SUPERSYMMETRIC DARK MATTER

G. JUNGMAN[a], M. KAMIONKOWSKI[b,c], K. GRIEST[d]

[a] *Department of Physics, Syracuse University, Syracuse, NY 13244, USA. jungman@npac.syr.edu*
[b] *Department of Physics, Columbia University, New York, NY 10027, USA. kamion@phys.columbia.edu*
[c] *School of Natural Sciences, Institute for Advanced Study, Princeton, NJ 08540, USA*
[d] *Department of Physics, University of California, San Diego, La Jolla, CA 92093, USA. kgriest@ucsd.edu*

ELSEVIER

AMSTERDAM – LAUSANNE – NEW YORK – OXFORD – SHANNON – TOKYO

ELSEVIER

Physics Reports 267 (1996) 195–373

PHYSICS REPORTS

Supersymmetric dark matter

Gerard Jungman[a], Marc Kamionkowski[b,c], Kim Griest[d]

[a] *Department of Physics, Syracuse University, Syracuse, NY 13244, USA. jungman@npac.syr.edu,*
[b] *Department of Physics, Columbia University, New York, NY 10027, USA. kamion@phys.columbia.edu,*
[c] *School of Natural Sciences, Institute for Advanced Study, Princeton, NJ 08540, USA,*
[d] *Department of Physics, University of California, San Diego, La Jolla, CA 92093, USA. kgriest@ucsd.edu*

Received June 1995; editor: D.N. Schramm

Contents

SSDI 0370-1573(95)00058-5

Abstract

There is almost universal agreement among astronomers that most of the mass in the Universe and most of the mass in the Galactic halo is dark. Many lines of reasoning suggest that the dark matter consists of some new, as yet undiscovered, weakly interacting massive particle (WIMP). There is now a vast experimental effort being surmounted to detect WIMPs in the halo. The most promising techniques involve direct detection in low-background laboratory detectors and indirect detection through observation of energetic neutrinos from annihilation of WIMPs that have accumulated in the Sun and/or the Earth. Of the many WIMP candidates, perhaps the best motivated and certainly the most theoretically developed is the neutralino, the lightest superpartner in many supersymmetric theories. We review the minimal supersymmetric extension of the standard model and discuss prospects for detection of neutralino dark matter. We review in detail how to calculate the cosmological abundance of the neutralino and the event rates for both direct- and indirect-detection schemes, and we discuss astrophysical and laboratory constraints on supersymmetric models. We isolate and clarify the uncertainties from particle physics, nuclear physics, and astrophysics that enter at each step in the calculations. We briefly review other related dark-matter candidates and detection techniques.

1. Introduction

In recent years, there has been a growing interaction between particle physics and astrophysics. The theoretical interest lies in the potential for particle-physics ideas to explain some of the thornier problems of cosmology, and the potential for astrophysical and cosmological observations to constrain ideas in particle physics. Although particle astrophysics was initially often dominated by theoretical speculation, it has recently reached a new level of maturity due to an active experimental thrust. In some areas, the connection between particle physics and astrophysics has become increasingly precise, and astrophysics has been able (or will soon be able) to provide empirical information that complements the results of accelerator experiments. The link between supersymmetry and dark matter is exemplary. In this review, we will explore the details of this link.

The standard model of particle physics provides an excellent description of physical processes at energies thus far probed by experiments. This includes those energies available in accelerator experiments, as well as those probed by measurements of, or bounds on, rare processes. Yet, virtually every particle theorist will agree that physics beyond the standard model is likely. In particular, new phenomena may well appear at the electroweak scale. Unitarity of electroweak interactions breaks down at energy scales $\lesssim$O(TeV) in the absence of a mechanism to account for electroweak-symmetry breaking. In the minimal model, electroweak symmetry is broken with a single Higgs doublet. Although consistent at low energies, the existence of a fundamental scalar field in the theory (the Higgs field) leads to an instability at higher energies, requiring a fine tuning of the high-energy parameters. Furthermore, the gauge structure in the standard model suggests the existence of a grand unified theory (GUT) at an energy scale of roughly 10^{16} GeV. Finally, there is the question of a more fundamental theory which would include quantum gravitational effects, presumably becoming strong at the Planck scale, 10^{19} GeV. Thus it seems quite possible that the standard $SU(3)\times SU(2)\times U(1)$ model for particle interactions is a low-energy limit of some underlying theory whose true structure will only become apparent when higher-energy scales are probed.

When Dirac combined special relativity with quantum mechanics, his equation contained a new charge-conjugation symmetry which required the existence of an antiparticle for each known particle. Dirac's initial hope that the electron might be the partner of the proton was soon dashed, but the discovery of the positron vindicated Dirac's theory. Today, this "doubling" of the number of particles is taken for granted to such an extent that antiparticles are not generally listed in the particle data book [1]. It is interesting that attempts to combine general relativity with quantum field theory (through the introduction of local supersymmetry) can lead to a supersymmetric doubling of the number of particles. Here, the symmetry relates bosonic integral-spin particles to fermionic half-integral-spin superpartners and vice versa. The discovery of supersymmetric partners has not followed quickly behind the theory, as did the discovery of the positron, although the hypothetical particles have been thoroughly studied. Searches for these particles are taking place at all the major accelerators. Examples of superpartners are the squarks and sleptons, the spin-0 partners of the quarks and leptons, and neutralinos, the spin-$\frac{1}{2}$ Majorana particles which are linear combinations of the supersymmetric partners of the photon, Z^0 and Higgs bosons (e.g., photino, higgsino, Z-ino).

Supersymmetry (SUSY) is an ingredient that appears in many theories for physics beyond the standard model. This is primarily because supersymmetry can cure the theoretical difficulty of

fundamental scalar particles which was mentioned above; it can render a theory stable to the radiative corrections which would otherwise force a fine tuning of high-energy parameters. This instability is the infamous "naturalness" problem (see, e.g., [2]), and we will discuss this technical point in Section 4. We mention here that, in order for the supersymmetric solution of this naturalness problem to work, it is necessary that the supersymmetry become manifest at relatively low energies, less than a few TeV. In other words, the required superpartner particles must have masses below this scale and must appear as final states in scattering experiments at these energies.

There are several other arguments for supersymmetry. An interesting motivation comes from the success of certain simple grand unified theories (GUTs) in explaining the pattern of electroweak-symmetry breaking. These theories would fail in the absence of supersymmetry [3]. In non-SUSY grand unified theories, it is found that the low-energy couplings for the U(1), SU(2), and SU(3) interactions do not unify at the GUT scale, in the simplest models. The convergence is tremendously improved with the introduction of supersymmetry [4]. As mentioned above, supersymmetry also seems to be an essential ingredient in theories (such as string or supergravity theories) which unify gravity with the other forces. In fact, gauging supersymmetry, in a manner analogous to the gauging of symmetries in the standard model, leads directly to gravitational interactions. Finally, there are some arguments based on accelerator phenomenology which might suggest the existence of low-energy supersymmetry [5]. We will discuss these issues as well in Sections 4 and 5.

In this background of many suggestions for physics beyond the standard model, astronomy also faces some curious problems. In astronomy, there is overwhelming evidence that most of the mass in the Universe is some nonluminous "dark matter", of as yet unknown composition. There are also reasons to believe that the bulk of this dark matter is nonbaryonic, that is, that it consists of some new elementary particle.

The most convincing observational evidence for the existence of dark matter involves galactic dynamics. There is simply not enough luminous matter ($\Omega_{\rm lum} \lesssim 0.01$) observed in spiral galaxies to account for their observed rotation curves. From gravitational effects, one infers a galactic dark halo of mass 3–10 times that of the luminous component, and by applying Newton's laws to the motion of galaxies in clusters, one infers a universal mass density of $\Omega \simeq 0.1$–0.3. There are also a few theoretical reasons for the existence of dark matter. First, if the mass density contributed by the luminous matter were the major contribution to the mass density of the Universe, the duration of the epoch of structure formation would be very short, thereby requiring (in almost all theories of structure formation) fluctuations in the microwave background which would be larger than those observed. These considerations imply $\Omega \gtrsim 0.3$ [6]. Second, if the current value of Ω is of order unity today, then at the Planck time it must have been 1 ± 10^{-60} leading us to believe that Ω is precisely 1 for aesthetic reasons. A related argument comes from inflationary cosmology, which provides the most compelling explanation for the smoothness of the microwave background. To account for this smoothness, inflation must set $\Omega_{\rm total}$ to unity.[1]

So, we see that conservative observational limits give $\Omega \gtrsim 0.1$, many others suggest $\Omega \gtrsim 0.3$, and $\Omega = 1$ is by far the most attractive possibility from theoretical arguments. On the other hand, big-bang nucleosynthesis suggests that the baryon density is $\Omega_{\rm b} \lesssim 0.1$ [7], too small to account for

[1] Here, $\Omega_{\rm total} = \Omega_{\rm matter} + \Omega_\Lambda$ can (but does not need to) include the contribution from a cosmological constant Λ as well as that from nonrelativistic matter. Throughout, we use Ω to denote the *matter* contribution to the mass density.

the dark matter in the Universe. Although a neutrino species of mass O(30 eV) could provide the right dark-matter density, N-body simulations of structure formation in a neutrino-dominated Universe do a poor job of reproducing the observed structure of the Universe. Furthermore, it is difficult to see (from phase-space arguments) how such a neutrino could make up the dark matter in the halos of galaxies [8]. It appears likely then, that some nonbaryonic, nonrelativistic matter is required in the Universe, and particle physics can provide candidates in abundance.

In this way, cosmology provides fuel to stoke the particle physicists' fire. Consider the case for supersymmetry. The presence of an exact discrete symmetry, R-parity, in most (but not all) supersymmetric theories guarantees that the lighest supersymmetric particle (LSP) is stable. In most cases, this particle is the neutralino, a linear combination of the SUSY partners of the photon, Z^0, and Higgs bosons. Therefore, supersymmetry predicts the existence of a new stable elementary particle having a mass less than a few TeV and having weak interactions with ordinary matter. As we will show in Section 3, if such a weakly interacting massive particle (WIMP) exists, then it has a cosmological abundance $\Omega \sim 1$ today, and could therefore account for the dark matter in the Universe.

Lest we mislead the reader, we should clarify several points. There is at present no *direct* accelerator evidence for the existence of supersymmetry; furthermore, it is not *absolutely* certain that there is dark matter which is neither baryons nor neutrinos. These are still unproven ideas. But current thinking in cosmology and particle physics has led in this direction. Supersymmetric theories of physics beyond the standard model provide perhaps the most promising candidates to solve the composite conundrums of particle physics and cosmology, providing a common paradigm for new particle physics and for cosmology. Although speculative, supersymmetric dark matter is very well motivated and based on a simple physical principle. This "coincidence" between new physics at the electroweak scale and a solution to the dark-matter problem is highly suggestive and should not be ignored.

Of course, it is certainly true that there exist "conservative" cosmological models which describe a Universe only in terms of baryons, and perhaps neutrinos. But these models often require several additional, and often poorly motivated, speculative assumptions.

Motivated by the above considerations, a far-ranging effort to discover supersymmetric dark matter is now afoot. In the simple picture, the dark matter in the Galactic halo is assumed to be composed, at least in part, by WIMPs, which we denote χ. If these particles account for Galactic rotation curves, then the local halo density is roughly $0.3\,\mathrm{GeV\,cm^{-3}}$, and the WIMPs have a Maxwell–Boltzmann distribution with a velocity dispersion of about $220\,\mathrm{km\,s^{-1}}$. The interactions of the WIMPs must be such that their cosmological density today is $\Omega_\chi \sim 1$. As explained in Section 3, this implies that they have interaction strengths characteristic of electroweak interactions. The mass of the WIMP in most supersymmetric models is somewhere between roughly 10 GeV and a few TeV.[2]

Although dark, in the sense that they neither emit nor absorb electromagnetic radiation, WIMPs must have some nonzero coupling to ordinary matter, because they must annihilate into it during the freezeout epoch in the early Universe. For example, this means that they will scatter from

[2] Actually, according to many supersymmetric-model builders, a few TeV is an overly conservative upper limit to the WIMP mass. These theorists will consider a few hundred GeV to be a more palatable upper bound.

nuclei. A first class of experiments searches for the O(keV) energy deposited in a low-background detector when a WIMP elastically scatters from a nucleus therein [9,10]. A second class of experiments searches for energetic neutrinos from the core of the Sun and Earth, which are produced by WIMP annihilation. Halo WIMPs can accrete in the Sun and Earth and annihilate therein to produce high-energy neutrinos which can be detected in neutrino telescopes [11–15]. Such neutrinos would have energies of roughly a third of the WIMP mass, so they would be much more energetic than, and could not be confused with, standard solar neutrinos. A third class of experiments, subject to far greater theoretical uncertainties, searches for anomalous cosmic rays produced by annihilation of WIMPs in the Galactic halo. Of course, the couplings to ordinary matter can lead to direct production in a particle accelerator as well.

This experimental effort has been complemented by a vast and sophisticated theoretical literature devoted to calculation of rates for both direct and indirect detection of supersymmetric dark matter, as well as accelerator searches for new particles. There has been no shortage of publications in which cosmological abundances, direct- and indirect-detection rates, and laboratory constraints are discussed for various supersymmetric models. Although the basic ideas underlying supersymmetric dark matter are simple, the literature devoted to rate calculations can be quite complicated. For example, implementation of supersymmetry in a realistic model is an involved process. Supersymmetry requires the introduction of numerous additional parameters. In the standard model, there are already 18 experimentally accessible parameters (6 quark masses, 3 lepton masses, 4 parameters in the Cabibbo–Kobayashi–Maskawa matrix, 3 gauge couplings, the W-boson mass, and Higgs-boson mass). It should be no surprise that in supersymmetry, where the number of degrees of freedom are (more than) doubled, there are many new parameters (we count 63), even in minimal supersymmetric extensions of the standard model. Logistical complications arise. Since such a large technical apparatus must be introduced when discussing supersymmetry, there are often significant variations in notation and implementation which alone cause confusion. There are also more significant complications. It is almost impossible (although we have not checked exhaustively) to find two authors (let alone two papers) using all the same assumptions about the various masses and couplings in the supersymmetric theory.

Given a supersymmetric model, the rate calculations are straightforward, but they can be quite lengthy and require input physics from supersymmetry, quantum chromodynamics, nuclear physics, astrophysics, solar physics, and some detector physics as well. As a result, it can be difficult for particle theorists to test the cosmological consequences of a given supersymmetric model or compare it with direct- and indirect-detection experiments. In some cases, it may be difficult to assess the significance of new calculations of neutrino spectra, nuclear matrix elements, cross sections for WIMP–nucleus scattering, etc. for event rates. The implications for detector design and search strategies can also be unclear.

In this Report, we review the cosmology of supersymmetric dark matter and the methods with which these ideas can be tested. We discuss the evidence for the existence of exotic dark matter and explain why supersymmetry provides an excellent candidate. We discuss direct detection of WIMPs and energetic neutrinos from WIMP annihilation. The main purpose of this work is to provide a handbook, useful to both theorists and experimentalists, which explains how to calculate direct and indirect-detection event rates. We collect here all the results from particle physics and astrophysics needed for the study of supersymmetric dark matter, and we include and make explicit all the information needed to calculate recoil spectra in detectors of almost any composition and to

calculate neutrino fluxes from annihilation of supersymmetric particles in the Sun and Earth. We isolate and clarify the uncertainties from particle physics, nuclear physics, and astrophysics that enter at each step in the calculation.

In Section 2, we begin with a review of the evidence for the existence of exotic (non-baryonic and non-light-neutrino) dark matter in the Universe and in our Galactic halo. Estimates of the local halo density of dark matter and its velocity distribution are discussed, as are the uncertainties in these.

In Section 3, the relic-abundance calculation is discussed, and we explain how to determine whether or not a given particle is cosmologically consistent, and if so, to determine if its abundance is suitable for accounting for the dark matter in the Universe. We argue that if a stable weakly interacting massive particle, such as the lightest supersymmetric particle, does indeed exist, then its relic abundance is likely suitable for accounting for the dark matter in the Universe.

In Section 4, we describe the minimal supersymmetric standard model (MSSM) and list the parameters which specify a model. Exploration of what is essentially a 63-dimensional parameter space is in fact tractable. In practice, some of the parameters are constrained by accelerator experiments, and many have well-motivated theoretical constraints. Furthermore, there are many simplifying relations usually (though not always) based on GUTs, supergravity, or string models employed which relate various masses and couplings. As a result, most of the relevant particle physics can be described with only a handful of parameters. We explain how the masses and couplings needed for cross sections appearing in cosmological-abundance and detection calculations are obtained from the input parameters.

Once the supersymmetric model is specified, it must satisfy a number of constraints from accelerator experiments. A comprehensive account of these constraints is beyond the scope of this review, but in Section 5, we list the most robust of these results and explain how to apply them to the MSSM.

The cosmological abundance depends primarily on the cross section for annihilation of two WIMPs to ordinary particles. Furthermore, the flux of energetic neutrinos from WIMP annihilation in the Sun and Earth as well as the flux of anomalous cosmic rays from WIMP annihilation in the halo depend on these cross sections. In Section 6, calculations of these annihilation cross sections are reviewed, and complete formulas for all the relevant annihilation channels are provided.

Both direct-detection and energetic-neutrino rates are controlled by the cross section for elastic scattering of WIMPs from nuclei, and these cross sections are discussed in Section 7. Complete formulas for WIMP–nucleus scattering are given for a variety of nuclei. These cross sections depend primarily on the coupling of the WIMP to protons and neutrons. The calculation of the WIMP-nucleon coupling is described, as are the uncertainties that arise from imprecise knowledge of low-energy strong-interaction physics, such as the scalar strange-quark density or spin content of the nucleon. Cross sections for scattering from heavier nuclei are obtained from the WIMP–nucleon couplings. The results from nuclear physics needed to obtain these cross sections are included here, and uncertainties in the nuclear modeling are also discussed. WIMPs generally couple to nuclei via an axial-vector (spin) interaction or a scalar (spin-independent) interaction. In the spin interaction, the WIMP couples to the spin of the nucleus, and in the scalar interaction, the WIMP couples to the nuclear mass. The two interactions have different consequences for detection, so care is taken to distinguish between the physics of these two processes.

Given the cross section for WIMP–nucleus scattering and a halo density and velocity distribution, it is straightforward to calculate the rate for scattering in a low-background detector. This is the subject of Section 8. The results are applicable to detectors of almost any composition. In many experiments, the nuclear-recoil spectrum is needed to compare theory with experiment, so in addition to total event rates, we show how to calculate the recoil spectrum as well. The dependences on the assumed WIMP halo density and velocity dispersion are made clear. We briefly review some of the current and forthcoming experiments and some of the expected backgrounds.

In Section 9, we discuss energetic neutrinos from WIMP annihilation in the Sun and Earth. The neutrinos from decays of WIMP-annihilation products may be detectable in high-energy neutrino telescopes. To obtain the flux of such neutrinos, the capture rate in the Sun and Earth and the spectrum of neutrinos from decays of the WIMP-annihilation products must be calculated. Absorption of neutrinos in the Sun and Earth must also be included. The signal in most neutrino telescopes is observation of an upward-going muon produced by a charged-current interaction of the neutrino in the material below the detector. These calculations are quite a bit more involved than the direct-detection calculations, but all the needed information is included here. We discuss and estimate the various uncertainties in the capture rates and neutrino spectra. We briefly review some of the neutrino telescopes and consider the irreducible background of atmospheric neutrinos.

Another possible avenue towards discovery of particle dark matter is observation of anomalous cosmic rays produced by WIMP annihilation in the halo, the subject of Section 10. Although it is plausible that WIMPs could produce a recognizable cosmic-ray signature, it is difficult to make precise predictions for a given supersymmetric candidate due to uncertainties in the dark-matter distribution, the propagation of cosmic rays, and an imprecise knowledge of the cosmic-ray background. Therefore, we survey briefly the various cosmic-ray signatures of WIMPs which have been considered, but we do not step through the calculations in great detail.

In Section 11, we give numerical examples of the results of earlier sections, and demonstrate the various relations between model parameters, direct- and indirect-detection rates, and relic abundances. A wide variety of model parameters are explored and several results which include a survey of the ratio of spin-dependent to spin-independent elastic cross sections, a comparison of indirect and direct detection, and the effect of various accelerator constraints and model uncertainties are illustrated here.

In this paper, we focus specifically on dark matter that arises from the minimal supersymmetric standard model. However, it should be pointed out that virtually any other stable massive particle with interaction strength characteristic of the electroweak interactions should also have a relic abundance of order unity. Furthermore, the direct- and indirect-detection experiments discussed here should also be sensitive to these WIMPs in our halo. For example, the first WIMP candidate considered was a heavy (possibly fourth-generation) Dirac or Majorana neutrino. In Section 12, we discuss briefly the heavy Dirac neutrino with standard-model couplings as the halo dark matter. The cosmology and phenomenology are much simpler than in the supersymmetric case. Furthermore, the Dirac neutrino with standard-model couplings is an interesting example, since it has in fact been ruled out as a halo dark-matter candidate by a variety of complementary experiments of the type described here. It should be noted that the neutralino of the MSSM and heavy neutrinos in other models do not exhaust the possibilities for WIMP dark matter. Such particles also arise in nonminimal supersymmetric models, and they may also arise as a consequence of some underlying

theory that is not yet born. We briefly discuss gravitinos, axinos, and neutralinos in nonminimal models.

In the conclusions, we summarize the discussion of supersymmetric dark matter by providing a diagram which shows the interrelation of all the calculations and experimental probes reviewed. We also list the central calculational results of the paper, and we make some concluding remarks.

Appendix A contains additional discussion of the MSSM. We briefly review supersymmetry and details about the construction of the minimal supersymmetric standard model. Numerous couplings and masses that appear, for example, in cross sections throughout the paper, are given here. The squark interactions are discussed in detail. In much previous work, it was assumed that squark and slepton mixing is flavor diagonal. In the standard-model lepton sector, there is no mixing between the various generations since neutrinos are (thought to be) massless. However, it is well known that the standard-model quark eigenstates are indeed linear superpositions of the weak-interaction eigenstates, and that this mixing is described by the Cabibbo–Kobayashi–Maskawa matrix. Although it is often assumed (for reasons of simplicity) that the squark and slepton sectors are flavor diagonal, there is no a priori reason for believing that this is so. In fact, the radiative corrections for all models show that flavor-asymmetric terms must arise, since flavor symmetry is broken by Yukawa couplings. The existence of such mixing terms is of interest since they play a role in probes of supersymmetry based on rare processes. Such probes are becoming very important at the present time, especially with regard to rare radiative b-quark decays. Therefore, it is worth presenting the details of flavor physics in a complete form. The MSSM interactions in Appendix A accommodate general flavor mixing.

Although it should be straightforward for a reader to code the information in this Report in order to study abundances, laboratory constraints, and detection rates for various supersymmetric models, the procedure is quite lengthy. Therefore, the preparation of this work was accompanied by the construction of a comprehensive, modular, exportable, and documented computer code (written in ANSI C). The program is briefly described in Appendix B. With this code, interested parties can reproduce the numerical results presented here, explore detection rates, abundances, and laboratory constraints in various regions of the MSSM, check numerically the sensitivity of results to various input assumptions, assess the significance of new calculations, etc. It should also be possible to interface this code to data-analysis software. The code is available upon request from the authors.

This review is meant to be useful to experimentalists and theorists interested in getting to the connection between particle theory, cosmology, and dark-matter experiments. Quite sophisticated calculations of relic abundance and detection rates which provide very accurate results for given model parameters have been carried out. However, we still have only vague clues about the detailed structure of the supersymmetric theory that may be relevant to reality. Masses and couplings vary over several orders of magnitude in the allowed MSSM parameter space. Moreover, some of the relevant cosmological and astrophysical parameters are uncertain by factors of two or so. The current experimental effort is aimed at discovery, not precise measurement of parameters in a class of theories which have yet to be discovered. Therefore, the accuracy of the calculational techniques presented here is generally O(10–20%), and in some cases only O(50%). For almost every calculation we describe, there exists another more sophisticated calculation with better accuracy. However, these calculations tend to be far more complicated and are rarely general or easily applied. The simpler results presented here should suffice for most current applications. We

should stress, however, that we have *not* simplified by limiting ourselves to certain regions of parameter space. In every case, we have sought to include results that will apply to as broad a class of supersymmetric dark-matter candidates as possible. For example, all the calculations simplify tremendously if one considers only WIMPs with masses less than the W-boson mass or WIMPs which are pure photinos or higgsinos. Here, we have tried to include results for neutralinos of any mass or composition that could arise in the MSSM.

In this work, we do not attempt to review all of the models which have been discussed, nor do we attempt to survey exhaustively the entire MSSM parameter space. In Section 11, we provide numerical results of surveys of supersymmetric parameter space for the purposes of illustration, and we occasionally work out the details of simple models also for illustration. We have attempted to clarify all the steps in each calculation and the effects of various assumptions on the results. The qualitative conclusions about abundances, laboratory constraints, and detection rates should be clear. Furthermore, with the formulas presented here (and if desired, the accompanying numerical code), interested readers can explore more carefully any specific region of parameter space themselves. The accompanying code has also been written in modular fashion, so readers can add to it more detailed formulas for any process they find of particular interest.

In studying supersymmetric dark matter, it is possible to become overwhelmed with all the details and lose sight of the big picture, which is actually quite simple. Therefore, where possible (especially in Sections 9.6 and 9.7), we provide approximate expressions for abundances and detection rates that are largely independent of the details of the model. For example, direct- and indirect-detection rates depend primarily on the WIMP–nucleon coupling. To a large extent, most of the details of the supersymmetric model enter into detection-rate calculations only through this coupling. Much of the remaining calculation can then be discussed without reference to any specific supersymmetric model, and we can reach some model-independent conclusions for detection strategies.

Before continuing, we mention some related reviews that may be of interest. It would be futile to attempt to list all the reviews and monographs on supersymmetry. For an introduction to supersymmetry, we recommend, for example, the monographs by Wess and Bagger [16] and West [17]. The minimal supersymmetric extension of the standard model is introduced quite well in Ref. [18], and some of the important phenomenology, especially in the Higgs sector, is reviewed clearly in Ref. [19]. Ref. [20] remains perhaps the most comprehensive review of the phenomenology of the MSSM. Reviews of the ideas and prospects for detection of WIMP dark matter which precede this review are Refs. [21, 22], although these did not focus specifically on supersymmetry. A more recent review of dark-matter detection, which focuses primarily on the relevant nuclear physics, is that by Engel et al. [23]. The experimental aspects of direct detection of dark matter are discussed in Ref. [24], and Ref. [25] is a collection of papers on recent developments in direct-detection technologies. Energetic-neutrino experiments are reviewed in Ref. [26]. The evidence for dark matter in galaxies is collected in Ref. [27], and the evidence for dark matter in the Universe is summarized in Ref. [28]. For a discussion of the mass distribution in our Galaxy, see Ref. [29], and for a pedagogical introduction to the relevant issues in galactic dynamics, see the monograph by Binney and Tremaine [30]. A good fraction of all the literature in astrophysics and cosmology today is devoted to issues relevant to dark matter. For a good introduction to some of the relevant cosmology, see, for example, the books by Kolb and Turner [31] and Peebles [32].

2. Dark matter in the Universe

It is remarkable that we still do not know what the primary constituent of the Universe is. This "dark matter" does not emit or absorb electromagnetic radiation at any known wavelength, yet its gravitational interactions dominate on scales from tiny dwarf galaxies, to large spirals such as the Milky Way, to clusters of galaxies, to the largest scales yet observed. Since the original suggestion of the existence of dark matter [33], the evidence has become overwhelming. The question has changed from "Does dark matter exist?" to "What is this most common of substances?"

The evidence for dark matter exists on many scales and it is important to keep in mind that the dark matter on different scales may consist of different materials. Many different substances can qualify as being "dark" in the astronomical meaning of this word. So it is quite possible that the dark matter in dwarf spirals is not the same as the dark matter which contributes $\Omega = 1$; in fact, the $\Omega = 1$ dark matter may not even exist. This consideration is especially important when discussing dark-matter detection, since detection is done in the Milky Way, and evidence for dark matter outside the Milky Way is only of secondary importance in this pursuit.

2.1. Inventory of dark matter

The cosmological density of a given population or species is quoted using $\Omega = \rho/\rho_{\rm crit}$, where ρ is the density of that species averaged over the Universe, and $\rho_{\rm crit} = 1.88h^2 \times 10^{-29}\,{\rm g\,cm^{-3}}$ is the critical density. Here $h = 0.4$–1 parameterizes the uncertainty in the Hubble constant, $H_0 = 100h\,{\rm km^2\,s^{-1}\,Mpc^{-1}}$. Most determinations of Ω are made by measuring the mass-to-light ratio Υ of some system and then multiplying this by the average luminosity density of the Universe: $j_0 = 1.7 \pm 0.6 \times 10^8\, hL_\odot\,{\rm Mpc^{-3}}$ (in V band) [30, 34, 35]. Then the cosmological density of that system is given by $\Omega = 6.1 \times 10^{-4} h^{-1}(\Upsilon_{\rm V}/\Upsilon_\odot)$, where $\Upsilon_\odot = M_\odot/L_\odot$ is the mass-to-light ratio of the Sun. The factor of two uncertainty in the luminosity density means that determinations of Ω which use this method will be uncertain by at least this amount. In fact, most determinations of Ω which involve an "inventory" of the dark matter in the Universe use this method. For example, the mass-to-light ratio in the solar neighborhood is $\Upsilon \approx 5\Upsilon_\odot$, giving $\Omega_{\rm lum} \approx 0.003h^{-1} = 0.003$–$0.007$. If the solar neighborhood is typical, the amount of material in stars, dust and gas is far below the critical value.

Spiral galaxies: The most robust evidence for dark matter comes from the rotation curves of spiral galaxies. Using 21-cm emission, the circular velocities of clouds of neutral hydrogen can be measured as a function of r, the distance from the center of the galaxy. In almost all cases, after a rise near $r = 0$, the velocities remain constant out as far as can be measured. By Newton's law this implies that the density drops like r^{-2} at large radii, and that the mass interior to r is $M(r) \propto r$ at large radii. Once r becomes greater than the extent of the mass, one expects the velocities to drop $\propto r^{-1/2}$, but this is not seen, implying that we do not know how large the extended dark halos around the spirals are. Fig. 1 shows the rotation curve for the spiral galaxy NGC 6503 [36].[3] The luminous disk extends no further than about 5 kpc from the center of the galaxy. If the luminous

[3] We thank A. Broeils for providing this figure.

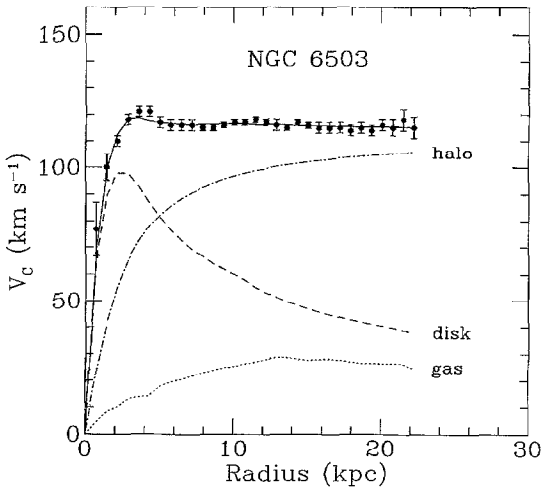

Fig. 1. Rotation curve for the spiral galaxy NGC 6503. The points are the measured circular rotation velocities as a function of distance from the center of the galaxy. The dashed and dotted curves are the contribution to the rotational velocity due to the observed disk and gas, respectively, and the dot–dash curve is the contribution from the dark halo. (From Ref. [36].)

matter was all there was, the rotation curve would drop at larger radii. From the discrepancy between the observed rotation curve and the rotation curve due to the luminous disk and gas, we infer the existence of a dark halo. This galaxy is typical. Similarly, the rotation curve of NGC 3198 [30] implies $\Upsilon > 30h\Upsilon_\odot$, or $\Omega_{\rm halo} > 0.017$. The large discrepancy between this number and $\Omega_{\rm lum}$ is seen in many external galaxies and provides the most robust evidence for dark matter.

Observations of tracers other than neutral hydrogen give similar results. For external galaxies, Zaritsky [37] used a sample of 69 small satellite galaxies around 45 spirals similar to the Milky Way to estimate the total mass for a "typical" spiral. He found that $M \approx 10^{12} M_\odot$ at 200 kpc from the center, implying $\Omega_{\rm spirals} \approx 0.087 h^{-1}$ out to this radius. It is interesting that even out to this rather large radius, there is no strong evidence that rotation speeds drop, so again there is no good upper limit to $\Omega_{\rm spiral}$. The number found by this satellite galaxy method is similar to the number found by the Local Group Timing and other methods (see, e.g., Refs. [29, 30]).

Clusters of galaxies: Moving to larger scales, the methods of determining Ω become less secure, but give larger values. There is a great deal of new evidence on dark matter in clusters of galaxies, coming from gravitational lensing [38], from X-ray gas temperatures [39, 40] and from the motions of cluster member galaxies. For example, consider the Coma cluster which contains roughly a thousand galaxies. White et al. [40] recently collated some of the data on the Coma cluster, reporting separate measurements of the amount of mass in stars, hot gas, and in total. Within a radius of $1.5h^{-1}$ Mpc, they give

$$M_{\rm star} = 1.0 \pm 0.2 \times 10^{13} h^{-1} M_\odot, \quad M_{\rm gas} = 5.4 \pm 1 \times 10^{13} h^{-5/2} M_\odot,$$

$$M_{\rm total} = (5.7 - 11) \times 10^{14} h^{-1} M_\odot, \tag{2.1}$$

where the total mass is estimated in two completely different ways. The first method is a refinement of Zwicky's method of using the radial velocities of the member galaxies, and the assumption of virialization to gauge the depth of the gravitational potential well. The second method makes use of the ROSAT X-ray maps and the assumption of a constant-temperature equilibrium to get the same information. Remarkably the two methods give the same mass within errors. Thus, with a mass-to-light ratio of $\Upsilon = 330\text{–}620\Upsilon_\odot$, one finds $\Omega = 0.2\text{–}0.4$, if the inner 1.5 Mpc of Coma is representative of the Universe as a whole.

There is, however, a very disconnecting fact about the above numbers. As pointed out by White et al. [40],

$$M_{\text{baryon}}/M_{\text{total}} > 0.009 + 0.05h^{-3/2} . \tag{2.2}$$

Now the Coma cluster is large enough that one might expect its baryon-to-dark-matter ratio to be the universal value, $(\Omega_b/\Omega_{\text{total}} = M_{\text{baryon}}/M_{\text{total}})$, and in fact, White et al. argue that this is the case. Then the inequality above should apply to the entire Universe. But, as we discuss later, big-bang nucleosynthesis limits the baryon density to $\Omega_b < 0.015h^{-2}$ [7,41,42]. If $\Omega_{\text{total}} = 1$, the two inequalities are in quite strong disagreement for any value of h. So this is a big puzzle. The conclusions of White et al. are that either Ω is not unity, or that big-bang nucleosynthesis is flawed. However, there are other possible explanations, notably that measurements of the total mass in clusters by weak or strong gravitational lensing tend to give larger total mass than the X-ray and virial methods, and that mass and velocity bias may mean that clusters are not so representative of the Universe as a whole [38,43]. Again it may also be that the Universe is open or that there is a significant cosmological constant [44].

Large-scale flows: It would be best to measure the amount of dark matter on the largest possible scales so that the sample is representative of the entire Universe. Within the past several years a host of large-scale flow methods have been tried and are giving impressive results [45,46]. These methods have the advantage stated above but have the disadvantage that they depend upon assumptions about galaxy formation, that is, they depend upon gravitational instability theory, biasing. etc. Also, the errors in these measurements are still large and the calculations are complicated, but they do have great promise, and tend to give values of Ω near unity.

The simplest example comes from the observation that the local group of galaxies moves at $627 \pm 22\ \text{km s}^{-1}$ with respect to the cosmic microwave background (CMB) (measured from the amplitude of the CMB dipole). If this motion comes from gravity, then the direction of the motion should line up with the direction where there is an excess of mass, and the velocity should be determined by the size of this excess. Thus, taking into account the expansion of the Universe, one has

$$v \propto \Omega^{0.6}(\delta\rho/\rho) = (\Omega^{0.6}/b)(\delta n/n) , \tag{2.3}$$

where the linear bias factor b has been introduced to relate the observed excess in galaxy number counts $\delta n/n$ to the excess in mass density $\delta\rho/\rho$. Using galaxy counts from the IRAS satellite survey, Yahil et al. [47] find that the direction of the $\delta n/n$ excess agrees with the direction of the velocity vector to within $\sim 20^\circ$, and that

$$\beta \equiv \Omega^{0.6}/b = 0.9 \pm 0.2. \tag{2.4}$$

Thus with the very conservative limit $b > 0.5$, one has $\Omega > 0.2$, and with the reasonable limit $b > 1$, one finds $\Omega > 0.5$. For this method to be reliable, $\delta n/n$ must be measured on very large scales to ensure that convergence has been reached, and this has yet to be convincingly demonstrated.

The above technique is only one of many related methods used to determine Ω on large scales. Another example is the detailed comparison of the peculiar velocities of many galaxies with the detailed maps of $\delta n/n$. This should not only determine Ω, but serve as a stringent test for the theory that large-scale structure is formed by gravitational instability. The difficulty is the measurement of the peculiar velocities, which requires subtraction of the much larger Hubble-flow velocity from the observed redshift velocity. Since the redshift measurements give only the radial component of velocity, it seems difficult to obtain complete enough information, but Bertschinger and Dekel [48] proposed a method in which it is assumed that the velocity field is curl free, allowing the entire three-dimensional field to be reconstructed. They use

$$\nabla \cdot v = -(\Omega^{0.6}/b)(\delta n/n)\,, \tag{2.5}$$

and solve for $\beta = \Omega^{0.6}/b$. In a recent application of this technique, it was found that $\beta \simeq 0.6$ [49], suggesting $\Omega \gtrsim 0.3$. Especially notable is that the detailed $\delta n/n$ maps agree remarkably well with the reconstructed velocity fields, thereby providing evidence that gravitational instability is the most likely cause of the structure. The review of Dekel [45] shows that many large-scale flow methods now predict $\Omega > 0.3$ and show reasonable to excellent agreement with the theory of gravitational collapse. Although this technique holds much promise, it should be noted that different analyses of the same data sometimes lead to different conclusions. So for the time being, these estimates of β should not be viewed as robust [50].

In conclusion, the observational evidence for large amounts of dark matter on galactic-halo scales is overwhelming. On larger scales, the observational evidence for Ω in the 0.1 to 0.2 range is strong. On the largest scales, substantial observational evidence exists for $\Omega > 0.3$, and some evidence for Ω near unity exists, although this may be in conflict with observations on cluster scales.

2.2. *Theoretical arguments*

From an aesthetic point of view, the value $\Omega = 1$, is quite heavily favored. The basic argument is that $\Omega = 1$ is the only value which does not change rapidly as the Universe expands. Since Ω is measured to be within an order of magnitude of unity today, then it must have been 1 ± 10^{-60} at the Planck time. Thus $\Omega = 1$ is the natural value, and if it is not unity, it will soon be very different from unity, meaning that we live at a rather special time in the history of the Universe. This argument has been given a concrete form with the advent of inflationary cosmology. An extremely striking feature of the Universe is the isotropy of the CMB. To date, by far the most attractive mechanism for explaining this homogeneity is inflation, which almost certainly sets $\Omega = 1$. In addition, inflation also provides a mechanism for producing primordial density perturbations that are quite similar to those observed. Therefore, the inflationary Universe is an intriguing paradigm that should be taken very seriously.

Structure formation and CMB: Theoretical and semi-empirical arguments involving large-scale structure formation and the cosmic microwave background also suggest a large value of Ω. Density perturbations grow after the Universe becomes matter dominated but before it becomes curvature

dominated. If the Universe consisted solely of luminous matter, then the epoch of structure formation would have been very short, probably requiring initial perturbations that would have given rise to CMB anisotropies larger than those observed. For example, in standard models of structure formation with cold dark matter and adiabatic primordial density perturbations, such considerations suggest $\Omega \gtrsim 0.3$ [6, 51]. Although these arguments are somewhat model dependent, alternative models for the origin of structure in a low-Ω Universe, such as the primordial isocurvature baryon (PIB) model, also seem to be in trouble with CMB measurements [52]. Finally, we should point out that, in the forthcoming years, measurement of the angular spectrum of the CMB on small angular scales will potentially provide a very precise determination of Ω [53].

Age of the Universe and Hubble constant: The biggest problem for an $\Omega = 1$ Universe may turn out to be the discrepancy between the large observed value for the age of the Universe, t_U, and the large measured values for the Hubble constant, h (in units of 100 km s^{-1} Mpc^{-1}). If $\Omega = 1$ and the cosmological constant $\Lambda = 0$, then $h \simeq (7\ \text{Gyr}/t_U)$. Globular-cluster ages suggest $t_U \gtrsim 13$ Gyr [54] while numerous recent measurements of the Hubble constant fall near $h \simeq 0.7$ [55–57]. If these numbers hold up, then the matter density in the Universe must be small, and a significant cosmological constant may also be required. This is shown in Fig. 2, where the relations between the Hubble constant, Ω, Λ, and the age of the Universe are displayed.

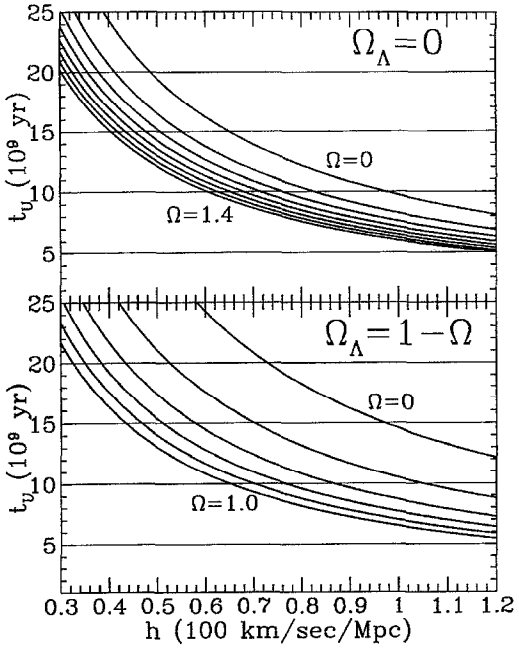

Fig. 2. Age of the Universe for various values of h, the Hubble constant, and Ω, the matter density. The top panel shows a Universe with no cosmological constant ($\Lambda = 0$), while the bottom panel shows a flat Universe with a cosmological constant ($\Omega + \Omega_\Lambda = 1$). In the top panel, the curves range from $\Omega = 0$ to $\Omega = 1.4$ in steps of 0.2, and in the bottom panel, Ω ranges from 0 to 1 also in steps of 0.2.

2.3. Baryonic content of the Universe

An important ingredient in the motivation for nonbaryonic dark matter comes from big-bang-nucleosynthesis limits on the average baryonic content of the Universe. To agree with the measured abundances of helium, deuterium, and lithium, the baryonic content of the Universe must be between $0.01 \lesssim \Omega_b h^2 \lesssim 0.015$ [7,41,42]. Given the large uncertainty in h, this means $0.01 \lesssim \Omega_b \lesssim 0.1$. These values are far below unity, so the predilection for $\Omega_{\text{total}} = 1$ (or the observational evidence for $\Omega \gtrsim 0.3$) forces the bulk of the dark matter to be nonbaryonic. The lower limit of this range is actually *above* the abundance of known stars, gas, etc., and so there also seems to be evidence for substantial *baryonic* dark matter as well.

For some time, it was proposed that the observed abundances of light elements could be produced with a larger baryon density if inhomogeneities were produced during a first-order QCD phase transition [58]; however, results from recent lattice simulations showing a smooth transition [59], as well as careful studies of the required phase transition parameters [60], make this possible loophole increasingly unlikely. So, it seems that in any case, if $\Omega_{\text{total}} \gtrsim 0.3$, the bulk of the dark matter must be nonbaryonic.

However, there are several other issues relevant to big-bang nucleosynthesis. The most serious problem may be the X-ray baryon crisis discussed above. It is not entirely clear what these observations imply for big-bang nucleosynthesis. Also, the standard value for primordial deuterium abundance has recently been challenged by a possible detection of a large primordial deuterium/hydrogen ratio (D/H) in a Lyman-limit cloud at large redshift, implying a baryon density from big-bang nucleosynthesis much smaller than previously thought [61]. However, another high-redshift detection of deuterium [62] has not confirmed this high value and is more in line with the older interstellar determinations of D/H. Finally, we note that the MACHO surveys [63–66] seem to suggest that there may be some dark baryons, although the event rates are not high enough to pose a problem for big-bang nucleosynthesis.

2.4. Distribution of dark matter in the Milky Way

It is fortunate that the most secure evidence for dark matter is in spiral galaxies, since direct searches for dark matter can be made only in spiral galaxies; in fact, only in our spiral, the Milky Way. Unfortunately, the rotation curve of the Milky Way is poorly constrained (it is much easier to measure rotation curves in other galaxies than in our own), which leads to uncertainty in the amount and distribution of dark matter in our Galaxy. However, there are numerous arguments that the Milky Way, like most other spiral galaxies, is immersed in a dark halo which outweighs the luminous component by about a factor of ten [29,67]. The first is a variant of the Copernican principle. To the extent that it can be determined, the Milky Way seems to be an ordinary spiral galaxy. For example, when plotted versus the observed Galactic rotation speed, the infrared luminosity of the Milky Way measured by COBE is that given by the Tully–Fisher relation. Since the typical spiral galaxy has a dark halo, it suggests that ours does as well.

There are additional theoretical arguments. As discussed above, there are a variety of reasons for believing that most of the mass of the Universe is in the form of cold dark matter. If so, then dark matter should cluster with galaxies. During gravitational collapse and subsequent virialization ("violent relaxation"), the collisionless dark matter should form a halo that is roughly spherical

[68]. In other words, if there is cold dark matter, there should be a halo. There are also arguments that a dark halo is needed to stabilize the disk, although these are controversial.

More directly, there are several dynamical arguments for the existence of a Galactic dark halo. For example, by studying the motion of dwarf galaxies (especially Leo I at a distance of 230 kpc), Zaritsky et al. [69] find a mass of the Milky Way of $M_{\rm MW} = 1.25^{+0.8}_{-0.3} \times 10^{12} M_\odot$, yielding $\Upsilon_{\rm MW} \approx 90 \Upsilon_\odot$. There are only a limited number of small satellite galaxies around the Milky Way, so the uncertainty in this measurement is large. The Local Group Timing method (which involves the dynamics of our Galaxy and its neighbor, M31) gives a similar result. Finally, if they are bound, the fastest stars in the local neighborhood suggest that the escape velocity from the Galaxy is $\gtrsim 450\ {\rm km\,s^{-1}}$, much larger than can be accounted for by the luminous matter. When assembled, these data suggest a Galactic circular rotation speed, at radii ≈ 100 kpc (much larger than the extent of the luminous component), of $\approx 230\ {\rm km\,s^{-1}}$ [67], although it should be noted that there may be significant systematic uncertainties in this result. Without a model or more understanding of the systematics, it is difficult to come up with an accurate value for the total mass of the Galaxy. However, from a broad survey of the evidence for dark matter in our halo, Fich and Tremaine conclude that dark matter outweighs the luminous matter in our Galaxy by a factor of ten or so [29].

There is also evidence for a Galactic halo from observations at much smaller radii. The measured rotation curve remains flat (to roughly 15%) from 4 kpc out to 18 kpc. This distance is about 6 times the exponential scale length (~ 3 kpc) of the luminous disk determined by COBE data [70]. The flaring of atomic hydrogen layers at distances larger than the optimal disk provides additional evidence for a dark halo. The rms scale height of the atomic-hydrogen gas rises from 200 pc at the solar-circle radius to 1700 pc at thrice this radius. This suggests that the matter responsible for the flat rotation curves cannot be confined to a thin disk and most likely has more of a spheriodal distribution [70, 71].

Local dark-matter density – overview: The two quantities which are crucial to both the direct and indirect methods of dark-matter detection are the *local* dark-matter density, ρ_0, and the velocity dispersion of dark-matter particles, $\bar{v} = \langle v^2 \rangle^{1/2}$. (Note, as discussed in Section 8, the form of the velocity distribution also enters.) Throughout this review we will use, as canonical values for these quantities, $\rho_0 = 0.3\ {\rm GeV\,cm^{-3}}$ and $\bar{v} = 270\ {\rm km\,s^{-1}}$, although as discussed below, there is considerable uncertainty and model dependence in these numbers. In this section we discuss some issues regarding the determination of these quantities.

In determining ρ_0 and $\bar{v}$, the rotation curve is the most important observational quantity since it measures the change in density and sets the scale for the depth of the Galactic potential well. The rotation curve of the Milky Way has been measured repeatedly, but due to our unfortunate location inside the Galaxy, it has been difficult to obtain accurate measurements at large Galactic radii, and the errors are larger than those for external galaxies. The IAU standard value for the rotation velocity at the Sun's distance from the Galactic center is $v_{\rm tot}(r_0) = 220\ {\rm km\,s^{-1}}$ [72]. Recent studies favor values near $v_{\rm tot}(r_0) \approx 200\ {\rm km\,s^{-1}}$ [73], and several studies show that $v_{\rm tot}(r)$ is constant to within 15% out to twice the solar circle (e.g., Ref. [74]).

The distribution of mass in other Galactic components such as the bulge, the stellar disk, and possibly a dark disk is also needed to determine the local halo density. The rotation curve measures the *total* gravitational potential and so includes contributions from both the assumed

dissipationless dark-matter halo and these other components. For example, considering the contribution of the stellar and dark disks (the most important components), the total rotation speed is

$$v_{\rm tot}(r) = [v_{\rm d}^2(r) + v_{\rm h}^2(r)]^{1/2}, \tag{2.6}$$

where $v_{\rm d}$ is the disk contribution, $v_{\rm h}$ is the halo contribution, and r is the distance to the center of the Galaxy in the plane of the disk. Since the density of particle dark matter depends only upon $v_{\rm h}$, in principle $\rho_0 = \rho(r_0)$ can be determined using only the local value and slope of the halo rotation curve:

$$\rho(r) = (1/4\pi G r^2)(\mathrm{d}/\mathrm{d}r)[r v_{\rm h}^2(r)], \tag{2.7}$$

where $r_0 \approx 8.5$ kpc is the distance from the Sun to the Galactic center. In practice, however, this equation is not used, since one wants to incorporate sampling of the rotation curve at several points, as well as additional dynamical information. Typically, the various Galactic components are modeled and then fit to the rotation curve (and perhaps other dynamical constraints) to obtain the local halo density. Thus we see that uncertainty in ρ_0 will come from (i) the uncertainty in the measured rotation curve, (ii) the uncertainty in the model of the dark halo considered, and (iii) the uncertainty in the contribution of the disk, etc. to the rotation curve, which must be subtracted [64, 75–81].

Using a variety of such techniques, the value of the local dark-matter density has been estimated by several groups. Bahcall et al. find a central value of $\rho_0 = 0.34\ \mathrm{GeV\,cm^{-3}}$ [82], while Caldwell and Ostriker find a slightly smaller central value, $\rho_0 = 0.23\ \mathrm{GeV\,cm^{-3}}$ [83], and Turner obtains $\rho_0 = 0.3$–$0.6\ \mathrm{GeV\,cm^{-3}}$ [84]. With additional theoretical modeling of the possible formation mechanism for the halo, Flores argues for a local dark-matter density in the range 0.3–$0.43\ \mathrm{GeV\,cm^{-3}}$ [85]. A recent analysis by Gates et al., which includes constraints on the microlensing optical depths to the Bulge and LMC, yields a central value of the local dark-matter (i.e., *not* MACHOS) halo density of $0.5\ \mathrm{GeV\,cm^{-3}}$ [81] (although the local halo densities in their consistent models range from 0.05–$1\ \mathrm{GeV\,cm^{-3}}$, in agreement with the results of Griest [86]). Their central value is higher than those previously obtained because they considered the possibility that the halos are elliptical. (Note that $M_\odot\,\mathrm{pc^{-3}} = 38\ \mathrm{GeV\,cm^{-3}}$.) As mentioned above, for numerical work in this review we adopt $\rho_0 = 0.3\ \mathrm{GeV\,cm^{-3}}$ and $\bar{v} = 270\ \mathrm{km\,s^{-1}}$, though given the large allowed range of values, we are not advocating these as the best values. Below we use a simple model to illustrate the sources of uncertainty.

Local dark-matter density – simple model: In order to illustrate the source of uncertainties in determining ρ_0, and to make our discussion concrete, consider a simple and commonly used model for the halo, the cored spherical isothermal halo [87],

$$\rho(r) = \rho_0(a^2 + r_0^2)/(a^2 + r^2), \tag{2.8}$$

where a is the core radius of the halo. The distribution in Eq. (2.8) produces rotation curves which are flat at large radii and it seems similar to (although not exactly like) those produced in N-body simulations. The local velocity distribution in this model is Maxwellian,

$$f(v)\,\mathrm{d}^3v = (\mathrm{e}^{-v^2/v_0^2}/\pi^{3/2}v_0^3)\,\mathrm{d}^3v\,. \tag{2.9}$$

Technically, one is not free to pick the density and velocity distributions independently since the phase-space distribution must satisfy Jean's equation [30]. The exact solution for the density distribution for the cored spherical isothermal halo, which can be obtained numerically [87], differs slightly from the analytic form, although it agrees with Eq. (2.8) in the small- and large-radius limits.

In this model, the circular rotation speed at a radius r due to the halo alone is

$$v_h^2(r) = 4\pi G\rho_0(r_0^2 + a^2)(1 - (a/r)\tan^{-1}(r/a)) . \tag{2.10}$$

Define v_∞ as the circular rotation velocity as $r \to \infty$. Since the stellar-disk density is thought to drop exponentially at radii much larger than the extent of the disk, this circular velocity should be due only to the halo $v_\infty = v_h(\infty) = v_{tot}(\infty)$. Then the rotation velocity due to the halo at the solar-circle radius, $v_h(r_0)$, is given by

$$(a/r_0)\tan^{-1}(r_0/a) = 1 - v_h^2(r_0)/v_\infty^2 , \tag{2.11}$$

and this determines the ratio a/r_0 in terms of the ratio, $v_h(r_0)/v_\infty$. The local halo density can be written as

$$\begin{aligned}\rho_0 &= v_\infty^2/\{4\pi G r_0^2[1 + (a/r_0)^2]\} \\ &= 0.47\,\mathrm{GeV\,cm^{-3}}(v_\infty/220\,\mathrm{km\,s^{-1}})^2/\{(r_0/8.5\,\mathrm{kpc})^2[1 + (a/r_0)^2]\} .\end{aligned} \tag{2.12}$$

Eqs. (2.11) and (2.12) show how the local halo density and core radius can be determined in the isothermal-sphere model in terms of v_∞ and $v_h(r_0)$. Also, it can be shown (see, e.g. Ref. [30]) that the parameter v_0 that appears in Eq. (2.9) is simply the rotation speed at large radii, $v_0 = v_\infty$, and that the velocity dispersion is given by $\bar{v} = \langle v^2\rangle^{1/2} = (3/2)^{1/2}v_0 \approx 270\,\mathrm{km\,s^{-1}}$. Eqs. (2.11) and (2.12) also show how the parameters $v_h(r_0)$ and v_∞ affect the local halo density.

Local dark-matter density – disk contribution: Some (or even most) of the rotation curve of the Milky Way at the solar radius is due to a stellar or dark-matter disk.[4] In canonical models, the disk contributes about half the rotation velocity, but larger disks have been suggested [88], and recent microlensing results may imply an even larger disk mass [66, 80] (or perhaps structure in the bulge [89]). Consider, for example, a thin exponential disk with scale length $H \approx 3.5$ kpc and $\Sigma(r) = \Sigma_0 \exp[-(r - r_0)/H]$, where $\Sigma(r)$ is the *surface* density of the disk. The quantity Σ models both the stellar disk and any possible disk dark matter. Dynamical measurement of Σ_0 remains controversial and may be somewhat model dependent. If the vertical motions of local stellar populations are modeled as being due to a disk and a dark halo, the disk surface density is found to be $46 \pm 9 M_\odot\,\mathrm{pc}^{-2}$ by Kuijken and Gilmore [90] and $53 \pm 12 M_\odot\,\mathrm{pc}^{-2}$ by Flynn and Fuchs [91]. Bahcall et al. [92] report a larger value, $85 \pm 25 M_\odot\,\mathrm{pc}^{-2}$; however, this value includes some of the

[4] Any dark matter in a thin disk probably cannot consist of WIMPs since WIMPs would have been unable to dissipate their kinetic energy.

contribution from a dark halo component. The rotation speed at a radius r due to an exponential disk is [30].

$$v_d^2(r) = 4\pi G\Sigma_0 H y^2 e^{r/H}[I_0(y)K_0(y) - I_1(y)K_1(y)]$$
$$\simeq (137\ \mathrm{km\,s^{-1}})^2\,(\Sigma_0/50M_\odot\,\mathrm{pc}^{-2}), \quad \text{for } r = r_0, \tag{2.13}$$

where $y = r/(2H)$, and the I's and K's are Bessel functions. For a spherical density distribution, the rotation velocity at the solar circle is due solely to the mass inside the solar circle. However, for a disk distribution, the mass density at radii larger than the solar radius can also affect the rotation speed at the solar circle.

Local dark-matter density – discussion: As an example, consider a conservative range of disk column densities $\Sigma_0 = 37$–$65M_\odot\,\mathrm{pc}^{-2}$, implying from Eq. (2.13) a range of disk rotation speeds (at the solar circle) of $118 < v_d(r_0) < 155\ \mathrm{km\,s^{-1}}$. Eq. (2.6) then determines a range in $v_h(r_0)$ once the value of and uncertainty in $v_{tot}(r_0)$ are specified. For example, if we set $v_{tot}(r_0) = 220\ \mathrm{km\,s^{-1}}$, then $150 < v_h(r_0) < 185\ \mathrm{km\,s^{-1}}$, while if one takes a wide range $190 < v_{tot}(r_0) < 240\ \mathrm{km\,s^{-1}}$, one finds a wider allowed range, $110 < v_h(r_0) < 210\ \mathrm{km\,s^{-1}}$.

Since ρ_0 in Eq. (2.10) is a function of both a and $v_h(r)$, we need to specify $v_h(r)$ at a minimum of two positions to solve for ρ_0. In a careful analysis, one would use several points along the Milky Way rotation curve, but for simplicity consider using $r = \infty$ and $r = r_0$. At $r = \infty$ there is no disk contribution, and a usual argument for obtaining v_∞ is that the flatness of the rotation curve (to about 15%, as mentioned above) between the solar-circle radius and twice the solar-circle radius suggests that the asymptotic rotation speed has been reached and that it is $v_\infty = 220\ \mathrm{km\,s^{-1}}$. In fact, the rotation speed beyond about 2.5 times the solar-circle radius is not directly measured; it could conceivably still be rising or begin falling and the disk contribution to the rotation speed at twice the solar-circle radius may be non-negligible (and quite uncertain).

With $v_\infty = 220\ \mathrm{km\,s^{-1}}$, Eq. (2.11) implies a range $0.06 \lesssim a/r_0 \lesssim 0.9$ for the wider range of solar-circle halo rotation speeds given above. Therefore, for v_∞ fixed at $220\ \mathrm{km\,s^{-1}}$, the uncertainty in the disk contribution to the solar-circle rotation speed leads to a range of local halo densities of $\rho_0 = 0.26$–$0.47\ \mathrm{GeV\,cm^{-3}}$. For the central values $\Sigma_0 = 50M_\odot\,\mathrm{pc}^{-2}$ and $v_{tot}(r_0) = v_\infty = 220\ \mathrm{km\,s^{-1}}$, $a/r_0 = 0.6$ and $\rho_0 = 0.35\ \mathrm{GeV\,cm^{-3}}$. If the *disk* contribution to the local disk surface density is larger than the values used above, then the local halo density will be accordingly smaller. Similarly, if $v_{tot}(r_0)$ is decreased, then the local halo density is also decreased.

Eq. (2.12) also shows how ρ_0 depends on v_∞. To first order, $\rho_0 \propto v_\infty^2$, but there is also an additional dependence on v_∞ through a/r_0, as given in Eq. (2.11). It should be noted that, in this analysis, the quantity v_∞ is a parameter; the rotation speed at $r = \infty$ cannot really be measured.

The above example shows how the measured rotation curve interacts with the disk and halo models to produce uncertainty in ρ_0. The more careful analyses quoted earlier thus find a wide or narrow range of acceptable local densities depending upon the range of rotation curves and models the authors considered. By taking values of v_∞, $v_{tot}(r_0)$, r_0, and Σ_0 within the ranges allowed by reasonable estimates of the systematic uncertainties, it is possible to find values of the local halo density as low as $0.06\ \mathrm{GeV\,cm^{-3}}$ [81, 86], or perhaps even smaller. However, the central values of all the studies are considerably higher than this, and it would most likely be difficult to reconcile

such a small local halo density with the observed flaring of atomic-hydrogen layers, or with other observations.

There are some additional uncertainties that arise from the halo model. For example, it is quite possible that the halo of our Galaxy is flattened into an ellipsoid, is triaxial, or has a component of velocity which is rotational and not isotropic. For example, Spergel and Richstone [93] find a factor-of-four uncertainty in the detection rates due to the change in the local halo density and velocity distribution in a triaxial halo. If one takes into account the evidence that halos of spiral galaxies may be flattened by a factor of 1–2.5 [94], then the local halo density may be enhanced by a factor of two [81]. Furthermore, other phenomena, such as the effect of adiabatic growth of the disk on the halo [95] and the effect of spiral arms and molecular clouds on dark-matter particles [96] could potentially alter the local dark-matter density. The good news for dark-matter detection is that these possible distortions of the standard spherical halo generally increase the rate for dark-matter detection.

In this article, we adopt $\rho_0 = 0.3$ GeV cm^{-3} and $\bar{v} = 270$ km s^{-1} (which implies $a = 6.4$ kpc) as our central values of local halo density and velocity dispersion. The standard lore currently says that the uncertainty in the local halo density is roughly a factor of two. But as our discussion of the disk and the measured rotation curve shows, the local density of dark matter and therefore the rate in dark-matter detectors depends sensitively on many aspects of our Galaxy's structure, and the uncertainties may be larger than usually assumed. It should be clear that improved understanding of Galactic dynamics and the mass distribution in the Milky Way is of utmost importance for dark-matter searches.

2.5. *Overview of dark-matter candidates*

There is an enormous wealth of possible dark-matter candidates. In mass, candidates range from axions with $m = 10^{-5}$ eV $= 9 \times 10^{-72} M_\odot$, to black holes of mass $m = 10^4 M_\odot$. The basic fact of being dark does not supply much information. There are, however, several categorization schemes which are helpful in organizing the candidates and deciding how searches should proceed.

The first is the baryonic versus nonbaryonic distinction. The main baryonic candidates are massive compact halo objects (MACHOs) [97–102]. These include, for example, brown dwarfs, jupiters, stellar black-hole remnants, white dwarfs, and neutron stars. Brown dwarfs are balls of H and He with masses below $0.08 M_\odot$, so they never begin nuclear fusion of hydrogen. Jupiters are similar but with masses near $0.001 M_\odot$. Black holes with masses near $100 M_\odot$ could be the remnants of an early generation of stars that were massive enough that not many heavy elements were dispersed when they underwent their supernova explosions. Other possibilities are white dwarfs and neutron stars, although one would expect observable supernova remnants around neutron stars. While there are some theoretical arguments against the dark matter consisting entirely of MACHOs [103], an all-MACHO halo would not violate the big-bang nucleosynthesis constraint. There are now several searches underway which are probing the halo for MACHOs in the mass range $10^{-7} M_\odot \lesssim M \lesssim 10 M_\odot$ [63, 65]. Although the statistics are still too poor to securely eliminate MACHOs as the primary halo component, especially given the uncertainty in the total mass of the halo, recent results suggest a halo MACHO fraction of roughly $\frac{1}{5}$, and seem to rule out an all-MACHO halo of the form of Eq. (2.8) [64, 78–80]. Other, less popular, baryonic possibilities

include fractal or specially conditioned neutral-hydrogen or molecular clouds [104–106], although Blitz has argued that such clouds are inconsistent [70].

The rest of the dark-matter candidates are nonbaryonic. Among the nonbaryonic candidates, an important categorization scheme is the "hot" versus "cold" classification. A dark-matter candidate is called "hot" if it was moving at relativistic speeds at the time galaxies could just start to form (when the horizon first contained about $10^{12} M_\odot$). It is called "cold" if it was moving nonrelativistically at that time. This categorization has important ramifications for structure formation, and studies of galaxy formation may provide clues as to whether the dark matter is hot or cold. Hot dark matter cannot cluster on galaxy scales until it has cooled to nonrelativistic speeds, and so gives rise to a considerably different primordial fluctuation spectrum [107].

The leading hot dark-matter candidate is a light neutrino. If a light ($m_\nu \lesssim 100$ eV) Majorana neutrino exists, its cosmological density would be $\Omega_\nu h^2 \simeq (m_\nu/93\ \text{eV})$. However, N-body simulations of structure formation in a universe dominated by hot dark matter do a poor job of reproducing the observed structure [107]. Although this could be remedied, possibly by topological defects, it still remains difficult to see how light neutrinos could account for the dark matter in dwarf galaxies [8, 108]. There have been some suggestions that perhaps part of the dark matter is hot, say $\Omega_\nu \simeq 0.25$, and that the rest is cold [109]. In these models the bulk of the dark matter (especially in galactic halos) is still cold dark matter, and WIMP detection is changed little.

The nonbaryonic cold-dark-matter candidates are basically elementary particles which have not yet been discovered. The leading nonbaryonic cold-dark-matter candidates are axions and weakly interacting massive particles (WIMPs). The axion [110, 111] is motivated as a possible solution to the strong-CP problem. Astrophysical arguments and laboratory experiments constrain the axion mass to be near 10^{-5} eV. If such an axion exists, then a cosmologically interesting (i.e., $\Omega \sim 1$) density of axions would have been produced at the QCD phase transition. If these axions populate our halo, they can potentially be detected via resonant conversion to photons in a magnetic field. Experiments which will probe a large fraction of the available axion parameter space are currently being mounted [112]. There are yet other pseudo-Nambu–Goldstone bosons, similar to the axion, which have also been proposed as dark-matter candidates [113, 114].

The largest class of cold-dark-matter candidates, the WIMP class, is the main subject of this review. These are stable particles which arise in extentions of the standard model of electroweak interactions. Those discussed most often are heavy fourth-generation Dirac and Majorana neutrinos and the neutralino and sneutrino in supersymmetric models (although Dirac neutrinos and sneutrinos are most likely ruled out by a variety of arguments; see Section 12). WIMP masses are typically in the range from 10 GeV to few TeV, and they have interactions with ordinary matter which are characteristic of the weak interactions. The most promising WIMP candidate is the neutralino, and it is this possibility on which we focus, although much of the discussion will apply to other WIMPs as well.

Finally, there are other possibilities, such as nontopological solitons, primordial black holes, or technibaryons which do not fit easily into the above classification scheme. In our opinion, the theoretical arguments for these other dark-matter candidates are not as compelling as those for WIMPs, although they are certainly within the realm of possibility.

There is yet another possibility which does not get much attention, but which should be kept in mind until the nature of the dark matter is discovered. This is non-Newtonian gravity, in which the strength of the gravitational force decreases less rapidly than r^{-2} at large distance. See Refs.

[115, 116] for provocative discussions of this possibility. However, upcoming results from gravitational lensing may place very strong constraints on this form of non-Newtonian gravity.

3. Cosmological abundance of a WIMP

As early as 1965 [117–119], it was realized that if a new, stable particle (call it χ) existed, it could have a significant cosmological abundance today. The basic idea is simple. Such a particle exists in thermal equilibrium and in abundance in the early Universe, when the temperature of the Universe exceeds the mass m_χ of the particle. The equilibrium abundance is maintained by annihilation of the particle with its antiparticle $\bar{\chi}$ into lighter particles l ($\chi\bar{\chi} \to l\bar{l}$) and vice versa ($l\bar{l} \to \chi\bar{\chi}$). In many cases, the particle is a Majorana particle in which case $\bar{\chi} = \chi$. As the Universe cools to a temperature less than the mass of the particle, the equilibrium abundance drops exponentially until the rate for the annihilation reaction ($\chi\bar{\chi} \to l\bar{l}$) fall below the expansion rate H, at which point the interactions which maintain thermal equilibrium "freeze out," and a relic cosmological abundance freezes in.

This idea was revived in the late 1970s and used to constrain the mass of a heavy neutrino [120–122], and subsequently to suggest that the dark matter could be composed of weakly interacting massive particles (WIMPs) [120, 123–125]. Since then, calculations of the cosmological abundance have become standardized and improved [31, 126–129], and have been applied to numerous candidate relic particles, such as the neutralino, the lighest supersymmetric particle in most supersymmetric theories. The result of the cosmological-abundance calculation for a thermal relic is crucial to the arguments for WIMP dark matter.

In this section, we will first review the standard calculation of the abundance of a WIMP. For pedagogical purposes, an approximate calculation will be performed for the simple case where the WIMP-annihilation cross section is energy independent. We will then pause to review the arguments for WIMP dark matter. The relic-abundance calculation in the more general case where the annihilation cross section is energy dependent will be outlined, and simple and accurate results for the relic abundance will be given. The constraints to the cosmological abundance of a WIMP imposed by the lower limits to the age of the Universe will be reviewed, and we will estimate the abundance required to account for the dark matter in the Galactic halo. There are some cases where the simple results for the relic abundance do not apply, and these will be listed. We close the section by listing possible loopholes and by making some comments on the significance of the relic-abundance calculation.

3.1. Simple estimates

Suppose that in addition to the known particles of the standard model there exists a new, yet undiscovered, stable (or long-lived) weakly interacting massive particle, χ. In thermal equilibrium, the number density of χ particles is

$$n_\chi^{\mathrm{eq}} = \frac{g}{(2\pi)^3} \int f(\boldsymbol{p})\, \mathrm{d}^3\boldsymbol{p}\,, \tag{3.1}$$

where g is the number of internal degrees of freedom of the particle and $f(\boldsymbol{p})$ is the familiar Fermi–Dirac or Bose–Einstein distribution. At high temperatures ($T \gg m_\chi$, where m_χ is the mass of χ), $n_\chi^{\rm eq} \propto T^3$ (that is, there are roughly as many χ particles as photons), while at low temperatures ($T \ll m_\chi$), $n_\chi^{\rm eq} \simeq g(m_\chi T/2\pi)^{3/2} \exp(-m_\chi/T)$, so that their density is Boltzmann suppressed. If the expansion of the Universe were so slow that thermal equilibrium was always maintained, the number of WIMPs today would be exponentially suppressed (essentially, there would be no WIMPs). However, the Universe is not static, so equilibrium thermodynamics is not the entire story.

At high temperatures ($T \gg m_\chi$), χ's are abundant and rapidly converting to lighter particles and vice versa ($\chi\bar{\chi} \leftrightarrow l\bar{l}$, where $l\bar{l}$ are quark–antiquark and lepton–antilepton pairs, and if m_χ is greater than the mass of the gauge and/or Higgs bosons, $l\bar{l}$ could be gauge-and/or Higgs-boson pairs as well). Shortly after T drops below m_χ the number density of χ's drops exponentially, and the rate for annihilation of χ's, $\Gamma = \langle\sigma_{\rm A} v\rangle n_\chi$, where $\langle\sigma_{\rm A} v\rangle$ is the thermally averaged total cross section for annihilation of $\chi\bar{\chi}$ into lighter particles times the relative velocity v, drops below the expansion rate, $\Gamma \lesssim H$. At this point, the χ's cease to annihilate, fall out of equilibrium, and a relic cosmological abundance remains.

This simple picture is described quantitatively by the Boltzmann equation, which describes the time evolution of the number density $n_\chi(t)$ of WIMPs:

$$\frac{{\rm d}n_\chi}{{\rm d}t} + 3Hn_\chi = -\langle\sigma_{\rm A} v\rangle[(n_\chi)^2 - (n_\chi^{\rm eq})^2]\,, \tag{3.2}$$

where $H = \dot{a}/a$ is the Hubble expansion rate, a is the scale factor of the Universe, and the dot denotes derivative with respect to time. This equation is easily understood. The second term on the left-hand side accounts for the expansion of the Universe. In the absence of number-changing interactions, the right-hand side would be zero, and we would find $n_\chi \propto a^{-3}$, as we should. The first term in brackets on the right-hand side of Eq. (3.2) accounts for depletion of WIMPs due to annihilation, and the second term arises from creation of WIMPs from the inverse reaction. It can be derived by noting that, in equilibrium, the rate for depletion and creation of particles is equal. This equation describes both Dirac particles as well as Majorana particles which are self-annihilating (that is, $\chi = \bar{\chi}$), such as neutralinos. For the case of Majorana particles, the annihilation rate is $\langle\sigma_{\rm A} v\rangle n_\chi^2/2$, but in each annihilation, two particles are removed, which cancels the factor of 2 in the annihilation rate. For Dirac particles with no particle–antiparticle asymmetry, $n_{\bar{\chi}} = n_\chi$, so Eq. (3.2) is true; however, the total number of particles plus antiparticles is then $2n_\chi$. In the case of Dirac particles with a particle–antiparticle asymmetry, the relic abundance is generally that given by the asymmetry [128]. For example, the relic proton density is fixed by the proton–antiproton asymmetry, i.e., the baryon number of the Universe.

Although there is no closed-form analytic solution to the Boltzmann equation, there exists a fairly simple analytic approximation that yields a solution that is good to about 10% for an annihilation cross section with a rather arbitrary dependence on energy. The derivation of this solution is straightforward, but somewhat lengthy, and has been described clearly elsewhere [31, 127]. Instead of fully reproducing the derivation, we will first work out an approximate solution for the case that $\langle\sigma_{\rm A} v\rangle$ is energy independent for the purpose of illustration. Afterwards, we will write down the more general solution.

The early Universe is radiation dominated, so the Hubble-expansion rate falls with temperature as $H(T) = 1.66 g_*^{1/2} T^2/m_{Pl}$, where $m_{Pl} \simeq 10^{19}$ GeV is the Planck mass. The quantity g_* is the effective number of relativistic degrees of freedom. It is approximately equal to the number of bosonic relativistic degrees of freedom plus $\frac{7}{8}$ times the number of fermionic relativistic degrees of freedom. This slowly varying function of temperature is plotted as a function of temperature in Fig. 3. At early times ($T \gtrsim m_\chi$), $H \propto T^2$, while $n_\chi \propto T^3$, so the expansion rate decreases less rapidly than the number density of χ's. Therefore, at early times, the expansion term, $3Hn_\chi$, in Eq. (3.2) is negligible compared with the right-hand side, and the number density tracks its equilibrium abundance. At late times, the right-hand side becomes negligible compared with the expansion term, and the comoving abundance of χ's remains unchanged. The temperature T_f at which the χ's freeze out is given by $\Gamma(T_f) = H(T_f)$. Using typical weak-scale numbers, the freezeout temperature turns out to be $T_f \simeq m_\chi/20$; there is a small logarithmic dependence on the mass and annihilation cross section. After freezeout, the abundance of χ's per comoving volume remains constant.

Barring exotic entropy-producing phenomena, the entropy per comoving volume in the Universe remains constant so that n_χ/s remains constant, where $s \simeq 0.4 g_* T^3$ is the entropy density.

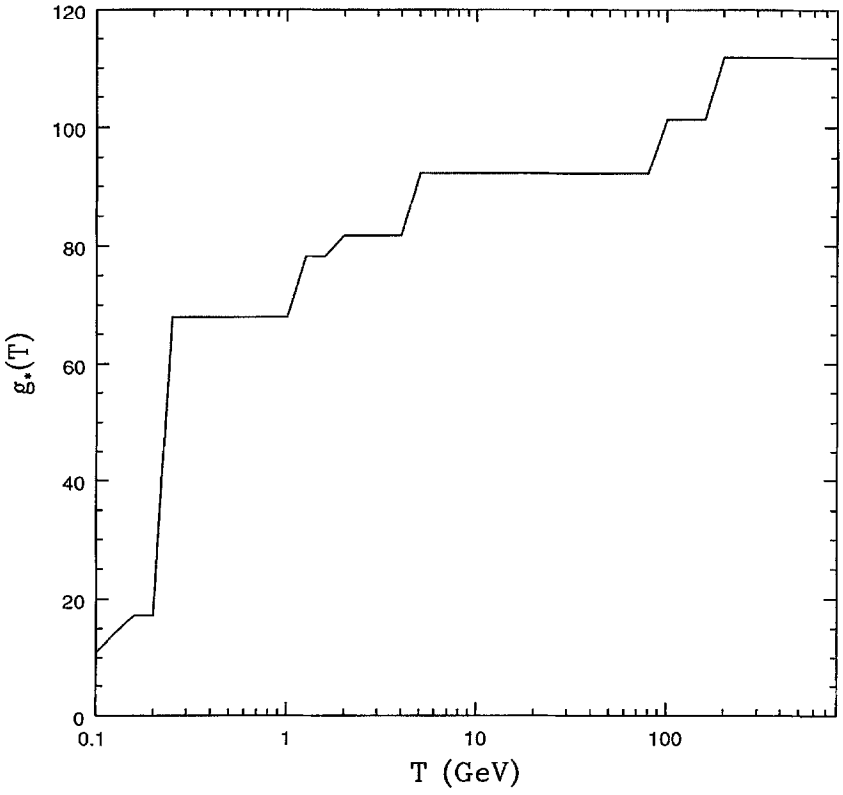

Fig. 3. The number of effective relativistic degrees of freedom, $g_*(T)$ as a function of temperature.

Using the above relations ($H = 1.66 g_*^{1/2} T^2/m_{\rm Pl}$ and the freezeout condition $\Gamma = n_\chi \langle \sigma_A v \rangle = H$), we find

$$(n_\chi/s)_0 = (n_\chi/s)_{\rm f} \simeq 100/(m_\chi m_{\rm Pl} g_*^{1/2} \langle \sigma_A v \rangle)$$
$$\simeq 10^{-8}/[(m_\chi/{\rm GeV})(\langle \sigma_A v \rangle/10^{-27}\,{\rm cm^3\,s^{-1}})], \tag{3.3}$$

where the subscript f denotes the value at freezeout and the subscript 0 denotes the value today. The current entropy density is $s_0 \simeq 4000\,{\rm cm^{-3}}$, and the critical density today is $\rho_{\rm c} \simeq 10^{-5} h^2\,{\rm GeV\,cm^{-3}}$, where h is the Hubble constant in units of $100\,{\rm km\,s^{-1}\,Mpc^{-1}}$, so the present mass density in units of the critical density is given by

$$\Omega_\chi h^2 = m_\chi n_\chi/\rho_{\rm c} \simeq (3 \times 10^{-27}\,{\rm cm^3\,s^{-1}}/\langle \sigma_{\rm A} v \rangle)\,. \tag{3.4}$$

The result is independent of the mass of the WIMP (except for logarithmic corrections), and is inversely proportional to its annihilation cross section.

Fig. 4 shows numerical solutions to the Boltzmann equation. The equilibrium (solid line) and actual (dashed lines) abundances per comoving volume are plotted as a function of $x \equiv m_\chi/T$

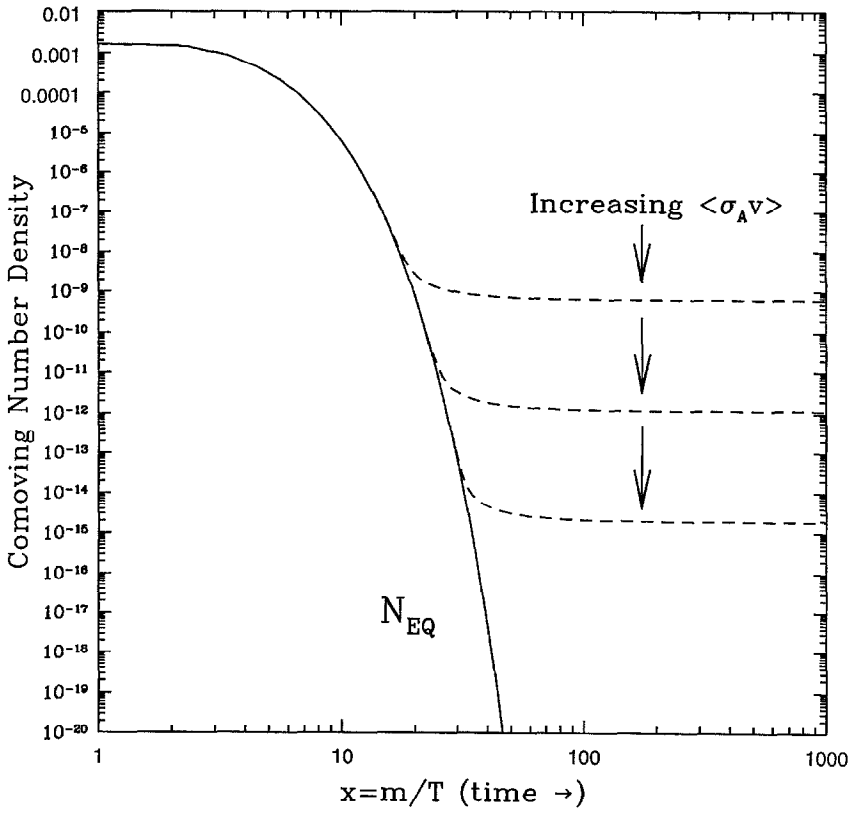

Fig. 4. Comoving number density of a WIMP in the early Universe. The dashed curves are the actual abundance, and the solid curve is the equilibrium abundance. From [31].

(which increases with increasing time). As the annihilation cross section is *increased* the WIMPs stay in equilibrium longer, and we are left with a *smaller* relic abundance.

3.2. Why WIMPs?

Now is a good time to pause and review the arguments for WIMP dark matter. We just showed that if such a stable particle exists, its relic abundance is $\Omega_\chi h^2 \simeq 3 \times 10^{-27}\,\mathrm{cm^3\,s^{-1}}\,\langle\sigma_A v\rangle^{-1}$. If a new particle with weak-scale interactions exists, then its annihilation cross section can be estimated to be $\langle\sigma_A v\rangle \sim \alpha^2(100\,\mathrm{GeV})^{-2} \sim 10^{-25}\,\mathrm{cm^3\,s^{-1}}$, for $\alpha \sim 10^{-2}$. This is remarkably close to the value required to account for the dark matter in the Universe, especially if we realize that there is no a priori reason for a weak-scale interaction to have anything to do with closure density, a cosmological parameter! This striking coincidence suggests that if there is a stable particle associated with new physics at the electroweak scale, it *is* the dark matter. This idea has been followed by extensive theoretical work, and has led to an enormous experimental effort to detect these WIMPS.

The identity of the WIMP remains a mystery. The earliest idea was that the WIMP was a heavy fourth-generation Dirac or Majorana neutrino. Since then, numerous other candidates have been put forth; however, of all the candidates, perhaps the most well-motivated and certainly the most theoretically well-developed WIMP candidate is the lightest supersymmetric particle (LSP). Low-energy supersymmetry is an idea for new weak-scale physics beyond the standard model which embodies an entire class of theories [20], so that even within the context of supersymmetry, the exact identity of the WIMP is uncertain. In most theories, the LSP is the neutralino, a linear combination of the supersymmetric partners of the photon, Z^0, and Higgs bosons. In some models, the neutralino may be a photino or higgsino, but in the general case it is some arbitrary linear combination. Extensive calculations which will be reviewed below have surveyed broad classes of supersymmetric models and backed up the rather simple conclusions about WIMPs above: That is, in broad regions of parameter space in minimal supersymmetric extensions of the standard model, the cosmological abundance of the LSP is close to unity and suitable for solving the dark matter problem, independent of the specific composition of the LSP [125, 130–135].

Since it is perhaps the best-motivated and certainly the most studied WIMP, we focus on the neutralino in this Report. But it should be kept in mind that the cosmological abundance and detectability of other candidate WIMPs will in general be similar.

3.3. Standard calculation of relic abundance

Most generally, the annihilation cross section is *not* energy independent. As pointed out above, the χ freezes out at a temperature, $T_f \simeq m_\chi/20 \ll m_\chi$, so the particles are moving at nonrelativistic velocities ($v \ll 1$) when they freeze out. This suggests that the total annihilation cross section be written as

$$\sigma_A v = a + bv^2 + \cdots , \tag{3.5}$$

where v is the relative velocity (so in the center-of-mass frame, each χ moves with a velocity $v/2$). It can be shown that the first term (a) comes from s-wave annihilation, the second term (bv^2) comes from both s- and p-wave annihilation, etc. In the simplest case, the s wave is unsuppressed, $\langle\sigma_A v\rangle$ is

largely energy independent, and only the a term is needed. However, in many cases, χ is a Majorana particle, and s-wave annihilation into light fermions is helicity suppressed [136]. Then the b term must be included as well. In virtually every case considered, the first two terms are sufficient in Eq. (3.5). If so, then an approximate analytic solution to the Boltzmann equation is easily obtained. The equation is solved both in the early-time and late-time limits, and the two solutions are matched near the time at which the WIMP freezes out. The solution is reviewed clearly and in a pedagogic fashion in Refs. [31, 126, 127], so we do not review it here.

The result for the relic abundance is

$$\Omega_\chi h^2 = Y_\infty s_0 m_\chi/(\rho_{\rm crit}/h^2) \approx 2.82 \times 10^8\, Y_\infty (m_\chi/{\rm GeV}) , \tag{3.6}$$

where

$$Y_\infty^{-1} = 0.264 g_*^{1/2}\, m_{\rm Pl} m_\chi \{a/x_{\rm f} + 3(b - \tfrac{1}{4}a)/x_{\rm f}^2\} . \tag{3.7}$$

The freezeout epoch $x_{\rm f} = m_\chi/T_{\rm f}$ is determined by

$$x_{\rm f} = \ln[0.0764 m_{\rm Pl}(a + 6b/x_{\rm f}) c(2 + c) m_\chi/(g_* x_{\rm f})^{1/2}] , \tag{3.8}$$

which can be solved iteratively to the required precision. Here $m_{\rm Pl} = 1.22 \times 10^{19}$ GeV is the Planck mass, g_* is evaluated at $T_{\rm f}$, and c is a constant of order unity which determines precisely when the late-time and early-time solutions are matched. In practice, c is chosen for optimum agreement with numerical solutions to the Boltzmann equation; the value $c = \frac{1}{2}$ results in a typical accuracy of about 5–10% – more than sufficient for our purposes here.

The contribution proportional to a in the second term in Eq. (3.7) results from a relativistic thermal-averaging procedure [129],[5] and was not included in much of the previous literature; it is roughly a 5% effect.

Note that the cosmological abundance is roughly inversely proportional to the thermally averaged annihilation cross section: If $a \gg b$, then $\langle \sigma_{\rm A} v \rangle = a$; if $a \ll b$ then $\langle \sigma_{\rm A} v \rangle \simeq 6b/x_{\rm f}$ at freezeout. Note also that the dependence on the WIMP mass is only logarithmic.

To summarize, given a particle-physics theory with a stable WIMP, the prescription for determining the abundance of the WIMP is as follows: Calculate the cross section for annihilation of the WIMP into all lighter particles, expand in velocity as in Eq. (3.5), and then obtain the relic abundance from Eq. (3.6).

If desired, a more careful calculation can be performed [129]. For example, the Boltzmann equation can be solved numerically. Given the uncertainty in the Hubble constant and the broad range of models to be surveyed, the simpler formulas listed above should be sufficient for most purposes.

3.4. *Special cases*

In certain easily identifiable cases (for example, if the WIMP mass very nearly matches the mass of some other particle or if annihilation occurs through a resonant channel), naive application of the standard analytic solution to the Boltzmann equation, Eqs. (3.6) and (3.7), yields results for the

[5] We thank Mark Srednicki for discussions of this term.

relic abundance which may be erroneous by factors of two or more. In general, these models must be dealt with on a case-by-case basis, but calculation of the relic abundance is still straightforward.

Techniques have been developed for dealing with some of the most common of such situations which may arise [137–139], and we will review these here briefly. Solutions to the Boltzmann equations in these cases may become quite complicated and may be model dependent, and these special cases occur for only a small fraction of the WIMP candidates. Therefore, here we will simply point out when the standard calculation breaks down, and indicate in which direction it errs.

The first case occurs when annihilation takes place near an s-channel pole in the cross section [137,138]. If two WIMPs annihilate via s-channel exchange of a virtual particle, for example, a Z or Higgs boson and the mass of the exchanged particle closely matches twice the WIMP mass, then the annihilation cross section can be approximated by [137]

$$\sigma v \simeq \alpha^2 s/[(m_{\rm ex}^2 - s)^2 + m_{\rm ex}^2 \Gamma_{\rm ex}^2] \,, \tag{3.9}$$

where $m_{\rm ex}$ and $\Gamma_{\rm ex}$ are the mass and width of the exchanged particle, respectively, s is the square of the center-of-mass energy, and $\alpha \sim 0.01$ is the square of some coupling constant. In this case, the nonrelativistic expansion, Eq. (3.5), does not apply. Naive application of the standard analytic result underestimates the true result, and when plotted against WIMP mass, the standard analytic approximation will show a sharp dip near the pole at $m_\chi \simeq \frac{1}{2} m_{\rm ex}$. More careful analysis shows that the naive analytic calculation will underestimate the correct result by roughly a factor of 3 for annihilation on the Z pole, and by larger factors for more narrow resonances, and that the dip in relic abundance for WIMP masses near the pole is not as dramatic as suggested by the standard result. This is because the annihilation rate at any given time depends on an average of a thermal distribution of energies. Contributions from the tails of the distribution smear the effect of the pole.

The second case involves annihilation near mass thresholds [137,138]. In the treatment in the previous subsection, it was assumed that if the WIMP mass is just below threshold for annihilation into a given channel, then annihilation into that channel is kinematically forbidden. If the WIMP mass is just above threshold, then annihilation to that channel can proceed. According to the standard result, the abundance of WIMPs with masses above threshold may be dramatically smaller than that for WIMPs below threshold, and the drop in abundance is sudden. Actually, this is not the case. Even if the WIMP mass is below threshold, there will be WIMPs in the high-energy tail of the thermal distribution with energies above threshold which can annihilate. If the WIMP mass is within $\sim 15\%$ of threshold, it is possible that the "forbidden" channel can dominate the cross section and determine the relic abundance. In fact, the relic abundance varies smoothly with mass, and there is no sharp drop near threshold.

The third case, dubbed "coannihilation" by Griest and Seckel, occurs when another particle is only slightly heavier than the WIMP and shares a quantum number with it [137]. In this case, conversion of the WIMP to the heavier particle may occur via scattering from standard-model particles. If the cross section for annihilation of the heavier particle is larger than that for annihilation of the WIMP, then the abundance of both species will be controlled by annihilation of the heavier and more strongly interacting particle, and the relic abundance can be reduced. Another possibility is that a WIMP could annihilate readily with the heavier particle, in which case this reaction could determine the relic abundance. For example, in SUSY models, if the WIMP is a neutralino and there is a squark with a mass that only slightly exceeds the neutralino mass, then coannihilation will occur. The relic abundance will be controlled by annihilation of squarks, and it

will be smaller than suggested by the results of the previous subsection. Also, if the neutralino is very nearly a pure higgsino, there will often be another higgsino and a chargino with masses very near the higgsino mass, and coannihilation occurs [140]. Generally, if there are additional particles with masses within 10% of the WIMP mass, then coannihilation will occur, and the proper calculation must be performed using the techniques developed in Ref. [137].

3.5. *Possible loopholes*

There are several effects which could alter the relic abundance from the results of the canonical calculation. Generally, these loopholes involve additional speculative assumptions, and none should be regarded as likely; however, they are within the realm of possibility and can be easily summarized.

The relic-abundance calculation involves determination of the abundance at the epoch at which the particle freezes out. Following this epoch, the number per comoving volume remains constant. In the standard cosmology, the entropy per comoving volume remains constant, in which case the ratio of the WIMP number density to the entropy density remains constant, and the WIMP abundance today then depends on the current entropy density, which we know. However, if the entropy density is increased (it can never decrease) for some reason, the entropy density no longer provides a reliable measure of the comoving volume. Then, the WIMP relic abundance is diluted accordingly, relative to the results of the canonical calculation, even though the number per comoving volume remains constant.

There are several mechanisms that could produce entropy after freezeout. For example, if some other massive particle which is decoupled from the plasma decays after freezeout, it will produce entropy [31].

Another possibility is entropy production at a first-order phase transition. For WIMPs, this could be the QCD phase transition, which takes place at temperatures [O(100 MeV)] well below the freezeout temperature, or if the WIMP is heavy enough, possibly the electroweak phase transition which could plausibly occur at temperatures O(100 GeV), below freezeout for very heavy WIMPs ($m_\chi \sim 1000$ GeV). If the QCD phase transition is strongly first order, then a significant amount of entropy could be produced, and the relic abundance could be reduced substantially. However, lattice simulations seem to indicate that the transition is second order, or maybe very weakly first order [59]. Therefore, it is unlikely that the QCD transition will affect the results of the relic-abundance calculation. Far less is known about the electroweak transition. In the minimal standard model with a Higgs boson heavy enough to have evaded detection, the transition should be only weakly first order [141], or perhaps second order; however, in the minimal supersymmetric model, for example, the Higgs sector will be different, and a strongly first-order phase transition is plausible [142, 143]. Although we do not really know the transition temperature, it would require that the WIMP be quite heavy and the transition temperature quite low for the transition to occur after freezeout (recall $T_f \simeq \frac{1}{20} m_\chi$). Therefore, it is unlikely that entropy production at the electroweak phase transition will dilute the WIMP abundance, although it remains as a possibility for very heavy WIMPs.

An inflationary epoch that occurs after freezeout could also produce a significant amount of entropy. Although there has been some discussion of inflation at the electroweak scale [144], inflation is commonly believed to occur at much higher temperatures associated with the

Peccei–Quinn, GUT, or Planck scales. We consider inflation at temperatures below the freezeout temperature to be unlikely.

Entropy production always reduces the relic abundance; however, there are also mechanisms which would increase the WIMP abundance. Freezeout occurs roughly when the expansion rate is equal to the annihilation rate. If, for some reason, the expansion rate was larger at the epoch of freezeout, then freezeout would occur earlier and thereby leave a larger relic abundance of WIMPs. This could occur in an anisotropic Universe where the shear contributes an effective energy density which increases the expansion rate at freezeout [145, 146]. Other possibilities are that the expansion rate at freezeout could be enhanced by the rolling of a scalar field, or by a variable Newton's constant [146]. All of these mechanisms are quite exotic (and unlikely), yet they illustrate that the abundance of a thermal relic could plausibly be larger than predicted by the standard calculation.

Yet another possibility is that the cosmological WIMP abundance is enhanced by some nonthermal production mechanism in the early Universe. It has been suggested that WIMPs could be produced by decay of heavier particles. For example, it has been pointed out in supergravity models that neutralinos might be produced by decays of gravitinos [147], and in models with SUSY and Peccei–Quinn symmetry that neutralinos could be produced by decays of axinos, the SUSY partners of axions. If so, then the neutralino abundance could be greater than its thermal-relic abundance [148].

3.6. Constraints on the WIMP density

Lower limits to the age of the Universe are often used to provide constraints to $\Omega_\chi h^2$. It is often misstated that if $\Omega_\chi > 1$, then WIMPs will "overclose" the Universe. This is not quite the correct argument; adding matter to the Universe will not change its geometry. However, adding matter to the Universe will cause the Universe to expand more rapidly and reach its present size in a shorter period of time. Thus, lower limits to the age of the Universe provide upper bounds to Ωh^2, and therefore, to $\Omega_\chi h^2$ (see Fig. 2 and, e.g., Ref. [31]).

A fairly conservative lower bound to the age t_U of the Universe, provided by cooling of white dwarfs [149], is about 10 Gyr. This results in a conservative upper bound of $\Omega h^2 \lesssim 1$ for $h \gtrsim 0.4$; if for some reason, h is even smaller (as has recently been suggested [150]) the bound is relaxed only slightly. Globular-cluster ages suggest an older Universe, $t_U \gtrsim 13$ Gyr, in which case $\Omega h^2 \lesssim 0.4$ (see Fig. 2(a)). The limits to Ωh^2 for a given t_U are obtained assuming the Universe is matter dominated. It is unlikely that the Universe is radiation dominated today, but if for some reason it is, then the constraints of Ωh^2 become stronger. In addition, the limit to Ωh^2 (where Ω does *not* include the contribution of the cosmological constant) cannot be relaxed by introducing a cosmological constant (see Fig. 2(b)).

Obviously, the mass density in WIMPs must be less than the total mass density; therefore, requiring $t_U \gtrsim 10$ Gyr leads to the constraint

$$\Omega_\chi h^2 \lesssim 1 \,, \tag{3.10}$$

on the WIMP cosmological abundance. If $t_U \gtrsim 13$ Gyr, then the constraint is stronger: $\Omega_\chi h^2 \lesssim 0.4$.

It should be noted that the upper bounds on Ωh^2 apply regardless of geometry. In fact there is little observational evidence that the Universe is closed. Most astronomical observations suggest that $\Omega \lesssim 1$, and some are perhaps consistent with a flat Universe, but few observers would say that

the evidence points to a closed Universe. Moreover, a number of theoretical arguments suggest the Universe is flat. If the Universe is open or flat, $\Omega \leq 1$, then the age-of-the-Universe constraint is stronger: For $t_U \gtrsim 10$ Gyr, the constraint is $\Omega_\chi h^2 \lesssim 0.5$, and for $t_U \gtrsim 13$ Gyr, the constraint is $\Omega_\chi h^2 \lesssim 0.25$.

Limits to the WIMP mass: According to dimensional arguments, the annihilation cross section is generally expected to decrease as the WIMP mass is increased, so the relic abundance should increase. Therefore, heavier WIMPs should be more likely to dominate the mass of the Universe and be cosmologically inconsistent. In fact, partial-wave unitarity provides a firm upper limit $\propto m_\chi^{-2}$ to the coefficients a and b in the nonrelativistic expansion of the annihilation cross section, Eq. (3.5). This can be used to place a model-independent lower bound [151],

$$\Omega_\chi h^2 \gtrsim (m_\chi/300\ \text{TeV})^2, \tag{3.11}$$

to the cosmological density of any stable thermal relic. Unitarity and the age-of-the-Universe constraint, $\Omega_\chi h^2 \lesssim 1$, then lead to the conclusion that the mass of a stable thermal relic must be $m_\chi \lesssim 300$ TeV [151]. This conclusion will *not* be altered substantially if the relic density is determined by annihilation near a pole or threshold or by coannihilation. Although the unitarity limit is a model-independent upper bound, the limit to the WIMP mass is roughly two orders of magnitude larger than the WIMP masses usually considered (e.g., in SUSY). However, the upper limit on the mass applies heuristically to a particle whose coupling is of order unity. In models (such as SUSY models) usually considered, the cross sections are proportional to a coupling $\alpha^2 \sim 10^{-4}$, so the largest cosmologically acceptable WIMP masses should be roughly a factor $\alpha \sim 10^{-2}$ smaller than the most conservative unitarity bound – about 3 TeV. This conclusion is supported, for example, by careful surveys of SUSY parameter space [134].

If the theorists' vision of a flat Universe is indeed justified, then a WIMP with an abundance $\Omega_\chi \simeq 1$ ($\Omega_\chi h^2 \simeq 0.25$ for acceptable values of h for $\Omega = 1$), is the most attractive theoretically. On the other hand, it is conceivable that the WIMPs could be the dark matter we are searching for in the Galactic halo, even if they do not contribute closure density. In order of magnitude, the luminous matter in galaxies contributes roughly $\Omega_{\text{lum}} \simeq 0.01$, and the dark matter outweighs the bright component by at least a factor of ten, so $\Omega_{\text{halo}} \gtrsim 0.1$. Therefore, $0.025 \lesssim \Omega_\chi h^2 \lesssim 1$ is a more conservative range for the relic density of a WIMP which could account for the dark matter in the Galactic halo. Although cosmologically consistent, WIMPs with smaller densities are not quite as astrophysically interesting, as they would not be suitable for solving the dark-matter problem, and heavier WIMP's would violate the lower bound on the age of the Universe.

4. Supersymmetric models

4.1. Motivation, goals, and some formalities

The fundamental motivation for introducing supersymmetry remains the argument that theories describing physics over an energy range of many decades must incorporate supersymmetry in order to remain technically natural. It is worth reiterating the details of this technical naturalness, which we will do shortly. Further motivation derives from the observation that a combination of

supersymmetry transformations gives a spacetime transformation, so that theories of *local* supersymmetry necessarily contain local spacetime transformations, and thus they contain gravity. It remains an open problem to construct a viable theory of elementary-particle physics which contains gravity, but much can be said in the context of supersymmetric theories. We will discuss this briefly as well. For more than the telegraphic details provided here, we refer the reader to some of the many excellent reviews on the subject of supersymmetry (see, e.g., [20, 152, 153]).

First consider what is meant by technical naturalness. Suppose that we wish to write down a Lagrangian for interactions of elementary particles, which we hope will describe all interactions up to some high-energy scale, such as the Planck scale, $E_{\text{Planck}} \simeq 10^{19}$ GeV, or a grand unification scale, $E_{\text{GUT}} \simeq 10^{16}$ GeV. If such a Lagrangian described all physical interactions at any scale, then our work would be done! However, no such arguably correct theory has ever been written down. In fact, it may be impossible to admit the very idea of elementary-particle physics above the Planck scale, where the structure of spacetime itself becomes something unknown. So the Lagrangian that we write for the physics of elementary particles at or below our specified high-energy scale is an effective Lagrangian, not appropriate for calculating processes at energies above the scale where it is defined. It depends on whatever fields exist in the theory, Ψ_i, and on some coupling parameters g_i,

$$\mathscr{L}_{\text{eff}} = \mathscr{L}_{\text{eff}}(\Psi_i, g_i). \tag{4.1}$$

Suppose that this theory contains scalar fields, the vacuum expectation values (VEVs) of which will spontaneously break certain gauge symmetries, such as the electroweak symmetry. If we choose to break the electroweak symmetry by the Higgs mechanism, then there must exist in $\mathscr{L}_{\text{eff}}$ a scalar excitation which is the Higgs field of the Glashow–Weinberg–Salam theory. For such a generic Lagrangian, specified at a scale Λ, much larger than the electroweak scale, E_{weak}, we find by explicit calculation that the masses of scalar excitations are of order Λ (unless there is fine tuning). The scalar excitations acquire such large masses because of radiative corrections. Due to diagrams with a scalar loop such as that shown in Fig. 5, their self-energies will renormalize m^2_{scalar} by typically quadratic terms of order Λ^2; that is, $\delta m^2_{\text{scalar}} \sim g^2\Lambda^2$. Therefore, for example, there will be radiative corrections to the standard-model Higgs mass of order Λ_{GUT} that will destroy the hierarchy between the electroweak and GUT scales. Either these particles must decouple at high energies, in which case they could not break the electroweak symmetry at the weak scale, or there must be some strongly nonperturbative effect which invalidates the method of calculation. The

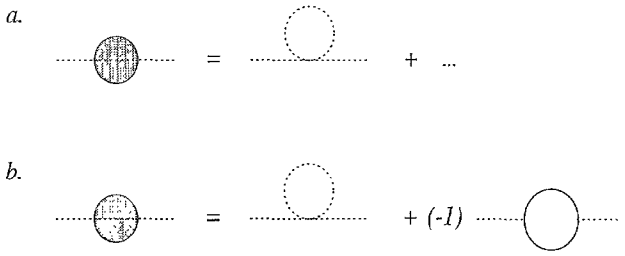

Fig. 5. Radiative corrections to the mass of a scalar particle. The dotted curves are scalar propagators, and the solid curves are fermion propagators: (a) Diagrams with no supersymmetry; (b) diagrams with supersymmetry.

latter alternative provides no comfort, and it is anyway difficult to see how such effects could appear if the couplings in $\mathscr{L}_{\text{eff}}$ are chosen to be sufficiently weak. Therefore, the only way to avoid this difficulty is to fine-tune the couplings g_i to one part in $\Lambda^2/E_{\text{weak}}^2 \gtrsim 10^{28}$. This is the fine-tuning or naturalness problem.

One could argue that there is no satisfying solution to this difficulty, in the sense that a more fundamental "theory of everything" may just produce the required finely tuned couplings. But what is the mechanism by which this fundamental theory of everything arranges to provide the Universe with something so useful to humanity as electroweak gauge-symmetry breaking at a scale $E_{\text{weak}} \simeq 200$ GeV? The physics of the theory of everything is not at all understood, but it would seem a priori to be a miraculous coincidence that such a scale should emerge from a theory which contains gravitational interactions, and perhaps other greatly complicated physics, occurring at energy scales greater than or equal to the Planck scale.

It seems that the only operable solutions to this problem are to excise the scalar excitations from the theory or to somehow eliminate the quadratic radiative corrections which are forcing the fine-tuning upon us. The first solution opens the door to the realm of dynamical electroweak-symmetry breaking and technicolor theories [154], which are not the topic here. Constructing realistic technicolor models has proven to be very difficult, and no completely realistic model has ever been constructed, though it is certainly possible that such a model exists. The second operable solution is provided by low-energy supersymmetry, and we now briefly discuss how this occurs.

Supersymmetry implies that the particles of a theory must appear in multiplets, related by supersymmetry transformations. The supersymmetry transformations turn bosons into fermions and vice versa, so that the members of supermultiplets have different spins. Supersymmetry thus provides an example of a symmetry which is entwined with the Poincare algebra in a nontrivial way; the commutator of two supersymmetry transformations, δ, gives the momentum operator

$$[\delta(\varepsilon_1), \delta(\varepsilon_2)] = \tfrac{1}{2}(\bar{\varepsilon}_2 \gamma^\mu \varepsilon_1)\partial_\mu, \tag{4.2}$$

where $\varepsilon_1, \varepsilon_2$ are the infinitesimal generators of the two transformations, which are fermionic fields. This equation is often verbalized as "supersymmetry is the square root of Poincare symmetry". In fact, supersymmetry is the only such entwined internal symmetry consistent with necessary symmetries of the S-matrix [155–157]. Fermionic intermediate states, fermion loops in diagrammatic perturbation theory such as those shown in the second equation in Fig. 5, carry a famous factor of -1. Thus, for every boson loop, there is a fermion loop in supersymmetric theories which cancels it. In this way, the momentum integrals of perturbation theory are softened. In fact, they are softened to the level that the quadratic dependence on a large ratio of energy scales is reduced to at most a logarithmic dependence, $\log(\Lambda/E_{\text{weak}})$. In some cases the dependence on this ratio is removed entirely, in which case the theories are formally finite in the ultraviolet and could in principle be extended to arbitrarily high energy without any fine-tuning problem.

Of course, we know that the known particles do not occur in supermultiplets; the required superpartners have never been observed. Thus supersymmetry cannot be an exact symmetry of the vacuum. It must be broken such that physics below the breaking scale, E_{SSB}, is phenomenologically acceptable. But the required cancelation of quadratic radiative corrections will only operate for intermediate states with momenta above E_{SSB}. Therefore, the quadratic corrections to the Higgs-boson mass should be $\delta m_{\text{H}}^2 \sim g^2(m_{\text{B}}^2 - m_{\text{F}}^2)$ where m_{B} and m_{F} are the masses of boson and fermion members of a supermultiplet. Therefore, if δm_{H}^2 is to be less than or of the order of the electroweak

gauge-boson masses, then the mass splittings in supermultiplets should be not too much greater than the electroweak scale. Thus, if supersymmetry is to be relevant to electroweak-symmetry breaking, the signs of supersymmetry must become visible near the electroweak scale, $E \lesssim \mathcal{O}(\text{TeV})$. If a supersymmetric particle spectrum does not become manifest by the time accelerator experiments reach such a scale, then the solution to the fine-tuning problem must be sought elsewhere. Thus supersymmetry is an interesting gamble. If it proves to be a winning bet, the rewards will be staggering. If it proves to be irrelevant to electroweak physics, then the absence of a viable treatment for the fine-tunning problem will be felt.

The second motivation which we mentioned arises from the connection between local supersymmetry and gravity. Supersymmetry is local if the transformations are allowed to depend on position and time (in other words, the symmetry is gauged); this means that the commutator of local supersymmetry transformations gives a local Poincare symmetry, as dictated by Eq. (4.2). But local Poincare symmetry is the basis of general relativity, so that "local supersymmetry is the square root of general relativity" [158]. Local supersymmetry is thus called supergravity (SUGRA). Combined with the idea of ultraviolet finiteness, as mentioned above, local supersymmetry held some initial promise as a true theory of everything, including gravity, extendible to arbitrarily high energies. This initial promise will probably remain unfulfilled, as it seems very likely that finiteness does not hold to arbitrary order in the diagrammatic expansion. Supergravity with added matter multiplets diverges at one loop [159], and it seems likely that pure supergravity diverges at three loops [160]. Therefore, supergravity has been adopted in a secondary manner, itself being considered as an effective theory which must give way to some more correct description at higher energies. The more fundamental theory that encompasses supergravity may be superstring theory, the status of which remains tentative. So the construction of a fundamental theory encompassing all the known interactions, including gravity, remains very much an open problem. However, current thinking makes it hard to understand an effective theory of softly broken global supersymmetry (such as the MSSM) out of the context of some fundamental locally supersymmetric scheme because of issues of the supersymmetry-breaking mechanism. Spontaneous breaking of local supersymmetry remains one of the most compelling models for the manifestation of supersymmetry in the Universe, and supergravity turns out to be the proper framework for spontaneous breaking of supersymmetry [161–166]. This provides an important motivation for the study of supergravity. We will discuss supergravity models in a bit more detail below.

From the above viewpoint, the existence of attractive dark-matter candidates in models possessing low-energy supersymmetry can be regarded as an independent and pleasant surprise. To our minds, this pleasant surprise provides an excellent motivation for studying these models. Supersymmetric dark matter remains one of the most interesting and viable candidates for cold particle dark matter. Finally, there are some arguments from coupling-constant unification which suggest the existence of low-energy supersymmetry [4].

Our immediate goal is to write down a well-motivated, viable, and adequately general supersymmetric model with which we can begin to calculate those things that interest us, such as cosmological relic abundances, detection rates, and event rates for accelerator experiments. We also need to explain the parameterization of the theory which we have chosen. To reach these goals, it is necessary that we take a small detour through the formalism of supersymmetric field theory; we introduce only as much formalism as is necessary to write the Lagrangian, and in writing the Lagrangian we establish the conventions for all the parameters of the theory. The necessity of this

step is obvious to anyone who has attempted to compare results from different calculations in the literature. Rather than present all the details in a linear fashion, we give a reduced account here and give the full exposition in Appendix A. This Appendix will be necessary for those readers interested in performing explicit calculations.

4.2. Minimal supersymmetric standard model

The object of immediate study in this review is the minimal supersymmetric standard model (MSSM). This theory contains all the known fields of the standard model and an extra Higgs doublet (for reasons discussed below), together with the partners required to form supersymmetric multiplets; no other fields are introduced in the MSSM. The interactions of the theory are all those which are allowed by the gauge symmetry $SU(3) \times SU(2) \times U(1)$ and by renormalizability. These specifications uniquely determine the MSSM, up to the prescription for transformations under the so-called R parity, although the various field assignments are not completely trivial. Writing the Lagrangian of the MSSM in its most manageable form requires the introduction of the machinery of superfields, and this will be left for Appendix A. The complexity of detail in the MSSM comes, not at the manifestly supersymmetric level, but at the level where the physics of supersymmetry breaking is specified. Following Girardello and Grisaru [167], as discussed in Appendix A, we construct the most general soft-breaking Lagrangian for the MSSM, which contains a large number of dimensionful parameters. The explicit form is given by Eq. (A.12).

Given an interest in supersymmetric dark matter, the most important ingredient is the realization of R parity. In terms of its action on the component fields of the theory, this discrete symmetry is $R = (-1)^{3(B-L)+2S}$, where B, L are the baryon and lepton number operators and S is the spin. This means that $R = 1$ for ordinary particles and $R = -1$ for their superpartners. If R parity is broken, then there are no special selection rules to prevent the decay of those supersymmetric particles in the spectrum with masses of order a few GeV or larger. In particular, the theory would possess no natural candidate for cold-dark-matter particles. However, this is only one of the many ills of a theory with broken R parity. Such theories also possess baryon- and lepton-number violating interactions with strengths controlled by the scale of R-parity violation. Therefore, very severe constraints on R-parity violation arise. In this review we will consider only models with strict R parity, so that the lightest R-odd particle will be absolutely stable. This is the so-called lightest supersymmetric particle (LSP). For discussions of the phenomenology of R-parity violation, see Refs. [168], and for related developments see Refs. [169].

Several points about the field assignments should be mentioned immediately, regarding neutrinos and the Higgs sector. First, one might ask whether or not a neutrino superfield is required, since one could imagine a neutrino arising as a Goldstone fermion for spontaneous supersymmetry breaking, which would also explain its masslessness. This particular speculation is ruled out by the phenomenology of neutrino interactions at low energy [170]. Second, it can be shown that two Higgs doublet fields are required in the MSSM, where only one is required in the standard model (see Appendix A). This enrichment of the Higgs sector provides some complication, but also provides an important phenomenological window. In many cases, the Higgs sector provides strong clues about the underlying supersymmetric theory, and constraints on the Higgs sector are an important area of supersymmetric phenomenology.

Table 1
Particle spectrum of the minimal supersymmetric standard model

Normal particles		SUSY partners	
Symbol	Name	Symbol	Name
$q = u, c, t$	up quarks	$\tilde{q}_u^1, \ldots, \tilde{q}_u^6$	up squarks
$q = d, s, b$	down quarks	$\tilde{q}_d^1, \ldots, \tilde{q}_d^6$	down squarks
$l = e, \mu, \tau$	leptons	$\tilde{l}_1, \ldots, \tilde{l}_6$	sleptons
ν	neutrinos	$\tilde{\nu}_1, \ldots, \tilde{\nu}_3$	sneutrinos
g	gluons	$\tilde{g}$	gluinos
$W^{\pm}$	W boson	$\tilde{\chi}_1^{\pm}, \tilde{\chi}_2^{\pm}$	charginos
$H^{\pm}$	charged Higgs		
γ	photon		
Z^0	Z boson		
h^0 (H_2^0)	light scalar Higgs	$\tilde{\chi}_1^0, \ldots, \tilde{\chi}_4^0$	neutralinos
H^0 (H_1^0)	heavy scalar Higgs		
A^0 (H_3^0, P_0)	pseudoscalar Higgs		

In supersymmetry, there is a fermionic degree of freedom for every bosonic degree of freedom and vice versa, so the particle spectrum is greatly extended in the MSSM. These are listed in Table 1. For each "normal" degree of freedom, there is a supersymmetric degree of freedom. Quarks have spin $\frac{1}{2}$, while squarks are scalars. Therefore, there are two squarks (left and right) for each quark. In general, the up quarks mix amongst themselves, and similarly for the down quarks, so there are six up squarks and six down squarks in the particle spectrum. In most of the models discussed in the literature, there is no mixing between different flavors, and each squark is associated with a given quark. Similarly for the leptons. In these models, left–right sfermion mixing is proportional to the corresponding fermion mass; thus, there is little left–right mixing for u, d, and s squarks or selectrons or smuons, but mixing of staus and c, b, and especially t squarks can be substantial.

The superpartners of the W and charged Higgs bosons, the charged higgsino and gaugino, carry the same $SU(3) \times U(1)$ quantum numbers. Thus, they will in general mix after electroweak-symmetry breaking, and the two resulting mass eigenstates are linear combinations known as charginos. The same is true of the superpartners of the photon, Z^0, and neutral Higgs bosons. These fields generally mix to create four mass eigenstates called neutralinos. We also list (in parentheses) some alternate symbols for the various neutral Higgs bosons that have appeared in some of the previous literature. The tilde is often used to denote superpartners. However, to avoid cluttered equations, in this paper we often omit the tilde for neutralinos and charginos, since there can be no ambiguity in this case. As we will argue below, the lightest superpartner is most likely the lightest neutralino, and it is stable. It is then the dark-matter candidate on which we focus, and very often we refer to it as *the* neutralino. When there can be no confusion that we are referring to the LSP, we may refer to it simply as χ.

The spectrum of the normal, R-even, particles is specified in the same manner as for nonsupersymmetric models. Quark mass matrices determine the masses and the mixing angles, which are encoded in the Cabibbo–Kobayashi–Maskawa matrix [171]. The pattern of gauge-symmetry

breaking is unchanged from the standard model, and gives the same tree-level relation between the masses of the W and Z bosons [172, 173]. The most important technical difference occurs in the Higgs sector. As mentioned above, the Higgs sector is required to contain two weak isospin doublets, as opposed to the one doublet required in the standard model. This doubling gives rise to five physical states, which are shown in Table 1, along with some of their properties.

Let us summarize the parameters of the model, referring to the detailed form of the terms in Appendix A. We count 63 parameters as follows, not including those parameters which appear in the nonsupersymmetric standard model, i.e., gauge couplings, fermion masses, etc. First there are the three gaugino mass parameters M_1, M_2, M_3, and the parameter μ (often referred to as the "higgsino-mass parameter") which appears in the superpotential. These are important for their role in the neutralino mass matrix in particular. There is the ratio of Higgs VEV's, $\tan\beta$, which appears in the neutralino mass matrix as well as in the relation between Higgs masses.

We choose the mass of the pseudoscalar Higgs particle, m_A, as a free parameter, and this together with $\tan\beta$ and the gauge couplings determines the Higgs boson spectrum. The remaining parameters are elements of matrices of dimensionful couplings in the soft-breaking Lagrangian, which appear in the sfermion mass matrices. There are three 3×3 symmetric matrices of squark mass-squared parameters, $M_{\tilde{u}}^2$, $M_{\tilde{d}}^2$, and $M_{\tilde{Q}}^2$, where the first pair are associated to the right-handed states and the third is associated to the left-handed states. There are similarly two slepton mass-squared parameter matrices, $M_{\tilde{e}}^2$ and $M_{\tilde{L}}^2$. These five matrices constitute 30 parameters. The remaining soft-breaking parameter matrices are three 3×3 Yukawa matrices, A_u, A_d, and A_e, which we choose to have dimensions of mass. These constitute 27 parameters.

The spectrum of superpartners of quarks and leptons possesses maximum model dependence. This is because of the large number of soft-breaking parameters which involve these particles directly; of the 63 parameters counted above, notice that 57 of them are parameters which specify the masses and mixings of the squarks and sleptons.

For the full details of the discussion in this section, the reader should consult Appendix A.

Which is the LSP?: Before discussing the properties of the neutralino, it is worth reprising the arguments of Ellis et al. [125] that the neutralino is most likely the lightest supersymmetric particle in the MSSM. Although these arguments are not fully airtight, they are indeed suggestive.

Suppose a charged uncolored particle, such as a chargino or slepton, were the LSP. Then the relic number density of such particles would be roughly $10^{-6}\,(M/\mathrm{GeV})\,n_B$ where M is the mass of the particle and n_B is the baryon number density [174]. Such particles would show up in searches for anomalously heavy protons [174]. Null results from such searches [175] rule out such charged particles over a broad mass range.

What if a squark or gluino were the LSP? Such particles would be expected to form hadrons. If charged, they would show up in anomalous proton searches, but it is possible that stable strongly interacting superpartners would form only neutral hadrons which, unlike neutrons, would not bind to nuclei and thus would evade detection. For these particles, one must turn to theory. Grand-unified models predict relations between the superparticle masses, and in most cases, the gluino is more massive than the neutralino, and the squarks are heavier than the sleptons. If so, then neither is the LSP.

Finally, consider sneutrinos. In most models, there is a slepton with mass similar to, but slightly smaller than, the sneutrino mass. If this is not the case for some reason, then there are cosmological

arguments against a stable sneutrino. As discussed in Section 12, most (but not all) regions of sneutrino parameter space are ruled out by WIMP direct-detection experiments [176].

This leaves the lightest neutralino as the LSP. The neutralino would be stable and weakly interacting, and thus be a good dark-matter candidate. Although constraints on neutralino parameter space exist, the vast majority of neutralino parameter space is still unprobed by various accelerator and dark-matter experiments.

The neutralino: As argued above, the lightest superpartner (LSP) in most cases is the lightest neutralino, a linear combination of the supersymmetric partners of the photon, Z^0, and neutral-Higgs bosons,

$$\chi = N_{10}^* \tilde{B} + N_{20}^* \tilde{W}^3 + N_{30}^* \tilde{H}_1^0 + N_{40}^* \tilde{H}_2^0, \tag{4.3}$$

where $\tilde{B}$ and $\tilde{W}^3$ are the supersymmetric partners of the U(1) gauge field B and the third component of the SU(2) gauge field W^3 that mix to make the photon and Z^0 boson. The coefficients N_{i0}, as well as the mass m_χ of the neutralino come from diagonalization of the neutralino mass matrix which appears in Eq. (A.20), and the subscript 0 denotes the lightest neutralino. The phenomenology and cosmology of the neutralino are governed primarily by its mass and composition. A useful parameter for describing the neutralino composition is the gaugino fraction, $f_g = |N_{10}|^2 + |N_{20}|^2$ [134]. If $f_g > 0.5$, then the neutralino is primarily gaugino and if $f_g < 0.5$, the neutralino is primarily higgsino.

Although discussions of neutralinos can become very involved, many results can be understood in terms of the neutralino properties displayed in Figs. 6 and 7. The broken curves are neutralino mass contours in the M_2–μ plane, and the solid curves are the gaugino fraction of the neutralino. We have taken $\tan\beta = 2$, but these curves are relatively insensitive to the value of $\tan\beta$. Although M_1 and M_2 are independent gaugino mass parameters in the MSSM that appear in the neutralino mass matrix, in most GUT models, there is a relation between the two which is adopted in almost all the literature on the MSSM. Therefore, we have also assumed this GUT relation: $M_1 = \frac{5}{3} M_2 \tan^2\theta_w$. The mass contours are hyperbolas that asymptote to $m_\chi = |\mu|$ for large M and to $m_\chi = M_1 \approx \frac{1}{2} M_2$ for large $|\mu|$. For large values of $|\mu|$ and M_2, models where the neutralino is half higgsino and half gaugino fall along the line $\mu = \frac{5}{3} M_2 \tan^2\theta_w \approx M_2/2$. In the regions where the gaugino fraction is greater than 0.99, the neutralino is almost a pure B-ino state ($N_{01} \approx 1$ and $N_{0i} \approx 0$ for $i \neq 1$). (When $M_1 = \frac{5}{3}\tan^2\theta_w$, the lightest neutralino cannot both be a pure photino and heavier than the W.) When the gaugino fraction is less than 0.01, the neutralino is very nearly a pure higgsino state ($N_{01} \approx N_{02} \approx 0$).

4.3. SUSY-GUT and supergravity models

As we remarked above, one of the main motivations for introducing supersymmetry is to provide a natural framework for discussing theories with large hierarchies of scales. Such large hierarchies invariably arise in grand-unified theories since the unification of running gauge couplings occurs at very high scales, greater than 10^{15} GeV. Thus supersymmetry goes hand-in-hand with grand unification, and supersymmetric grand-unified theories are attractive as descriptions of physics at and below the unification energy scale. In fact, precision measurements of the standard-model

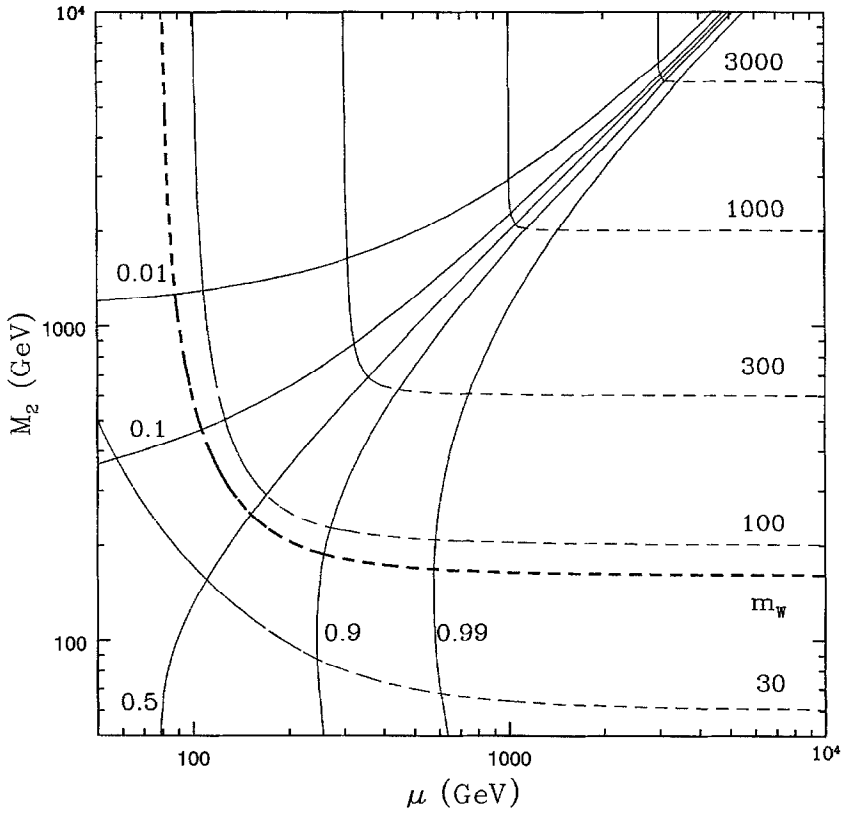

Fig. 6. Contour plot of the neutralino mass and composition in the M_2–μ plane. The broken curves are contours of constant neutralino mass m_χ (in GeV), and the solid curves are contours of constant gaugino fraction f_g. Here, $\tan\beta = 2$ and the GUT relation, $M_1 = \frac{5}{3} M_2 \tan^2\theta_W$ has been used. Only positive values of μ are shown. From Ref. [134].

gauge couplings at $\sqrt{s} \simeq m_Z$ indicate that nonsupersymmetric grand-unified theories with no intermediate scales are not viable [4]. However, by calculating the renormalization group running of the couplings with the assumption that a supersymmetric spectrum of particles becomes visible at scales roughly in the range 100 GeV–1 TeV, it is found that the simplest grand-unification scheme works quite well [4, 177, 178]. This observation has inspired some renewed interest in these models.

Supersymmetric grand unification has several novel features compared to the nonsupersymmetric case. The unification scale in these theories is always larger than the corresponding scale in a nonsupersymmetric theory because the supersymmetric additions to the particle spectrum decrease the beta functions, slowing the running of the couplings [179–181]. Proton decay via dimension-six operators is thereby suppressed, but one must also consider the effect of baryon-number violating dimension-five operators [181]. The most likely channel for proton decay turns out to be $p \to \bar{\nu}_\tau K^+$ [181].

The most important problem for supersymmetric theories remains that of supersymmetry breaking. In the MSSM, we parametrized the soft breaking in the most general way, according to

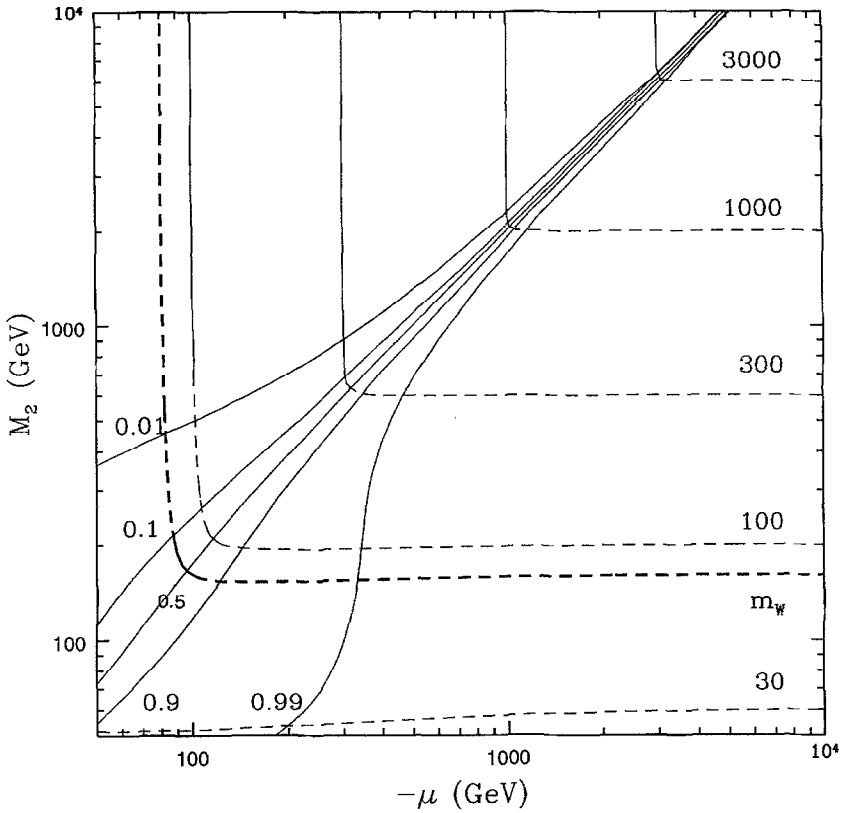

Fig. 7. Same as Fig. 6, but for negative values of μ.

the results of Girardello and Grisaru [167], and we noted that this description is purely an effective description, with no hint at the mechanism which must operate to produce these terms in the low-energy limit. In order that the underlying theory be truly supersymmetric, we must consider some form of spontaneous supersymmetry breaking. As discussed in Appendix A, the natural framework for such supersymmetry breaking is that of *local* supersymmetry, which is supergravity. In many cases this breaking is accomplished in a so-called hidden sector, and the effects of the breaking are transferred to the visible sector by gravitational interactions. These hidden sector models can be realized in superstring models, where the hidden sector is comprised of the fields transforming under one factor of E_8 in the full $E_8 \times E_8$ gauge group.

Within this framework of spontaneously broken supergravity, there remains a choice for the mechanism of electroweak-symmetry breaking. Tree-level breaking of electroweak symmetry manifests certain difficulties with regard to fine-tuning in the superpotential [182], as well as problems with naturalness of the necessary singlet superfields [183–187]. These problems are avoided by models which break the electroweak symmetry through radiative corrections [188–191]. It could as well be argued that such a mechanism is more attractive due to its minimality.

Thus we arrive at the minimal model of supergravity which encompasses the known interactions, where supersymmetry is broken in a hidden sector, and electroweak symmetry is broken by radiative corrections.

The parameters which specify such a supergravity model are as follows. First, there is a common unified gauge coupling given at the unification scale M_X. This gauge coupling is determined along with the scale M_X by the requirement of coupling unification [192]. Second, there is the superpotential, which is in precisely the same form as Eq. (A.10). Therefore we have a higgsino paramter μ as well as the Yukawa coupling matrices h_u, h_d, and h_e. Note that since supergravity does not solve the problem of generation replication, this Yukawa coupling data is required. Third are the gaugino mass terms, which are equal at the unification scale, $M_1(M_X) = M_2(M_X) = M_3(M_X) = M$. Fourth is the area in which supergravity provides great simplification, and that is with regard to the remaining soft-breaking terms. Assuming a global U(N) symmetry between the N chiral superfields, the general form of the scalar potential is [193]

$$V = \sum_i \left| \frac{\partial W}{\partial \phi_i} \right|^2 + |m|^2 \sum_i |\phi_i^2| + AW_3 + BW_2 + (2B - A)W_1 + D \text{ terms}, \tag{4.4}$$

where W_n is the part of the superpotential W which is nth order. The parameter m is seen to be a common mass parameter for all the sfermions in the theory, and the breaking is flavor-blind so that the sfermion matrices, $\tilde{M}^2$, are proportional to the identity at the unification scale. We have chosen the parameters A and B to have dimensions of mass. Also note that there exist different conventions in the literature regarding numerical factors in the definitions. We have followed Ref. [194] in our choices. Furthermore, some authors assume a minimal Kähler potential, which implies the further constraint $B = A - m$.

If one is not interested in questions of generational mixing, then the Yukawa couplings of the light generations can be ignored, leaving only the three heavy couplings h_τ, h_b, and h_t. Often one assumes the relation $h_b(M_X) = h_\tau(M_X)$, which is a prediction of many simple GUTS, based on certain minimal choices for the Higgs representations [195, 196]. This relation is phenomenologically successful; however, it is worth keeping in mind that there are often corrections to this relation in the presence of some common Higgs representations, which may in fact be required in some models for other reasons, and it is important to know exactly what model one intends when speaking of a "minimal" model. See Ref. [197] for an example of such a minimal model.

So the simplest model that can be considered has nine parameters, $\mu(M_X)$, $h_b(M_X)$, $h_\tau(M_X)$, $h_t(M_X)$, α_X, M_X, A, M, and m. We have already remarked that α_X and M_X are fixed by using the measured values of the low-energy gauge couplings. The Yukawa couplings can be fixed in terms of the measured masses, though the solution of the full renormalization group required to do this can be technically complicated. Furthermore, the relatively poor precision of the measured b-quark mass allows for some freedom. The Higgs parameter $\mu(M_X)$ basically sets the scale for electroweak-symmetry breaking, though the relation is quite complicated; it can be eliminated by using an electroweak mass scale, such as the mass of the Z^0.

The most important constraint on the free parameters is that they do in fact allow for electroweak-symmetry breaking. The electroweak symmetry in this model is broken only by radiative corrections, and one must solve the renormalization group equations which describe the evolution of the Higgs potential in order to implement this constraint [194, 198].

Thus far we have said nothing about superstring theory. It is hoped that superstring theory will lead to an effective supergravity theory below the string scale. However, the form that such a model would take is unknown. It appears that many possibilities exist. In particular, it is unclear whether or not superstring theory will lead to a minimal model of supergravity such as we have discussed.

5. Laboratory constraints

5.1. Remarks

In this section we will briefly address the constraints on supersymmetric models from laboratory experiments. We will avoid a detailed enumeration of search techniques and current results, and instead try to indicate a few important points. For more discussion of these issues, we refer the reader to some of the extant lectures and review articles as a starting point [20, 152, 199, 200]. The effect of these constraints on neutralino dark matter is discussed in Section 11.

5.2. Constraints on the Higgs sector

The most distinctive feature of the Higgs sector in the MSSM is the relation between couplings in the Higgs potential and gauge couplings. At tree level, these relations lead to the important prediction $m_{h^0} < m_Z$. In principle, this prediction provides the most definitive method to rule out the MSSM, in the context of a direct search for the h^0 boson.

However, it has been realized that radiative corrections in the Higgs sector will upset the tree-level mass relations and raise the upper limit on the lightest Higgs boson mass [201–206]. The full results for the radiative corrections are quite complicated, but can be simplified in a leading-logarithm approximation [202]. The corrections are generically important if the top quark is heavy, and the upper limit on the mass of the h^0 can be raised to values as high as $m_{h^0} \lesssim 130$ GeV [207–211]. This result implies that the h^0 of the MSSM could possibly evade detection at LEP-II, running at $\sqrt{s} \simeq 200$ GeV. Nevertheless, the search for the Higgs bosons of the MSSM remains one of the most important tests of the scenario.

Limits from LEP-I derive from searches for the processes $Z^0 \to h^0 \bar{f}f$ and $Z^0 \to h^0 A^0$. The rate for decay of an on-shell Z to neutral Higgs bosons is [19]

$$\Gamma(Z \to A^0 h^0)/\Gamma(Z \to \bar{\nu}\nu) = 4\cos^2(\beta - \alpha)\,(|\boldsymbol{p}|/m_Z)^3, \tag{5.1}$$

where $|\boldsymbol{p}|$ is the three momentum of one of the final-state Higgs bosons, and $\Gamma(Z \to \bar{\nu}\nu)$ is the standard-model rate for Z-boson decay to one massless neutrino species. The current limits derived from these searches are $m_{h^0} > 44$ GeV [212, 213], and $m_{A^0} > 39$ GeV [214, 215]. Some dependence on the top-quark mass exists for the A^0 limit; see Ref. [212].

The limit on m_{h^0} is based on the assumption $\tan\beta > 1$. If this constraint is relaxed, the limit reduces to $m_{h^0} \gtrsim 30$ GeV [216]. The limit on m_{A^0} is also dependent on the assumption $\tan\beta > 1$, and can be relaxed to $m_{A^0} > 12$ GeV if this constraint is relaxed [216].

Although it is now believed that the absolute upper limit for the mass of the h^0 can allow it to evade discovery at LEP-II, the projected coverage of parameter space provided by such experiments is still excellent.

5.3. Constraints on the chargino/neutralino sector

As discussed above, the Higgs sector may provide the simplest method to rule out the MSSM. Of course, the discovery of Higgs bosons with masses in a range consistent with the MSSM does not provide proof for the existence of low-energy supersymmetry! Low-energy supersymmetry can be said to be absolutely confirmed only in the case that superpartner particles are discovered by direct production in high-energy collisions.

As one might expect, details of the model parameters become important in discussing the production of supersymmetric particles. Because of the possible complexity of the couplings and of the mass spectrum, it is extremely difficult to place bounds on the model without making some assumptions.

Consider the simplest production process, the pair production of neutralinos or charginos in e^+e^- collisions at the Z^0 resonance [217, 218]. The width for decay of a Z^0 boson to a neutralino pair is [219]

$$\Gamma(Z^0 \to \chi_i^0 \chi_j^0) = \tfrac{4}{3} S(\alpha(O''^{L}_{ij})^2/\sin^2 2\theta_w)\beta m_Z [1 - \tfrac{1}{2}(x_i + x_j) - \tfrac{1}{2}(x_i - x_j)^2 - 3x_i x_j], \quad (5.2)$$

where $x_i = (m_{\chi_i}/m_Z)^2$, $\beta = \sqrt{1 - 2(x_i + x_j) + (x_i - x_j)^2}$, and S is a symmetry factor which equals $\frac{1}{2}$ for identical particles in the final state. The couplings O''^{L}_{ij} are as introduced in Eq. (A.53) and are dependent on the mixing of the neutralinos. The same expression applies for chargino pair production with the substitution $2(O''^{L}_{ij})^2 \to (O'^{L}_{ij})^2 + (O'^{R}_{ij})^2$.

Due to the simple nature of chargino mixing, it is possible to derive a bound on the chargino masses independent of any assumptions, $m_{\chi^+} > 45.2$ GeV [220]. Prospects for chargino detection at LEP-II have also been discussed [221, 222]. For the case of neutralinos, some assumptions regarding the mixing of the states are required in order to translate bounds on the branching ratios into bounds on neutralino masses. For example, if the grand-unification relation is imposed on the gaugino mass parameters, then it is possible to derive the bound $m_{\chi^0} > 18.4$ GeV for the mass of the lightest neutralino [223]. This limit is comparable to the limits from the cosmological neutralino abundance. Note that the signals for neutralino production depend on the nature of the neutralinos as well. Production of a pair of LSP neutralinos contributes to the invisible width of the Z. Production of one LSP neutralino and another heavier neutralino can produce spectacular one-sided events; however, in most models, the mass of the second lightest neutralino is too large for this Z-decay channel to open.

5.4. Sleptons

Charged sleptons can be produced in e^+e^- collisions [217, 218]. Generically, the signal for such events is the presence of acoplanar leptons in the final state, coming from the decays of the sleptons. Neutralinos appear in the final state of these decays as well, and assumptions about the lightest neutralino mass must be made in the analysis. For example, assuming the lightest neutralino is

lighter than 41 GeV, a limit on the selectron mass can be derived, $m_{\tilde{e}} > 45$ GeV [220]. Similar limits exist for the smuon and stau [220].

5.5. Squarks and gluinos

Strongly interacting supersymmetric particles could be produced in hadronic collisions. Significant model dependence enters because the signal will depend on the particular decay chain taken by the squark or gluino, and assumptions about these decay chains enter the data analysis directly.

For example, consider squark production. A squark will generically undergo two-body decay to a quark and a neutralino or chargino with subsequent cascade decay of the neutralino (or escape from the detector if it is the lightest neutralino). The signal is missing energy, which escapes with an LSP neutralino at the end of the cascade. Clearly, assumptions about the neutralino sector will be very important in the search for such processes. For example, if the grand-unification condition is assumed, then a relation exists between the lightest neutralino mass and the gluino mass, and if one assumes that the gluino mass is less than 410 GeV, then a bound $m_{\tilde{q}} > 90$ GeV can be derived [224]. Other assumptions involving the squark sector and the nature of the cascade decays enter in Ref. [224], and we refer the reader there for further discussion.

Another possible signal in $p-\bar{p}$ collisions is the trilepton signal from decays of charginos and neutralinos produced through an intermediate off-shell W boson. With some assumptions typical of supergravity models, sensitivity to gluino masses up to about 250 GeV can be obtained [225]. For some current thinking on squark and gluino production in supergravity models, see Ref. [226].

Gluino mass limits are somewhat controversial at the present time, due to claims that a mass window remains open in the range 1–4 GeV. The suggestion of such a possibility derives essentially from the observation that it would lead to a better fit between low and high energy values for the running strong-coupling constant [227]. All or part of this window can be closed by invoking model assumptions of various sorts, such as unification conditions [223], or supergravity assumptions [228].

Squarks could also be produced at e^+e^- colliders [217], but squarks in the currently accessible mass range have been ruled out by hadron-collider experiments.

5.6. Limits from rare processes

In this subsection we will note a few constraints on the MSSM which arise upon consideration of rare processes and precision experiments. In particular, the most stringent constraints arise from consideration of flavor-changing neutral-current (FCNC) interactions. Most important among these is the decay $b \to s\gamma$, which has recently received a great deal of attention.

We have seen above that the general MSSM Lagrangian actually possesses FCNC interactions at tree level, which arise from flavor asymmetries in the soft-breaking terms. These direct flavor-changing interactions all involve superpartner particles, so that they are not directly accessible to low-energy experiments. However, the effect of these interactions will be felt through radiative corrections to measured processes. In some cases, the effects will appear as corrections to FCNC processes which are already known to exist in the standard model, such as $\Delta S = 2$ or $\Delta S = 1$ processes. In other cases the effects will appear through the existence of processes which are strictly forbidden in the standard model, such as $\mu \to e\gamma$. One may ask why we might expect some flavor

dependence in the soft-breaking terms at all. The best answer is that, even if they do not exist at tree level, radiative corrections involving the Yukawa couplings will lead to small deviations from flavor-blind soft breaking. Our above discussion of supersymmetric grand unification and supergravity models already mentioned this possibility.

The $\Delta S = 2$ mixing in the K^0–$\bar{K}^0$ system historically provided very important clues to flavor physics, beginning with the prediction of the charm-quark mass [229]. The basic point is that the extreme smallness of this mixing, corresponding to a mass difference of 3.5×10^{-12} MeV, requires a careful cancelation of FCNC interactions [230]. In the standard model, Cabibbo–Kobayashi–Maskawa mixing of quarks provides the necessary flavor asymmetry to explain mixing in the K^0–$\bar{K}^0$ system at the observed magnitude.

In the MSSM, flavor asymmetry in the squark sector will also give contributions to K^0–$\bar{K}^0$ mixing. One can see this immediately by "supersymmetrizing" the standard box-diagram calculation, replacing quark lines with squark lines and W-boson lines with gaugino lines [231–234]. There also exist contributions from gluino exchange. The full results of these calculations are somewhat complicated, and the numerical values of the resulting bounds are dependent on certain assumptions; however, as a generic feature, one finds that the squark masses must be degenerate to a precision of about a few percent. This assumes that the squark mixing angles are of the same order as the corresponding quark mixing angles. For a discussion of supersymmetric FCNC phenomenology in the K^0–$\bar{K}^0$ system, including CP-violation, see Refs. [235, 236].

In the standard model, processes such as $\mu \to e\gamma$ are strictly forbidden because the absence of neutrino mass leads to exact conservation of the individual lepton numbers. However, in the MSSM, mixing in the scalar lepton sector will violate these separate conservation laws. Again, these violations will manifest themselves through radiative corrections, in this case providing the sole cause of such processes in the model. A calculation of the $\mu \to e\gamma$ amplitude [233] combined with the current limit on $\Gamma(\mu \to e\gamma)$ gives a constraint similar to that derived on the squark sector from K^0–$\bar{K}^0$ mixing. The scalar leptons must generically be degenerate to a precision of a few percent. This assumes that the slepton mixing angles are of the same order as the quark Cabibbo–Kobayashi–Maskawa mixing angles.

$b \to s\gamma$ *constraints:* Recently, the CLEO collaboration has announced the observation of a $\Delta S = 1$ process in the B system, in the exclusive mode $B \to K^*\gamma$ and in the inclusive mode $B \to X_s\gamma$. The values for the branching ratios at the time of this review are [237, 238]

$$B(B \to K^*\gamma) = (4.3 \pm 1.5 \pm 0.9) \times 10^{-5}, \qquad B(B \to X_s\gamma) = (2.32 \pm 0.57 \pm 0.35) \times 10^{-4}. \quad (5.3)$$

Due to strong-interation modeling uncertainties, the quantitative import of the exclusive measurement is unclear. However, the inclusive process $B \to X_s\gamma$ provides an interesting window on physics beyond the standard model. The standard-model prediction is approximately $(2–3) \times 10^{-4}$, and the inclusive measurement is consistent with this value. In the context of the MSSM, there exist contributions to the amplitude both from the extended Higgs sector and from intermediate superparticles. The contributions from the extended Higgs sector have been known for some time and have the interesting feature that they necessarily increase the rate compared to the standard-model prediction [239]. However, the intrinsically supersymmetric contributions to the rate do not share this feature [240, 241]. Therefore, the consequences for the most general supersymmetric models are generally model dependent.

Analyses of the $b \to s\gamma$ process split into two classes. First are those analyses which treat the amplitude as if it were dominated by the charged-Higgs-boson exchange, as in the standard calculations for the two-doublet model. Second are those which consider the detailed contributions from exchange of supersymmetric particles. Analyses of the first class have the feature of simplicity, while those of the second class are more complete.

In Ref. [242], dominance of charged-Higgs exchange is assumed. A resulting bound on the Higgs sector can be written as $m_A > 130$ GeV, for a top quark mass of 150 GeV. This type of analysis is generally applicable to supergravity models, but is not strictly binding in the general MSSM. In Ref. [243], similar assumptions are made, and it is pointed out that the measurement of the inclusive rate can narrow the available parameter space for the Higgs sector.

In Ref. [241], a more general situation is considered. There it is pointed out that the required magnetic moment operator must vanish in the limit of exact supersymmetry, so that the size of the effect is strongly dependent on the supersymmetry-breaking terms. This is an important point which deserves further consideration. Simplified analyses tend to be more relevant to supergravity models because the spectrum in these models often implies the dominance of charged-Higgs exchange. Note that the example numerical calculations in Ref. [241] contain some unrealistic assumptions, apparently made for the sake of simplicity, and the numerical results given there should not be understood as generic, although they are illustrative of the point which is made in the paper. Other treatments include that in Ref. [244], which considers the contributions of a light s-top state, and that in Ref. [245], which treats the contributions of chargino exchange. These calculations support the point that one must consider a more detailed treatment of the sparticle contributions in order to claim a complete calculation.

The inclusive branching ratio for $b \to s\gamma$ is given by the following expression [241, 245, 246]:

$$\frac{B(B \to X_s\gamma)}{B(B \to X_c e\nu)} = \frac{6\alpha_{em}}{\pi} \frac{|\eta^p \mathscr{A}_\gamma + \frac{8}{3}(\eta^q - \eta^p)\mathscr{A}_g + \mathscr{C}|^2}{I(x_{cb})(1 - (2/3\pi)\alpha_s(m_b) f(x_{cb}))}. \tag{5.4}$$

Here, η is a ratio of running strong-coupling constants at the high- and low-energy scales, $\eta = \alpha_s(M_Z)/\alpha_s(m_b)$, and p, q are renormalization group exponents, $p = 16/23$, $q = 14/23$. The amplitude $\mathscr{A}_\gamma$ is from the photon penguin vertex, the amplitude $\mathscr{A}_g$ is from the gluon penguin vertex, and the amplitude $\mathscr{C}$ is from mixing with four-quark operators, $C \simeq 0.175$. The function $I(x) = 1 - 8x^2 + 8x^6 - x^8 - 24x^4 \ln x$ is a phase space factor; $x_{cb} = m_c/m_b$. The function $f(x)$ is a QCD correction factor, $f(x_{cb}) \simeq 2.41$ [247].

The amplitudes $\mathscr{A}_\gamma$ and $\mathscr{A}_g$ receive contributions from supersymmetric particle exchange as well as from $W^\pm$ and charged-Higgs exchange. Following Refs. [241, 245], we consider only those supersymmetric contributions from chargino exchange. This is a useful simplification for most models; the terms ignored are those due to gluino exchange, which can be important only in models with large squark flavor mixing. Neglecting terms with more than one insertion of a down squark mass matrix gives the amplitudes

$$\mathscr{A}^W_{\gamma,g} = \frac{3}{2}\frac{m_t^2}{m_W^2} f^{(1)}_{\gamma,g}\left(\frac{m_t^2}{m_W^2}\right), \tag{5.5}$$

$$\mathscr{A}^H_{\gamma,g} = \frac{1}{2}\frac{m_t^2}{m_{H^\pm}^2}\left[\frac{1}{\tan^2\beta} f^{(1)}_{\gamma,g}\left(\frac{m_t^2}{m_{H^\pm}^2}\right) + f^{(2)}_{\gamma,g}\left(\frac{m_t^2}{m_{H^\pm}^2}\right)\right], \tag{5.6}$$

and

$$\mathscr{A}^{\chi}_{\gamma,g} = \frac{1}{(V^{CKM}_{ts})^* V^{CKM}_{tb}} \sum_{j=1}^{6} \sum_{n=1}^{2} (-) \frac{m_W^2}{m^2_{\chi_n^+}} f^{(1)}_{\gamma,g}\left(\frac{m^2_{\tilde{q}_j}}{m^2_{\chi_n^+}}\right) \left[K^{Lu}_{bjn} - \frac{J^{Ru}_{bjn}}{\sqrt{2}\sin\beta}\right]\left[K^{Lu}_{sjn} - \frac{J^{Ru}_{sjn}}{\sqrt{2}\sin\beta}\right]$$
$$+ \frac{m_W}{m_b}\frac{m_W}{m_{\chi_n^+}} \frac{J^{Lu}_{bjn}}{\sqrt{2}\cos\beta} f^{(3)}_{\gamma,g}\left(\frac{m^2_{\tilde{q}_j}}{m^2_{\chi_n^+}}\right)\left[K^{Lu}_{sjn} - \frac{J^{Ru}_{sjn}}{\sqrt{2}\sin\beta}\right], \tag{5.7}$$

where the sum on n is over the two charginos, and the sum on j is over the six up squarks. The J's and K's are the chargino–quark–squark couplings defined in Eqs. (A.37–A.39). The total amplitudes are sums of the above, $\mathscr{A}_{\gamma,g} = \mathscr{A}^{W}_{\gamma,g} + \mathscr{A}^{H}_{\gamma,g} + \mathscr{A}^{\chi}_{\gamma,g}$. The functions $f_a^{(i)}$ are given by

$$f_\gamma^{(1)}(x) = \frac{7 - 5x - 8x^2}{36(x-1)^3} + \frac{x(3x-2)}{6(x-1)^4}\ln x$$
$$f_\gamma^{(2)}(x) = \frac{3 - 5x}{6(x-1)^2} + \frac{3x-2}{3(x-1)^3}\ln x$$
$$f_\gamma^{(3)}(x) = (1-x) f_\gamma^{(1)}(x) - \tfrac{1}{2}x f_\gamma^{(2)}(x) - \tfrac{23}{36}, \tag{5.8}$$
$$f_g^{(1)}(x) = \frac{2 + 5x - x^2}{12(x-1)^3} - \frac{x}{2(x-1)^4}\ln x$$
$$f_g^{(2)}(x) = \frac{3 - x}{2(x-1)^2} - \frac{1}{(x-1)^3}\ln x$$
$$f_g^{(3)}(x) = (1-x) f_g^{(1)}(x) - \tfrac{1}{2}x f_g^{(2)}(x) - \tfrac{1}{3}, \tag{5.9}$$

These expressions are taken from Ref. [241] and are consistent with those in Ref. [240] and in Ref. [245], with the appropriate specialization of the flavor structure in the latter case.

A numerical example of the effect of chargino exchange is shown in Fig. 8. The charged-Higgs boson mass and the couplings at the quark–squark–chargino vertices are held fixed. This illustrates the dependence of the effect on the chargino mass. The example does not correspond to any fixed MSSM model, but is meant to be illustrative.

b → sγ *and dark-matter detection:* In Ref. [248], the detectability of neutralino dark matter is linked to the amplitude for b → sγ. Some assumptions about the supersymmetry-breaking terms are made there; for instance, it is assumed that all sfermions have the same soft-breaking mass parameter. This implies that no contributions to the amplitude can come from neutralino or gluino exchange. These assumptions are typical of those which lead to dominance of the Higgs-exchange contribution. The interesting point is that, when the amplitude is dominated by Higgs exchange, it is often true that elastic scattering of neutralinos off ordinary matter is also controlled by Higgs exchange. This provides the link, and implies that models with large elastic-scattering cross sections will have a large b → sγ rate, inconsistent with the CLEO results. Ref. [249] discusses this issue as well, though the model-dependence in that analysis is unclear. On the other hand, these conclusions are not fully general and may not hold true, for example, in models where the elastic-scattering cross section is mediated by squark exchange. These rare decays may provide stringent constraints on SUSY parameters, but more work is needed to fully assess the impact of

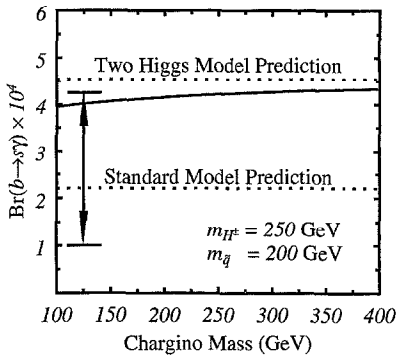

Fig. 8. Example of the effect of chargino exchange on Br(b → sγ). The mixing angle appearing in the quark–squark–chargino vertex has been fixed at 0.1, and the only parameter allowed to vary is $m_{\chi^\pm}$. The solid line is the result for the branching ratio; the upper dotted line is the result ignoring the chargino contribution; the lower dotted line is the result ignoring both the chargino contribution and the charge-Higgs contribution, which is the usual standard-model result. The arrows show the CLEO 95% CL limits.

the b → sγ constraint on dark-matter detection rates. We will discuss this point further with regard to the examples of Section 11.

For a comprehensive discussion of B physics in supersymmetric models, see Ref. [250]. For a general discussion of FCNC processes in $N = 1$ supergravity, see Ref. [236]; for special emphasis on nonminimal Kähler potentials in supergravity, see Ref. [251].

6. Neutralino annihilation

6.1. Remarks

The two processes which govern nearly all of neutralino cosmology are annihilation of neutralino pairs and scattering of neutralinos off ordinary matter. In this section we discuss the annihilation cross sections. We provide results for all the final states that appear at tree level and for those one-loop final states that are also important, and we discuss some of their properties. Annihilation cross sections are needed in cosmology for calculations of the cosmological neutralino relic abundance (see Section 3), the flux of energetic neutrinos from neutralino annihilation in the Sun and Earth (Section 9), and fluxes of anomalous cosmic rays produced by neutralino annihilation in the Galactic halo (Section 10). For these purposes, it is generally sufficient to expand the annihilation cross section in the nonrelativistic ($v \to 0$ where v is the neutralino–neutralino relative velocity) limit,

$$\sigma_A v = a + bv^2 + O(v^4), \tag{6.1}$$

where a is the s-wave contribution at zero relative velocity and b contains contributions from both the s and p waves. Neutralinos in the Galactic halo, Sun, and Earth move with velocities $O(10^{-3})$, so only the a term in Eq. (6.1) is needed for calculations involving relic neutralinos. When

neutralino interactions freeze out in the early Universe, their relative velocities are approximately $v \simeq \frac{1}{2}$ (see Section 3), so both the a and b terms are generally needed for relic-abundance calculations [see Eqs. (3.6) and (3.7)].

There are numerous final states into which the neutralino can annihilate. By far, the most important of these are those which appear in lowest order in perturbation theory, i.e., the two-body final states which occur at tree level. Specifically, these are fermion–antifermion pairs ($f\bar{f}$ where $\bar{f}$ are the standard-model neutrinos, leptons and quarks), W^+W^-, Z^0Z^0, W^-H^-, W^-H^+, Z^0A^0, Z^0H^0, Z^0h^0, H^+H^-, and all six combinations of A^0, h^0, and H^0. Several Feynman diagrams contribute to each of these processes, so the computation of the total annihilation cross section is quite a task. Both the a and b contributions for all of these final states have now been calculated. These are all the final states that should be needed for relic-abundance calculations. In addition, the s-wave contributions for the two-gluon (gg) and $q\bar{q}g$ final states have been calculated. These may be important for indirect-detection calculations in some regions of parameter space, but should not affect the relic-abundance results [252]. The s-wave contributions for the $\gamma\gamma$ final states have also been calculated. These are needed for calculation of the fluxes of cosmic gamma rays (see Section 10.3), but can be neglected for abundance calculations.

The analytic results for the a terms are always tractable (i.e., they can be written on one line). In this section, we will include explicit expressions for a (in other words, the $v \to 0$ limit of the annihilation cross sections). These limits are simple, and they are useful for the calculations of indirect-detection rates. They may also be useful in many cases for estimating the relic abundance.

On the other hand, calculation of the b terms can be quite involved. Several techniques have been used to obtain these terms. Standard "brute-force" evaluation of the Feynman diagrams can be done (e.g., [134]). Although the resulting expressions are long, they are valid for any value of the center-of-mass energy, s, including values outside the nonrelativistic limit. One can use these complete expressions to check the high-energy behavior of the cross sections for consistency with unitarity. More recently, the cross sections have been determined by evaluation of helicity amplitudes [253]. When expanded in the non-relativistic limit, these helicity amplitudes provide the nonrelativistic cross-section results needed for cosmological calculations. These analytic expressions are not necessarily shorter than the brute-force results, but the physical origin of each term is easier to understand. Finally, it has been pointed out that the amplitudes may first be expanded in v^2, and the b coefficient subsequently extracted [254, 255], but this technique has not yet been applied to all the supersymmetric annihilation channels.

Although available, the complete analytic results for the b terms are quite lengthy. We will give complete results for the $f\bar{f}$ final states in what follows. For other final states, we will write expressions in terms of the helicity amplitudes listed in the paper by Drees and Nojiri [253], the most recent and complete work on these annihilation cross sections, rather than reproduce all the relevant results here. Our conventions agree with theirs, so it should be clear how to incorporate those results with the others presented here. Since we choose to consider the most general flavor structure in the squark sector, our expressions for the $f\bar{f}$ final states are slightly different from those in Ref. [253]. They agree with previous results in the appropriate limits.

We clarify that we have included all the a and b terms for all the two-body final states that appear at tree level in our numerical work. In particular, the complete results for the b terms are included in the computer code that we are making available for distribution (see Appendix B).

We will discuss in turn the relatively straightforward cases of annihilation to gauge and Higgs bosons and then to fermion pairs. Then we will discuss QCD corrections to the $f\bar{f}$ processes and annihilation to gg and $q\bar{q}g$, which can be competitive in some regions of parameter space [252]. Finally, we will discuss the two-photon annihilation cross section which is needed for calculating the expected flux of gamma rays from neutralino annihilation in the Galactic halo.

6.2. *Weak gauge-boson final states*

Annihilation to weak gauge bosons will occur when the neutralino mass is high enough for such channels to be open ($m_\chi > m_W$). The cross sections for neutralino annihilation to W^+W^- and Z^0Z^0 were first calculated for pure B-inos and higgsinos in Refs. [132] and [133], and for the general neutralino state in Ref. [134]. There is no s-wave suppression mechanism for these annihilations, and thus they can be very important when the neutralino is heavy enough to make these final states available. In particular, they are often important in models where the neutralino is primarily higgsino.

Some simplification of the results of Refs. [132–134] were obtained in Ref. [253] by the use of the helicity formalism. Our notation agrees with theirs, so we simply summarize those results rather than reproduce them in their entirety. The cross sections are expressed as sums of squares of helicity amplitudes.

The expression for the cross section is not written in the form $\sigma_A v \simeq a + bv^2 + O(v^4)$, but it *does* contain all terms of order v^2. Therefore, a and b can be extracted from these expressions analytically, by Taylor expansion.

First, let us define some kinematic quantities that will be used for annihilation into any two particles, X and Y. The square of the total energy is $s \simeq 4m_\chi^2(1 + \frac{1}{4}v^2)$, and we define the kinematic invariant.

$$\bar{\beta}_{XY}(v) = \sqrt{1 - 2(m_X^2 + m_Y^2)/s + (m_X^2 - m_Y^2)/s^2}\,. \tag{6.2}$$

We define $\beta_{XY} = \bar{\beta}_{XY}(v = 0)$.

The diagrams for the process $\chi\chi \to W^+W^-$ are shown in Fig. 9. Annihilation to W^+W^- pairs occurs by s-channel exchange of Z^0, h^0, and H^0 bosons and by t- and u-channel exchange of charginos. The result for the cross section for annihilation to the W^+W^- final state is [253]

$$\begin{aligned}\sigma(\chi\chi \to W^+W^-)v = {} & \tfrac{1}{4}(\bar{\beta}_{WW}/8\pi s)\{2|(A12a)|^2 + \tfrac{1}{3}[|(A12b)|^2 + 2|(A12c)|^2 \\ & + 4|(A12d)|^2 + |(A12e)|^2 + 2|(A12f)|^2 + 2|(A12g)|^2 \\ & + 2|(A12h)_{\lambda_f=1}|^2 + 2|(A12h)_{\lambda_f=-1}|^2 + 2|(A12i)|^2 + |(A12j)|^2]\}.\end{aligned} \tag{6.3}$$

Here, the expressions $(A12x)$ refer to equation numbers in Ref. [253]. These are amplitudes for the various possible final helicity states, and it should be noted that they are in general complex quantities. The expression, $(A12h)$ must be evaluated once for positive total helicity, $\lambda_f = 1$ and once for negative total helicity, $\lambda_f = -1$.

The diagrams for $\chi\chi \to Z^0Z^0$ are shown in Fig. 10. Annihilation to Z^0 pairs proceeds via t- and u-channel exchange of four neutralinos and by s-channel exchange of H^0 and h^0 bosons. The cross

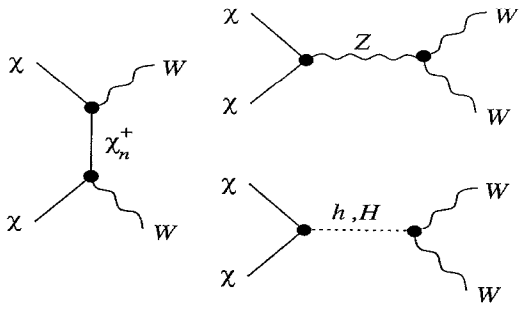

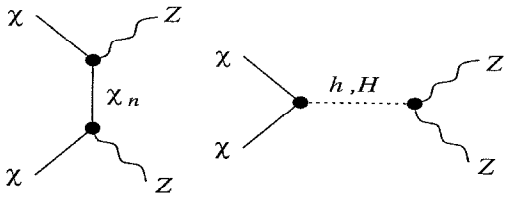

Fig. 9. Diagrams contributing to neutralino annihilation to W^+W^- pairs.

Fig. 10. Diagrams contributing to neutralino annihilation to Z^0Z^0 pairs.

section for annihilation to ZZ pairs is

$$\sigma(\chi\chi \to Z^0Z^0)v = \tfrac{1}{4}(\bar{\beta}_{ZZ}/16\pi s)\{2|(A15a)|^2 + \tfrac{1}{3}[|(A15b)|^2 + 2|(A15c)|^2 + 4|(A15d)|^2 + 2|(A15e)|^2 + 4|(A15f)|^2 + 2|(A15g)|^2 + |(A15h)^2|]\}. \tag{6.4}$$

Once again, the expressions (A15x) refer to equation numbers in Ref. [253].

Cross sections in the $v \to 0$ limits: These expressions simplify tremendously when $v \to 0$, the limit needed for indirect-detection calculations, and rough estimates of the relic abundance. The zero-velocity amplitude for annihilation to a pair of W bosons is determined solely by chargino exchange and is given by

$$\mathscr{A}(\chi\chi \to W^+W^-)_{v\to 0} = 2\sqrt{2}\,\beta_W g^2 \sum_{n=1}^{2} [(O_{0n}^L)^2 + (O_{0n}^R)^2]\frac{1}{P_n} \tag{6.5}$$

where $P_n = 1 + (m_{\chi_n^\pm}/m_\chi)^2 - (m_W/m_\chi)^2$, and the sum is over the two chargino states which can couple to the neutralino and the W boson. The zero-velocity amplitude for annihilation to a pair of Z bosons is determined solely be neutralino exchange and is given by

$$\mathscr{A}(\chi\chi \to Z^0Z^0)_{v\to 0} = 4\sqrt{2}\,\beta_Z \frac{g^2}{\cos^2\theta_W} \sum_{n=1}^{4} (O_{0n}^{\prime\prime L})^2 \frac{1}{P_n} \tag{6.6}$$

where $P_n = 1 + (m_{\chi_n}/m_\chi)^2 - (m_Z/m_\chi)^2$, and $\beta_Z = \sqrt{1 - m_Z^2/m_\chi^2}$, m_χ^2 and the sum is over the four neutralino states, χ_n. In terms of these amplitudes, the zero-velocity cross sections for these annihilations are given by

$$\sigma(\chi\chi \to VV)_{v\to 0} v = \frac{1}{S_V}\frac{\beta_V}{128\pi m_\chi^2}|\mathscr{A}(\chi\chi \to VV)|^2, \tag{6.7}$$

where V indicates the vector boson W or Z. The coefficient S_V is a symmetry factor, $S_W = 1$ and $S_Z = 2$, which accounts for the fact that the Z-boson final state contains two identical particles.

6.3. *Final states containing Higgs bosons*

Annihilation to Higgs bosons may also be important when such channels are open. The exceptions are those cases when the s-wave amplitude vanishes identically because of the inability of the Higgs bosons to produce the appropriate final state quantum number, CP = −1, in an s wave. In this case, the process may have some effect on the relic density but will not be relevant for indirect detection. The cases where the s-wave amplitude vanishes identically are $\chi\chi \to h^0h^0$, $\chi\chi \to H^0H^0$, $\chi\chi \to A^0A^0$, $\chi\chi \to H^+H^-$, and the mixed final state $\chi\chi \to Z^0A^0$. The processes which have nonvanishing s-wave contributions are $\chi\chi \to h^0A^0$, $\chi\chi \to H^0A^0$, $\chi\chi \to Z^0h^0$, $\chi\chi \to Z^0H^0$, and $\chi\chi \to W^\pm H^\mp$. The *a* and *b* contributions for annihilation of pure higgsinos and B-inos to two neutral Higgs bosons were first calculated in Refs. [132, 133], and for the general neutralino in Ref. [134]. The *a* contribution for the mixed gauge/Higgs-boson final states was computed in Ref. [256] and the *b* contribution was subsequently computed in Refs. [253, 257, 258].

First consider the processes $\chi\chi \to Z^0H^0$ and $\chi\chi \to Z^0h^0$. The diagrams for these processes are shown in Fig. 11. These receive contributions from exchange of all four neutralinos in the *t* and *u* channels, and from Z^0 and A^0 exchange in the *s* channel. The result for the cross section [correct to $\mathcal{O}(v^2)$] is

$$\sigma(\chi\chi \to Z^0H^0)v = \tfrac{1}{4}(\bar{\beta}_{ZH}/8\pi s)\{|(A17a)|^2 + \tfrac{1}{3}[2|(A17b)|^2 + |(A17c)|^2 + 2|(A17d)|^2]\}, \quad (6.8)$$

where the $(A17x)$ refer again to equation numbers in Ref. [253]. The expression for annihilation to the Z^0h^0 final state is similar, but the H^0 couplings and masses-need to be replaced by those for h^0, as discussed in Ref. [253].

The diagrams for the process $\chi\chi \to Z^0A^0$ are shown in Fig. 12. This process receives contributions from *t*- and *u*-channel exchange of all four neutralinos, and by *s*-channel exchange of Z^0, H^0, and h^0 bosons, The expression for the cross section is [253]

$$\sigma(\chi\chi \to Z^0A^0)v = \tfrac{1}{4}(\bar{\beta}_{ZA}/8\pi s)\tfrac{1}{3}[|(A19a)|^2 + 2|(A19b)|^2 + 2|(A19c)|^2 + |(A19d)|^2]. \quad (6.9)$$

For this final state, s-wave annihilation is forbidden by CP conservation, so $\sigma(\chi\chi \to Z^0A^0)_{v\to 0} = 0$.

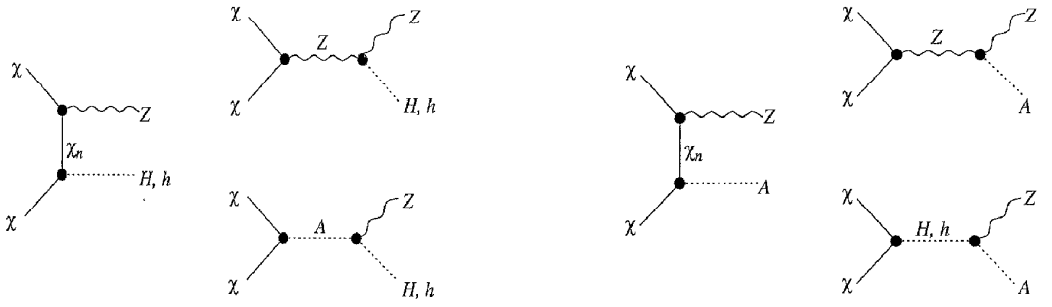

Fig. 11. Diagrams for the processes $\chi\chi \to Z^0H^0$ and $\chi\chi \to Z^0h^0$.

Fig. 12. Diagrams for the processes $\chi\chi \to Z^0A^0$.

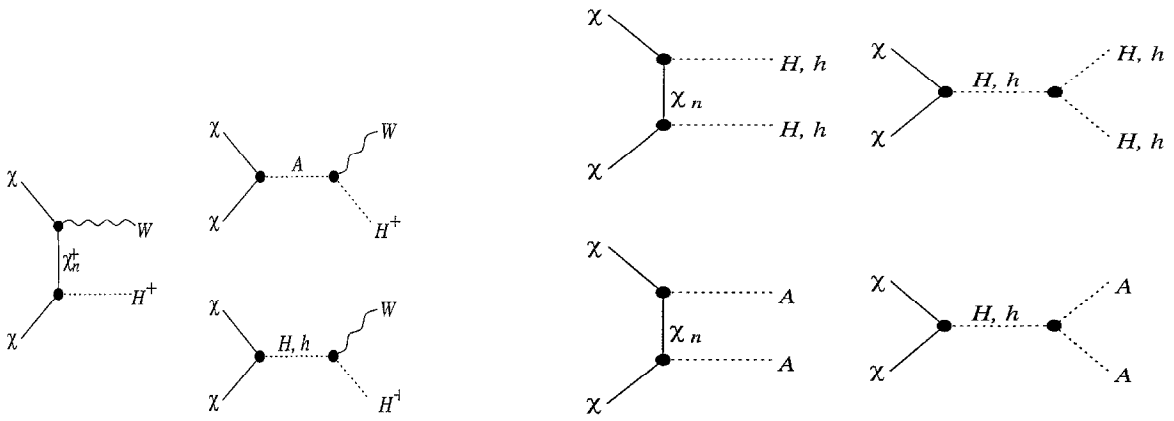

Fig. 13. Diagrams for the process $\chi\chi \to W^+H^-$. The charge-conjugate process is similar.

Fig. 14. Diagrams for neutralino–neutralino annihilation to the H^0H^0, H^0h^0, h^0h^0, and A^0A^0 final states.

Next consider the process $\chi\chi \to W^+H^-$ (and its charge conjugate). This receives contributions from chargino exchange and from all three neutral Higgs bosons in the s channel, see Fig. 13. The result is [253]

$$\sigma(\chi\chi \to W^+H^-)v = 2\tfrac{1}{4}(\bar{\beta}_{WH^+}/8\pi s)\{|(A21a)|^2 + \tfrac{1}{3}[|(A21b)|^2 + |(A21c)_{\lambda=1}|^2 + |(A21c)_{\lambda=-1}|^2 + |(A21d)|^2 + |(A21e)_{\lambda=1}|^2 + |(A21e)_{\lambda=-1}|^2 + |(A21f)|^2]\}. \tag{6.10}$$

Note that the leading factor of 2 is included to count the charge-conjugate process, $\chi\chi \to W^-H^+$, as well.

Next, consider annihilation into the two Higgs-boson final states, H^0H^0, h^0h^0, H^0h^0, and A^0A^0. The diagrams for these channels are shown in Fig. 14. Annihilation to these final states occurs by t- and u-channel exchange of the four neutralinos and by s-channel exchange of H^0 and h^0 bosons. The cross sections for annihilation to these final states may be written

$$\sigma(\chi\chi \to \phi_1\phi_2)v = \frac{1}{4S}\frac{\bar{\beta}_{\phi_1\phi_2}}{8\pi s}\{\tfrac{1}{3}[|(A23a)|^2 + |(A23b)|^2]\}, \tag{6.11}$$

where ϕ_1 and ϕ_2 are any of the scalars in the combinations H^0H^0, h^0h^0, H^0h^0, and A^0A^0, and $(A23x)$ refer to equations in Ref. [253]. The relevant couplings to be used in the expressions, $(A23x)$, for each of the final states are explained therein. Here, S is a symmetry factor: $S = 2$ for two identical particles in the final state and $S = 1$ otherwise. Note that s-wave annihilation to these final states is forbidden by CP conservation, so $\sigma(\chi\chi \to \phi_1^0\phi_2^0)_{v\to 0} = 0$ for these combinations of Higgs bosons.

We now consider the processes with one CP-even scalar and one CP-odd scalar A^0 in the final state; i.e., $\chi\chi \to H^0A^0$ and $\chi\chi \to h^0A^0$. The diagrams for these channels are shown in Fig. 15. These receive contributions from neutralino exchange, from Z^0 exchange in the s-channel, and

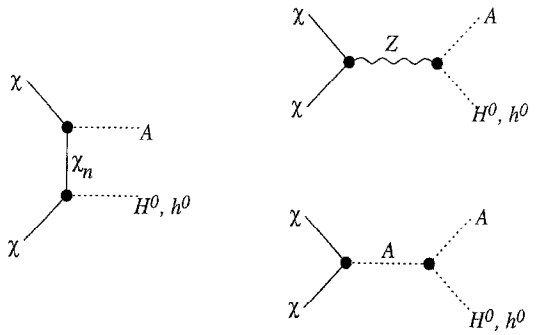

Fig. 15. Diagrams for the amplitudes containing one pseudoscalar Higgs boson in the final state.

from A^0 exchange in the s-channel. The cross section for this process may be written

$$\sigma(\chi\chi \to A^0H^0)v = \frac{1}{4}\frac{\bar{\beta}_{HA}}{8\pi s}\{|(A25a)|^2 + \tfrac{1}{3}|(A25b)|^2\}, \tag{6.12}$$

where again, the amplitudes are those given in Ref. [253], and the cross section for the A^0h^0 final state is similar, with the appropriate substitution of the couplings as discussed therein.

Finally, consider the cross section for the process $\chi\chi \to H^+H^-$. This proceeds via t- and u-channel exchange of the two charginos and by s-channel exchange of the Z^0, H^0, and h^0 bosons. The result is [253],

$$\sigma(\chi\chi \to H^+H^-)v = \frac{1}{4}\frac{\bar{\beta}_{\phi_1\phi_2}}{8\pi s}\{\tfrac{1}{3}[|(A27a)|^2 + |(A27b)|^2]\}, \tag{6.13}$$

where $(A27x)$ are amplitudes from Ref. [253]. The s-wave amplitude for this process is zero due to CP conservation.

Cross sections in the $v \to 0$ limit: We now give complete and self-contained expressions for the zero-velocity limits of the cross sections for annihilation to two-body final states containing Higgs bosons, for those final states in which the limit is nonvanishing . We list the amplitudes for each process, and then provide the expression for the cross sections in terms of these amplitudes. The supersymmetric couplings and masses that appear throughout are given in Appendix A.

In the zero-velocity limit, the amplitude for the process $\chi\chi \to Z^0H^0$ becomes [253, 256]

$$\mathscr{A}(\chi\chi \to Z^0H^0)_{v\to 0} = -2\sqrt{2}\,\beta_{ZH}\frac{m_\chi}{m_Z}\frac{g^2}{\cos\theta_W}\left[-2\sum_{n=1}^{4} O''_{L0n}\,T_{H0n}\frac{m_{\chi_n}-m_\chi}{m_\chi P_n}\right.$$
$$\left. + O''_{L00}\frac{m_\chi\cos(\alpha-\beta)}{m_Z\cos\theta_W} - \frac{2\sin(\alpha-\beta)\,T_{A00}}{4 - m_A^2/m_\chi^2 + i\Gamma_A m_A/m_\chi^2}\right] \tag{6.14}$$

and that for the process $\chi\chi \to Z^0 h^0$ becomes

$$\mathscr{A}(\chi\chi \to Z^0 h^0)_{v\to 0} = -2\sqrt{2}\,\beta_{Zh}\frac{m_\chi}{m_Z}\frac{g^2}{\cos\theta_W}\left[-2\sum_{n=1}^{4} O''_{L0n}\,T_{h0n}\,\frac{m_{\chi_n}-m_\chi}{m_\chi P_n} + O''_{L00}\,\frac{m_\chi \sin(\beta-\alpha)}{m_Z\cos\theta_W} - \frac{2\cos(\alpha-\beta)\,T_{A00}}{4-m_A^2/m_\chi^2 + i\Gamma_A m_A/m_\chi^2}\right], \tag{6.15}$$

where Γ_A is the width of the A^0 boson, and is given for the general model in Appendix B of Ref. [19]. Unless the neutralino mass is very nearly half the A^0-boson mass, $m_\chi \simeq \frac{1}{2}m_A$, the A^0 width can be taken to be zero. If $m_\chi \simeq \frac{1}{2}m_A$, then annihilation occurs on the A^0 pole, and it is likely that the neutralino relic abundance is too small to be astrophysically interesting anyway, Here, $P_n = 1 + (m_{\chi_n}/m_\chi)^2 - \frac{1}{2}(m_Z/m_\chi)^2 - \frac{1}{2}(M/m_\chi)^2$, where M is either m_{h^0} or m_{H^0}, as appropriate.

In the zero-velocity limit, annihilation to W^+H^- occurs only by exchange of charginos and the A^0 boson, and the amplitude is given by [253, 256]

$$\mathscr{A}(\chi\chi \to W^\pm H^\mp)_{v\to 0} = 4\sqrt{2}\,\beta_{WH}\,g^2\left[-\frac{1}{2}\sum_{n=1}^{2}\frac{m_\chi}{m_W}\frac{O^R_{0n}Q'^R_{0n} - O^L_{0n}Q'^L_{0n}}{P_n} + \frac{1}{2}\sum_{n=1}^{2}\frac{m_{\chi_n^+}}{m_W}\frac{O^R_{0n}Q'^L_{0n} - O^L_{0n}Q'^R_{0n}}{P_n} - \frac{m_\chi}{m_W}\frac{T_{A00}}{4-m_A^2/m_\chi^2}\right]. \tag{6.16}$$

Here, $P_n = 1 + (m_{\chi_n^\pm}/m_\chi)^2 - \frac{1}{2}(m_{H^\pm}/m_\chi)^2 - \frac{1}{2}(m_W/m_\chi)^2$.

The zero-velocity limit of the amplitude for the process $\chi\chi \to A^0H^0$ is [134, 253]

$$\mathscr{A}(\chi\chi \to H^0A^0)_{v\to 0} = \sqrt{2}\,g^2\left\{-4\sum_{n=1}^{4} T_{H0n}\,T_{A0n}\left[\frac{m_{\chi_n}}{m_\chi P_n} - \frac{m_A^2-m_H^2}{m_\chi^2}\right] + 2\frac{m_Z}{m_\chi}\frac{\cos(\alpha+\beta)\cos 2\beta}{2\cos\theta_W}\frac{T_{A00}}{4-m_A^2/m_\chi^2} - \frac{\sin(\alpha-\beta)\,O''_{L00}}{2\cos^2\theta_W}\frac{m_A^2-m_H^2}{m_Z^2}\right\}, \tag{6.17}$$

and that for the process $\chi\chi \to A^0H^0$ is [134, 253]

$$\mathscr{A}(\chi\chi \to h^0A^0)_{v\to 0} = \sqrt{2}\,g^2\left\{-4\sum_{n=1}^{4} T_{h0n}\,T_{A0n}\left[\frac{m_{\chi_n}}{m_\chi P_n} - \frac{m_A^2-m_h^2}{m_\chi^2}\right] - 2\frac{m_Z}{m_\chi}\frac{\sin(\alpha+\beta)\cos 2\beta}{2\cos\theta_W}\frac{T_{A00}}{4-m_A^2/m_\chi^2} - \frac{\cos(\alpha-\beta)\,O''_{L00}}{2\cos^2\theta_W}\frac{m_A^2-m_h^2}{m_Z^2}\right\}, \tag{6.18}$$

Here, $P_n = 1 + (m_{\chi_n}/m_\chi)^2 - \frac{1}{2}(m_A/m_\chi)^2 - \frac{1}{2}(M/m_\chi)^2$, where M is either m_{h0} or m_{H0} as appropriate.

The cross section for any of the above processes, in terms of its given amplitude, is

$$\sigma(\chi\chi \to XY)_{v\to 0}\,v = \frac{\beta_{XY}}{128\pi m_\chi^2}\,|\mathscr{A}(\chi\chi \to XY)_{v\to 0}|^2. \tag{6.19}$$

6.4. Fermion final states

The annihilation of neutralinos to a fermion–antifermion pair displays several important features. First, given the expectation that the neutralino mass is of order or greater than 10 GeV, the light fermions will always be an open annihilation channel. For many interesting neutralino masses, other channels will be closed or suppressed, so that fermionic final states are often the only open channels. Second, in the limit of zero relative velocity for the annihilating neutralino, there is a suppression of the cross section for the fermionic final state due to helicity constraints [136]. Neutralinos are Majorana fermions, equivalent to their own antiparticles, and thus two neutralinos in a relative s-wave must have their spins oppositely directed by Fermi statistics. Therefore, the final state fermion and antifermion must as well have their spins oppositely directed, and this implies that the amplitude for the process carries a factor of the fermion mass, accounting for the required helicity flip. This result can also be seen by noting that the initial state has CP $= -1$, and the final state must as well, since the interaction is assumed to be CP conserving. The resulting suppression of the s-wave amplitude for the cross section is of order m_f^2/m_χ^2. The suppression of the light fermionic final states is due purely to the fact that these fermions are relatively light compared to the energy scale, $2m_\chi$, for the process. Of course there is no suppression of the top-quark final state if that channel is open (unless the neutralino is much heavier than the top quark). In fact, since the cross section to fermion final states depends on the square of the fermion mass, the top-quark final state is the dominant annihilation channel in many models where the neutralino is heavier than the top quark.

The cross section for neutralino–neutralino annihilation to light fermions was first calculated for general neutralinos in Ref. [125] and subsequently in Refs. [130, 131]. More recently, these cross sections have been extended to include right–left sfermion mixing for the general neutralino in [253].

The diagrams for neutralino–neutralino annihilation to the $f\bar{f}$ final state are shown in Fig. 16. The cross section contains contributions from t- and u-channel exchange of all six sfermions which can couple to f, and from s-channel exchange of Z^0 and all three neutral Higgs bosons. The results of Ref. [253] are easily extended to include flavor-off-diagonal sfermion mixing. First we define the following helicity amplitudes:

$$
\begin{aligned}
A(^1S_0)_i = \sum_{j=1}^{6} \Bigg\{ & [(X'_{fij0})^2 + (W'_{fij0})^2] \left[1 + v^2 \left(-\frac{1}{2P_j} + \frac{\beta_f^2}{3P_j^2} \right) \right] \frac{m_{f_i}}{m_\chi P_j} \\
& + 2X'_{fij0} W'_{fij0} \frac{1}{P_j} \left[1 + v^2 \left(\frac{1}{4} - \frac{1}{2P_j} - \frac{\beta_f^2}{6P_j} + \frac{\beta_f^2}{3P_j^2} \right) \right] \Bigg\} \\
& + \frac{2g^2}{\cos^2\theta_W} O''^{L}_{00} T_3(f_i) \frac{m_{f_i} m_\chi}{m_Z^2} + \frac{4g T_{A00} h_{Aff}}{4 - (m_A/m_\chi)^2 + i\Gamma_A m_A/m_\chi^2} \left(1 + \frac{v^2}{4} \right); \qquad (6.20)
\end{aligned}
$$

$$
\begin{aligned}
A(^3P_{00})_i = \overline{\beta_f} \sum_{j=1}^{6} & \left\{ - X'_{fij0} W'_{fij0} \left(\frac{1}{P_j} - \frac{2}{3P_j^2} \right) + [(X'_{fij0})^2 + (W'_{fij0})^2] \frac{m_{f_i}}{m_\chi P_j^2} \right\} \\
& - \overline{\beta_f} \sum_{k = H^0, h^0, A^0} \frac{2g h_{kff} T_{k00}}{4 - (m_k/m_\chi)^2 + i\Gamma_k m_k/m_\chi^2}; \qquad (6.21)
\end{aligned}
$$

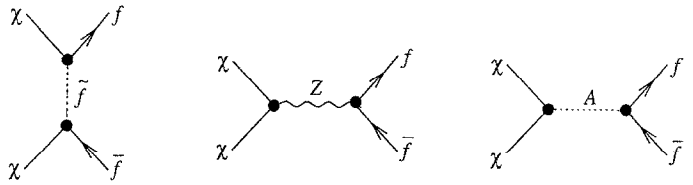

Fig. 16. Diagrams contributing to neutralino annihilation into fermions.

$$A(^3P_{10})_i = \sum_{j=1}^{6} \left\{ \frac{m_{f_i}}{m_\chi P_j} [(X'_{fijo})^2 - (W'_{fijo})^2] \right\}$$

$$- 2g^2 \frac{O''^{L}_{00}}{\cos^2\theta_W} \frac{m_{\tilde{f}_i}}{m_\chi} \frac{(T_3(f_i) - 2e_{f_i}\sin^2\theta_W)}{4 - (m_Z/m_\chi)^2 + i\Gamma_Z m_Z/m_\chi{}^2}; \tag{6.22}$$

$$A(^3P_{11})_i(\lambda) = \sum_{j=1}^{6} \left\{ \lambda\bar{\beta}_f [(X'_{fijo})^2 + (W'_{fijo})^2] \left(-\frac{1}{P_j} + \frac{1}{P_j^2} \right) \right.$$

$$\left. + [(X'_{fijo})^2 - (W'_{fijo})^2] \left(\frac{1}{P_j} - \frac{\bar{\beta}_f^2}{P_j^2} \right) + 2\bar{\beta}_f \lambda X'_{fijo} W'_{fijo} \frac{m_{f_i}}{m_\chi P_j^2} \right\}$$

$$+ \frac{2g_Z^2 O''^{L}_{00} [\lambda T_3(f_i)\bar{\beta}_f - (T_3(f_i) - 2e_{f_i}\sin^2\theta_W)]}{4 - (m_Z/m_\chi)^2 + i\Gamma_Z m_Z/m_\chi{}^2}; \tag{6.23}$$

$$A(^3P_{20})_i = \bar{\beta}_f \sum_{j=1}^{6} \left\{ \frac{1}{P_j^2} \left[\frac{m_f}{m_\chi} [(X'_{fijo})^2 + (W'_{fijo})^2] + 2X'_{fijo} W'_{fijo} \right] \right\}; \tag{6.24}$$

$$A(^3P_{21})_i(\lambda) = \bar{\beta}_f \sum_{j=1}^{6} \left\{ \frac{1}{P_j^2} \left[-[(X'_{fijo})^2 + (W'_{fijo})^2] + \bar{\beta}_f \lambda [(X'_{fijo})^2 - (W'_{fijo})^2] \right. \right.$$

$$\left. \left. - 2(m_{f_i}/m_\chi) X'_{fijo} W'_{fijo} \right] \right\}. \tag{6.25}$$

Where $P_j = 1 + (m_{\tilde{f}_j}/m_\chi)^2 - (m_{f_i}/m_\chi)^2$. The subscript i refers to the fermion type whose cross section is being considered. The sum on j is over the six sfermion states which can couple to the fermion. f_i. Recall that for each fermion there are two sfermions, corresponding to the superpartners of the right-handed and left-handed components of the fermion. Considering generational replication, this means that there are six sfermions which share the same charge. These sfermions will generically mix amongst themselves, as discussed in Appendix A. Often in the literature a less general sfermion mixing structure is assumed, but for completeness we have given the simple modification required to handle the most general case; in fact, for numerical purposes it is easier to consider the general case since all calculations can then be done in a basis independent fashion. The masses and couplings are defined in Appendix A. The weak isospin of the fermion is denoted

$T_3(f_i)$. The last index on the coupling matrices X' and W' is the neutralino index, which has been set to zero, indicating that we are interested in annihilations of the lightest neutralino.

The sum on k is over the three neutral Higgs bosons, and the T_{k00} are the Higgs–neutralino–neutralino couplings defined in Appendix A. The h_{kff} are the Higgs–fermion–antifermion Yukawa couplings also defined in Appendix A.

Given the above amplitudes, the cross section for annihilation into the fermion final state $f_i\bar{f}_i$ is

$$\sigma(\chi\chi \to f_i f_i)v = \frac{1}{4}\frac{c_f\beta_f}{8\pi s}\Big\{4|A(^1S_0)_i|^2 + \tfrac{1}{3}v^2[2|A(^3P_{00})|^2 + 2|A(^3P_{10})_i|^2 + 2|A(^3P_{11})_i(\lambda=1)|^2 + 2|A(^3P_{11})_i(\lambda=-1)|^2 + \tfrac{8}{3}|A(^3P_{20})|^2 + 2|A(^3P_{21})(\lambda=1)|^2 + 2|A(^3P_{21})(\lambda=-1)|^2]\Big\}, \tag{6.26}$$

where e_f is a color factor which equals three when the final state fermions are quarks. Again, note that both s and β_f in the prefactor, as well as in the amplitudes, contain contributions of $O(v^2)$. Therefore, to obtain the b contribution to the annihilation cross section [i.e., the $O(v^2)$ term], Eq. (6.26) must be Taylor expanded analytically to $O(v^2)$.

Cross section in the $v \to 0$ limit: Eq. (6.26) simplifies greatly in the $v \to 0$ limit, which is useful for indirect-detection calculations. The s-wave amplitude for annihilation to a fermion–antifermion pair has contributions from intermediate sfermion states, from an s-channel Z^0 boson, and from an s-channel A^0 boson [125, 130, 131, 253],

$$\mathscr{A}(\chi\chi \to \bar{f}_i\bar{f}_i)_{v\to 0} = \mathscr{A}_{sf} + \mathscr{A}_Z + \mathscr{A}_A. \tag{6.27}$$

The sfermion exchange contribution is

$$\mathscr{A}_{sf} = \sqrt{2}\sum_{j=1}^{6}\frac{1}{P_j}\left\{[(X'_{fij0})^2 + (W'_{fij0})^2]\frac{m_{f_i}}{m_\chi} + 2X'_{fij0}W'_{fij0}\right\}, \tag{6.28}$$

The sum is again over the six sfermion states which can generally couple to the fermion f_i. Note that this amplitude is proportional to the fermion mass both explicitly and through the fact that W'_f vanishes for vanishing fermion mass.

The Z^0 contribution is

$$\mathscr{A}_Z = 2\sqrt{2}\frac{g^2}{\cos^2\theta_W}O''^{L}_{00}T_3(f_i)\frac{m_{f_i}m_\chi}{m_Z^2}. \tag{6.29}$$

This amplitude is proportional to the fermion mass as it must be. In fact, the application of the CP $= -1$ condition to this amplitude explains why there is no contribution from an on-shell Z^0 and thus no resonant enhancement for $s \simeq m_Z^2$.

Finally, the Higgs contribution is

$$\mathscr{A}_A = 4\sqrt{2}g\,T_{A00}h_{Aff}\frac{1}{4-(m_A/m_\chi)^2 + i\Gamma_A m_A/m_\chi^2}, \tag{6.30}$$

Again note that the amplitude is proportional to the fermion mass (through the Yukawa couplings, h_{Aff}).

The cross section for the annihilation in the limit of zero velocity is given in terms of the zero-veloicty amplitude by

$$\sigma(\chi\chi \to \bar{f}_i f_i)_{v\to 0}\, v = \frac{c_f \beta_f}{128\pi m_\chi^2} |\mathscr{A}(\chi\chi \to \bar{f}_i f_i)|^2, \tag{6.31}$$

where $\beta_f = \sqrt{1 - m_f^2/m_\chi^2}$. As discussed above, the $v \to 0$ limit of the cross section for annihilation to fermion–antifermion pairs is proportional to the fermion mass. Therefore, the $v \to 0$ cross section for annihilation to neutrinos is zero. Furthermore, for the vast majority of neutralinos often considered, annihilation to light (i.e., u, d, and s) quarks and leptons (e and μ) is negligible in comparison with annihilation to the τ lepton and heavy (i.e., c, b, and t) quarks. Finally, if the neutralino is heavy enough to annihilate to top quarks ($m_\chi > m_t$), then annihilation occurs essentially entirely to top quarks in most models usually considered.

QCD corrections: The results presented above are strictly correct only at tree level. Radiative corrections to the cross sections for annihilation to leptons should be negligible. On the other hand, QCD corrections to the tree-level cross sections for annihilation to quarks can be significant, as seen in electron–positron annihilation to quarks in accelerators. These corrections, which come from virtual intermediate states and soft-gluon emission, can be accounted for, at leading logarithmic order, by use of the running quark masses in the above expressions [252]. Expressions for the running b and c quark masses are given in Eqs. (2.21)–(2.23) of Ref. [252]. To illustrate, if the neutralino mass is 80 GeV, the running e-quark mass is about $\frac{3}{5}$ times its tree-level value and the running b-quark mass is about $\frac{3}{4}$ times its tree-level value. The $v \to 0$ cross sections to quarks are proportional to the square of the quark mass, so QCD corrections reduce the $v \to 0$ cross sections to b and c quarks in this case by roughly a factor of two.

Although these corrections can be substantial for the $v \to 0$ limit of the cross section, they are less important for the terms proportional to v^2. Therefore, these QCD corrections must be included in the annihilation cross sections used in calculations of energetic-neutrino rates, but they may be ignored in relic-abundance calculations.

Now consider the process $\chi^0\chi^0 \to \bar{q}qg$, which falls under the general heading of QCD corrections to the tree-level annihilation to quark–antiquark pairs. Because of the possibility of emission of very soft unobserved gluons, the two processes are in fact inextricably linked. In order to calculate the complete $\mathcal{O}(\alpha_s)$ amplitude, one must calculate the vertex correction at the $\bar{q}$–q emission point as well as the graphs with the final state gluon radiation. The complete infrared finite result is then obtained according to the Bloch–Nordsieck prescription for such radiative processes [259, 260]. This $\mathcal{O}(\alpha_s)$ amplitude has been calculated [261] with the result that the correction is never more than 15% of the total cross section and will not substantially effect relic-abundance calculations. However, the correction can be important for s-wave annihilation, under conditions similar to those for which the two-gluon annihilation is important. The amplitude has also been calculated in the limit that the quark mass vanishes, in which case it turns out that the resulting gluon radiation graphs are actually infrared finite [252]. Although this calculation does not provide a complete $\mathcal{O}(\alpha_s)$ result, it is arguably useful in the case of interest, i.e., the case that the quark mass is negligible.

6.5. *Gluon final states*

In models where the neutralino annihilates predominantly to light fermions, the two-gluon final state may be important for indirect-detection calculations. WIMPs in the halo, Sun, and Earth move with velocities $v \lesssim 10^{-3}$, so annihilation proceeds only through the s wave. But s-wave annihilation to light fermions is suppressed by a factor $(m_f/m_\chi)^2$. On the other hand, annihilation to two gluons is *not* helicity suppressed in the $v \to 0$ limit. Therefore, even though annihilation to gluons is formally suppressed by a factor α_s^2, s-wave annihilation into gluons may in some cases be comparable to, or even stronger than, annihilation into fermions [252, 262, 263]. This effect could be important, for example, if the neutralino is too light to annihilate to gauge or Higgs bosons. It could also be important in models-such as those in which the neutralino is primarily gaugino-where although heavier than the W boson and lighter than the top quark, the neutralino still annihilates primarily into light fermions. The two-gluon final state will almost always be negligible for models where $m_\chi > m_t$. Furthermore, it can always be neglected in relic-abundance calculations, since annihilation into light-fermion final states can proceed through the p wave, short-circuiting the helicity suppression.

The cross section for annihilation to a pair of gluons is complicated since it arises first at one-loop order [252]. The diagrams for the process $\chi\chi \to gg$ are shown in Fig. 17. Annihilation to gluons in the $v \to 0$ limit proceeds by quark–squark loops and by s-channel exchange of A^0 and Z^0 bosons. Define an amplitude for this process, $\mathscr{A}_{gg}$, so that the cross section is given by

$$\sigma_{gg} v = |\mathscr{A}_{gg}|^2 \, [\alpha_s^2 \, m_\chi^2/(8\pi^3)]. \tag{6.32}$$

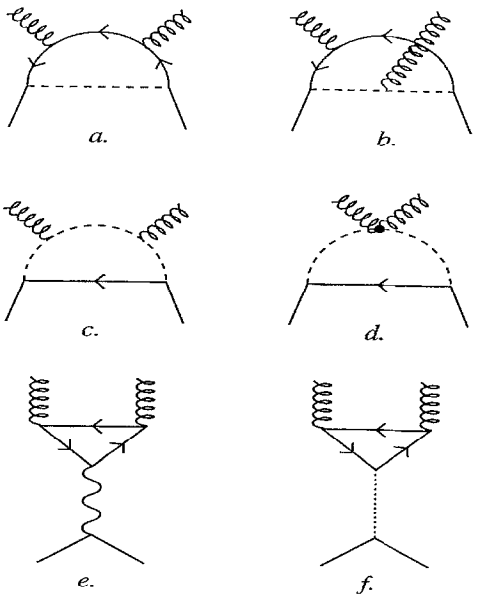

Fig. 17. Diagrams contributing to neutralino annihilation into gluons: (a)–(d) Quark–squark loops; (e), (f) the exchange of the Z^0 boson or the pseudoscalar Higgs boson A^0. From Ref. [252].

The imaginary part of the amplitude is given by

$$\mathrm{Im}\,\mathscr{A}_{gg} = -\pi \sum_{q_i} \theta(m_\chi^2 - m_{q_i}^2) \ln \frac{1+\beta_{q_i}}{1-\beta_{q_i}} \times \left\{ \sum_{\tilde{q}_j} \left[\frac{1}{m_{\tilde{q}_j}^2 + m_\chi^2 - m_{q_i}^2} \left(\frac{1}{2}\right) \left(S_{ij} \frac{m_{q_i}^2}{m_\chi^2} + D_{ij} \frac{m_{q_i}}{m_\chi} \right) \right] \right.$$
$$\left. + \frac{m_{q_i}}{m_\chi} \frac{h_{Aqq}\, T_{A00}}{(4m_\chi^2 - m_A^2)} - \frac{m_{q_i}^2}{m_\chi^2 m_Z^2}\, T_3(q_i)\, \frac{g^2 O''_{L00}}{4\cos^2\theta_W} \right\}, \tag{6.33}$$

where $\beta_q = \sqrt{1 - m_q^2/m_\chi^2}$ The real part of $\mathscr{A}_{gg}$ is given by

$$\mathrm{Re}\,\mathscr{A}_{gg} = \sum_{q_i} \left[\sum_{\tilde{q}_j} \tilde{S}(a_j, b_{ij}, i, j) + 2I\left(\frac{m_{q_i}^2}{m_\chi^2}\right) \frac{m_{q_i}}{m_\chi} \left(-\frac{T_{A00} h_{Aqq}}{(4m_\chi^2 - m_A^2)} + \frac{m_{q_i}}{m_\chi}\, T_3(q_i)\, \frac{g^2 O''_{L00}}{m_Z^3 4\cos^2\theta_W} \right) \right], \tag{6.34}$$

where the squark exchange term is

$$S(a,b,i,j) = -\frac{1}{2m_\chi^2} \int_0^1 dx \left(\frac{S_{ij}}{x} \ln \left| \frac{x^2 a + x(b-1-a) + 1}{-x^2 a + x(b-1+a) + 1} \right| \right.$$
$$+ \frac{S_{ij} b + D_{ij}\sqrt{ab}}{1+a-b} \left(\frac{1}{1-x} + \frac{1}{1+x} \right) \ln \left| \frac{x^2 a + x(b-a-1) + 1}{b + a(1-x^2)} \right|$$
$$+ \frac{1}{1-b+xa} \left[S_{ij} b \left(\frac{1}{x} + \frac{1}{1-x} \right) + D_{ij}\sqrt{ab}\, \frac{1}{1-x} \right] \ln \left| \frac{b}{x^2 a - x(a+b-1) - 1} \right|$$
$$\left. + \frac{1}{b-1+ax} \left[S_{ij} b \left(\frac{1}{x} - \frac{1}{1+x} \right) - D_{ij}\sqrt{ab}\, \frac{1}{x+1} \right] \ln \left| \frac{b}{x^2 a + x(b-1-a) + 1} \right| \right) \tag{6.35}$$

and where $a_j \equiv m_\chi^2/m_{\tilde{q}_j}^2$ and $b_{ij} \equiv m_{q_i}^2/m_{\tilde{q}_j}^2$, and it is important to note that the sign of $\sqrt{a_j b_{ij}}$ is the sign of m_χ. The couplings which appear here are combinations of the fundamental quark–squark–neutralino coupling matrices X'_q and W'_q, $S_{ij} = ((X'_{qij0})^2 + (W'_{qij0})^2)/2$ and $D_{ij} = X'_{qij0} W'_{qij0}$.

The function $I(x)$ appearing in the contribution from A^0 and Z^0 exchange is a one-loop three-point integral,

$$I(x) = \begin{cases} -\frac{1}{4}\left[\ln^2 \dfrac{1+\sqrt{1-x}}{1-\sqrt{1-x}} - \pi^2 \right] & \text{for } x \le 1, \\ \left[\arctan \dfrac{1}{\sqrt{x-1}} \right]^2 & \text{for } x > 1. \end{cases} \tag{6.36}$$

The sum over quarks in the above is taken over all up-type and down-type quarks, and for each such quark the sum over squarks is taken over the six squark states coupling to the quark.

When evaluated numerically, it is found that annihilation to the two-gluon final state can dominate annihilation to tree-level final states when the neutralino is very nearly pure gaugino (but lighter than the top quark), and it can be comparable when the neutralino is a mixed state. It is generally not significant when the neutralino is purely higgsino.

In addition to the two-gluon final state, the three-body $q\bar{q}g$ final state (which arises at lower order in perturbation theory) should also be considered [252, 261]. It seems to be the case, however, that the $q\bar{q}g$ final state may be more important than the gg final state only in regions of parameter space where the gg final state is itself unimportant. Therefore, the $q\bar{q}g$ final state can safely be ignored in most models [252].

6.6. *Photon final states*

Annihilation to photon pairs may have interesting observational consequences [263–266]. and will be further discussed in Section 10.3. This annihilation process is the most complicated of the two-body annihilation channels, possessing all the structure of the two-gluon channel plus several extra contributions.

The diagrams for the process $\chi\chi \to \gamma\gamma$ are shown in Fig. 18. Annihilation proceeds via sfermion–fermion and charged–Higgs–chargino loops, which are similar to those that appear in the two-gluon amplitude (see Fig. 17), and by chargino –W-boson loops. The calculation of the amplitude for annihilation to photon pairs has a long history, and there exist several partial calculations in the literature. The calculation of Ref. [263] was carried out assuming that the neutralino was a pure photino or higgsino state, and in the limit of large sfermion masses. The calculation of Ref. [265] was also carried out in the limit of large sfermion masses but with an

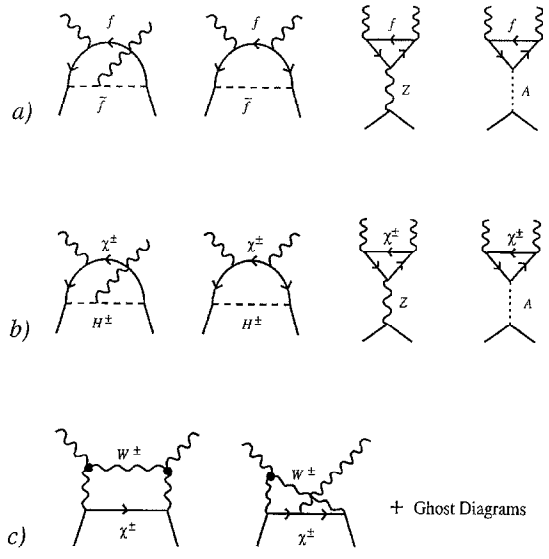

Fig. 18. Diagrams contributing to neutralino annihilation into photons: (a) fermion–sfermion loops, (b) charged-Higgs–chargino loops, and (c) chargino–W-boson loops. From Ref. [266].

arbitrary neutralino state mixture. Ref. [264] calculated the fermion–sfermion loop contributions for arbitrary squark masses, but only for a pure photino. In Ref. [267], the contribution from intermediate W-boson states was calculated in a leading-logarithmic approximation, and subleading terms were further included the Ref. [266]. These diagrams are potentially of interest if the neutralino is heavier than the W boson and primarily higgsino. A complete calculation of the W-boson loops has yet to be done. These results for the $\chi\chi \to \gamma\gamma$ cross section including all the contributions shown in Fig. 18 for a neutralino of arbitrary mass and composition were recently collected in Ref. [266]. The expressions in Ref. [266] are given in the same notation as used here, so we refer the reader there for the detailed results.

In addition, s-wave annihilation to the $Z^0\gamma$ final state is also accessible at the same order in perturbation theory through gauge-boson loops [267]. This should be most important for a neutralino that is primarily higgsino. The final state photon will again be monoenergetic, and for large neutralino masses, $m_\chi \gg m_Z$, its energy should be very nearly the same as the energy of the photons in the two-photon channel, $E_\gamma \simeq m_\chi$. A complete calculation of the cross section for this process has not been done. However, in the leading-logarithmic approximation, one can show that for annihilation through gauge-boson loops, the cross section for the process $\chi\chi \to Z^0\gamma$ should be roughly $\cot^2\theta_W \simeq 3.4$ times as large as that for the process $\chi\chi \to \gamma\gamma$.

6.7. *Summary of neutralino annihilation*

Table 2 summarizes the results for the neutralino annihilation cross sections. Listed are all the two-body final states that occur at tree level, as well as those one-loop amplitudes we have discussed that may also be important.

Table 2
Neutralino–neutralino annihilation channels. The numbers refer to equation numbers in which the cross sections are given. For the fermion–antifermion final states, $f = \nu_l\nu_l$, ll, qq, for $l = e, \mu, \tau$ and $q = u, d, s, c, b, t$. For the $f\bar{f}$ final states, $a \propto m_f^2$, so in particular, $(\sigma v)_{v\to 0} = 0$ for annihilation to $\bar{\nu}\nu$. In addition, for annihilation into u, d, and s quarks, $(\sigma v)_{v\to 0}$ is essentially negligible. N/A indicates that the p-wave annihilation cross section (i.e., b) has not been computed for these final states. However, b is required only for the relic-abundance calculation, and for this purpose, the b contribution for these final states should be negligible

Annihilation channel	σv	$(\sigma v)_{v\to 0}$
$f\bar{f}$	(6.26)	(6.31)
W^+W^-	(6.3)	(6.5), (6.7)
Z^0Z^0	(6.4)	(6.6), (6.7)
W^+H^-, W^-H^+	(6.10)	(6.16), (6.19)
Z^0A^0	(6.9)	0
Z^0H^0, Z^0h^0	(6.8)	(6.14), (6.15), (6.19)
A^0A^0, H^0H^0, h^0h^0, H^0h^0	(6.11)	0
A^0H^0, A^0h^0	(6.12)	(6.17), (6.18), (6.19)
H^+H^-	(6.13)	0
gg	N/A	(6.32)
$\gamma\gamma$	N/A	Eq. (2.2) in Ref. [266]

7. Elastic-scattering cross sections

7.1. The basic ingredients

When it comes to detection, the cross section for elastic scattering of a WIMP from ordinary material is perhaps its most important property. This cross section determines the detection rate in the direct-detection experiments (Section 8). It also determines the rate at which particles from the Galactic halo accrete into the Earth and Sun, and so determines the signal in the indirect-detection experiments (Section 9). We have already seen in Section 3 that if the WIMP is to have a cosmological density of order unity, then it must have some small but finite coupling to ordinary matter; otherwise, it would not have annihilated in the early Universe and it would be unacceptably overabundant today. By crossing symmetry, the amplitude for WIMP annihilation to quarks is related to the amplitude for elastic scattering of WIMPs from quarks. Therefore, a WIMP that solves the dark-matter problem is generically expected to have some small, but non zero, coupling to nuclei (through the coupling to quarks). As a result, we expect there to be finite (although small) detection rates in generic models.

The WIMP–nucleus elastic-scattering cross section depends fundamentally on the WIMP–quark interaction strength; however, since it is the WIMP–nuclei cross sections which enter, the distribution of quarks in the nucleon and the distribution of nucleons in the nucleus play a crucial role. Thus the calculation of WIMP–nuclei interactions must take place in three steps.

The first step is the calculation of the interactions of WIMPs with quarks and gluons. In practice, straightforward diagrammatic calculations give the effective interactions of neutralinos at the microscopic level. Such calculations yield the coefficients in an effective Lagrangian for the interactions of neutralino with quarks and gluons. Since diagrams with internal quark loops appear, the couplings of neutralinos with all six quarks as well as gluons are required. These couplings, as well as the masses of the exchanged particles and other important quantities, are determined by parameters of the supersymmetric model, and even in simplified versions of the model there are typically many possible values allowed. Thus, the fundamental elastic-scattering cross section cannot be determined uniquely and is subject to a great deal of model uncertainty. Limits from accelerator searches for SUSY particles, as well as cosmological constraints, reduce the parameter space somewhat, but this model uncertainty is probably the largest uncertainty in the predicted rate for detection of SUSY dark matter.

The next step is translation of the microscopic interactions into interactions with nucleons, using the matrix elements of the quark and gluon operators in a nucleon state. One extracts these hardronic matrix elements from appropriate scattering data whenever possible. Subtleties such as the strangeness content of the nucleon enter. In addition, in the effective-Lagrangian approach there are several qualitatively different types of interaction: vector, axial-vector, scalar, pseudoscalar, and tensor, and in principle these add very differently inside the nucleon. For example, axial-vector interactions probe the up, down, and strange contributions to the spin of the nucleon, quantities which are still not well determined either theoretically or experimentally. All this implies additional uncertainty in the final elastic-scattering cross section.

In the final step, using nuclear wave functions, the spin and scalar components of the nucleons must be added coherently to give the matrix element for the WIMP–nucleus cross section as a function of momentum transfer. This is done by sandwiching the nucleon operators from the

above step in a nuclear state. This step introduces a form-factor suppression (or "coherence loss") analogous to that in low-energy electromagnetic scattering of electrons from nuclei, which reduces the cross section for heavy WIMPs and heavy nuclei. It also means that results can depend upon complicated calculations of nuclear wave functions, another source of uncertainty. For a more complete discussion of the nuclear physics of dark-matter detection, see Ref. [23].

An important simplification in these calculations occurs because the elastic scattering of dark-matter WIMPs takes place in the extreme nonrelativistic limit. In particular, the axial-vector current becomes an interaction between the quark spin and the WIMP spin, while the vector and tensor currents assume the same form as the scalar interaction. Furthermore, neutralinos do not have vector interactions since they are Majorana fermions. So generically, only two cases need to be considered: the spin–spin interaction and the scalar interaction. In the case of the spin–spin interaction, the WIMP couples to the spin of the nucleus; in the case of the scalar interaction, the WIMP couples to the mass of the nucleus. This division was recognized early by Goodman and Witten [9] in their seminal paper on direct detection. Since then, much work has been done, and several new contributions to the cross section have been found, but it is still only these two cases which are important. For the neutralino, both scalar and spin interactions contribute and the two cases will be considered separately. The complete elastic-scattering cross section is the sum of these two pieces.

In the following, we will examine each type of interaction, noting the results of the microscopic calculations and the results of the translation to an interaction with nuclei.

7.2. *Axial-vector (spin) interaction*

The Feynman diagrams which give rise to the WIMP–nucleus axial-vector interaction are shown in Fig. 19. The microscopic axial-vector interaction of a neutralino with a quark q is given by

$$\mathscr{L}_{\mathrm{A}} = \mathrm{d}_{\mathrm{q}} \bar{\chi}\gamma^{\mu}\gamma_5\chi\,\bar{q}\gamma_{\mu}\gamma_5 q\,, \tag{7.1}$$

where d_{q} is a coupling which can be written in terms of the fundamental couplings of the theory as [9, 23, 130, 131, 268, 269]

$$d_{\mathrm{q}_i} = -\frac{g^2 T_{3\mathrm{q}}}{4m_{\mathrm{W}}^2} O''^{\mathrm{R}}_{00} + \frac{1}{8}\sum_{j=1}^{6} \frac{(X'_{\mathrm{q}ij0})^2 + (W'_{\mathrm{q}ij0})^2}{m^2_{\tilde{\mathrm{q}}_j} - (m_{\chi} + m_{\mathrm{q}_i})^2}\,. \tag{7.2}$$

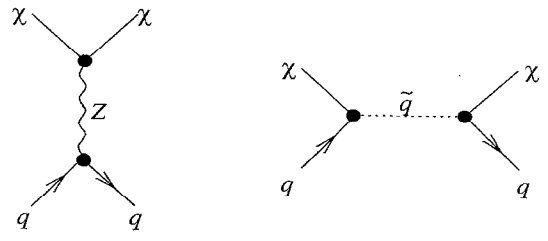

Fig. 19. Feynman diagrams contributing to the spin-dependent elastic scattering of neutralinos from quarks.

The subscript q_i refers to quark type; the subscript q denotes the quark sector (up or down), and $i = 1, 2, 3$ is used to denote the flavor of the quark within that sector (e.g., $q_i = d, s, b$ if q refers to the down-quark sector). The first term in Eq. (7.2) comes from Z^0 exchange, and the second term comes from squark exchange. Thus, the sum on j is over all six squarks which can couple to a given quark. For further clarification, one can check the definition of the couplings X' and W' given in Eq. (A.32).

Spin content of the nucleon: The first step in the calculation is to evaluate the matrix element of the above quark axial-vector current in a nucleon. These matrix elements are proportional to the spin of the nucleon, with coefficients that can be extracted from data on polarized deep-inelastic scattering. We write

$$\langle n | \bar{q}\gamma_\mu\gamma_5 q | n \rangle = 2s_\mu^{(n)} \Delta q^{(n)} , \tag{7.3}$$

where the quantities Δq are extracted from data obtained in lepton–proton scattering, and $s_\mu^{(n)}$ is the spin of the nucleon n, which can be either a proton or a neutron. The values of the Δq's are not determined experimentally to great precision, and the values obtained are somewhat puzzling from a theoretical point of view. In Table 3, we give several determinations of these parameters. In terms of the quantities determined by measurements of the nucleon spin structure functions (that is, the first moment of the proton spin-dependent structure function, Γ, the total quark spin contribution to the nucleon spin, $\Delta\Sigma$, and $\Delta s^{(p)}$), the u- and d-quark matrix elements are $\Delta u^{(p)} = 6\Gamma - \frac{1}{3}\Delta\Sigma$ and $\Delta d^{(p)} = \frac{4}{3}\Delta\Sigma - 6\Gamma - \Delta s$ (neglecting small corrections due to the running of the strong-coupling constant) [270]. We list the quantities predicted by the naive quark model (NQM) [9, 271, 272], as well as values determined by an earlier experiment (EMC) [270, 273], a more recent experiment (SMC) [274], as well as a compilation of all the experimental data (All) [274]. Also listed are values obtained using the 1σ error on $\Delta\Sigma$ from the compilation. The uncertainties in the Δq's are illustrated by the spread of the values in Table 3; the most significant uncertainties are those associated with Δs.

The related quantities for a neutron are obtained from these by an isospin rotation, $u \leftrightarrow d$; that is $\Delta s^{(p)} = \Delta s^{(n)}$, $\Delta u^{(p)} = \Delta d^{(n)}$, $\Delta d^{(p)} = \Delta u^{(n)}$. So we write the effective interaction of neutralinos with a nucleon as

$$\mathcal{L}_A = \bar{\chi}\gamma^\mu\gamma_5\chi\bar{n}s_\mu n \sum_{q=u,\,d,\,s} 2d_q \Delta q^{(n)} . \tag{7.4}$$

Table 3
Quark spin content of the proton determined from the SU(3) naive quark model (NQM) [9, 271, 272] and for measured spin-dependent structure functions from EMC [270, 273], SMC [274], and a compilation (All) [274]. Also listed are values using the 1σ error on $\Delta\Sigma$ from the compilation [296]

	NQM	EMC	SMC	All	$\text{All}_{\Delta\Sigma+1\sigma}$
Γ	0.188	0.137	0.136	0.145	0.145
$\Delta\Sigma$	0.60	0.12	0.22	0.30	0.42
$\Delta s^{(p)}$	0	−0.16	−0.12	−0.09	−0.09
$\Delta u^{(p)}$	0.93	0.78	0.74	0.77	0.73
$\Delta d^{(p)}$	−0.33	−0.50	−0.40	−0.38	−0.22

Uncertainties in the experimentally determined values for the quantities Δ_q can lead to significant variations in the WIMP–nucleon axial-vector coupling, and therefore to the predicted rates for detection of WIMPs which have primarily spin couplings to nuclei. For example, neutralinos that are pure B-ino in models with no squark mixing are among the likeliest candidates for detection via the axial-vector interaction. However, by varying the Δ_q's within the acceptable experimental uncertainty, the coupling of such particles to neutrons may be reduced by more than an order of magnitude relative to the value obtained by using the central values for Δ_q. This comes about because there is a potential cancellation between the various Δ_q's that can occur. On the other hand, for the particular case of pure B-inos, the coupling of WIMPs to protons is much more robust. Future measurements of the spin structure functions are likely to reduce this uncertainty somewhat, but for the time being there will be a significant uncertainty in the predicted event rates for detectors with nuclei in which the spin is carried primarily by an unpaired neutron.

Nuclear matrix elements and form factors: The next step is evaluation of the matrix elements of the nucleon spin operators in the nuclear state. At zero momentum transfer, this is equivalent to calculating the average spins for neutrons and protons in the given nucleus; at nonzero momentum transfer there is also a form-factor suppression which must be calculated from nuclear wave functions. At this stage, it is convenient to introduce the isoscalar (a_0) and isovector (a_1) parameterization of the matrix element, since this decomposition is natural in terms of nuclear physics. We write

$$a_p = \sum_{q=u,d,s} \frac{d_q}{\sqrt{2}G_F} \Delta q^{(p)}, \qquad a_n = \sum_{q=u,d,s} \frac{d_q}{\sqrt{2}G_F} \Delta q^{(n)},$$

$$a_0 = a_p + a_n, \qquad a_1 = a_p - a_n . \tag{7.5}$$

The interference of the isoscalar and isovector parts of the scattering amplitude gives rise to three distinct form factors, which are functions of the absolute value of the momentum transfer $q = |\boldsymbol{q}|$, and the differential cross section takes the form [23, 269]

$$\frac{d\sigma}{d|\boldsymbol{q}|^2} = \frac{8}{\pi v^2} \Lambda^2 G_F^2 J(J+1) \frac{S(|\boldsymbol{q}|)}{S(0)}, \tag{7.6}$$

where v is the velocity of the WIMP relative to the target,

$$S(q) = a_0^2 S_{00}(q) + a_1^2 S_{11}(q) + a_0 a_1 S_{01}(q), \tag{7.7}$$

and the independent form factors $S_{ij}(q)$ are obtained from detailed nuclear calculations. The quantity J is the total angular momentum of the nucleus, Λ is given by

$$\Lambda = (1/J)[a_p \langle S_p \rangle + a_n \langle S_n \rangle], \tag{7.8}$$

$\langle S_p \rangle = \langle N | S_p | N \rangle$ is the expectation value of the spin content of the proton group in the nucleus, and similarly for $\langle S_n \rangle$. Note that the cross section does not grow like J^2 because of the factor of J which appears in the normalization of Λ; this is a common misunderstanding. These quantities are found either from a detailed nuclear calculation (e.g., [269, 275]) or from a simple nuclear model.

For many nuclei, detailed nuclear calculations have not been made, and in many of these cases they are not needed, since reasonably accurate estimates can be made using the "odd-group" model [23]. This model assumes all the nuclear spin is carried by the "odd" group, either the protons or the neutrons, whichever is most unpaired. So only one of either $\langle S_n \rangle$ or $\langle S_p \rangle$ is nonzero. The value of the odd-group spin is found using the measured nuclear magnetic moment μ,

$$\langle S_{odd} \rangle = \frac{\mu - g^l_{odd} J}{g^s_{odd} - g^l_{odd}}, \tag{7.9}$$

where "odd" stands for either the proton or the neutron, $g^s_n = -3.826$, $g^s_p = 5.586$, $g^l_n = 0$, and $g^l_p = 1$. Thus for ^{29}Si, which has $J = \frac{1}{2}$, $\mu = -0.555$, and has unpaired neutrons, $\langle S_p \rangle_{29} \approx 0$, and $\langle S_n \rangle_{29} \approx 0.15$, in good agreement with the detailed nuclear shell-model calculations which have been performed for this element [269]. For ^{73}Ge, however, the odd-group model gives a very poor estimate, in disagreement with the detailed calculations of Refs. [269, 276]. Table 4 provides a summary of values for $\langle S_p \rangle$ and $\langle S_n \rangle$ from the odd-group model as well as from more detailed calculations for several nuclei commonly considered for detection of spin-coupled WIMPs.

For completeness, we mention the single-particle shell model used originally by Goodman and Witten [9], and subsequently by many authors, to estimate the spin content in the nucleus. This model assumes the entire spin of the nucleus comes from the single last unpaired proton or neutron. Thus it predicts,

$$\langle S_n \rangle = \frac{[j(j+1) - l(l+1) + \frac{3}{4}]}{(2j+2)}, \tag{7.10}$$

and $\langle S_p \rangle = 0$ for a nucleus with an unpaired neutron, and vice versa for a nucleus with an unpaired proton. However, the single-particle shell model rarely gives accurate results, and it is better to use a detailed nuclear calculation if it exists, and if it does not, the odd-group model will almost always give a more accurate estimate than the single-particle shell model.

Table 4
Comparison of odd-group model results with best estimates from more detailed calculations. EOGM is the extended odd-group model, and IBFM is the interacting–boson–fermion model

Nucleus	$\langle S_p \rangle_{OGM}$	$\langle S_n \rangle_{OGM}$	$\langle S_p \rangle$	$\langle S_n \rangle$	Model [Ref.]
^{19}F	0.46	0.0	0.415	−0.047	EOGM1 [23]
			0.368	−0.001	EOGM2 [23]
^{27}Al	0.25	0.0	−0.343	0.030	Shell model [321]
^{29}Si	0.0	0.15	−0.002	0.13	Shell model [269]
^{35}Cl	−0.15	0.0	−0.094	0.014	EOGM1 [23]
			−0.083	0.004	EOGM2 [23]
^{39}K	−0.24	0.0	−0.18	0.05	Perturbation theory [321]
^{73}Ge	0.0	0.23	0.011	0.491	Shell model [269]
			0.030	0.378	Hybrid [276]
^{93}Nb	0.36	0.0	0.46	0.08	Shell model [275]
^{131}Xe	−0.041	−0.236	0.0	−0.166	IBFM [419, 296]

The full momentum dependence of the form factors must be calculated from detailed nuclear models, and the results are especially important for heavier nuclei. We choose to fit these form factors to polynomials, with an explicit cutoff on the range of validity of the fit. In terms of the variable $y = 0.25b^2|\boldsymbol{q}|^2$, where $b = (1\text{ fm})A^{1/6}$, and A is the atomic mass number of the nucleus, we write

$$S_{ij} = \sum_k c_{ij}^{(k)} y^k. \tag{7.11}$$

The fit coefficients for several nuclei are given in Table 5.

Cross section: In general, we will write the differential cross section as

$$\frac{\mathrm{d}\sigma}{\mathrm{d}|\boldsymbol{q}|^2} = G_F^2 \frac{C}{v^2} F^2(|\boldsymbol{q}|) = \frac{\sigma_0}{4m_r^2 v^2} F^2(|\boldsymbol{q}|)\,, \tag{7.12}$$

where C is a dimensionless number that carries all the particle-physics model information, the form factor F is normalized so that $F(0) = 1$, the reduced mass is $m_r = m_N m_\chi/(m_N + m_\chi)$ where m_N is the

Table 5
Polynomial fits to momentum dependence of the spin-dependent form factors for several nuclei. The polynomial fits are valid for values of y less than y_{cut}. For larger values of y, the form factor should be set equal to zero. Results for ^{73}Ge are based on Ref. [276], and those for ^{27}Al and ^{39}K from Ref. [321]. Results for ^{29}Si are adapted from the exponential fits given in Ref. [269]

	$c^{(0)}$	$c^{(1)}$	$c^{(2)}$	$c^{(3)}$	$c^{(4)}$	$c^{(5)}$	$c^{(6)}$
				^{73}Ge, $y_{cut} = 1.3$			
S_{00}	0.159705	− 1.100053	3.219129	− 4.907739	4.110591	− 1.796717	0.320255
S_{01}	0.114796	− 0.910499	2.936698	− 4.808584	4.254926	− 1.941010	0.357707
S_{11}	− 0.271006	2.018922	− 6.226466	9.860608	− 8.502157	3.800620	− 0.689352
				^{29}Si, $y_{cut} = 0.25$			
S_{00}	0.00818	− 0.0362	0.0802	− 0.118	0.131	0	0
S_{01}	0.00867	− 0.0543	0.170	− 0.355	0.556	0	0
S_{11}	− 0.0169	0.0912	− 0.247	0.445	− 0.603	0	0
				^{27}Al			
S_{00}	0.0929516	− 0.472059	1.05996	− 1.01148	0	0	0
S_{01}	0.1563300	− 0.935958	2.45779	− 2.72621	0	0	0
S_{11}	0.0657232	− 0.44984	1.35041	− 1.68508	0	0	0
				^{39}K			
S_{00}	0.0094999	− 0.0619718	0.162844	− 0.194282	0.0891054	0	0
S_{01}	0.0332044	− 0.2319430	0.638528	− 0.798523	0.3809750	0	0
S_{11}	0.0298127	− 0.2176360	0.623646	− 0.814418	0.4050270	0	0

nuclear mass, and v is the WIMP speed relative to the target. For later use, we define a "standard" total cross section at zero momentum transfer:

$$\sigma_0 = \int_0^{4m_r^2v^2} \frac{\mathrm{d}\sigma(q=0)}{\mathrm{d}|\boldsymbol{q}|^2}\mathrm{d}|\boldsymbol{q}|^2 = 4G_F^2 m_r^2 C \,. \tag{7.13}$$

Note that σ_0 is *not* really the total cross section. The total cross section is obtained by integrating (7.12) over $\mathrm{d}|\boldsymbol{q}|^2$, which includes the form-factor suppression. However, it is the quantity σ_0 defined in (7.13) that appears in our expressions for direct- and indirect-detection rates in the following sections. This is discussed in further detail in Section 8.

For the spin-interaction case above,

$$C_{\mathrm{spin}} = (8/\pi)\Lambda^2 J(J+1)\,, \tag{7.14}$$

with

$$F^2(|\boldsymbol{q}|) = S(|\boldsymbol{q}|)/S(0)\,, \tag{7.15}$$

so that

$$\sigma_{0\mathrm{spin}} = (32/\pi)G_F^2 m_r^2 \Lambda^2 J(J+1)\,. \tag{7.16}$$

7.3. Scalar interaction

Microscopic interactions other than the axial-vector interaction can be very important and will often dominate the spin interaction for heavier nuclei. The scalar neutralino–nucleon interaction arises from several sources. First, as illustrated in Fig. 20, there are contributions from squark exchange and Higgs exchange which give rise to couplings to quark currents. Second, there are one-loop amplitudes for interactions of neutralinos with gluons, as shown in Fig. 21. The importance of the neutralino coupling to gluons through heavy-quark loops was pointed out in Ref. [131] following a similar argument for coupling of heavy Majorana neutrinos to nucleons [277]. The neutralino–gluon coupling which arises through exchange of the light (h^0) [278] and heavy (H^0) [256] Higgs bosons can be very important because the lightest Higgs boson may often be far lighter than the squarks. In Ref. [279], it was pointed out that the scalar coupling of the neutralino to the quark current, especially the strange quarks, which arises from the diagrams in Fig. 20, may also be quite substantial. Significant scalar couplings to nuclei arise if the neutralino is a mixed gaugino/higgsino state. As pointed out in Ref. [280], and emphasized in Refs. [281, 282], mixing of right and left squarks leads to a significant scalar coupling even for neutralinos which are pure higgsino or pure gaugino.

In this subsection, we follow primarily the paper by Drees and Nojiri [282], which contains the most complete results to date for the scalar neutralino–nucleon matrix elements. In particular, the quark–squark loops are evaluated explicitly; in all previous work, these diagrams were evaluated only in the limit of large squark masses. Although the complete one-loop results for the scalar (and tensor) interactions are quite complicated, they often differ from the large-squark-mass limits, which are analytically much simpler, by more than a factor of two. Therefore, since the scalar interaction often dominates the elastic-scattering cross section, it is important to evaluate this

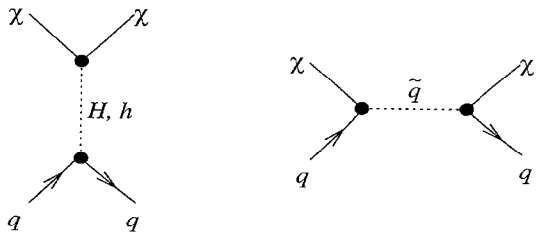

Fig. 20. Feynman diagrams contributing to the scalar elastic-scattering amplitude of a neutralino from quarks.

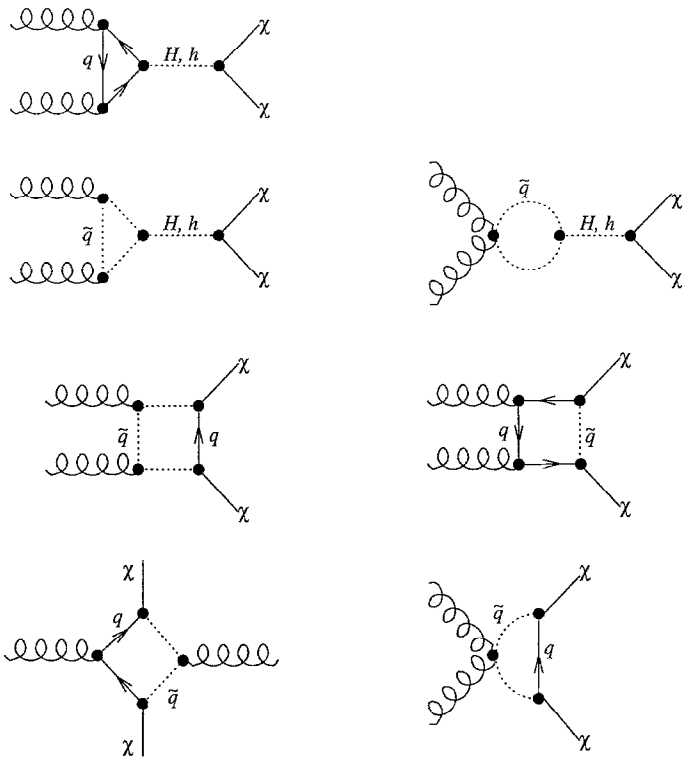

Fig. 21. Feynman diagrams contributing to the gluonic interaction with neutralinos, which contributes to the scalar elastic-scattering amplitude for neutralinos from nuclei.

contribution accurately. After we present the complete results, we will list the simpler large-squark-mass results for readers interested in obtaining quick estimates of the cross sections.

In the notation of Ref. [282], the microscopic effective Lagrangian for scalar and tensor neutralino–quark and neutralino–gluon interactions is

$$\begin{aligned}\mathscr{L}_{\mathrm{ST}} = {} & f_{\mathrm{q}}\bar{\chi}\chi\bar{q}q + g_{\mathrm{q}}[-2\mathrm{i}\bar{\chi}\gamma^{\mu}\partial^{\nu}\chi\mathscr{O}^{(2)}_{\mathrm{q}\mu\nu} - \tfrac{1}{2}m_{\mathrm{q}}m_{\chi}\bar{\mathrm{q}}\mathrm{q}\bar{\chi}\chi] \\ & + b\alpha_{\mathrm{s}}\bar{\chi}\chi G^{a}_{\mu\nu}G^{a\mu\nu} - \alpha_{\mathrm{s}}(B_{1\mathrm{D}} + B_{1\mathrm{S}})\bar{\chi}\partial_{\mu}\partial_{\nu}\chi\mathscr{G}^{(2)\mu\nu} \\ & + \alpha_{\mathrm{s}}B_{2\mathrm{S}}\bar{\chi}(\mathrm{i}\partial_{\mu}\gamma_{\nu} + \mathrm{i}\partial_{\nu}\gamma_{\mu})\chi\mathscr{G}^{(2)\mu\nu}\,, \end{aligned} \tag{7.17}$$

where the twist-two quark and gluon operators are defined by

$$\mathcal{O}^{(2)}_{q\mu\nu} = i\tfrac{1}{2}[\bar{q}\gamma_\mu \partial_\nu q + \bar{q}\gamma_\nu \partial_\mu q - \tfrac{1}{2} g_{\mu\nu} \bar{q} \not{\partial} q] ,$$
$$\mathcal{G}^{(2)\mu\nu} = G^{a\mu}_\rho G^{a\rho\nu} + \tfrac{1}{4} g^{\mu\nu} G^{a\sigma\rho} G^a_{\sigma\rho} , \tag{7.18}$$

and the coefficient b is given by

$$b = -T_{\tilde{q}} + B_D + B_S - \tfrac{1}{2} m_\chi B_{2S} - \tfrac{1}{4} m_\chi^2 (B_{1D} + B_{1S}) , \tag{7.19}$$

and $G^{\mu\nu}_a$ is the gluon field-strength tensor. The couplings to quarks are given by

$$f_{q_i} = -\frac{1}{4} \sum_{\tilde{q}_j} \frac{X'_{qij0} W'_{qij0}}{m^2_{\tilde{q}_j} - (m_\chi + m_{q_i})^2} + f^{(H)}_{q_i} ,$$
$$f^{(H)}_{q_i} = \sum_{h = h^0, H^0} \frac{g T_{h00} h_{hq_iq_i}}{2 m_h^2} ,$$
$$g_{q_i} = -\frac{1}{8} \sum_{\tilde{q}_j} \frac{(X'_{qij0})^2 + (W'_{qij0})^2}{[m^2_{\tilde{q}j} - (m_\chi + m_{q_i})^2]^2} , \tag{7.20}$$

where T_{h00} are the Higgs–neutralino–neutralino couplings given in Eq. (A.61), and $h_{hq_iq_i}$ are the Higgs–quark–quark Yukawa couplings given in Eqs. (A.66–A.67). Again, we note that the subscript q_i labels the quark type. The subscript q refers to the quark sector (up or down), while the subscript $i = 1, 2, 3$ is the flavor index within that sector.

This effective Lagrangian is specified at a high-energy scale, for example, $\mu_0 \simeq m_\chi$. Our definitions of the coefficients B_i and $T_{\tilde{q}}$ differ from those in Ref. [282] by a factor of α_s. The reason we extract these factors of α_s is that it is more natural to consider the object $\alpha_s G^{\mu\nu} G_{\mu\nu}$ as a single entity, since it is a renormalization-group invariant. In addition, the form of these coefficients is changed slightly as well when one considers the most generic flavor structure for squarks:

$$B_D = \frac{1}{32\pi} \sum_{q_i, \tilde{q}_j} m_{q_i} X'_{qij0} W'_{qij0} I_1(m_{q_i}, m_{\tilde{q}_j}, m_\chi) ,$$
$$B_S = \frac{1}{32\pi} \sum_{q_i, \tilde{q}_j} m_\chi \frac{1}{2} [(X'_{qij0})^2 + (W'_{qij0})^2] I_2(m_{q_i}, m_{\tilde{q}_j}, m_\chi) ,$$
$$B_{1D} = \frac{1}{12\pi} \sum_{q_i, \tilde{q}_j} m_{q_i} X'_{qij0} W'_{qij0} I_3(m_{q_i}, m_{\tilde{q}_j}, m_\chi) ,$$
$$B_{1S} = \frac{1}{12\pi} \sum_{q_i, \tilde{q}_j} m_\chi \frac{1}{2} [(X'_{qij0})^2 + (W'_{qij0})^2] I_4(m_{q_i}, m_{\tilde{q}_j}, m_\chi) ,$$
$$B_{2S} = \frac{1}{48\pi} \sum_{q_i, \tilde{q}_j} \frac{1}{2} [(X'_{qij0})^2 + (W'_{qij0})^2] I_5(m_{q_i}, m_{\tilde{q}_j}, m_\chi) ,$$
$$T_{\tilde{q}} = \frac{1}{96\pi} \sum_{h = h^0, H^0} \frac{g}{2} \frac{T_{h00}}{m_h^2} \sum_{\tilde{q}_j} \frac{g_{h\tilde{q}_j\tilde{q}_j}}{m^2_{\tilde{q}_j}} \tag{7.21}$$

where the I_k are as given in Eqs. (B.1a–B.1e) of Ref. [282], and the squark–squark–Higgs couplings $g_{h\tilde{q}_j\tilde{q}_k}$ are given in Eqs. (A.43–A.46). As pointed out to us by the authors, Eq. (B.1d) of Ref. [282] has

Table 6
Estimates for the nucleon parameters f_{Tq}. The u- and d-quark values are obtained from Ref. [284], and we list values reported for f_{Ts} by several authors

Nucleon	f_{Tu}	f_{Td}	f_{Ts} [285]	F_{Ts} [283, 284]	F_{Ts} [288]
n	0.023	0.034	0.14	0.46	0.08
p	0.019	0.041	0.14	0.46	0.08

three typographical errors. The factor in the first term should read $(m_{\tilde{q}}^2 - m_q^2 - m_\chi^2)$, with a corrected exponent for m_χ; the term immediately following should read $-1/m_{\tilde{q}}^2 m_\chi^4$, again with a corrected exponent for m_χ; finally, a sign in the last term should be corrected so that it reads $[\cdots - m_{\tilde{q}}^2 + m_\chi^2]L$.

Nucleonic matrix elements: The next step is to evaluate the matrix elements of the quark and gluon operators in a nucleon state. The matrix elements of the light-quark currents are obtained in chiral perturbation theory from measurements of the pion–nucleon sigma term [283–285]. For each of the three light quarks, (q = u, d, s), we write

$$\langle n | m_q \bar{q} q | n \rangle = m_n f_{Tq}^{(n)}. \tag{7.22}$$

The determination of the pion–nucleon sigma term from the data is fraught with significant uncertainties [285], which lead to uncertainties in the parameters f_{Tq} [286]. There are additional corrections that may arise from higher orders in chiral perturbation theory, but these are generally smaller. Thus, the uncertainty in the pion–nucleon sigma term is perhaps the largest source of uncertainty in this calculation.[6] Table 6 lists the values for these parameters obtained by various authors. In Refs. [283, 284], a value for the pion–nucleon sigma term of $\sigma_{\pi N} \simeq 60$ MeV was used, while Gasser et al. [285] argue that the pion–nucleon data suggest $\sigma_{\pi N} \simeq 45$ MeV, resulting in a smaller strange-quark content. In Ref. [288], even smaller values of f_{Tq} were considered, and it is worth noting that, in all the literature on supersymmetric dark matter prior to Ref. [279], the f_{Tq} were taken to be zero for the light quarks. In our numerical work, we use $f_{Ts} = 0.14$ [285].

The f_{Tq} for u and d quarks in the nucleon are included here for completeness, but they are generally small. In most models, little accuracy is lost in setting them to zero. (In some pathological cases, this might not be the case. For example, if for some reason, the up and down squarks are significantly lighter than the other squarks, the u- and d-quark currents could be important.) Furthermore, the error made in taking $f_{Tq} = 0$ for u and d quarks is usually smaller than the theoretical error due to the spread in f_{Ts}.

As pointed out by Shifman, Vainshtein, and Zakharov, heavy quarks contribute to the mass of the nucleon through the anomaly [289, 290]. Under the heavy-quark expansion, the following substitution can be made for the heavy quarks Q = c, b, t, in a nucleon matrix element [289]:

$$m_Q \bar{Q} Q \to \frac{-2\alpha_s}{24\pi} GG. \tag{7.23}$$

[6] There is a possibility that lattice calculations may be able to provide the sigma term in the near future [287].

The trace of the QCD energy-momentum tensor can therefore be written

$$\theta^{\mu}_{\mu} = m_u \bar{u}u + m_d \bar{d}d + m_s \bar{s}s + \sum_{Q=b,c,t} m_Q \bar{Q}Q - \frac{7\alpha_s}{8\pi} GG$$

$$= m_u \bar{u}u + m_d \bar{d}d + m_s \bar{s}s - \frac{9\alpha_s}{8\pi} GG \,. \tag{7.24}$$

The matrix element of this quantity is the nucleon mass,

$$m_n = \langle n | m_u \bar{u}u | n \rangle + \langle n | m_d \bar{d}d | n \rangle + \langle n | m_s \bar{s}s | n \rangle + \left\langle n \left| \frac{-9\alpha_s}{8\pi} GG \right| n \right\rangle , \tag{7.25}$$

so we find that for each of the heavy quarks, Q = c, b, t,

$$\langle n | m_Q \bar{Q}Q | n \rangle = \frac{2}{27} m_n \left[1 - \sum_{q=u,d,s} f_{Tq}^{(n)} \right] \equiv \frac{2}{27} m_n f_{TG} \,, \tag{7.26}$$

and so define the quantity f_{TG}. This result arises because the heavy-quark current couples to gluons through the triangle diagram with heavy quark loops. The coupling of squarks or Higgs bosons to heavy quarks leads to a coupling to gluons through such loops, as shown in Fig. 21.

From Eq. (7.26) and the large-squark-mass limit of the effective Lagrangian (below), we can see that the elastic-scattering cross section should generally increase as the strangeness content of the nucleon is increased. The coupling to heavy quarks is maximized if the strangeness content is zero, but as we increase the strangeness content the coupling to the strange-quark scalar density more than makes up for the decrease in the heavy-quark coupling (assuming, of course, similar couplings and masses for the various flavors). In order of magnitude, if couplings and masses were the same for the various flavors, this would mean that the elastic-scattering cross section for $f_{Ts} = 0.5$ would be roughly 7 times larger than that for $f_{Ts} = 0$. This enhancement should not occur, however, for neutralinos which are either pure higgsino or B-ino. Usually in these cases, the coupling to the strange-quark scalar density will be negligible since strange-squark mixing is generally negligible compared with the mixing in the heavier flavors. In such models, increasing the strangeness content should decrease the cross section.

The matrix elements of the twist-two operators, at zero momentum transfer, can be written

$$m_n \langle n | \mathcal{O}^{(2)}_{q\mu\nu} | n \rangle = (p_\mu p_\nu - \tfrac{1}{4} m_n^2 g_{\mu\nu}) \int_0^1 \mathrm{d}x \, x [q(x, \mu_0^2) + \bar{q}(x, \mu_0^2)] \,,$$

$$m_n \langle n | \mathcal{G}^{(2)}_{q\mu\nu} | n \rangle = (p_\mu p_\nu - \tfrac{1}{4} m_n^2 g_{\mu\nu}) G(\mu_0^2) \,, \tag{7.27}$$

where p_μ is the momentum of the nucleon. The functions $q(x, \mu^2)$ and $G(\mu^2)$ are the quark and gluon densities in the nucleon at the scale μ. As in the case of the axial-vector interaction, we would like to use deep-inelastic scattering data to fix these matrix elements. A small technical complication exists due to the fact that the data is best specified at a fixed low-energy scale, and therefore the twist-two operators must be evolved up to the high-energy scale μ_0 using the renormalization group. The solution for this evolution is described in Ref. [282]; the effect is typically of order 30%.

Given the above, we can write down the effective couplings of neutralinos to protons and neutrons, f_p and f_n:

$$\frac{f_p}{m_p} = \sum_{q=u,d,s} \frac{f_{Tq}}{m_q}\left[f_q - \frac{m_\chi m_q}{2} g_q\right] + \frac{2}{27} f_{TG} \sum_{q=c,b,t} \frac{f_q^{(H)}}{m_q}$$
$$- \frac{3}{2} m_\chi \sum_{q=u,d,s,c,b} g_q(\mu_0) q(\mu_0^2) - \tfrac{8}{9}\pi b f_{TG}$$
$$+ \tfrac{3}{2} m_\chi G(\mu_0^2)\alpha_s(\mu_0^2)[B_{2S} + \tfrac{1}{2} m_\chi (B_{1D} + B_{1S})] , \tag{7.28}$$

with a similar expression for f_n. The couplings f_q are proportional to m_q, so the fraction f_q/m_q does not become large for small m_q. The quantity $G(\mu_0^2)\alpha_s(\mu_0^2)$ which appears in the last term is a renormalization-group invariant (in other words, independent of μ_0). Typical values of $G(\mu_0^2 = m_b^2)$ obtained by various authors (0.471–0.514) are listed in Table 1 of Ref. [282], and $\alpha_s(\mu_0^2 = m_b^2) \simeq 0.18$. Instead of writing separate expressions for the parton densities $q(\mu_0^2)$ that appear in the third term in Eq. (7.28), a single expression for the sums of the combinations $g_q(\mu_0^2)q(\mu_0^2)$ is given in Eq. (32) of Ref. [282]. It is to be evaluated at $\mu_0^2 = m_\chi^2$, and the couplings f_q and g_q are those given in Eq. (7.20). The expressions for f_p and f_n differ in the slightly different values for F_{Tq} in the proton and neutron, as discussed above, and these quantities are essentially the same (within the theoretical uncertainty) and generally very small. The quantities f_p and f_n also differ since the u and d valence-quark densities differ for the proton and neutron. This will result in a difference between f_p and f_n if the neutralino couples differently to u and d quarks (as it usually does). However, these terms are suppressed by a factor $m_{\tilde{q}}^{-4}$. Therefore, it is usually (although not always) safe to assume that $f_p \simeq f_n$.

The first term in Eq. (7.28) comes from the neutralino coupling to the light-quark scalar densities in the nucleon, via squark and Higgs exchange. The two terms proportional to f_{TG} come from the neutralino coupling to the gluon scalar density in the nucleon that arise via the loop diagrams in Fig. 21. The terms proportional to g_q come from terms of order $m_{\tilde{q}}^{-4}$ in the expansion of the squark propagator in the neutralino–quark diagram (Fig. 20). The remaining terms are due to higher-dimension operators which arise from the quark–squark loop diagrams of Fig. 21.

Limit of large squark masses: In the limit of large squark masses, $m_\chi \ll m_{\tilde{q}}$ and $m_q \ll m_{\tilde{q}}$, the integral I_1 becomes

$$I_1(m_q, m_{\tilde{q}}, m_\chi) \simeq \frac{2}{3 m_q^2 m_{\tilde{q}}^2} + O\left(\frac{1}{m_{\tilde{q}}^4}\right), \tag{7.29}$$

and the other I_i are higher order in $m_{\tilde{q}}$. Therefore, to lowest order in $m_{\tilde{q}}^{-1}$, the neutralino couplings to nucleons, f_p and f_n, become,

$$\frac{f_{p,n}}{m_{p,n}} \simeq \frac{f_{Ts} f_s}{m_s} + \frac{2}{27} f_{TG} \sum_{q=c,b,t} \frac{f_q}{m_q} , \tag{7.30}$$

where we have neglected the (usually) small contributions due to the light-quark scalar density. Except for the addition of the last term, these results agree with those obtained earlier [131, 256,

278, 279]. Strictly speaking, there is an additional term (that with $T_{\tilde{q}}$) of order $m_{\tilde{q}}^{-1}$, which arises from diagrams with squark loops and an exchanged Higgs boson, but this term also contains a Higgs-boson propagator, and should therefore be negligible compared to the Higgs-exchange terms in Eq. (7.28) in the large-squark-mass limit.

Nuclear form factors: Finally, we must evaluate the effective interaction with nuclei by evaluating the matrix elements of the nucleon operators in a nuclear state. As opposed to the case of the axial-vector interaction, there is no spin structure in the required nucleon operators at zero momentum transfer. Therefore, the nuclear physics is greatly simplified. In fact, the operators simply count the nucleons, so that the amplitude is proportional to the nucleon number. This gives a substantial enhancement for heavy nuclei.

At nonzero momentum transfer, the form factor associated with the nucleon-number operator is simply the Fourier transform of the nucleon density, which has a well-determined form, in contrast to the axial-vector form factors which require significant effort for their calculation. Several form factors have been used in the literature. The most commonly used form factor is the exponential form factor, first used in this context by Ahlen et al. [291] and Freese et al. [292]:[7]

$$F(Q) = \exp(-Q/2Q_0), \quad \text{exponential} \tag{7.31}$$

where Q is the energy transferred from the WIMP to the nucleus, $Q_0 = 1.5/(m_N R_0^2)$ is the nuclear "coherence energy" and

$$R_0 = 10^{-13}\,\text{cm}\,[0.3 + 0.91(m_N/\text{GeV})^{1/3}]\,, \tag{7.32}$$

is the radius of the nucleus. The exponential form factor implies that the radial density profile of the nucleus has a Gaussian form. A more accurate form factor is that suggested by Engel [293],

$$F(Q) = \left[\frac{3j_1(qR_1)}{qR_1}\right]^2 \exp[-(qs)^2], \quad \text{Woods–Saxon} \tag{7.33}$$

where the momentum transferred is $q = \sqrt{2m_N Q}$, m_r is the reduced mass, $R_1 = (R^2 - 5s^2)^{1/2}$, $R \simeq 1.2\,\text{fm}\,A^{1/3}$, j_1 is a spherical Bessel function, and $s \simeq 1$ fm. Although this form factor is *not* that obtained from the Fourier transform of the Woods–Saxon density distribution, it is very similar, so we refer to it as the "Woods–Saxon" form factor. Note that $F(Q)$ is normalized to 1 at zero energy transfer, and that it is implicitly a function of $|\boldsymbol{q}|$. However, for most practical purposes, the exponential form factor of Eq. (7.31) is adequate, and it is much easier to manipulate analytically.

The differential cross section for the scalar interaction can now be written,

$$\frac{d\sigma}{d|\boldsymbol{q}|^2} = G_F^2 \frac{C_{\text{scalar}}}{v^2} F^2(Q) = \frac{\sigma_{0\text{scalar}}}{4m_r^2 v^2} F^2(Q) = \frac{1}{\pi v^2}[Zf_p + (A - Z)f_n]^2 F^2(Q)\,, \tag{7.34}$$

where Z is the nuclear charge (i.e., the number of protons), A–Z is the number of neutrons, and

$$C_{\text{scalar}} = \frac{1}{\pi G_F^2}[Zf_p + (A - Z)f_n]^2\,. \tag{7.35}$$

[7] It should be noted that in some of the papers on WIMP detection, the form factor is defined to be the square of what we call the form factor. We have chosen our conventions to agree with the nuclear physicists'.

As in the spin case, we have defined a "standard" cross section at zero momentum transfer,

$$\sigma_{0\mathrm{scalar}} = \int_0^{4m_r^2v^2} \frac{\mathrm{d}\sigma(q=0)}{\mathrm{d}|\boldsymbol{q}|^2} = \frac{4m_r^2}{\pi}[Zf_p + (A-Z)f_n]^2 \,. \tag{7.36}$$

In most instances, $f_p \simeq f_n$, so $C_{\mathrm{scalar}} \propto A^2 \propto m_N^2$. Furthermore, for heavy WIMPs, $m_\chi \gg m_N$, the reduced mass is $m_r \simeq m_N$, so the "standard" scalar elastic-scattering cross section scales with the nuclear mass as $\sigma_{0\mathrm{scalar}} \propto m_N^4$. However, note again that σ_0 is *not* really the total cross section. The actual cross section is obtained by integrating (7.34) over $\mathrm{d}|\boldsymbol{q}|^2$ with the exponential or Woods–Saxon form factor.

7.4. General axial-vector, vector, and scalar interactions

Consider WIMPs, not necessarily supersymmetric, which interact with quarks via an axial-vector interaction of the form given in Eq. (7.1). If the WIMP is the lightest neutralino in the MSSM, then the WIMP–quark axial-vector couplings, d_q, are given by Eq. (7.2). For other WIMPs, such as Majorana neutrinos, there might be a similar interaction with different d_q. If those d_q are known, then the WIMP–nuclei "standard" total cross sections will again be given by Eq. (7.16) where A is given in terms of a_p and a_n in Eq. (7.16), and a_n and a_p are given in terms of d_q in Eq. (7.5).

Among similar lines, consider a generic WIMP with a scalar WIMP–quark interaction (for example, the fourth-generation neutrino considered in Ref. [277]),

$$\mathscr{L}_{\mathrm{scalar}} = f_q \bar{\chi}\chi\bar{q}q \,. \tag{7.37}$$

The "standard" total cross section for scalar WIMP–nuclear scattering for such a particle will be given by Eq. (7.36) with $f_p = f_n$ given in terms of f_q by Eq. (7.30).

In addition to these two interactions, WIMPs which are *not* Majorana particles may have vector interactions with nuclei,

$$\mathscr{L}^q_{\mathrm{vec}} = b_q\, \bar{\chi}\gamma_\mu\chi\, \bar{q}\gamma^\mu q \,. \tag{7.38}$$

Due to the conservation of the vector current, the contributions of each quark in the nucleus add coherently, so the resulting WIMP–nuclear cross section can be large for large nuclei. Furthermore, there is no uncertainty that can arise in going from the WIMP–quark to the WIMP–nucleus interaction from considerations like spin or strangeness content of the nucleon or from the spin structure of the nucleus. This is because sea quarks and gluons cannot contribute to the vector current. Therefore, the WIMP–neutron interaction is $\mathscr{L}^n_{\mathrm{vec}} = b_n\bar{\chi}\gamma_\mu\chi\bar{n}\gamma^\mu n$, and similarly for the WIMP–proton interaction, with $b_p = 2b_u + b_d$ and $b_n = b_u + 2b_d$. The WIMP–nucleus interaction is then $\mathscr{L}^N_{\mathrm{vec}} = b_n\bar{\chi}\gamma_\mu\chi\bar{N}\gamma^\mu N$, with $b_N = 2Zb_p + (A-Z)b_n$. The "standard" total cross section for the WIMP–nucleus vector interaction is then

$$\sigma_{0\mathrm{vec}} = \frac{m_\chi^2 m_N^2 b_N^2}{64\pi(m_\chi + m_N)^2} \,. \tag{7.39}$$

For example, a heavy fourth-generation Dirac neutrino with standard-model couplings to the Z^0 boson would have a WIMP–quark interaction of the form Eq. (7.38). This leads to

a WIMP–nuclear interaction with

$$b_{\mathrm{N}}^{\nu} = \frac{4}{\sqrt{2}} G_{\mathrm{F}}[(A-Z) - (1 - 4\sin^2\theta_{\mathrm{W}})Z] \,, \tag{7.40}$$

where the first term in brackets comes from the coupling to neutrons and the second from the protons. Since. $\sin^2\theta_{\mathrm{W}} \simeq \frac{1}{4}$, it turns out that the Dirac-neutrino coupling to protons is negligible compared to the coupling neutrons.

The standard electromagnetic interaction is a vector interaction, so the vector interaction leads to an interaction proportional to the charge distribution in the nucleus. To a good approximation, the charge distribution in the nucleus traces the mass distribution, so the scalar form factors discussed above can be applied to the vector interaction as well.

Sneutrinos, the spin-0 supersymmetric partners of neutrinos, have couplings to the Z^0 similar to the neutrino couplings. Therefore, they also scatter via a vector interaction, although the form of the effective Lagrangian for scalar partners differs from that in Eq. (7.38). The sneutrino–nucleus cross section turns out to be 4 times the Dirac-neutrino–nucleus cross section [176].

7.5. Comparison of spin and scalar cross sections

For some years it was thought that the axial-vector coupling provided the only interaction of neutralinos with ordinary matter. However, it was then realized [277, 131] that due to the heavy-quark expansion, there may be a significant scalar coupling of neutralinos to nuclei if the neutralino is a mixed gaugino/higgsino state. For mixed neutralino states, the scalar coupling would be enhanced additionally by the exchange of the lightest Higgs boson [278], and since the lightest Higgs boson is relatively light, this contribution could be significant. More recently, the contribution to the scalar coupling from squark mixing [280] has been shown to be important [282]. This contribution is proportional to the quark/squark mass ratio, and now that the top quark is known to be quite heavy, squark mixing may have a significant effect on the scalar neutralino–nucleus coupling, even if the neutralino is a pure state.

The spin and scalar interactions correspond to two different detection strategies. The technology of low-background detectors with spin-zero target nuclei is highly developed, in the main due to its use in double-beta decay experiments [294]. The development of low-background detectors enriched with isotopes of nonzero spin is more recent and has been driven primarily by the effort to detect spin-coupled WIMPs [25].

Obviously, the question of theoretical expectation for the relative strengths of the scalar and spin couplings is a model-dependent one. However, since the two detection schemes may involve significantly different detection strategies, estimates of the relative importance of the two interactions are needed for developing these strategies. Perhaps the best hints can be obtained by broad numerical surveys of supersymmetric parameter space [295], and these will be discussed later in Section 11. Here, we give a brief analytic comparison of the spin and scalar interactions in the MSSM, but it should be kept in mind that there are significant model dependencies that cannot be taken into account by such a discussion.

It is worthwhile to separate the model-dependent factors from the nuclear physics as much as possible. The nuclear dependence of the A^2 factor in the spin cross section is not easily separated

Table 7
Nuclear dependence in comparison of spin and scalar cross sections. Values for the spin moments are from previous discussion in this section

Method	Nucleus	η_A
Odd Group	^{1}H	3
Odd Group	^{3}He	0.41
Odd Group	^{17}O	0.0047
Odd Group	^{19}F	0.0071
Odd Group	^{23}Na	2.8×10^{-4}
Shell Model	^{29}Si	2.4×10^{-4}
Odd Group	^{35}Cl	1.2×10^{-4}
Perturbation Theory	^{39}K	2.1×10^{-4}
Shell Model	^{73}Ge	2.0×10^{-4}
Shell Model	^{93}Nb	1.6×10^{-4}
IBFM	^{131}Xe	1.7×10^{-5}

from the model dependence. But we will write

$$\frac{\sigma_{0\mathrm{spin}}}{\sigma_{0\mathrm{scalar}}} = \eta_A\left[a_p\frac{\langle S_p\rangle}{S_T} + a_n\frac{\langle S_n\rangle}{S_T}\right]^2\left[\frac{(Z/A)f_p}{\sqrt{2}G_F} + \left(1-\frac{Z}{A}\right)\frac{f_n}{\sqrt{2}G_F}\right]^{-2}, \tag{7.41}$$

where the nuclear dependence is given mainly by the factor

$$\eta_A = 4S_T^2 J(J+1)/A^2\,, \tag{7.42}$$

and $S_T = |\langle S_p\rangle| + |\langle S_n\rangle|$. In the odd-group model, S_T^2/J^2 is precisely the parameter λ^2 of Ref. [295]. In more general nuclear calculations it can differ from the odd-group model value. Some values of η_A are given in Table 7.

In order to proceed, assume that one type of nucleon dominates the spin-dependent interaction. As a numerical example, we will take the case of a B-ino in the large-squark-mass limit (and assume degenerate squark masses), for which [296]

$$a \simeq 0.1(m_W^2/m_{\tilde{q}}^2)\,. \tag{7.43}$$

For the scalar interaction, take the numerical example provided by Fig. 2 of Ref. [282], where $m_{\tilde{q}} = 200$ GeV. Thus $f_p \simeq f_n \simeq 10^{-8}\ \mathrm{GeV}^{-2}$. With this example, we find

$$\sigma_{0\mathrm{spin}}/\sigma_{0\mathrm{scalar}} \approx 250\,\eta_A\,. \tag{7.44}$$

This implies dominance of the scalar interaction for $A \gtrsim 20$, roughly speaking.

Before continuing, we reemphasize that there is no substitute for a complete SUSY-model calculation in the case of light nuclei, say for definiteness $A \lesssim 40$, because we know that the amplitudes involved can vary by an order of magnitude depending on the model parameters. It is also useful to remember that there are significant theoretical uncertainties, both from nuclear physics and from the spin content of the proton, that enter into the spin-dependent cross section [269, 296], and theoretical uncertainties from the pion–nucleon sigma term that enter into the scalar cross sections as well. However, the basic conclusion seems to be confirmed by numerical

experiments. In surveys of supersymmetric parameter space, one finds that the scalar interaction almost always dominates for nuclei with $A \gtrsim 30$. This has been noted in Ref. [282] and more recently stressed in Ref. [295].

8. Direct detection of neutralinos

If the halo of the Milky Way consists of WIMPs, then hundreds to thousands of WIMPs must pass through every square centimeter of the Earth's surface each second. The most satisfying proof of the WIMP hypothesis would be direct detection of these particles, by, for example, observation of nuclear recoil after WIMP–nucleus elastic scattering. The very low cross section of WIMPs on ordinary material makes these interactions quite rare, but as suggested a decade ago [9, 10, 297], specialized detectors may make such direct detection possible. The basic idea is to somehow measure, and distinguish from background, the tiny energy deposited by the very occasional WIMP–nucleus interaction. During the past decade, enormous technical progress on a host of techniques has been made, and direct detection is now one of the most promising methods of detecting Galactic WIMPs. Dozens of groups have built or are building detectors with direct detection of WIMPs in mind, and results from the first-generation detectors have already set strong limits on or eliminated several WIMP candidates (see Section 12). Along with the tremendous experimental advances, many theoretical papers aimed at understanding this process have been written, and increasingly more subtle effects and uncertainties have been explored. In this section, we review and summarize the highlights of both the theoretical and experimental situations. We have attempted to give easily applied formulas which can take into account as much or as little theoretical sophistication as desired, but our survey of the experimental efforts is brief. For more complete discussions of the experimental aspects, see Refs. [21, 24]. For a survey of experiments, see Ref. [25].

8.1. Theory

The rate in a detector depends upon the density ρ_0 of WIMPs near the Earth, and the velocity distribution $f(v)$ of WIMPs in the Galactic halo near the Earth [Eqs. (2.8) and (2.9)]. As a function of energy deposited, Q, direct-detection experiments measure the number of events per day per kilogram of detector material. Qualitatively, this event rate is simply $R \approx n\sigma\langle v\rangle/m_{\mathrm{N}}$, where the WIMP number density is $n = \rho_0/m_\chi$, σ is the elastic-scattering cross section, $\langle v\rangle$ is the average speed of the WIMP relative to the target, and we divide the detector mass M_{det} by the target nucleus mass m_{N}, to get the number of target nuclei.

More accurately, one should take into account the fact that the WIMPs move in the halo with velocities determined by $f(v)$, that the differential cross section depends upon $f(v)$ through a form factor $\mathrm{d}\sigma/\mathrm{d}|\boldsymbol{q}|^2 \propto F^2(Q)$, and that detectors have a threshold energy E_{T}, below which they are insensitive to WIMP–nuclear recoils. In addition, the Earth moves through the Galactic halo and this motion should be taken into account via $f(v)$. The potential field of the Sun [298] and the Galactic disk will also affect the local WIMP density and velocity dispersion, but these effects are relatively small and will not be discussed here.

In general, the differential rate (per unit detector mass) can be written

$$dR = (\rho_0/m_\chi m_N) v f_1(v) (d\sigma/d|\boldsymbol{q}|^2)\, d|\boldsymbol{q}|^2\, dv\,, \tag{8.1}$$

where $f_1(v)$ is the distribution of speeds relative to the detector, found by integrating the three-dimensional velocity distribution over angles (it is normalized to $\int f_1(v)\,dv = 1$). Since the momentum transferred $|\boldsymbol{q}|^2 = 2m_r^2 v^2(1-\cos\theta^*)$, where θ^* is the scattering angle in the center-of-momentum frame, and $m_r = m_\chi m_N/(m_\chi + m_N)$, the energy deposited in the detector (energy transferred to the nucleus) is

$$Q = |\boldsymbol{q}|^2/(2m_N) = (m_r^2 v^2/m_N)(1-\cos\theta^*)\,. \tag{8.2}$$

To find the total rate we must integrate dR over all possible incoming velocities and over deposited energies between E_T and $E_{max} = 2m_r^2 v^2/m_N$. Using Eqs. (7.12), (8.1), and (8.2), we have

$$\frac{dR}{dQ} = \frac{\sigma_0 \rho_0}{2m_\chi m_r^2} F^2(Q) \int_{v_{min}}^{\infty} \frac{f_1(v)}{v}\, dv\,, \tag{8.3}$$

where

$$v_{min} = (Qm_N/(2m_r^2))^{1/2}\,, \tag{8.4}$$

and $F(Q)$ is the form factor, which should be chosen from Eqs. (7.31), or (7.33) for scalar WIMPs, or from the fitted forms in Eqs. (7.15), (7.7), and (7.11), for spin-coupled WIMPs.

Note that by using the energy transfer Q, all the dependence on WIMP velocity has been put into one integral. So we can further define the dimensionless quantity

$$T(Q) = \frac{\sqrt{\pi}}{2} v_0 \int_{v_{min}}^{\infty} \frac{f_1(v)}{v}\, dv\,, \tag{8.5}$$

to get

$$dR/dQ = (\sigma_0 \rho_0/\sqrt{\pi} v_0 m_\chi m_r^2) F^2(Q) T(Q)\,, \tag{8.6}$$

where $v_0 \approx 220\ \mathrm{km\,s^{-1}}$ is the circular speed of the Sun around the Galactic center. The total rate for events per kilogram per day is found from

$$R = \int_{E_T}^{\infty} \frac{dR}{dQ}\, dQ\,. \tag{8.7}$$

This factoring of the differential rate into a form-factor piece and a piece which depends upon WIMP velocity lends itself to easier calculation for both simple and complicated examples.

For the purpose of illustration, consider a simple Maxwellian halo

$$f(v')\, d^3v' = (1/v_0^3 \pi^{3/2}) \exp(-v'^2/v_0^2)\, d^3v'\,. \tag{8.8}$$

If one were to use this (leaving out the motion of the Sun and Earth), one would integrate over angles to find the speed distribution

$$f_1(v')\, dv' = [4(v')^2/v_0^3 \sqrt{\pi}] \exp(-v'^2/v_0^2)\, dv'\,. \tag{8.9}$$

Thus for this case, Eq. (8.5) gives simply,

$$T(Q) = \exp(-v_{\min}^2/v_0^2) \quad \text{(pure Maxwellian)}\,, \tag{8.10}$$

where $v_{\min}$ is given in Eq. (8.4). If one considered light WIMPs where $F(Q) \approx 1$, one would get

$$\frac{dR}{dQ} = [\sigma_0\rho_0/(\sqrt{\pi}v_0 m_\chi m_r^2)]\exp(-Qm_N/(2m_r^2v_0^2)) \quad \text{(pure Maxwellian)}\,, \tag{8.11}$$

and integrating to find the total rate gives

$$R = [\sigma_0\rho_0/(m_\chi m_N)](2/\sqrt{\pi})v_0\exp(-E_T m_N/(2m_r^2v_0^2)) \quad \text{(pure Maxwellian)}\,, \tag{8.12}$$

With $E_T = 0$, this result is precisely the naive rate mentioned at the beginning of this section, since $\langle v\rangle = (2/\sqrt{\pi})v_0$ for the velocity distribution of Eq. (8.9).

More realistically, one should take into account the motion of the Sun and Earth. This increases the total rate and gives rise to an yearly modulation in the event rate which might serve as a method of distinguishing signal and noise if many events are found [292, 299]. Following Freese, Frieman, and Gould [292], and Sadoulet [300], one subtracts the Earth velocity v_e from v' in Eq. (8.8) to get the velocity v of the WIMP in the Earth frame.

$$\boldsymbol{v}' = \boldsymbol{v} + \boldsymbol{v}_e, \qquad v'^2 = v^2 + v_e^2 + 2vv_e\cos\chi, \tag{8.13}$$

where χ is the angle between the WIMP velocity in the Earth frame and the direction of the Earth's motion. As a function of time, v_e changes as the Earth's motion comes into and out of alignment with the Sun's motion around the Galaxy. This causes an yearly modulation in the event rate which peaks around June 2nd each year [298, 299]. This is taken into account using [292]

$$v_e = v_0\left[1.05 + 0.07\cos\left(\frac{2\pi(t - t_p)}{1\text{ yr}}\right)\right], \tag{8.14}$$

where $t_p =$ June 2nd $\pm$ 1.3 days. Changing variables, using $d^3v'/d^3v = (v'^2/v^2)(\cos\theta/\cos\chi)$, and integrating over angles one gets [292]

$$f_1(v)\,dv = \frac{v\,dv}{v_e v_0\sqrt{\pi}}\left\{\exp\left[-\frac{(v - v_e)^2}{v_0^2}\right] - \exp\left[-\frac{(v + v_e)^2}{v_0^2}\right]\right\}. \tag{8.15}$$

Then from Eq. (8.5) one has [300]

$$T(Q) = \frac{\sqrt{\pi}}{4v_e}v_0\left[\operatorname{erf}\left(\frac{v_{\min} + v_e}{v_0}\right) - \operatorname{erf}\left(\frac{v_{\min} - v_e}{v_0}\right)\right]. \tag{8.16}$$

so

$$\frac{dR}{dQ} = \frac{\sigma_0\rho_0}{4v_e m_\chi m_r^2}F^2(Q)\left[\operatorname{erf}\left(\frac{v_{\min} + v_e}{v_0}\right) - \operatorname{erf}\left(\frac{v_{\min} - v_e}{v_0}\right)\right]. \tag{8.17}$$

This equation is similar to the one obtained in Ref. [24] and is quite general. It is especially important for experimentalists who wish to fit the differential energy spectrum. It is also easily

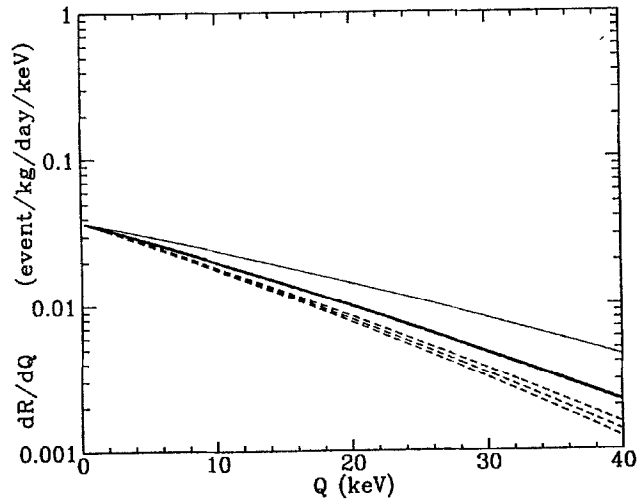

Fig. 22. Theoretical differential event rate [Eq. (8.17)] versus deposited energy for several different nuclear form factors. An arbitrary cross section of $\sigma_0 = 4 \times 10^{-36}\,\mathrm{cm}^2$ was chosen, with $m_\chi = 40$ GeV and $m_N = 68$ GeV, and standard values of the other parameters. The heavy solid line shows the best-estimate (i.e., the Woods–Saxon) form factor [Eq. (7.33)] for scalar interactions, while the long-dashed line (which falls on top of the heavy solid line) shows the exponential form factor [Eq. (7.31)]. The light solid line shows $F(Q) = 1$ (no form factor). The three spin form factors for germanium (Table 5) are shown as short-dashed lines.

integrated, either analytically (see below) or numerically, to get the total event rate. Eq. (8.17) is the main result of this section.

For a general WIMP, the rates from both spin and scalar interactions must be added together to get the total event rate. The procedure is to calculate $\sigma_{0\mathrm{scalar}}$ and $\sigma_{0\mathrm{spin}}$ [from Eqs. (7.16), and (7.36)], pick a form factor for each, and plug into Eq. (8.17). For the scalar interaction, $F(Q)$ can be chosen from Eq. (7.33) (more accurate) or Eq. (7.31) (more easily manipulated analytically). In Fig. 22 we show $\mathrm{d}R/\mathrm{d}Q$ from Eq. (8.17) for a variety of form factors for a 40-GeV WIMP hitting a Ge target. The cross section was arbitrarily picked as $\sigma_0 = 4 \times 10^{-36}\,\mathrm{cm}^2$, and standard values of the parameters were used. The form-factor dependence of $\mathrm{d}R/\mathrm{d}Q$ is small at small Q but becomes appreciable for larger recoil energies.

For the spin interaction, fitted form factors from Eqs. (7.15), (7.7), and (7.11), should be used if available. If not, one of the scalar form factors above or the form factor given in Ellis and Flores [268] could be used. We remind the reader that for spin–spin interactions and large nuclei, none of the simple analytic form factors listed above provide a very good approximation, since detailed calculations show spin form factors usually have non-exponential tails. These tails give larger cross sections at large Q than the simple form factors; they may be important for heavy WIMPs and for nuclei which couple axially. Thus the explicit nuclear calculations which have been done for several elements such as iodine, niobium germanium, silicon, etc. should be used when they exist. For example, ^{73}Ge, ^{29}Si, ^{27}Al, and ^{39}K results are shown in Table 5; for niobium see Ref. [275]. Fig. 22 also shows $\mathrm{d}R/\mathrm{d}Q$ for the germanium form factors of Table 5. As discussed in Section 7, there are actually three independent form factors for spin couplings, and these are displayed as the three short-dashed lines.

Finally, Eq. (8.17) can be integrated over Q, from the detector threshold energy, E_T, to infinity. In many cases a numerical integration is easiest, but for low-mass WIMPs and/or low-mass nuclei, one can approximate $F(Q) = 1$ and recover Eq. (2.19) from Ref. [292],

$$R_1 = \frac{\sigma_0 \rho_0}{\sqrt{\pi} m_\chi m_N} \frac{v_0^2}{v_e} [(\tfrac{1}{2} - A_+ A_-)\chi(A_-, A_+) + \tfrac{1}{2}(A_+ e^{-A_-^2} - A_- e^{-A_+^2})] , \tag{8.18}$$

where

$$\chi(x_1, x_2) = (\sqrt{\pi}/2)(\operatorname{erf} x_2 - \operatorname{erf} x_1) , \tag{8.19}$$

$$A_\pm = A_T \pm v_e/v_0, \qquad A_T^2 = m_N E_T (2 m_r^2 v_0^2)^{-1} . \tag{8.20}$$

Using the exponential form for $F(Q)$, from Eq. (7.31), one recovers Eq. (B1) of Ref. [292],

$$R_{exp} = \frac{\sigma_0 \rho_0}{\sqrt{\pi} m_\chi m_N} \frac{v_0^2}{v_e b} \left[e^{-E_T/E_0} \chi(A_-, A_+) - \frac{\chi(\check{A}_-, \check{A}_+)}{(1+b)^{1/2}} \exp\left(- \frac{b}{1+b} \frac{v_e^2}{v_0^2} \right) \right] , \tag{8.21}$$

where

$$\check{A}_\pm = (1+b)^{-1/2} [A_T (1+b) \pm (v_e/v_0)] , \qquad b = 2 v_0^2 m_r^2 (E_0 m_N)^{-1} . \tag{8.22}$$

We have given equations for the differential event rate, Eq. (8.17), in terms of an arbitrary form factor, $F(Q)$, and a standard total cross section at zero momentum transfer, σ_0 (discussed in the previous section). We have also given in Eq. (8.18), an analytic expression for the total event rate for a constant form factor, and in Eq. (8.21) an analytic expression for the total event rate for the exponential form factor [Eq. (7.31)]. A general WIMP will have both scalar and spin-dependent interactions with the nucleus, so there will be a scalar cross section, $\sigma_{0scalar}$, and a spin cross-section, $\sigma_{0,spin}$. The differential and total event rate will be the sum of the differential and total event rates due to the two interactions. For the scalar interaction, an analytic form factor can be used. For the spin interaction, the form factor will differ from nucleus to nucleus, and specific form factors for some commonly used nuclei with spin are given in the previous section. These must generally be integrated numerically to obtain a total cross section. Form-factor suppression becomes small for target nuclei of sufficiently low mass, so Eq. (8.18) should provide an increasingly accurate estimate of the total event rate for both scalar and spin interactions, as the mass of the target nucleus is decreased (e.g., Fig. 5 of Ref. [131]).

The formalism described above can be used to predict the "signal" expected in almost any direct-detection device. As an example, in Fig. 23 we show the theoretical dR/dQ for a germanium detector and several WIMP masses (see also Fig. 24). We used the Woods–Saxon form factor [Eq. (7.33)], an arbitrary cross section of $\sigma_0 = 4 \times 10^{-36}$ cm^2, and standard values of the other parameters. The expected shape of the spectrum is one method of discriminating against non-dark-matter background, and as discussed in the next section, should be compared with a typical background such as is shown in Fig. 25.

Eq. (7.36) in the previous section gives the standard total cross section for scattering from a given nucleus in terms of the WIMP–nucleon couplings f_p and f_n. As noted in the discussion following Eq. (7.36), it is almost always true that $f_p \simeq f_n$. If so, then the cross section for neutralino scattering from a nucleus m_N can be written [301] as

$$\sigma_{0scalar} = \{4 m_\chi^2 m_N^4 / [\pi (m_\chi + m_N)^2]\} (f_p/m_n)^2 , \tag{8.23}$$

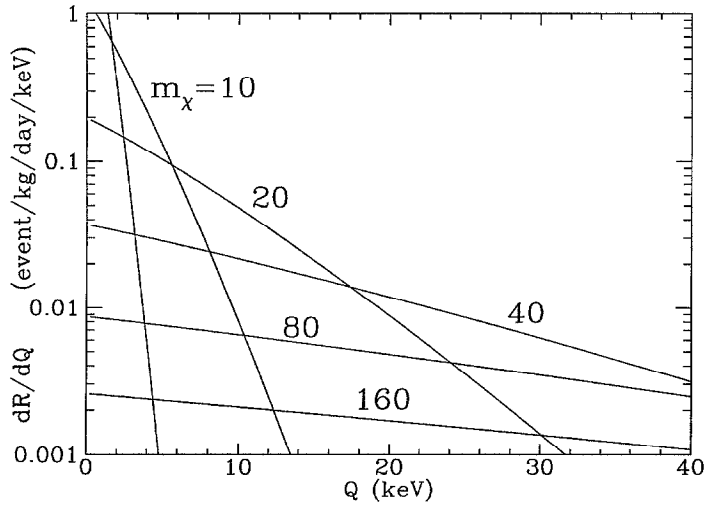

Fig. 23. Theoretical differential event rate for WIMPs of various masses hitting a germanium target. WIMP masses are labeled in GeV. An arbitrary cross section of $\sigma_0 = 4 \times 10^{-36}\,\mathrm{cm}^2$ was chosen with standard values for the other parameters. Compare these curves with a typical experimental gamma-ray background shown in Fig. 25. Note the rate axis scale is 100 times *smaller* than in Fig. 25, and the cross section chosen is very high for neutralinos (see Section 11).

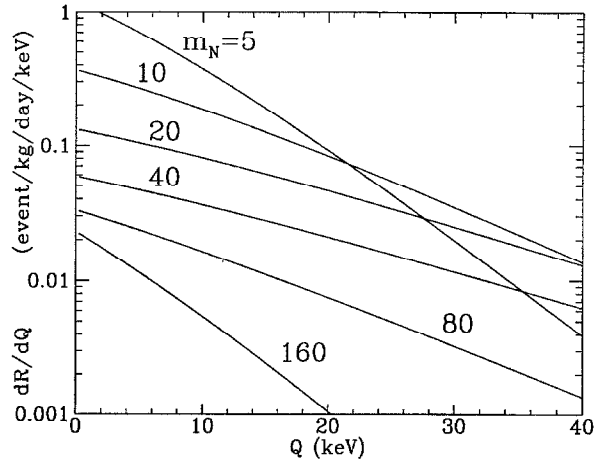

Fig. 24. Same as Fig. 23, but for a 40-GeV WIMP interacting with detectors made of different material. The detector-nuclei masses are labeled in GeV. An arbitrary cross section of $\sigma_0 = 4 \times 10^{-36}\,\mathrm{cm}^2$ was chosen with standard values for the other parameters. Compare these curves with a typical experimental gamma-ray background shown in Fig. 25. Note the rate axis scale is 100 times *smaller* than in Fig. 25, and the cross section chosen is very high for neutralinos (see Section 11).

where $m_n \simeq 0.94$ GeV is the nucleon mass. The important thing to note is that all the information needed about any specific MSSM (e.g., the neutralino composition, the masses and couplings of all the superpartners, etc.) for the scalar neutralino–nucleus interaction is encoded in f_p, and f_p is *in*dependent of the nuclear mass. Therefore, the nuclear-mass dependence of the

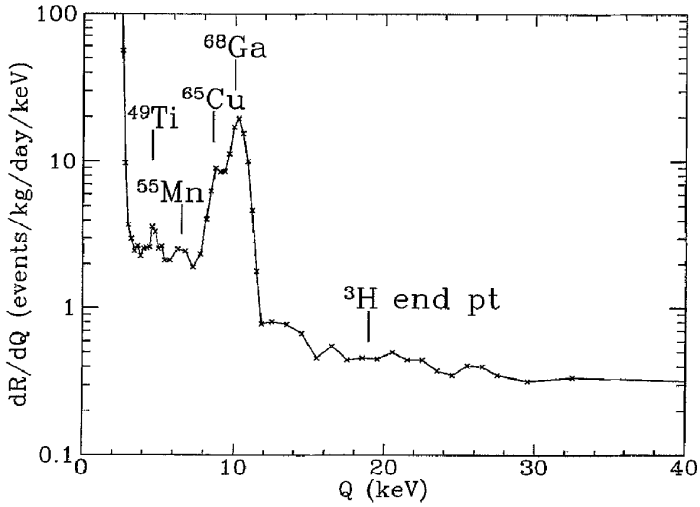

Fig. 25. Measured gamma-ray background in an underground high-purity germanium ionization detector (data acquired by the UCB/UCSB/LBL experiment at Oroville [307, 420]. Various gamma-ray lines are identified, as is the end point of the broad tritium spectrum. The rapid rise at low Q is the electronic noise. Compare with the potential WIMP signals shown in Figs. 23 and 24.

neutralino–nucleus standard total cross section is given in the prefactor in Eq. (8.23). As a result, the predicted event rate of a scalar-coupled WIMP in a detector of a given composition can be related to the event rate in a detector of a different composition with Eqs. (8.21) and (8.23). In Fig. 26, we show the integrated rate (neglecting detector thresholds) for detectors made of various nuclei, as compared to a ^{76}Ge detector [301]. Fig. 26 can be used to estimate the differences in expected rates for various detector materials, for WIMPs with predominantly scalar interactions.

The equations above give the differential and the total event rate, and by using different times of year in Eq. (8.14), the seasonal modulation [292, 299] in total event rate can be found. The event rate is about 5% larger when the Sun and Earth velocities through the Galactic halo are most closely aligned (in June), than when the velocities are most closely antialigned (in December). Due to the small size of the effect, a large number of events would be needed to have a significant detection. More striking than the seasonal modulation is the directional dependence of the recoil rate [302]. As the Earth and Sun move through the Galactic halo at $\sim 220\,\mathrm{km\,s^{-1}}$, the large preponderance of recoils are in the opposite direction. Thus, if the direction of the nuclear recoil could be determined, a clear dark-matter signature would exist. Experimental attempts at obtaining directionality are mentioned briefly in Section 8.2.

Finally, for very massive WIMPs there is the possibility of detection of a diurnal variation in event rate as the rotating Earth shields the experiment from the Galactic wind of WIMPs [303]. It has recently been proposed that ejection of target nuclei from solid surfaces induced by WIMP–nucleus elastic scattering could provide a unique WIMP signature [304].

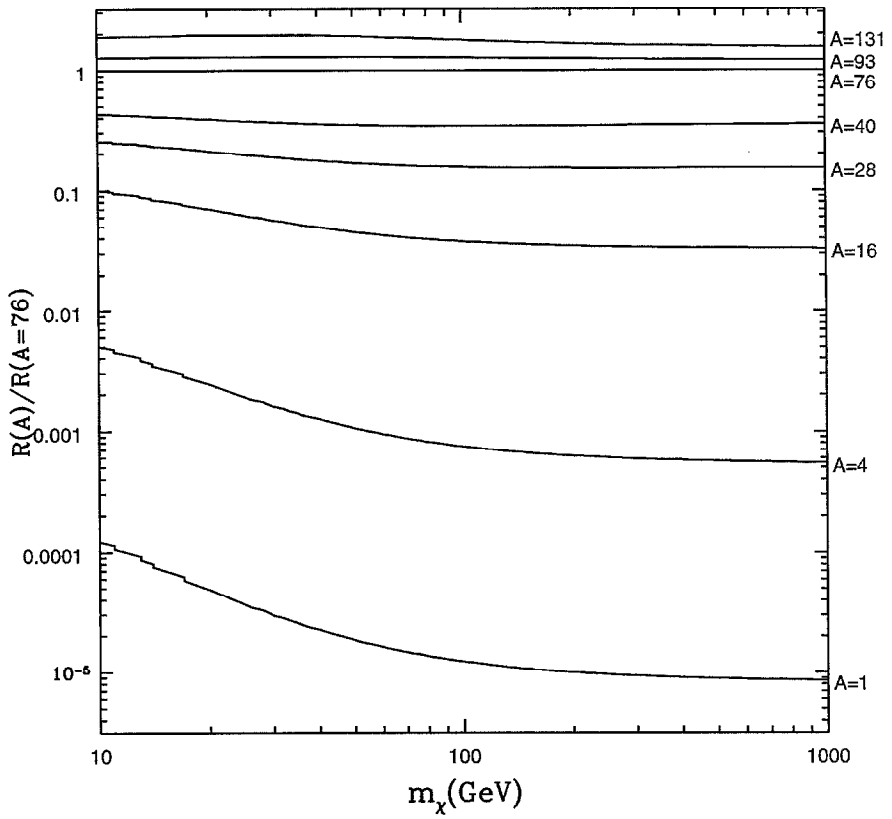

Fig. 26. Event rate (per kg of detector) for scalar-coupled WIMPs in a detector composed of nuclei with mass number A scaled by the rate in a ^{76}Ge detector as a function of WIMP mass m_χ. Threshold effects are neglected. (From Ref. [301].)

8.2. Detectors

There are a great many experiments actively searching for WIMP dark matter by trying to measure the energy deposited when a WIMP from the Galactic halo scatters from a nucleus in the detector. For reviews see Refs. [21, 24, 25]. A typical WIMP moving at about 270 km s^{-1}, with a mass in the range 20–400 GeV, hitting a nucleus with mass in the range 1–200 GeV, will deposit an energy of 1–100 keV [Eq. (8.2)] at a rate of about 10^{-4} to 1 event per day per kilogram of detector material (for sample supersymmetric particle-physics models, see Section 11). The more massive the WIMP, the more the energy deposited, but also the smaller the event rate. Both this energy and this event rate are extremely small by the usual standards of particle physics, and it is the small energy deposited and the low rate which makes these experiments difficult. The low count rate requires that the experiments have extremely good background discrimination, very large detectors, and/or very long counting times. The small energy deposited makes many esoteric background sources important, and background discrimination is essential and difficult. For example, on the Earth's surface, cosmic rays and cosmic-ray induced gamma rays with energies in the keV to MeV range occur at $\gtrsim 100$ event kg^{-1} d^{-1} and would completely swamp any dark-matter signal. Thus dark-matter direct-detection experiments are forced deep underground.

Even so, radioactive isotopes in the walls and equipment, along with residual cosmic-ray muons, create neutrons and gamma rays, thus requiring the use of sophisticated shielding and special attention to the radio purity of all the materials used in the experimental equipment. The low rates and small energy have also forced experimentalists to invent extremely sensitive detectors, using entirely new techniques, and generally to operate at very low temperatures to reduce thermal noise.

As an example, consider the Berkeley Center for Particle Astrophysics (CfPA) germanium detector [305, 306] being deployed as part of the Cryogenic Dark Matter Search collaboration at the Stanford University Underground Facility. The detector consists of a tower of very pure germanium crystals, each weighing approximately 160 g, made into thermal calorimeters by attaching NTD germanium thermistors to them. When cooled to 20 mK in a dilution refrigerator, the heat capacity ($\propto T^3$) is so low that even a few keV of deposited energy raises the temperature of one of the crystals by a measurable amount, allowing the amount of energy deposited to be determined. Threshold energies as low as a keV have been demonstrated. However, the first generation of dark-matter detectors discovered a gamma-ray background of about 2 event $kg^{-1}\,d^{-1}\,keV^{-1}$ in the 1–100 keV range (see Fig. 25), so to make the thermal calorimetric detectors sensitive to the necessary ~ 0.01 event $kg^{-1}\,d^{-1}$ level, the crystals are simultaneously run as ionization detectors [306]. A small voltage is placed across the crystal, and when a gamma ray enters and ionizes several atoms, the freed electrons are drifted to one side, the charge collected being a measure of the energy deposited in ionization. This technique of simultaneously measuring the heat and ionization energy gives excellent discrimination against the gamma-ray background [306]. Nuclear recoils caused by WIMP interaction deposit relatively less energy in ionization compared to phonons (heat), while gamma rays give relatively more energy in ionization compared to phonons. Thus, this experiment expects to reach a sensitivity of ~ 0.3 event $kg^{-1}\,d^{-1}$ in the near future, and a sensitivity of ~ 0.01 event $kg^{-1}\,d^{-1}$ in the next few years. We should point out that germanium crystals, running exclusively as ionization devices at liquid-nitrogen temperatures, have been run successfully underground for years and have already given strong limits on dark-matter candidates such as massive Dirac neutrinos [291, 307–309]. As discussed in Section 12, massive Dirac-neutrino dark matter would have resulted in event rates in the 30–300 event $kg^{-1}\,d^{-1}$ range, and have been ruled out as the primary constituent of the dark matter by these experiments [291, 307–309].

Besides the CDMS collaboration, many other collaborations are mounting experimental efforts with related technology. For example, the Munich group [310] has developed a detector using Al_2O_3 (sapphire) and have achieved a 90-eV energy resolution for 6-keV gamma rays in a 31-g detector. Crystals of lithium fluoride are also being used [311]. Besides thermal calorimetry, several techniques based on the superconducting–normal phase transition are being used to detect the energy deposited. For example, a thin film of tungsten can be grown on a silicon substrate (detector) and held just below the critical temperature [312]. Phonons created by a WIMP–nucleus interaction would heat the superconducting film, causing it to go normal, and the change in resistance could be measured. A related technique is to use small superconducting granules in a magnetic field, which, when heated by a nuclear recoil, would go normal and thereby cause a measurable change in the magnetic flux [9, 297, 313].

A problem common to all these techniques is illustrated by the fact that, in its current configuration, the CDMS collaboration will be unable to achieve a total detector mass of more than 10 kg. Given the small expected event rates, this may be a serious impediment to detecting

very weakly coupled supersymmetric WIMPs. However, several groups are investigating the use of NaI and CaF scintillation detectors [314–317], for which 100 kg detectors are feasible. Here, it is not a temperature rise in the crystal which is used to measure the nuclear recoil, but scintillation light caused by ionization – a classic particle-physics technique. The energy threshold for these detectors may be substantially higher than the thermal calorimeters, and the background may be problematic, but several methods for discriminating gamma rays from WIMP-induced recoil have been suggested [314, 315, 317]. Other techniques using rotons in superfluid helium [318] and scintillation in Xenon [317, 319] are also being developed and may allow both gamma-ray discrimination and large detector volumes.

As mentioned above, another way to beat the very low event rate is to count for a very long time. While for most experiments this means several years, recently one group has been exploiting ancient mica samples to increase the effective exposure time to several billion years [320]. A WIMP-induced nuclear recoil would form a stable "track" of crystal defects, which could be found by etching a thin sample of ancient mica. Longer tracks from MeV-scale radioactive decays can be discriminated from the short WIMP-induced tracks. In their preliminary search, no WIMP-induced tracks were found, leading to weak, but respectable, limits on WIMP halo dark matter. So far only a few nanograms of material have been analyzed, and a background may appear, but the ultimate sensitivity of this technique is still unknown. Mica is composed primarily of the spinless nuclei ^{16}O and ^{28}Si and the odd-A nuclei ^{27}Al, ^{39}K and H. The relevant nuclear form factors have recently been calculated [321] and the distinguishability of the recoiling potassium tracks has been analyzed [322].

A problem with all the above experiments is that, if a WIMP signal is seen, it will be difficult to prove the signal is from dark-matter particles and not from some unknown background. As shown in Figs. 23 and 24, the expected dark-matter signal is roughly an exponentially-distributed event rate, and as shown in Fig. 25, the gamma-ray background consists of various lines and noise peaks, some of which look similar to the WIMP signal. The rate shown in Fig. 23 is actually larger than the rate expected for most dark-matter neutralinos, so the need for excellent background discrimination is evident. Even assuming discrimination against gamma-rays, other unknown backgrounds could exist. Since the shape of the spectrum depends upon the WIMP and nuclear masses in a well-known way (assuming the WIMP halo velocity distribution is indeed Maxwellian), a possible way to distinguish signal from background is to use detectors of different material and to note the differences in detected recoil spectrum and total rate. Fig. 23 shows the theoretical dR/dQ for a WIMP of mass 40 GeV, and for various nuclear masses. As we have seen, a wide variety of materials are being proposed as detectors. However, since detectors made of different materials typically use different detection techniques, they will typically have different backgrounds, and this may make the comparison difficult. Other potential complications in the comparison of event rates from different materials are the particle- and nuclear-physics uncertainties in the WIMP-nucleus cross sections. As discussed in Section 7, the WIMP–nucleus cross section is the sum of a spin interaction and a scalar interaction, the values of which are dependent on the unknown details of the underlying particle-physics model. For example, some nuclei have no net spin, and so would be "invisible" to WIMPs which had only spin coupling. For such WIMPs, the difference in rate between detectors made of spinless nuclei and detectors made of nuclei with spin would be due to the unknown ratio of the WIMP spin and scalar interactions. The neutralino almost always has a dominant scalar coupling (Section 11), so this is unlikely to be the case for these particles, but

other WIMPs may have dominant spin couplings. In other words, a rate difference between different materials may also be due to differing nuclear matrix elements. Of course, once a signal is found, this effect could be used to separate the spin and scalar component of the WIMP couplings.

Another possible method for discriminating a dark-matter signal from background is the seasonal modulation of the event rate caused as the Earth travels around the Sun [292, 299]. The small size of the modulation means that this can only work if large numbers of events are found, implying the need for very large detectors. As mentioned above, the directional dependence (recoil away from direction of Earth motion) is much more striking than the seasonal modulation [302], and efforts to develop detectors sensitive to this effect have been made. In the bolometric devices, the nuclear recoil seems to quickly form a melted "hot spot" that is an isotropic (modulo the lattice) source of the phonons which eventually heat the crystal. It is possible that the initial "ballistic" phonons may preserve some of the directionality [312, 318, 323, 324], but at present, determination of the direction of the nuclear recoil seems unlikely in these devices. However, in gas detectors such a directional sensitivity has already been demonstrated [325]. Using hydrogen (and also argon) gas in a time projection chamber (TPC), clear tracks due to nuclear recoil caused by low-energy neutrons have been observed. This is another classic particle-physics technique, and by using a large magnetic field to bend the tracks, discrimination between electrons, muons and nuclear recoil is almost 100%. The main problem with this technique is the relatively small mass of detector gas (1–10 g at present). Thus, once again, the low interaction rate competes with background rejection in making the experimental detection of dark matter difficult.

Finally, it should be kept in mind that for any given detector, some experimental effects and efficiency factors will need to be considered in order to obtain results from the data that can be compared with the theoretical prediction in Eq. (8.17),[8] Here we list some of these, but we do not provide general expressions [326].

First of all, if a target consists of two or more nuclei (e.g., NaI), then the predicted recoil rate will be the sum of the recoil rates from the two nuclei. Furthermore, there may be a recoil efficiency (which takes into account the difference between the observed and recoil energy) which differs between the two nuclei. There may be corrections due to energy resolution or near threshold from, for example, Poisson fluctuations if there are only a few photoelectrons.

8.3. Inelastic-scattering techniques

All the above detection techniques relied on measuring energy deposited after an elastic scattering event. It is also possible that a WIMP interaction could leave a nucleus in an excited state. In this case, one might also be able to detect a gamma ray which resulted from de-excitation, and thereby have a redundancy which would greatly reduce the possible background [327]. However, the cross section to populate an excited state is usually extremely small. A possible exception may have been found for iodine [328]. Along similar lines, it has recently been proposed that scattering of WIMPs from orbital electrons could leave atoms in an excited state, and the photon from de-excitation subsequently detected [329].

[8] We thank P.F. Smith for suggestions.

9. Energetic neutrinos from WIMP annihilation in the Sun and/or Earth

9.1. General description

Another promising method for indirect detection of WIMPs in the halo is the observation of energetic neutrinos from annihilation of WIMPs that have accumulated in the Sun [11, 12] and/or Earth [13–15]. As we will argue, such neutrinos are easily distinguished from solar neutrinos, atmospheric neutrinos, or any other known background. If observed, these neutrinos could provide very convincing evidence for the existence of particle dark matter.

There has been a vast literature developed to address the expected rates for observation of neutrinos from WIMP annihilation, and the progress in the development of suitable neutrino telescopes has been tremendous. Kamiokande [330–332], IMB [333, 334], Frejus [335], and MACRO [336] have already reported (unfortunately null) results of searches for energetic neutrinos from the Sun and Earth. In addition, DUMAND [337], AMANDA [338], and NESTOR [339], will also be capable of energetic-neutrino searches with much greater sensitivity.

If neutralinos are the dark matter in the Galactic halo, then they will accumulate in the Sun and Earth. A WIMP with an orbit which passes through a given body (the Sun or Earth) has a small but finite probability of elastically scattering from a nucleus therein. If, in doing so, it scatters to a velocity smaller than the escape velocity, then it becomes gravitationally bound to the body. Once captured, the WIMP undergoes additional scatters from elements in the Sun or Earth and settles to the core of the body in a relatively short time. WIMPs which have accumulated in this way can annihilate with another WIMP into ordinary particles such as quarks and leptons, and if heavy enough, gauge and Higgs bosons and top quarks. The majority of the decay products of these particles are absorbed almost immediately and without consequence in the core of the Sun or Earth. However, decays of these annihilation products will also produce energetic muon neutrinos which can pass through the Sun or Earth and be detected in astrophysical neutrino detectors. In passing through the rock below the detector, an energetic muon neutrino can undergo a charged-current event in which a muon is produced. Therefore, neutrino-induced muons from the Sun or Earth provide a signature for particle dark matter.

The neutralino annihilates almost always to a two-body final state, so the energy of each annihilation product is equal to the WIMP mass. The annihilation products then undergo two- or three-body decays. The resulting neutrino energies are therefore broadly distributed, but the typical neutrino energy is roughly $\frac{1}{3}$ to $\frac{1}{2}$ the WIMP mass. Typical WIMP masses are in the range of 10 GeV to a few TeV. Therefore, neutrinos from WIMP annihilation in the Sun are far more energetic than, and cannot be confused with, solar neutrinos, which have energies in the MeV range. In fact, the experimental techniques used to search for neutrinos from WIMP annihilation are entirely different than those used to detect solar neutrinos.

Observation of energetic neutrinos from the Sun or Earth would provide a very distinctive signature for the existence of dark matter in the halo. The atmospheric-neutrino background is well modeled and is easily subtracted [340, 341]. There may also be a background of energetic neutrinos from the direction of the Sun due to interaction of cosmic rays in the Sun, but this is expected to be small [342]. Otherwise, there are no known phenomena which would produce neutrinos from the Sun or Earth. In this regard, energetic-neutrino searches have the advantage over direct-detection experiments (see Section 8): the backgrounds are better understood, so a positive detection is more

recognizable. Similarly, energetic-neutrino searches have several advantages over other indirect-detection techniques involving searches for anomalous cosmic-ray antiprotons or positrons or gamma rays from WIMP annihilation in the halo (see Section 10). Again, the neutrino background is understood better than the cosmic-ray background.

The prospects for discovery of particle dark matter by energetic-neutrino detection are generally (though not always) improved relative to other detection techniques for higher-mass WIMPs. Such WIMPs become increasingly favored as null results in accelerator searches raise the expected mass scale of supersymmetry. As we will see, the annihilation rate in the Sun or Earth is set by the capture rate, which is proportional to the number density n_χ, itself inversely proportional to the WIMP mass m_χ for a given halo density. So the annihilation rate and direct-detection rate have roughly the same scaling with WIMP mass. However, the probability of detecting a neutrino scales roughly with the square of the neutrino energy: one power comes from the charged-current cross section for producing a muon, and the second power comes from the fact that the range of a muon is roughly proportional to its energy. So the energetic-neutrino event rate generally increases relative to the direct-detection rate as the WIMP mass is increased. The flux of cosmic rays from WIMP annihilation in the halo is proportional to an integral over the volume of the Galaxy of the square of the number density, so the flux should fall off as the square of the WIMP mass as the mass is increased. Moreover, the local halo density is constrained better than the entire halo-density profile, so the rate predictions for a given model are less uncertain for energetic neutrinos (or direct detection) than they are for cosmic-ray searches.

Given this heuristic introduction, we can now move on and discuss more quantitatively the flux of such energetic neutrinos. For a given candidate WIMP, the calculation of the event rate is straightforward, although it can be quite lengthy and requires inputs from solar physics, neutrino physics, quark hadronization, etc. The flux of high-energy neutrinos of type i (e.g., $i = \nu_\mu, \bar{\nu}_\mu$, etc.) from neutralino annihilation in the Sun or Earth is

$$\left(\frac{\mathrm{d}\phi}{\mathrm{d}E}\right)_i = \frac{\Gamma_\mathrm{A}}{4\pi R^2}\sum_\mathrm{F} B_\mathrm{F}\left(\frac{\mathrm{d}N}{\mathrm{d}E}\right)_{\mathrm{F},i}(E_\nu, E_\mathrm{in})\,. \tag{9.1}$$

The quantity Γ_A is the rate of neutralino–neutralino annihilation in the Sun or Earth, and R is the Sun–Earth distance or radius of the Earth for neutrinos from the Sun or Earth, respectively. Neutralinos from the Galactic halo are accreted onto the Sun and their number in the Sun is depleted by annihilation. In most cases of interest these two processes come to equilibrium on a time scale much shorter than the age of the solar system, in which case $\Gamma_\mathrm{A} = \frac{1}{2}C$ where C is the rate for capture of neutralinos from the halo. The annihilation rate is discussed further in Section 9.3. The capture rate is determined by the flux of neutralinos incident on the Sun and a probability for capture, which in turn depends on kinematic factors and the cross sections for elastic scattering of the neutralino off of the elements in the sun. We discuss in detail the capture-rate computation in Section 9.4. The sum is over all annihilation channels F (e.g., pairs of gauge or Higgs bosons or fermion–antifermion pairs), B_F is the annihilation branch for channel F, and $(\mathrm{d}N/\mathrm{d}E)_{\mathrm{F}i}$ is the differential energy spectrum of neutrino type i at the *surface* of the Sun or Earth expected from injection of the particles in channel F in the *core* of the Sun or Earth. The spectra $(\mathrm{d}N/\mathrm{d}E)_{\mathrm{F}i}$ are functions of the neutrino energy E_ν and of the energy E_in of the injected particles. Determination of these spectra is quite complicated as it involves hadronization of the annihilation products,

interaction of the particles in the resulting cascade with the surrounding medium and the subsequent interaction of high-energy neutrinos with the solar medium as they propagate from the core to the surface of the Sun [343–345]. The spectra of neutrinos from the Sun are different than those from the Earth. These spectra are discussed in Section 9.5.

The best technique for inferring the existence of the neutrino is observation of an upward muon produced by a charged-current interaction in the rock below the detector. The cross section for production of a muon is proportional to the neutrino energy, and the range of the muon in rock is roughly proportional to the muon energy. Therefore, the rate for observation of energetic neutrinos is proportional to the second moment of the neutrino energy spectrum. Inserting the numerical values for the charged-current cross section and the effective range of the muon, and ignoring detector thresholds, the rate per unit detector area for neutrino-induced throughgoing-muon events may be written [256, 343]

$$\Gamma_{\text{detect}} = (2.54 \times 10^{-29}\,\text{m}^{-2}\,\text{yr}^{-1}) \frac{\Gamma_A}{\text{s}^{-1}} \left(\frac{m_\chi}{1\,\text{GeV}} \right)^2 \sum_i a_i b_i \sum_F B_F \langle N z^2 \rangle_{F,i}(m_\chi) \,, \tag{9.2}$$

for neutrinos from the Sun; the same expression multiplied by 5.6×10^8 (the square of the ratio of the Earth–Sun distance to the Earth's radius) gives the rate for neutrino events from the Earth. The a_i are neutrino-scattering coefficients, $a_\nu = 6.8$ and $a_{\bar{\nu}} = 3.1$, and the b_i are muon-range coefficients, $b_\nu = 0.51$ and $b_{\bar{\nu}} = 0.67$ [343]. The quantity

$$\langle N z^2 \rangle_{F,i}(E_{\text{in}}) \equiv \frac{1}{E_{\text{in}}^2} \int \left(\frac{dN}{dE} \right)_{F,i} (E_\nu, E_{\text{in}}) E_\nu^2 \, dE_\nu \,, \tag{9.3}$$

is the second moment of the spectrum of neutrino type i from final state F scaled by the square of the injection energy E_{in} of the annihilation products. The quantity $z = E_\nu / E_{\text{in}}$ is the neutrino energy scaled by the injection energy. In Section 9.5, we list analytic expressions for the scaled second moments for all the final states F which give rise to energetic neutrinos.

Strictly speaking, neutrino telescopes observe neutrinos only with energies above a given threshold. Therefore, the event rate is proportional to the contribution to the second moment from neutrinos with energies above threshold – that is, there is a lower bound to the integral in Eq. (9.3). To obtain the most accurate experimental information, a detailed calculation of the neutrino spectra should be folded in with the detector response. For example, an energetic-neutrino signal from the Sun must be distinguishable from the atmospheric-neutrino background. The direction of the neutrino-induced muon is correlated with the parent-neutrino direction only within an angular window of roughly $\sqrt{1\,\text{GeV}/E_\nu}$ radians. Therefore, a proper determination of the signal-to-noise ratio requires knowledge of the neutrino energy spectrum.

On the other hand, in cases where the WIMP is quite massive, most of the neutrinos have energies large enough to produce a muon with an energy much higher than the detector threshold. For example, if a 100-GeV WIMP annihilates to gauge bosons, the typical neutrino energy is roughly half that, and the typical muon energy is usually half that – about 25 GeV. Typical thresholds for current and next-generation detectors are no more than 10 GeV, so the vast majority of the neutrinos in this example are above threshold. In addition, even if a non-negligible fraction of the neutrinos have energies below the detector threshold, the total second moment of the energy distribution is still primarily determined by the higher-energy neutrinos. The contribution of

neutrinos with energies below threshold to the upward-muon flux will be $\mathcal{O}(E_{\rm thresh}^3/m_\chi^3)$ where $E_{\rm thresh}$ is the threshold energy. Therefore, in cases where the WIMP mass is significantly larger than the detector threshold, the expression for the rate for neutrino-induced upward muons, Eq. (9.2), together with the results for $\langle Nz^2\rangle$ presented here, will provide a good theoretical estimate to compare with experimental determinations of the flux of upward muons from the Sun and/or Earth.

The most promising method of detection of the energetic neutrinos, especially for higher-mass WIMPs, is the upward-muon signal. Neutrinos may also be detected by contained events in which a charged lepton is produced within the detector, but because this process is proportional only to the neutrino energy E (as opposed to E^2 for throughgoing events), the throughgoing muons should provide a more promising signature for heavy neutralinos. Of course, if the neutrino spectra $({\rm d}N/{\rm d}E)_{{\rm F},i}$ are known, then the rates for contained events can be calculated. Here we will focus primarily on the upward-muon signal. Therefore, we will list only expressions for the scaled second moments $\langle Nz^2\rangle$ of the neutrino spectra. If interested, the reader may find analytic expressions for the neutrino spectra $({\rm d}N/{\rm d}E)_{{\rm F},i}$ for all the relevant final states F in Ref. [345].

In the following subsection, we give a brief overview of the current and planned experiments suitable for searches for energetic neutrinos from WIMP annihilation. We then explain in Section 9.3 how the annihilation rates in the Sun and Earth are obtained from the capture rates. A detailed discussion of the capture rates as well as relatively simple analytic fits are given in Section 9.4. The neutrino spectra and the scaled second moments are discussed in the final subsection. We include in Sections 9.3–9.5 all the information needed for evaluating the event rate given in Eq. (9.2) for observation of neutrino-induced throughgoing muons from WIMP annihilation in the Sun and/or Earth.

9.2. Detectors and atmospheric-neutrino background

The search for energetic neutrinos from WIMP annihilation is already well underway. These detectors are generally large tanks of water instrumented with phototubes capable of detecting the Cerenkov light from neutrino-induced upward muons produced in the material below the detector. Due to the huge flux of cosmic-ray muons which dominates the neutrino signal from WIMP annihilation, neutrino observations of the Sun can be done only when the Sun is below the horizon. The experiments typically trigger only on muons which pass entirely through the detector; therefore, only muons with energies above a given threshold are counted. This threshold is about 2 GeV for the underground experiments and possibly 10 GeV for the ice and nearly 100 GeV for the ocean-water experiments now being constructed. Energy resolution above this threshold is quite difficult and has not yet been employed in the upward-muon analyses. Directional information is required to distinguish neutrinos from the Sun or core of the Earth from the atmospheric-neutrino background. However, the angular resolution required is fixed by the muon-energy threshold, not by the angular size of the Sun. The rms angle between a neutrino and the muon it produces is $\sim 20^\circ\,(E_\nu/10\ {\rm GeV})^{-1/2}$. In addition, the muon typically carries about half the neutrino energy. Therefore, when searching for energetic neutrinos from the Sun or core of the Earth, muons within an angular window with radius roughly $14^\circ\ (E_{\rm thresh}/10\ {\rm GeV})^{-1/2}$, where $E_{\rm thresh}$ is the detector threshold, must be accepted. Thus, when searching for a point source, the atmospheric-neutrino background falls as $E_{\rm thresh}^{-1}$ as the threshold energy is raised. For the large class of WIMPs with mass much larger than threshold, $m_\chi \gg E_{\rm thresh}$, the loss in signal is only a factor

$O(m_\chi^3/E_{\rm thresh}^3)$ [345], so the signal-to-noise ratio can be increased substantially with increased thresholds.

The energetic-neutrino background comes from atmospheric neutrinos, i.e., neutrinos produced by cosmic-ray spallation in the atmosphere. The theoretical calculation of the expected flux [346, 347] agrees quite well with measurements [332, 334]. For a muon-energy threshold cutoff of 1.7 GeV, the upward-muon flux at zenith is $6.4 \times 10^{-2}\,\mathrm{m}^{-2}\,\mathrm{yr}^{-1}\,\mathrm{sr}^{-1}$ [332, 334]. The atmospheric-neutrino spectrum falls steeply with energy, but this is counteracted when considering the energy spectrum of atmospheric-neutrino induced muons by the fact that the probability of detecting the neutrino is proportional to its energy squared. Thus, there is some reduction – in addition to that from better angular resolution discussed above – in the atmospheric-neutrino background from increased energy thresholds, but it is not dramatic.

Now we briefly review some of the detectors. The first class are underground detectors. These are multipurpose detectors suitable for searching for proton decay or magnetic monopoles, detecting supernovae, solar and atmospheric neutrinos and cosmic rays in addition to WIMP searches. The Irvine–Michigan–Brookhaven (IMB) detector, an 8000 t underground water detector designed to look for proton decay, had an exposure of roughly 400 m^2 yr [333, 334]. IMB detected muons with energies greater than $\gtrsim 2$ GeV. This detector is no longer in operation. After seven years of operation, the Kamiokande detector had an exposure of 215 m^2 yr to the Sun, and the muon-energy threshold is 1.7 GeV [331, 348]. These two experiments constrain the flux of energetic neutrinos from the Sun with energies $\gtrsim 2$ GeV to be less than $2.1 \times 10^{-2}\,\mathrm{m}^{-2}\,\mathrm{yr}^{-1}$ (90% C.L. limit). In addition, Kamiokande has analyzed upward muons from the Earth's core. With an exposure of 770 m^2 yr to the Earth's core, they obtain an upper limit of $1.3 \times 10^{-2}\,\mathrm{m}^{-2}\,\mathrm{yr}^{-1}$. The other detector currently in operation is the Monopole, Astrophysics, and Cosmic Ray Observatory (MACRO) with an area of exposure both to the Sun and Earth of about 850 m^2, also with a 2-GeV threshold [336]. After six months of operation, the limits on neutrinos from the Sun and Earth are slightly weaker, but almost competitive with those set by Kamiokande. It is expected that their sensitivity to energetic neutrinos from the Sun and Earth will improve the current Kumiokande sensitivities by a factor of 2 to 3 after five years of operation.

In addition to the underground detectors, there are several experiments under construction or beginning operation which rely on the novel idea of using sea water or antarctic ice as Cerenkov detectors. In addition to WIMP searches, these experiments will also be capable of doing atmospheric-neutrino and cosmic-ray physics as well as detecting ultra high-energy neutrinos from cosmic rays or active galactic nuclei, for example. Strings of phototubes which are simply placed in the water or in holes drilled in the ice are used to detect Cerenkov photons from throughgoing muons. The Deep Undersea Muon and Neutrino Detector (DUMAND) (see Fig. 27) [337], located off the coast of Hawaii, is expected to have an exposure area in the first phase of 300 m^2 which will later be expanded to 3000 m^2. The NESTOR (Neutrinos from Supernovae and TeV Sources Ocean Range) experiment is a similar effort located off the coast of Greece. An exposure area of 3×10^4 m^2 is forecast [339]. The Antarctic Muon and Neutrino Detector Array (AMANDA) (see Fig. 28) is situated at the South Pole [338]. Although ice near the surface is opaque, the ice a kilometer below the surface is relatively clear and has an attenuation length comparable to water. AMANDA is expected to have an exposure of 1000 m^2. Finally, the Baksan detector, located in North Caucasus, has an effective area of 289 m^2, and the collaboration is currently searching for neutrinos from WIMP annihilation [349].

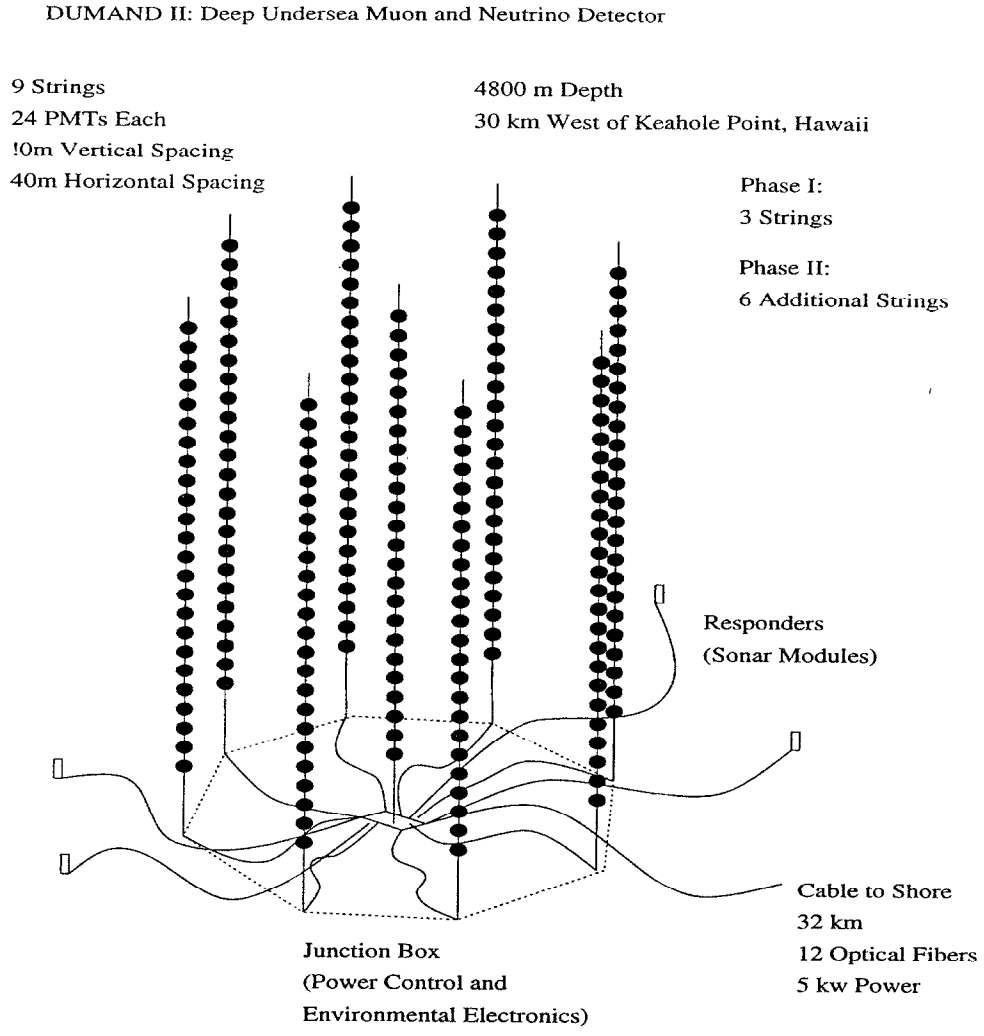

Fig. 27. Diagram of the DUMAND neutrino detector [337].

9.3. Annihilation rate in the Sun and Earth

The first step in calculating the rate for WIMP-induced neutrino events from the Sun is the determination of the rate at which WIMPs annihilate in the Sun. WIMPs accumulate in the Sun or Earth by capture from the Galactic halo and are depleted by annihilation. If N is the number of WIMPs in the Sun (or Earth), then the differential equation governing the time evolution of N is

$$\dot{N} = C - C_A N^2 , \tag{9.4}$$

where the dot denotes differentiation with respect to time. Here, C is the rate of accretion of WIMPs onto the Sun (or Earth). The determination of C is straightforward and will be discussed in detail below, and if the halo density of WIMPs remains constant in time, C is of course time-independent.

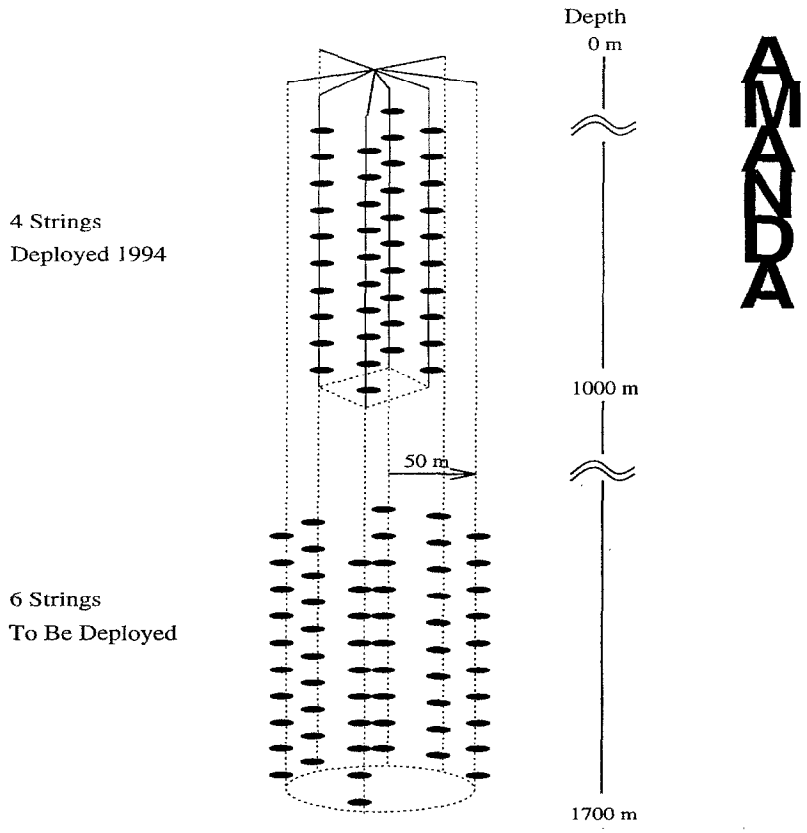

Fig. 28. Diagram of the AMANDA neutrino detector [338]. The final configuration may differ slightly from that shown here.

The second term on the right-hand side is twice the annihilation rate in the Sun (or Earth), $\Gamma_A = \frac{1}{2} C_A N^2$, and accounts for depletion of WIMPs. The quantity C_A depends on the WIMP annihilation cross section and the distribution of WIMPs in the Sun (or Earth) [128]

$$C_A = \langle \sigma_A v \rangle V_2 / V_1^2 , \tag{9.5}$$

where $\langle \sigma_A v \rangle$ is the total annihilation cross section times relative velocity in the limit of zero relative velocity (since captured WIMPs move *very* slowly), and is reviewed in Section 6, and the quantities V_j are effective volumes for the Sun or Earth [128, 350]

$$V_j = [3 m_{Pl}^2 T / (2 j m_\chi \rho)]^{3/2} , \tag{9.6}$$

where T is the temperature of the Sun or Earth, m_{Pl} is the Planck mass, and ρ is the core density of the Sun or Earth. In Ref. [128], it is found that $V_j = 6.5 \times 10^{28} (j m_\chi^{10})^{-3/2}\,\mathrm{cm}^3$, where m_χ^{10} is the WIMP mass in units of 10 GeV, for the Sun. In Ref. [350], it is found that $V_j = 2.0 \times 10^{25} (j m_\chi^{10})^{-3/2}\,\mathrm{cm}^3$ for the Earth.

Solving Eq. (9.4) for N, we find that the annihilation rate at any given time is

$$\Gamma_A = \tfrac{1}{2} C \tanh^2(t/\tau) , \tag{9.7}$$

where $\tau = (CC_A)^{-1/2}$ is the time scale for capture and annihilation to equilibrate. Therefore, if the age of the solar system is much greater than the equilibrium time scale ($t_\odot \simeq t_\oplus = 1.5 \times 10^{17}\,\mathrm{s} \gg \tau_A$), then the neutrino flux is at "full strength" ($\Gamma_A = \frac{1}{2}C$), but if $\tau \gg t_\odot$ then the annihilation rate is smaller and the neutrino signal is diluted accordingly.

Taking $t_\odot \simeq t_\oplus \simeq 4.5$ Gyr as the age of the solar system, we find

$$\frac{t_\odot}{\tau_\odot} = 330\left(\frac{C_\odot}{\mathrm{s}^{-1}}\right)^{1/2}\left(\frac{\langle\sigma_A v\rangle}{\mathrm{cm}^3\,\mathrm{s}^{-1}}\right)^{1/2}\left(\frac{m_\chi}{10\,\mathrm{GeV}}\right)^{3/4}, \tag{9.8}$$

and

$$\frac{t_\oplus}{\tau_\oplus} = 1.9 \times 10^4\left(\frac{C_\oplus}{\mathrm{s}^{-1}}\right)^{1/2}\left(\frac{\langle\sigma_A v\rangle}{\mathrm{cm}^3\,\mathrm{s}^{-1}}\right)^{1/2}\left(\frac{m_\chi}{10\,\mathrm{GeV}}\right)^{3/4}, \tag{9.9}$$

where $C_\odot$ and $C_\oplus$ are the capture rates in the Sun and Earth (see the following subsection), and $\langle\sigma_A v\rangle$ is the total annihilation cross section times relative velocity in the limit $v \to 0$. As we will see, the capture rate in the Earth is generally a factor $\lesssim 10^{-9}$ of that in the Sun while the value of V_j in the Earth is only about 3×10^{-4} of that in the Sun, so the value of τ is always larger in the Earth than in the Sun; consequently, the fraction of full signal in the Earth can never be greater than that in the Sun. In most cases where the signal is observable, the signal is at full strength, so the annihilation rates in the Sun and Earth are proportional to the capture rate. Therefore, we emphasize that it is generally the elastic-scattering cross section – not the annihilation cross section – that determines the annihilation rate.

Angular distribution of energetic neutrinos: Once WIMPs are captured, they settle (in a time much smaller than the solar-system age) to the core of the Sun or Earth with an isothermal distribution at a temperature equal to the core temperature of the Sun or Earth. Although the Sun is effectively a point source of energetic neutrinos from WIMP annihilation, the Earth is not. It can be shown [350] that roughly 98% of the signal originates within a $14^\circ\,(m_\chi/20\,\mathrm{GeV})^{-1/2}$ cone around the center of the Earth. If massive enough (greater than about 50 GeV), then the neutrino signal from the Earth is effectively a point source when we recall that the ability of the detector to resolve the direction of the incoming neutrino is limited by the finite angle at which the muon in a charged-current event is produced. For lower-mass WIMPs, the angular distribution [350] should be included in the analysis of upward-muon data.

Evaporation: It is conceivable that once captured, WIMPs could be ejected by hard elastic scattering from nuclei [14, 128, 351–353]. Heuristically, we might expect this to occur if the typical WIMP velocity, approximately $(T/m_\chi)^{1/2}$ where T is the temperature at the core of the Sun or Earth, was comparable to or exceeded the escape velocity. One finds that only WIMPs with masses $\lesssim 10$ GeV may undergo evaporation from both the Sun and Earth. More careful calculations [128, 352] support this order-of-magnitude estimate of the evaporation mass.

9.4. Capture rate in the Sun and Earth

The rate of accretion of WIMPs in the Sun was first calculated by Press and Spergel [351], and accretion in the Earth was first discussed by Freese [13] and by Krauss et al. [14]. A more careful

and accurate calculation of the capture rates was then carried out by Gould [350, 354]. Complete expressions for the capture rates in both the Sun and Earth are given in Refs. [350, 354]. The results depend on the velocity dispersion in the halo, the velocity at which the solar system passes through the halo, the local density of WIMPs, and the composition of the Sun and Earth. Results were presented without form-factor suppression of the WIMP–nucleus interaction and with a form-factor suppression approximated as an exponential. Although accurate, the expressions given therein are fairly involved. On the other hand, given the factor-of-two uncertainties in the local halo density and velocity dispersion, and the number of WIMP models to be explored, it is often desirable to have expressions for the capture rate which are accurate to O(10%) or so. Therefore, in this section we will provide approximations to the complete results of Gould [350, 354] which can be easily evaluated. One can refer to the original Gould papers for increased accuracy or for a more careful assessment of the dependence of the results on velocity dispersion or velocity of the Earth or Sun through the halo, for example.

Although the calculation of the rate for capture of WIMPs in an astrophysical object becomes quite involved, the basic idea is simple. Suppose a halo WIMP which has a velocity v_∞ far away from the object has a trajectory that passes through the object. At a point within the body where the escape velocity is $v_{\rm esc}$, the WIMP velocity will then be $(v_\infty^2 + v_{\rm esc}^2)^{1/2}$. If the WIMP elastically scatters from a nucleus of mass $m_{\rm N}$ to a velocity less than $v_{\rm esc}$, the WIMP will be captured. Kinematics tells us that the fractional energy loss (Q/E) of the WIMP in the collision must lie in the range

$$0 \le Q/E \le 4m_\chi m_{\rm N}/(m_\chi + m_{\rm N})^2 \,. \tag{9.10}$$

As discussed in Section 7, the WIMP generally scatters from nuclei with spin (which for the purpose of capture in the Sun or Earth includes only the hydrogen in the Sun) via an axial-vector or "spin-dependent" interaction. In addition, the WIMP may scatter from any nucleus via a scalar interaction in which the WIMP couples to the mass of the entire nucleus. In some cases (for example, the Dirac neutrino), there may be a vector coupling, although this does not occur for WIMPs which are Majorana particles. If so, then the WIMP coupling to the nucleus is similar to the scalar coupling.

If there is an axial-vector interaction, then the cross section for elastic scattering of the neutralino from nucleus i is isotropic, and the probability for a given energy loss is flat in the interval of Eq. (9.10). If the neutralino scatters via a scalar interaction, then at high momentum transfer there will be a form-factor suppression to the cross section. Then, the probability for a given energy loss is no longer flat in the interval given by Eq. (9.10). For the purpose of illustration, we will assume for now that the scattering is isotropic so that the probability for a given energy loss is flat in the interval in Eq. (9.10). The rate of capture of the WIMP by scattering from nucleus i at this point in the Sun is then the rate of elastic scattering, $\sigma_0^i n^i (v_{\rm esc}^2 + v_\infty^2)^{1/2}$ (where n^i is the number density of nucleus i, and σ_0^i is the cross section for elastic scattering of a WIMP from nucleus i), times the conditional probability that the WIMP is scattered to a velocity less than $v_{\rm esc}$;

$$\frac{1}{\beta_+}\left(\beta_+ - \frac{v_\infty^2}{v_\infty^2 + v_{\rm esc}^2}\right)\theta\left(\beta_+ - \frac{v_\infty^2}{v_\infty^2 + v_{\rm esc}^2}\right) = \frac{1}{v_{\rm esc}^2 + v_\infty^2}\left(v_{\rm esc}^2 - \frac{v_\infty^2}{\beta_-}\right)\theta\left(v_{\rm esc}^2 - \frac{v_\infty^2}{\beta_-}\right), \tag{9.11}$$

where $\beta_\pm = 4m_\chi m_{\rm N}/(m_\chi \pm m_{\rm N})^2$, and θ is the Heaviside step function.

The conditional probability that a WIMP will be captured in a scattering event is greatest when β_- is maximized, which occurs when the WIMP mass closely matches the mass of the nucleus from which it scatters. Furthermore, this resonance effect is much sharper in the Earth than in the Sun; the velocities of the WIMPs have a Maxwell–Boltzmann distribution with velocity dispersion of $\bar{v} = 270\ \mathrm{km\,s^{-1}}$ and the escape velocity from the Earth ranges from $11.2\ \mathrm{km\,s^{-1}}$ (at the surface) to $14.8\ \mathrm{km\,s^{-1}}$ (at the center), so the probability is nonzero only for the very slow WIMPs on the Boltzmann tail or for WIMPs with masses that very nearly match m_N. In a detailed analysis, Gould [350] finds that WIMPs in the "resonance range" of 10–80 GeV have masses which are sufficiently close to the mass of an element with a significant abundance in the Earth so that their capture is not kinematically suppressed. On the other hand, the escape velocity just at the surface of the Sun is $618\ \mathrm{km\,s^{-1}}$ (and v_{esc} is much greater at the center), so capture in the Sun is not kinematically suppressed unless β_- is quite small (i.e., the neutralino and nuclear masses are *very* mismatched) and the resonance range for capture in the Sun is much larger than in the Earth.

If the WIMP has scalar (or vector) interactions with the nucleus, and the momentum transfer q is not small compared to the inverse of the nuclear radius R, the neutralino does not 'see' the entire nucleus. If so, the cross section for scattering of neutralinos from nuclei is form-factor suppressed (like that for electromagnetic elastic scattering of electrons from nuclei). As discussed in Section 7, the form-factor suppression may be approximated in terms of the energy loss Q as [350]

$$F(Q) = \exp(-Q/2Q_0)\,, \tag{9.12}$$

where $Q_0 = 1.5/(2m_N R_0^2)$. Here, R_0 is the nuclear radius,

$$R_0 \simeq [0.91(m_N/\mathrm{GeV})^{1/3} + 0.3] \times 10^{-13}\ \mathrm{cm}\,. \tag{9.13}$$

Now let us consider the relevance of form-factor suppression for the capture of WIMPs in the Sun and Earth. First of all, for a WIMP with a kinetic energy $E_\infty = \frac{1}{2}m_\chi v_\infty^2$ in the halo to be captured, it must have an energy loss in the range

$$E_\infty \le Q \le \beta_+(E_\infty + E_{esc})\,, \tag{9.14}$$

where $E_{esc} = \frac{1}{2}m_\chi v_{esc}^2$ is the WIMP escape energy at the point of collision in the Sun. The lower limit comes from the condition that the WIMP scatter from a velocity $(v_\infty^2 + v_{esc}^2)^{1/2}$ to a velocity less than v_{esc}, and the upper limit is the kinematic limit. This implies that, in order to be captured, the WIMP energy in the halo must be $E_\infty \le \beta_- E_{esc}$, which in turn implies that the largest energy loss involved in capture of WIMPs from the halo is $Q_{max} = \beta_- E_{esc}$.

Consider the effect of form-factor suppression, first on capture in the Earth. Because of the factor of $(m_\chi - m_N)^2$ in the denominator of β_-, coherence loss will be most important for capture of WIMPs with masses that match those of nuclei in the Earth, roughly in the resonance range 10–80 GeV. In particular, coherence loss results in suppression factors of 0.99, 0.94, and 0.72 for capture on resonance (i.e., $m_\chi \simeq m_N$) by oxygen, silicon, and iron, respectively [350]. The value of Q_0 for iron, the heaviest element important for capture in both the Sun and Earth, is 4×10^{-5} GeV. The largest energy loss involved in capture in the Earth occurs at the center of the Earth and is roughly 2×10^{-6} GeV. Therefore, form-factor suppression is negligible for capture of WIMPs with mass $\gtrsim 80$ GeV in the Earth, and is never more than a 28% effect for capture of lighter WIMPs.

On the other hand, the escape velocity in the Sun greatly exceeds the escape velocity in the Earth, and E_{esc} in the Sun is at least three orders of magnitude greater in the Sun than in the Earth. So

a WIMP must generally undergo a much harder scatter when it is captured in the Sun. For example, the maximum energy loss for capture from iron in the Sun is 8×10^{-3} GeV, which implies that a proper calculation of capture in the Sun must include the effects of form-factor suppression of the coherent scalar interaction. From detailed calculations, one finds that the form-factor suppression of capture from hydrogen and helium is negligible, capture from scattering off elements with atomic masses 12–32 is moderately suppressed, while capture from scattering off iron can be suppressed by several orders of magnitude for WIMPs in the several hundred GeV range. If there were no form-factor suppression, owing to the factor of m_N^4 [see Eq. (7.36)] in the scalar (or vector) cross section, one would expect scattering from iron nuclei to dominate the capture of WIMPs in the Sun; however, because of the form-factor suppression, capture of heavy WIMPs in the Sun occurs primarily by scattering from oxygen [350]. Even so, capture from scattering off iron nuclei is still significant. When considering the complete capture rate due to scalar interaction of WIMPs from nuclei in the Sun, one finds that the form-factor suppression of the scalar elastic-scattering cross section decreases the capture rate by a factor of about 0.3 for WIMPs of mass 80 GeV and about 0.07 for WIMPs of mass of order 1 TeV. Incidentally, as the neutralino mass is increased beyond a few TeV, the form-factor suppression ceases to decrease with increasing WIMP mass; the reason is that if the nuclear mass is negligible compared to the WIMP mass, the momentum transfer does not depend on the WIMP mass.

Even if the exponential form factor is not necessarily a good approximation to the actual form factor at large momentum transfers [293], most capture occurs at small momentum transfer (since the correct form factor must also become very small at large momentum transfers) where the exponential form is a good approximation. Capture of WIMPs via the axial-vector interaction occurs only from hydrogen in the Sun, so detailed axial-vector form factors [23, 269] are not needed for capture-rate calculations. Therefore, the results obtained for the capture rate using the exponential approximation for the form factor for scalar (or vector) interactions will be fairly accurate. The exact form-factor suppression may be important for accurate determination of direct-detection rates (see Section 8).

The full capture-rate calculation assumes the astrophysical object moves through a homogeneous Maxwell–Boltzmann distribution of WIMPs and requires information about the elemental composition of the object and the distribution of elements in the object. One must integrate over the trajectories of the WIMP through the Sun and Earth and over the velocity distribution of the WIMPs [350, 354]. We write the total capture rate C as the sum of the capture rate via axial-vector scattering, C_{ax}, and capture via a scalar (or vector) interaction, C_{sc}.

For the case of accretion via scalar interactions, Gould's result for the capture rate in the Sun is

$$C_{sc}^{\odot} = \frac{\rho_\chi M_\odot v_*}{4m_\chi^2} \sum_i \frac{(m_\chi + m_{N_i})^2 \sigma_0^i f_i}{a m_{N_i}^2} \left[2 \frac{\exp(-a\hat{\eta}^2)}{(1+a)^{1/2}} \operatorname{erf}(\hat{\eta}) - \frac{\exp(-a\hat{\eta}^2)}{(A_c^2 - A_s^2)(1+a)^{3/2}} \right.$$
$$\times \left\{ \left(\hat{A}_+ \hat{A}_- - \frac{1}{2} - \frac{1+a}{a-b} \right) [\operatorname{erf}(\hat{A}_+) - \operatorname{erf}(\hat{A}_-)] + \frac{1}{\sqrt{\pi}} \left(\hat{A}_- e^{-\hat{A}_+^2} - \hat{A}_+ e^{-\hat{A}_-^2} \right) \right\}_{A=A_s}^{A_c}$$
$$\left. + \frac{\exp(-b\check{\eta}^2)}{(a-b)\,(A_c^2 - A_s^2)\,(1+b)^{1/2}} \{ [2\operatorname{erf}(\check{\eta}) - \operatorname{erf}(\check{A}_+) + \operatorname{erf}(\check{A}_-)]\, e^{-(a-b)A^2} \}_{A=A_s}^{A=A_c} \right], \tag{9.15}$$

where the sum is over the elements in the Sun, $v_* = \sqrt{2/3}\bar{v}/\eta$, $\eta \simeq 1$ is the dimensionless velocity of the solar system through the halo, ρ_χ is the local halo WIMP density, $M_\odot$ is the solar mass, and σ_0^i is the cross section for elastic scattering from nucleus i. Here,

$$a = m_\chi \bar{v}^2/(2Q_0), \qquad b = \beta_+ a, \qquad \hat{\eta} = \eta/(1+a)^{1/2}\,, \tag{9.16}$$

$$\check{\eta} = \eta/(1+b)^{1/2}, \qquad \hat{A} = A(1+a)^{1/2}, \qquad \check{A} = A(1+b)^{1/2}\,, \tag{9.17}$$

$$\hat{A}_\pm = \hat{A} \pm \hat{\eta}, \quad \check{A}_\pm = \check{A} \pm \check{\eta}, \quad A^2(v) = \beta_- v^2/\bar{v}^2, \quad A_c = A(v_c), \quad A_s = A(v_s)\,, \tag{9.18}$$

where $\beta_\pm = 4m_\chi m_N/(m_\chi \pm m_N)^2$. For the Sun, the escape velocity to be used at the center is $v_c = 1354\,\mathrm{km\,s^{-1}}$, and the escape velocity to be used at the surface is $v_s = 795\,\mathrm{km\,s^{-1}}$. (An approximation to the escape-velocity profile was used to obtain (9.15); thus the discrepancy with the actual escape velocities.) The analogous expression for capture in the Earth via the scalar interaction can be obtained by replacing $M_\odot \to M_\oplus$, and using the escape velocities appropriate for the Earth: $v_c = 11.2\,\mathrm{km\,s^{-1}}$ and $v_s = 14.8\,\mathrm{km\,s^{-1}}$. WIMPs undergo additional accretion in the Sun (but not the Earth; remember, only a negligible fraction of the Earth's mass is in nuclei with spin) via axial-vector interactions from hydrogen nuclei. The rate for capture in the Sun via axial-vector interactions can be obtained from Eq. (9.15) by summing over hydrogen only and replacing $\sigma_{0\,\mathrm{scalar}}^i$ by $\sigma_{0\,\mathrm{spin}}^{\mathrm{H}}$. Form-factor suppression is negligible for capture from hydrogen, so the $E \to \infty$ [$a \to 0$ limit of Eq. (9.15)] can be used when evaluating capture via axial-vector scattering.

In the simplest (and perhaps most likely) scenarios, $\eta \simeq 1$. For this case, we have obtained greatly simplified approximations to Eq. (9.15). The axial-vector interaction leads to capture in the Sun only (so $C_{\mathrm{ax}}^{\oplus} = 0$) with a rate

$$C_{\mathrm{ax}}^{\odot} = (1.3 \times 10^{25}\,\mathrm{s^{-1}}) \frac{\rho_{0.3}^{\chi} \sigma_{0\,\mathrm{spin}}^{\mathrm{H}(40)} S(m_\chi/m_{\mathrm{H}})}{(m_\chi/(1\,\mathrm{GeV}))\bar{v}_{270}}\,, \tag{9.19}$$

where $\sigma_{0\,\mathrm{spin}}^{\mathrm{H}(40)}$ is the cross section for WIMP–proton elastic scattering via the axial-vector interaction in units of $10^{-40}\,\mathrm{cm^2}$ [Eq. (7.16)], $\bar{v}_{270}$ is the dark-matter velocity dispersion in units of $270\,\mathrm{km\,s^{-1}}$, and $\rho_{0.3}^{\chi}$ is the local halo mass density in units of $0.3\,\mathrm{GeV\,cm^{-3}}$. Recall that the axial-vector interaction does not lead to accretion of WIMPs in the Earth. The rates for capture of WIMPs in the Sun and Earth via a scalar[9] interaction can be written [256]

$$C_{\mathrm{sc}} = c \frac{\rho_{0.3}^{\chi}}{(m_\chi/\mathrm{GeV})\bar{v}_{270}} \sum_i F_i(m_\chi)\, \sigma_{0\,\mathrm{scalar}}^{i(40)}\, f_i \phi_i S(m_\chi/m_{\mathrm{N}_i})/(m_{\mathrm{N}_i}/(1\,\mathrm{GeV}))\,, \tag{9.20}$$

where $c = 4.8 \times 10^{24}\,\mathrm{s^{-1}}$ for the Sun and $c = 4.8 \times 10^{15}\,\mathrm{s^{-1}}$ for the Earth. The sum is over all species of nuclei in the astrophysical object (here the Earth or Sun), m_{N_i} is the mass of the ith nuclear species in GeV, f_i is the mass fraction of element i, and $\sigma_{0\,\mathrm{scalar}}^{i(40)}$ is the cross section for elastic scattering of the neutralino from nucleus i via a scalar interaction [Eq. (7.36)] in units of $10^{-40}\,\mathrm{cm^2}$. The quantities ϕ_i describe the distribution of element i in the Sun or Earth, and are listed in Tables 8 and 9, as are the quantities f_i. These approximations are obtained assuming the solar system moves through the halo with a velocity equal to the dark-matter velocity dispersion. Increasing the solar-system velocity slightly decreases the capture rate and vice versa.

[9] This expression also applies for WIMPs, such as Dirac neutrinos, which have vector interactions with nuclei. The form-factor suppression for this case is similar to that for the scalar interaction, so the form of the $F_i(m_\chi)$ is similar.

Table 8
Solar composition

Element	Mass Number	f_i	ϕ_i
H	1	0.772	3.16
He	4	0.209	3.4
C	12	3.87×10^{-3}	3.23
N	14	9.4×10^{-4}	3.23
O	16	8.55×10^{-3}	3.23
Ne	20	1.51×10^{-3}	3.23
Mg	24	7.39×10^{-4}	3.23
Ni	28	8.13×10^{-4}	3.23
S	32	4.65×10^{-4}	3.23
Fe	56	1.46×10^{-3}	3.23

Table 9
Earth composition

Element	Mass Number	f_i	ϕ_i
O	16	0.3	1.2
Si	28	0.15	1.2
Mg	24	0.14	1.2
Fe	56	0.3	1.6
Ca	40	0.015	1.2
P	30	0.011	1.2
Na	23	0.004	1.2
S	32	0.05	1.6
Ni	59	0.03	1.6

The quantity $S(m_\chi/m_N)$ is the kinematic suppression factor for capture of a WIMP of mass m_χ from a nucleus of mass m_N, and is given by [256]

$$S(x) = [A^b/(1 + A^b)]^{1/b}\,, \tag{9.21}$$

where

$$A = \frac{3}{2}\frac{x}{(x-1)^2}\left(\frac{\langle v_{esc}\rangle^2}{\bar{v}^2}\right), \tag{9.22}$$

and $b = 1.5$. The quantity $\langle v_{esc}\rangle$ is a mean escape velocity obtained by fitting this analytic approximation to the exact result. For the Sun, $\langle v_{esc}\rangle = 1156\,\mathrm{km\,s^{-1}}$, and for the Earth, $\langle v_{esc}\rangle = 13.2\,\mathrm{km\,s^{-1}}$. Note that $S(x) \to 1$ for $x \to 1$, $S(x) \to 3/2\ (\langle v_{esc}\rangle^2/\bar{v}^2)x^{-1}$ for $x \to \infty$ and $S(x) \propto 3/2\,(\langle v_{esc}\rangle^2/\bar{v}^2)x$ for $x \to 0$. In other words, capture is kinematically suppressed if the WIMP mass differs from the nuclear mass, and there is no kinematic suppression if the two masses are similar.

The form-factor suppression $F_i(m_\chi)$ of the capture of a WIMP of mass m_χ from nucleus i is obtained simply by comparing the results for Gould's capture rates with and without coherence loss [350, 354]. For capture in the Earth, coherence is lost when the WIMP mass matches closely the mass of a nucleus in the Earth. Coherence loss is never more than a 6% effect for scattering from any nucleus except for iron, in which case it may be as large as a 28% suppression if the WIMP mass very closely matches the mass of iron. Thus, for O(5%) accuracy, $F_i(m_\chi)$ may be taken to be unity for scattering from all elements except for iron. For iron, we find that

$$F_{\mathrm{Fe}} \simeq 1 - 0.26[A/(1+A)]\,, \tag{9.23}$$

where A is given in Eq. (9.22), provides a good approximation to the form-factor suppression.

For capture in the Sun, the resulting $F_i(m_\chi)$ are plotted in Fig. 29. From Fig. 29 we see that the form-factor suppression for capture from scattering off hydrogen and helium is negligible, capture from scattering off of elements with atomic masses 12–32 is moderately suppressed, while capture from scattering off iron is suppressed by several orders of magnitude for WIMPs in the several hundred GeV range. For hydrogen, the form factor suppression is $F_{\mathrm{H}}(m_\chi) = 1$. For the other

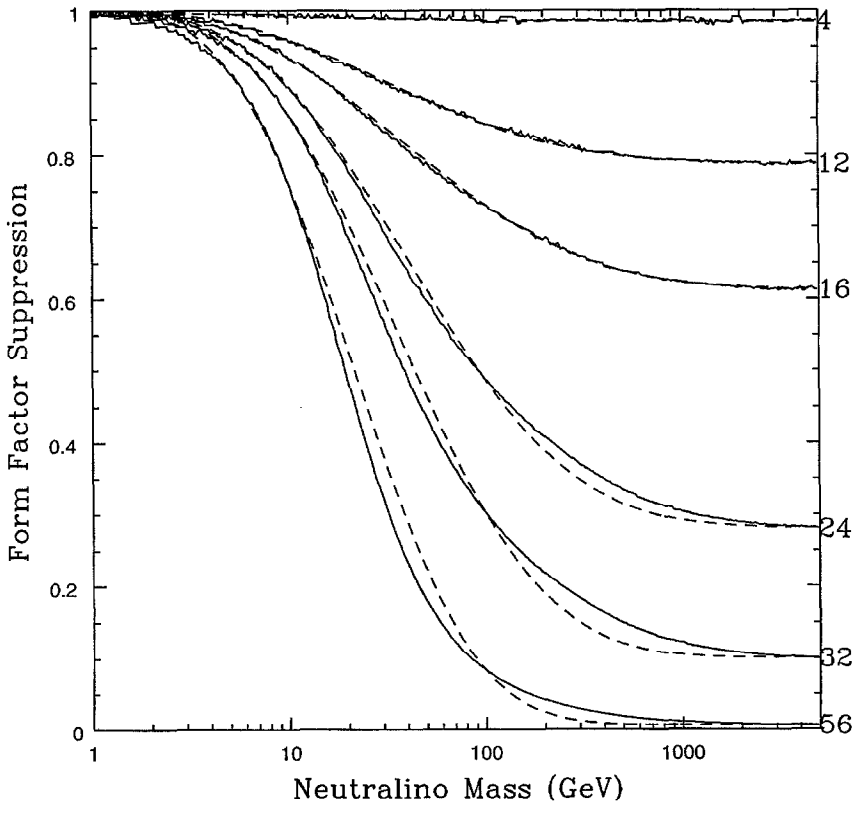

Fig. 29. Form-factor suppression of capture in the Sun as a function of WIMP mass for nuclei with mass numbers 4, 12, 16, 24, 32 and 56. The solid curves are the exact results, and the dashed curves are the analytic approximation given here.

Table 10
Fit parameters for form-factor suppression of capture in the Sun

Element	m_c^i (GeV)	$F_i^{\inf}$	α_i
He	18.2	0.986	1.58
C	61.6	0.788	2.69
N, O, Ne	75.2	0.613	2.69
Mg, Si	71.7	0.281	2.97
O	57.0	0.101	3.1
Fe	29.3	0.00677	3.36

elements, the following expression provides a fairly accurate analytic fit to the results:

$$F_i(m_\chi) = F_i^{\inf} + (1 - F_i^{\inf}) \exp\left[-\left(\frac{\log m_\chi}{\log m_c^i}\right)^{\alpha_i} \right], \tag{9.24}$$

where $F_i^{\inf}$ and α_i are fit parameters given in Table 10.

"Model-independent" capture rates: Evaluation of the expression, Eq. (9.19), for the rate for accretion of WIMPs onto the Sun via an axial-vector interaction is relatively simple. All it requires for a given model is the WIMP mass and the cross section for axial-vector scattering from hydrogen. On the other hand, the expression, Eq. (9.20), for capture in the Earth and Sun via the scalar interaction is more complicated since it requires for each model several additional cross sections for scattering from heavier nuclei. In general, each of these cross sections must be evaluated individually for each WIMP candidate. However, in most cases, simplifications can be made [301, 355].

As noted in Section 8 [Eq. (8.23)], in all but a few pathological cases, the scalar cross section for scattering from nucleus i can be written [301],

$$\sigma_i^{0\,\text{scalar}} = \frac{4m_\chi^2 m_N^4}{\pi(m_\chi + m_N)^2} (f_p/m_p)^2 , \tag{9.25}$$

where $f_p \simeq f_n$ is the scalar neutralino–nucleon coupling [Eqs. (7.28) and (7.30)]. As pointed out in the previous section, all the information needed about any specific MSSM for the scalar neutralino–nucleus interaction is encoded in f_p, and it is *independent* of the nuclear mass. Then, f_p can be taken outside the summation in Eq. (9.20), and the capture rates via scalar interactions in the Sun and Earth can be written as [301]

$$C_\odot = 2.4 \times 10^{37}\ \text{s}^{-1}\ \rho_\chi^{0.3} f_\odot(m_\chi)\,(f_p/\text{GeV}^{-2})^2 , \tag{9.26}$$

$$C_\oplus = 2.4 \times 10^{28}\ \text{s}^{-1}\ \rho_\chi^{0.3} f_\oplus(m_\chi)\,(f_p/\text{GeV}^{-2})^2 , \tag{9.27}$$

where the neutralino-mass dependence of the capture rates is encoded in the functions

$$f(m_\chi) = \sum_i f_i \phi_i S_i(m_\chi) F_i(m_\chi) m_{N_i}^3\, m_\chi/(m_\chi + m_{N_i})^2 . \tag{9.28}$$

These functions (for the Sun and Earth) are plotted in Fig. 30.

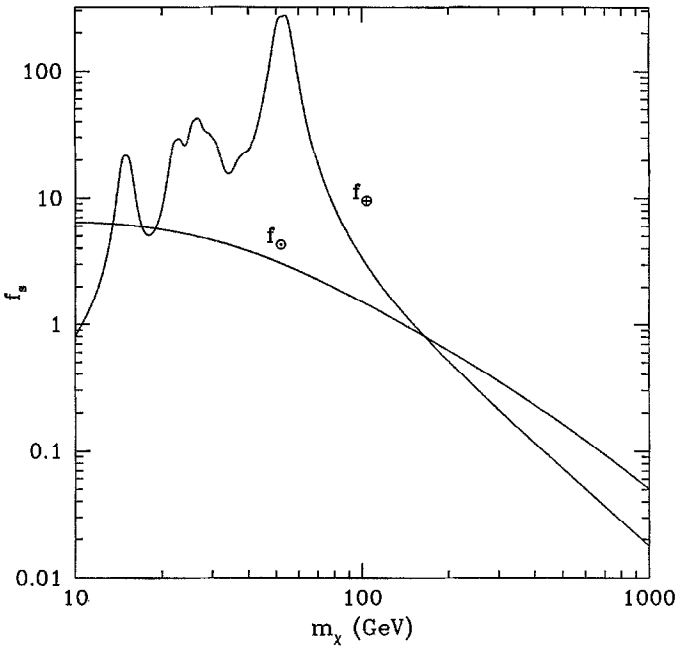

Fig. 30. Plot of the neutralino-mass dependence of the scalar capture rate in the Sun, $f_\odot(m_\chi)$, and Earth, $f_\oplus(m_\chi)$ as a function of neutralino mass.

9.5. Neutrino spectra

A proper calculation of the spectra $(\mathrm{d}N/\mathrm{d}E)_{\mathrm{F},i}$ of neutrinos of type i from injection of particles F is crucial in order to evaluate accurately the energetic-neutrino event rate. Hadronization, neutrino absorption and stopping, and stopping of heavy hadrons (those containing b and c quarks) must be included [343]; otherwise, the predicted event rates can be off by as much as an order of magnitude. The neutralino-annihilation products which produce energetic neutrinos are τ leptons, b, c, and t quarks, and gauge and Higgs bosons. Light (that is u, d, and s) quarks are relatively long lived, so they will come to rest in the center of the Sun or Earth before decaying. Consequently, the energy of the neutrinos from decays of these light particles will be small, and the probability of detecting them is negligible. Neutrino spectra from decays of τ leptons and b and c quarks were first calculated by Gaisser et al. [15]. Ritz and Seckel then pointed out the importance of hadronization, stopping of heavy hadrons, and stopping and absorption of neutrinos, and included them in a Monte Carlo calculation of the neutrino spectra for the same final states, and for a top quark which was assumed to have a mass of 60 GeV. More recently, an analytic calculation of the neutrino spectra which includes all the important effects (and an updated treatment of the top quark) was performed for *all* the final states [345]. In this subsection, we will briefly discuss the various effects and describe the steps in the calculation. We will then list results for all the scaled second moments, which are those results needed to calculate the throughgoing muon fluxes. The interested reader is referred to Ref. [345] for more details of the calculation as well as expressions for the complete spectra.

For all of the particles considered, the neutrino distribution $(\mathrm{d}N/\mathrm{d}E)^{\mathrm{rest}}(E_\nu)$, as a function of the neutrino energy E_ν, in the rest frame of the decaying particle, is that of a standard two- or three-body decay. Given the rest-frame distribution, the energy distribution of a particle moving with an energy E_d, velocity β, and $\gamma = (1-\beta^2)^{-1/2} = E_\mathrm{d}/m_\mathrm{d}$ (where m_d is the decaying-particle mass) is related to the rest-frame distribution by

$$\left(\frac{\mathrm{d}N}{\mathrm{d}E}\right)^{\oplus}(E_\mathrm{d}, E_\nu) = \frac{1}{2}\int_{E_-(E)}^{E_+(E)} \frac{d\varepsilon}{\varepsilon}\frac{1}{\gamma\beta}\left(\frac{\mathrm{d}N}{\mathrm{d}E}\right)^{\mathrm{rest}}(\varepsilon)\,, \tag{9.29}$$

where

$$E_\pm(E) = E_\nu/[\gamma(1 \mp \beta)]\,. \tag{9.30}$$

This assumes that the particles are unpolarized. In Ref. [345], it is shown that polarization is never more than a small ($\lesssim 10\%$) effect.

The Earth is thin enough that stopping of heavy hadrons and stopping and absorption of neutrinos as they pass through the Earth can be neglected. Therefore, if the rest-frame distribution from a particular decaying particle is known, Eq. (9.29) gives the correct $\mathrm{d}N/\mathrm{d}E$ for particle decay in the Earth; hence the superscript $\oplus$ in Eq. (9.29). This also implies that the neutrino and antineutrino spectra from injection of a given particle–antiparticle pair in the center of the Sun are the same. Also, if the scaled second moment in the rest frame of the decaying particle, $\langle Nz^2\rangle^{\mathrm{rest}}$, is known, then the scaled second moment for a particle that decays with a velocity β in the Earth is simply

$$\langle Nz^2\rangle(\beta) = \langle Nz^2\rangle^{\mathrm{rest}}(1 + \beta^2/3)\,. \tag{9.31}$$

Neutrino stopping and absorption: The calculation is more complicated for neutrinos injected in the core of the Sun. Energetic neutrinos will lose energy via neutral-current interactions with the solar medium and become absorbed via charged-current interactions as they pass through the Sun. In particular, a neutrino injected with an energy E leaves the Sun with energy

$$E_\mathrm{f} = \frac{E}{1 + E\tau_i}\,, \tag{9.32}$$

where $\tau_\nu = 1.01\times 10^{-3}\,\mathrm{GeV}^{-1}$ and $\tau_{\bar\nu} = 3.8\times 10^{-4}\,\mathrm{GeV}^{-1}$, and with probability

$$P_\mathrm{f} = \left(\frac{1}{1 + E\tau_i}\right)^{\alpha_i}\,, \tag{9.33}$$

where $\alpha_\nu = 5.1$ and $\alpha_{\bar\nu} = 9.0$ [343]. As a result, the neutrino spectrum for a particle decaying with energy E_d in the Sun, $(\mathrm{d}N/\mathrm{d}E)^{\odot}$, is related to the neutrino spectrum for a particle decaying with energy E_d in the Earth, $(\mathrm{d}N/\mathrm{d}E)^{\oplus}$, by

$$\left(\frac{\mathrm{d}N}{\mathrm{d}E}\right)_i^{\odot}(E_\mathrm{d}, E_\nu) = (1 - E_\nu\tau_i)^{\alpha_i - 2}\left(\frac{\mathrm{d}N}{\mathrm{d}E}\right)^{\oplus}(E_\mathrm{d}, E_\mathrm{m})\,, \tag{9.34}$$

where $E_\mathrm{m} = E_\nu/(1 - E_\nu\tau_i)$ is the energy a neutrino had at the core of the Sun if it exits with energy E_ν. Note that stopping and absorption are different for neutrinos and antineutrinos, so the spectrum of neutrinos from WIMP annihilation in the Sun is different than the spectrum of

antineutrinos. (The spectrum of neutrinos is the same as that for antineutrinos for decays in the Earth, so we neglect the subscript i on neutrino spectra from the Earth.)

Hadronization: If a b or c quark is injected into the center of the Earth, it will lose energy during hadronization. As a result, the energy at which the hadron decays in the Earth, E_d, is related to the energy E_{in} at which it is injected by $E_d = z_f E_{in}$. For c quarks, $z_f = 0.58$, and for b quarks, $z_f = 0.73$ [343, 345]. Actually, there is a distribution of z_f described by a fragmentation function [356], but this fragmentation function is highly localized around z_f. No more than 5% accuracy is lost by using the central value of the fragmentation function [345].

Stopping of heavy hadrons: In addition, the core of the Sun (but *not* the Earth) is dense enough that b- and c-quark hadrons will interact with the solar medium and be slowed appreciably before they decay [343]. If a hadron initially has an energy $E_0 = z_f E_{in}$ (after hadronization of a quark injected with energy E_{in}), then it will decay with an energy E_d picked from a decay distribution [343, 345][10]

$$\left(\frac{1}{N}\frac{dN}{dE_d}\right)^{\text{hadron}}(E_0, E_d) = \frac{E_c}{E_d^2}\exp\left[E_c\left(\frac{1}{E_0} - \frac{1}{E_d}\right)\right], \tag{9.35}$$

where $E_c = 250$ GeV for c quarks, $E_c = 470$ GeV for b quarks.

The average energy at which a hadron decays is

$$\langle E_d \rangle (E_0) = E_c \exp(E_c/E_0)\, E_1(E_c/E_0)\,, \tag{9.36}$$

where $E_1(x) = \int_x^\infty (e^{-y}/y)\, dy$ [357], and the rms value of the decay energy is [345]

$$E_d^{\text{rms}}(E_0) = \sqrt{\langle E_d^2 \rangle} = \sqrt{E_c(E_0 - \langle E_d \rangle)}\,. \tag{9.37}$$

These quantities will be used in the following.

Stopping of heavy hadrons is perhaps the greatest source of theoretical uncertainty in the calculation of the neutrino spectra; very little is known about the interaction of heavy-quark hadrons with dense matter. Although the functional form of the decay distribution, Eq. (9.35), is physically well motivated, the values of E_c listed here are subject to some (perhaps sizeable) uncertainty. However, this theoretical uncertainty also enters the Monte Carlo calculation. In this regard, Monte Carlo simulations offer no improvement over the analytic result. Also, the effect of hadron stopping is small at lower energies, so the uncertainty introduced into the neutrino spectra is relatively small. Stopping becomes much stronger – and the subsequent theoretical uncertainty much larger – at higher injection energies, but in most cases where the WIMP is massive enough that it can annihilate into top quarks, it annihilates almost exclusively to top quarks, gauge bosons, and/or Higgs bosons [132–134]. Therefore, the uncertainty in the *total* neutrino spectrum due to poor understanding of hadron stopping is never very large.

Neutrino spectra from the Earth: We will now list the results (from Ref. [345]) for all final states that produce energetic neutrinos (except for Higgs bosons) for the scaled second moments of the

[10] Note that this equation corrects a typographical error in Ref. [345].

neutrino spectra from injection of particles into the core of the Earth. Higgs-boson neutrino spectra for the Sun and Earth will be discussed below. Since neutrinos are not absorbed or stopped significantly in passing through the Earth, the results for muon neutrinos and antineutrinos are the same. Further details, as well as functional forms for the complete spectra can be found (with the same notation) in Ref. [345].

For injection of $\tau\bar{\tau}$ pairs with energy $E_{\rm in}$ and velocity $\beta = (1 - m_\tau^2/E_{\rm in}^2)^{1/2}$ in the core of the Earth, the scaled second moment is

$$\langle Nz^2\rangle^{\oplus}_{\tau\bar{\tau}}(E_{\rm in}) = (\Gamma_{\tau\to\mu\nu\nu}/10)\,(1 + \beta^2/3)\,, \tag{9.38}$$

where $\Gamma_{\tau\to\mu\nu\nu} \simeq 0.18$ is the branching ratio for τ decay to muons.

A b or c quark injected with energy $E_{\rm in}$ decays with energy $E_{\rm d} = z_{\rm f}E_{\rm in}$ and velocity $\beta = (1 - m_{\rm q}^2/E_{\rm d}^2)^{1/2}$ and $m_{\rm q}$ is the quark mass. The expression for decay of a b quark injected with energy $E_{\rm in}$ is then

$$\langle Nz^2\rangle^{\oplus}_{\rm b\bar{b}}(E_{\rm in}) = (z_{\rm f}^2\Gamma_{\rm b\to\mu\nu X}/10)\,(1 + \beta^2/3)\,, \tag{9.39}$$

where $\Gamma_{\rm b\to\mu\nu X} \simeq 0.103$ is the branching ratio for inclusive semileptonic decay of the b quark into muons [1], and that from c-quark decay is

$$\langle Nz^2\rangle^{\oplus}_{\rm c\bar{c}}(E_{\rm in}) = (2z_{\rm f}^2\Gamma_{\rm c\to\mu\nu X}/15)\,(1 + \beta^2/3)\,, \tag{9.40}$$

where $\Gamma_{\rm c\to\mu\nu X} \simeq 0.13$ is the branching ratio for inclusive semileptonic decay of the c quark into muons.

The second moment for neutrinos from the Earth from injection of $W^{\pm}$ pairs with energy $E_{\rm in}$ and velocity β is given by

$$\langle Nz^2\rangle^{\oplus}_{\chi\chi\to WW}(E_{\rm in}) = \Gamma_{W\to\mu\nu}\tfrac{1}{4}(1 + \tfrac{2}{5}\beta^2)\,, \tag{9.41}$$

where $\Gamma_{W\to\mu\nu} = 0.105$ is the branching ratio for W decay to a muon neutrino, and the second moment for neutrinos from the Earth from injection of ZZ pairs is given by

$$\langle Nz^2\rangle^{\oplus}_{\chi\chi\to ZZ}(E_{\rm in}) = 2\Gamma_{Z\to\nu_\mu\bar{\nu}_\mu}\tfrac{1}{4}(1 + \tfrac{2}{5}\beta^2)\,, \tag{9.42}$$

where $\Gamma_{Z\to\nu_\mu\bar{\nu}_\mu} = 0.067$ is the branching ratio for Z decay to muon neutrinos.

The top quark decays as $t \to Wb$ with a branching ratio near unity, so the neutrino spectrum is obtained from those of W and b-quark decay. The result for a top quark injected with energy $E_{\rm in}$ and velocity β is

$$\langle Nz^2\rangle^{\oplus}_{t\bar{t}}(E_{\rm in}) = \left(1 + \frac{\beta^2}{3}\right)\left\{\frac{\Gamma_{W\to\mu\nu}E_W^2}{4m_t^2}\left[1 + \tfrac{1}{5}\beta_W^2(2 - f_L)\right] + \Gamma_{b\to\mu\nu X}\frac{2z_f^2E_b^2}{15m_t^2}\right\}, \tag{9.43}$$

where $E_W = (m_t^2 + m_W^2)/(2m_t)$ is the energy of the W boson in the rest frame of the decaying top, $E_b = (m_t^2 - m_W^2)/(2m_t)$ is the energy of the b quark in this frame, and $\beta_W = E_b/E_W$ is the W-boson velocity in this frame. A fraction $f_L = (1 + 2m_t^2/m_W^2)^{-1}$ of the W bosons from top-quark decay are produced in the longitudinal-helicity state [5]. And the b-quark value for z_f should be used in Eq. (9.43).

Note that in all cases, the $\langle Nz^2\rangle(E_{\rm in})$ for particles with mass m go to a constant for $E_{\rm in} \gg m$ (i.e., $\beta \to 1$). Therefore, away from thresholds, we insert the numerical values lised above (and take $m_t = 174$ GeV [358]) and find that the $\langle Nz^2\rangle$ for decays of τ leptons, b and c quarks, W and

Z bosons, and top quarks are simply 0.024, 0.0073, 0.0078, 0.037, 0.047, and 0.012, respectively. So gauge bosons give the strongest neutrino signals, followed by τ leptons, top quarks, and finally b and c quarks.

Neutrino spectra from the Sun: For neutrinos from the Sun, stopping and absorption of neutrinos and stopping of heavy hadrons must be included, so the expressions for the neutrino spectra from the Sun are far more complicated than the corresponding results for the Earth. Stopping and absorption of neutrinos in the Sun are significant effects, so the spectra for neutrinos from particle decay in the Sun are different than those for antineutrinos.

For $\tau\bar{\tau}$ pairs injected in the core of the Sun, the results are

$$\langle Nz^2\rangle^{\odot}_{\bar{\tau}\tau,i}(E_{\rm in}) = \Gamma_{\tau\to\mu\nu\nu}\, h_{\tau,i}(E_{\rm in}\tau_i)\,, \tag{9.44}$$

where the τ_i are the neutrino stopping coefficients given above. For muon neutrinos, the function $h_{\tau,i}(y)$ is given by

$$h_{\tau,\nu_\mu}(y) = \tfrac{1}{30}\,[(4+y)/(1+y)^4]\,, \tag{9.45}$$

and for antineutrinos, the appropriate function is

$$h_{\tau,\bar{\nu}_\mu}(y) = \tfrac{1}{1260}\,[(168 + 354y + 348y^2 + 190y^3 + 56y^4 + 7y^5)/(1+y)^8]\,. \tag{9.46}$$

Calculation of neutrino spectra from b and c quarks injected in the core of the Sun must include the effects of heavy-quark stopping. An accurate (to a few percent) approximation to the exact results for quark f (where f = c, b) is provided by

$$\langle Nz^2\rangle_{{\rm f},i}(E_{\rm in}) \simeq \frac{\langle E_{\rm d}\rangle^2}{E_{\rm in}^2}\, h_{{\rm f},i}\left(\sqrt{\langle E_{\rm d}^2\rangle}\,\tau_i\right), \tag{9.47}$$

where the subscript i refers to neutrino type (ν_μ or $\bar{\nu}_\mu$), and the moments $\langle E_{\rm d}^n\rangle$ are those that were given above. For b quarks, the functions $h_{{\rm b},i}$ are the same as those for τ leptons given previously: $h_{{\rm b},i}(y) = h_{\tau,i}(y)$ [cf. Eqs. (9.45) and (9.46)]. For neutrinos, the c-quark functions are,

$$h_{{\rm c},\nu_\mu}(y) = \tfrac{1}{180}\,[(32 + 25y + 5y^2)/(1+y)^5]\,, \tag{9.48}$$

and for antineutrinos,

$$h_{{\rm c},\bar{\nu}_\mu}(y) = \tfrac{1}{7560}\,(1344 + 3186y + 3834y^2 + 2786y^3 + 1242y^4 + 315y^5 + 35y^6)/(1+y)^9\,. \tag{9.49}$$

The result for the scaled second moment of the neutrino distribution from decay of W bosons with energy $E_{\rm in}$ and velocity β in the Sun is [256]

$$\langle Nz^2\rangle^{\odot}_{{\rm WW},i} = \frac{\Gamma_{{\rm W}\to\mu\nu}}{\beta}\,\frac{2 + 2E\tau_i(1+\alpha_i) + E^2\tau_i^2\alpha_i(1+\alpha_i)}{E_{\rm in}^3\tau_i^3\alpha_i(\alpha_i^2-1)\,(1+E\tau_i)^{\alpha_i+1}}\Bigg|_{E=E_{\rm in}(1-\beta)/2}^{E=E_{\rm in}(1+\beta)/2}\,. \tag{9.50}$$

The expression for ZZ pairs is obtained by replacing $\Gamma_{{\rm W}\to\mu\nu}$ with $2\Gamma_{{\rm Z}\to\nu_\mu\bar{\nu}_\mu}$, where the factor of two counts the Z bosons.

The expression for $\langle Nz^2\rangle$ as a function of the top-quark injection energy, $E_{\rm in}$, for top quarks injected into the Sun, is obtained by integrating the expressions for $\langle Nz^2\rangle$ for the W boson and

b quark from top-quark decay,

$$\langle Nz^2\rangle_{t\bar{t}}^{\odot}(E_{in}) = \frac{1}{E_{in}^2}\sum_{f=b\bar{b},WW}\frac{1}{2\gamma_t E_f\beta_f\beta_t}\int_{\gamma_t E_f(1-\beta_t\beta_f)}^{\gamma_t E_f(1+\beta_t\beta_f)} E^2\langle Nz^2\rangle_f^{\odot}(E)\,dE\,, \tag{9.51}$$

where we have included the sum over both the W bosons and b quarks from top-quark decay. The integral is over the injection energy of the decay particles, and the moments $\langle Nz^2\rangle_f^{\odot}$ include the effects of interactions with the solar medium. For W bosons, $\langle Nz^2\rangle^{\odot}$ is given by Eq. (9.50), and for b quarks by Eq. (9.47). The quantities E_{in}, $\beta_t = (1 - m_t^2/E_{in}^2)^{1/2}$, and $\gamma_t = (1-\beta_t^2)^{-1/2}$ are the energy, velocity, and γ factors of the top quark. The quantities E_W and β_W are the energy and velocity of the W boson and E_b and $\beta_b \simeq 1$ are the energy and velocity of the b quark in the rest frame of the top, as given above. Also, recall that the $\langle Nz^2\rangle$ for neutrinos from the Sun are different than those for antineutrinos.

In Fig. 31, we plot the second moments, $m_\chi^2\langle Nz^2\rangle_\nu^{\odot}$, of the neutrino spectra from the various annihilation channels for particles injected with energy equal to the neutralino mass m_χ, as a function of m_χ. Fig. 32 shows the same for antineutrinos. Gauge bosons, τ leptons, and top quarks all decay before they can hadronize or be slowed, so the neutrino signal from these final states are all roughly comparable. On the other hand, b and c quarks hadronize and are slowed in the Sun before they decay, so the neutrino signals from these final states are suppressed significantly relative to those from the other final states. The decrease in the neutrino signal from gauge bosons at large m_χ shown in Figs. 31 and 32 are due to neutrino absorption in the Sun. The neutrino signal for the other final states is similarly attenuated at energies larger than those shown in the figures here.

Neutrinos from Higgs-boson decay in the Sun and Earth: Finally, consider neutrinos from Higgs-boson decay, $H \to l_1 l_2$, to lighter particles l_1 and l_2, which then decay to energetic neutrinos. In general, decays of both scalar Higgs bosons, h^0 and H^0, the pseudoscalar Higgs boson, A^0, and the charged Higgs bosons, $H^{\pm}$, will produce energetic neurinos. The lighter particles will be τ leptons, b and c quarks, and if heavy enough, perhaps top quarks, gauge bosons, or other Higgs bosons, l_2,

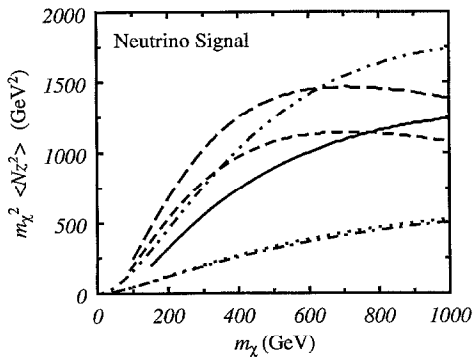

Fig. 31. The second moment, $m_\chi^2\langle Nz^2\rangle$, of the neutrino energy distribution from injection of particles with energy equal to the WIMP mass m_χ in the Sun. The solid curve is for $t\bar{t}$ pairs, the upper (lower) dashed curve is for W^+W^- (ZZ) pairs, and the upper dot–dash curve is for $\tau\bar{\tau}$ pairs. At the bottom are the $b\bar{b}$ and $c\bar{c}$ curves, and the $b\bar{b}$ curve is slightly higher than the $c\bar{c}$ curve.

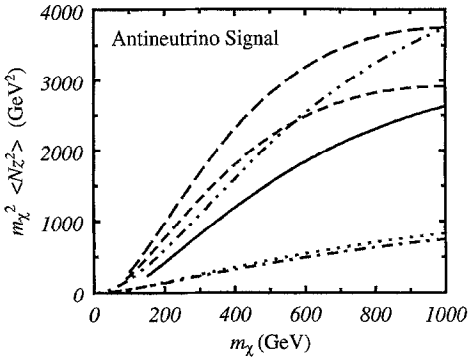

Fig. 32. Same as Fig. 31, but for antineutrinos.

which then decay to energetic neutrinos. In the rest frame of the decaying H, the energies of the two light particles are $E_1 = (m_H^2 + m_1^2 - m_2^2)/(2m_H)$ and $E_2 = (m_H^2 + m_2^2 - m_1^2)/(2m_H)$, and their velocities are $\beta_1 = (1 - m_1^2/E_1^2)^{1/2}$ and $\beta_2 = (1 - m_2^2/E_2^2)^{1/2}$, where m_H, m_1, and m_2 are the masses of H, l_1, and l_2, respectively. Suppose that the scaled second moment of the neutrino spectrum from decay of l_1 for a given injection energy E_{in} is $\langle Nz^2 \rangle_1 (E_{in})$, and similarly for neutrinos from decays of l_2. Then the scaled second moments of the neutrino spectrum from Higgs bosons which decay with energy E_{in}, velocity β_H, and Lorentz factor γ_H, are given by

$$\langle Nz^2 \rangle_H (E_{in}) = \frac{1}{E_{in}^2} \sum_D B_D \sum_{f=1,2} \frac{1}{2\gamma_H E_f \beta_f \beta_H} \int_{\gamma_H E_f (1-\beta_H \beta_f)}^{\gamma_H E_f (1+\beta_H \beta_f)} E^2 \langle Nz^2 \rangle_f (E)\, dE\,, \tag{9.52}$$

where the sum on D is over all decay channels of the Higgs, B_D is the Higgs-decay branch to D, and E_f and β_f are the decay-particle energies in the rest frame of the Higgs boson. Note that Eq. (9.52) works for neutrino spectra from both the Sun and Earth.

The branching ratios B_D and decay-product energies E_f and velocities β_f for each Higgs boson can only be evaluated once the Higgs-sector model parameters (tan β and one of the Higgs-boson masses) are specified, so the Higgs-boson $\langle Nz^2 \rangle$ will be model-dependent. The branching ratios for Higgs-boson decay may be obtained from the formulas in Appendix B in Ref. [19]. In some cases, superpartners may be among the decay products of some of the Higgs bosons; however, if the neutralino is assumed to be the LSP, then the Higgs bosons produced in neutralino annihilation will never decay to superpartners.

9.6. *Model-independent analysis and summary*

Neutralinos in the Galactic halo will accrete onto the Sun and Earth and annihilate therein, giving rise to a high-energy neutrino signal that could potentially be observed in terrestrial detectors. The differential energy flux of such neutrinos is given in terms of the annihilation rate, Γ_A, by Eq. (9.1). This annihilation rate is given in terms of the capture rate, C by Eq. (9.7), and the capture rate is discussed in Section 9.4. In addition, the neutrino spectra from various annihilation channels must be known, and these are discussed in Section 9.5. The most promising technique for detection of such energetic neutrinos is via observation of upward muons produced by

charged-current interactions of the neutrinos in the rock below the detector. The probability for detecting such a neutrino in this fashion is proportional to the square of the neutrino energy, so only the second moments of the neutrino spectra are needed.

There are many steps that enter the calculation, and for each model, there are factors that affect the final result for the event rate. Both the scalar and axial-vector elastic-scattering cross sections for a given model are needed for the capture rates. The annihilation cross sections are needed to determine the branching ratios into the final states whose decays produce energetic neutrinos. Furthermore, all these enter into determination of the equilibration time which affects the total annihilation rate. As a result, there are many cranks to turn before an event rate can be obtained for any given model, and it may be difficult to understand in a qualitative sense how the end results may depend on the input parameters.

Here, we briefly discuss how event rates may be estimated for generic models in a somewhat model-independent way [301, 355]. Although there will always be cases that deviate from these estimates, the majority of supersymmetric (and other WIMP) dark-matter candidates will be properly described. To do so, we consider first WIMPs with only scalar couplings and then WIMPs with only axial-vector couplings. A realistic WIMP will couple both ways, so the total event rate will be the sum of the two.

We begin with WIMPs with only scalar couplings. First, note that if the scattering cross sections can be written in the form (9.25), the flux of WIMPs from annihilation in the Sun or Earth can be written [301],

$$\Gamma^{\rm sc}_{\rm detect} = d \tanh^2(t/\tau) \frac{\rho_\chi^{0.3}}{\bar{v}_{270}} f(m_\chi)\xi(m_\chi)\,(m_\chi/{\rm GeV})^2\,(f_{\rm p}/{\rm GeV}^{-2})^2\,, \tag{9.53}$$

where $d_\odot = 3.3\times10^8\,{\rm m}^{-2}\,{\rm yr}^{-1}$, and $d_\oplus = 1.7\times10^8\,{\rm m}^{-2}\,{\rm yr}^{-1}$, and it should be noted that the quantities $f(m_\chi)$, $\xi(m_\chi)$, and t/τ are different for annihilation in the Earth than they are for the Sun. Here, the function $\xi(m_\chi)$, which describes the neutrino energy spectrum from WIMP annihilation for a given mass, is given by,

$$\xi(m_\chi) = \sum_{\rm F} B_{\rm F}[3.47\,\langle Nz^2\rangle_{{\rm F},\nu}(m_\chi) + 2.08\,\langle Nz^2\rangle_{{\rm F},\bar{\nu}}(m_\chi)]\,, \tag{9.54}$$

where the sum is over all annihilation channels F available to the WIMP, and $B_{\rm F}$ is the branching ratio for annihilation into F.

Although $\xi(m_\chi)$ depends on the various annihilation channels, we can generally constrain $\xi(m_\chi)$ to lie between a lower and upper limiting value for a given WIMP mass. For example, if the neutralino is less massive than the W boson, then it generally annihilates primarily to b quarks and τ leptons, and to a much lesser extent, c quarks. The largest (smallest) value of ξ in this mass range occurs when the WIMP annihilates to τ leptons (b quarks), which often occurs, for example, if the neutralino is primarily B-ino (higgsino). If the neutralino annihilates to some combination of light fermions, then the resulting ξ will be somewhere between these limiting values. Similarly, for WIMPs heavier than the top quark, the upper (lower) limit to $\xi(m_\chi)$ comes from annihilation into top quarks, which often occurs when the neutralino is primarily B-ino (W and Z bosons, which occur when the neutralino is primarily Higgsino). Although lighter fermions give smaller neutrino fluxes than either, in all but a few pathological cases the branching ratio for annihilation into

lighter fermions is negligible if the WIMP annihilates to top quarks. And for WIMP masses between the W and top-quark masses, $\xi(m_\chi)$ is bound above (below) by the values of ξ obtained for neutralinos which annihilate only to gauge bosons (τ leptons).

These results are plotted in Fig. 33. The upper and lower solid curves show the limiting values for $\xi(m_\chi)$ as a function of WIMP mass for neutrino spectra from annihilation in the Earth. The upper and lower dashed curves show the same for annihilation in the Sun. It is indeed possible that, in some cases, the value of ξ may fall outside the indicated range. For example, if the WIMP has a significant annihilation branch into pure-Higgs-boson or gluon final states [252], then the resulting value of ξ would be lower. On the other hand, other candidate WIMPs, such as Dirac particles, could annihilate directly into neutrinos, in which case the value of ξ would be higher. However, we have checked by explicit numerical evaluation of ξ in thousands of supersymmetric models that the vast majority of the models yield a value of ξ in the regions indicated in Fig. 33.

Finally, there is the equilibration-timescale factor $\tanh^2(t/\tau)$ in Eq. (9.53). To evaluate this factor in a general fashion, we must make some additional (reasonable) assumptions. For example, if neutralinos are indeed the dark matter needed to account for a flat universe, then $\Omega_\chi h^2 \simeq 0.25$ which generally (although not always) fixes $\sigma_A v \simeq 10^{-26}$ cm^2. We then consider only models which give neutrino fluxes in the range $10^{-4} \lesssim \Gamma_{\rm detect}/({\rm m}^{-2}\ {\rm yr}^{-1}) \lesssim 10^{-2}$. Models with larger fluxes would have been observed already, and the lower limit is roughly the sensitivity obtainable with next-generation O(km^2) detectors (accounting for the atmospheric background with current energy thresholds and energy resolution; the sensitivity can in principle be improved with higher thresholds and/or better energy resolution). With these assumptions and Eq. (9.53), we can

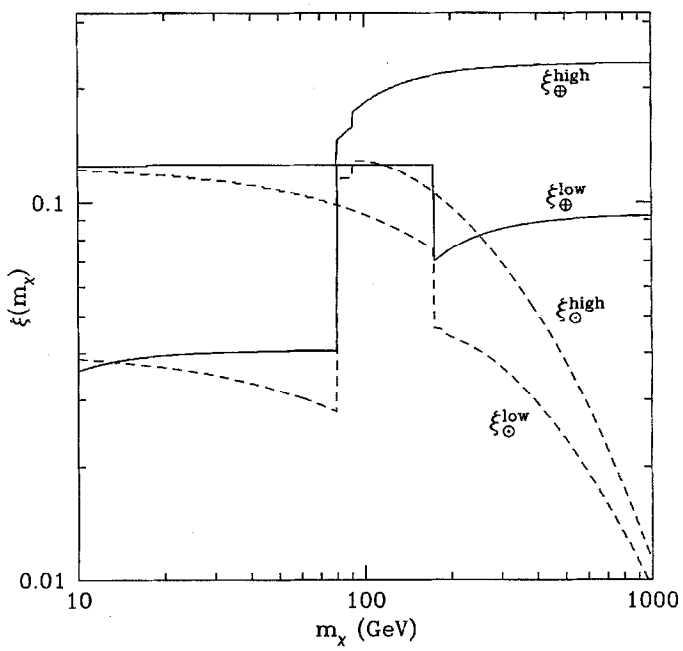

Fig. 33. Upper and lower limiting values for the function $\xi(m_\chi)$ for the Earth (solid curves) and Sun (dashed curves).

constrain the values of f_p that give rise to neutrino signals in the allowed detection range. As a result, we can show that if $\Gamma_{\rm detect}(\sigma_A v)_{26}(m_\chi/{\rm GeV})^{-1/2} r^2 \gtrsim d\xi(m_\chi)$, where $r_\odot = 2.9\times 10^7$ and $r_\oplus = 5.2\times 10^4$, then the signal is at full strength. Taking $\Gamma_\odot > 10^{-4}\,{\rm m}^{-2}\,{\rm yr}^{-1}$, and $\xi(m_\chi)\lesssim 0.25$ (the maximum value of ξ for any annihilation branch is 0.25), we find that the neutrino signal from the Sun is at full strength unless $m_\chi \gtrsim 10$ TeV. On the other hand, the signal from the Earth is potentially suppressed for any $m_\chi \gtrsim 10$ GeV. Although not fully general, these results imply that for annihilation in the Sun, $\tanh(t/\tau)$ will generally be of order unity, in which case the neutrino event rate from the Sun is easily evaluated given a mass and f_p with Eq. (9.53) and Fig. 30. The Earth signal will generally be suppressed; a more involved calculation is usually required for an accurate estimate.

With Eq. (9.53), the limiting values for $\xi(m_\chi)$, and the assumptions regarding equilibration timescales just described, we can compare rates for energetic-neutrino events from the Sun with those from the Earth for WIMPs with only scalar interaction. This comparison is to a large extent independent of the model. The results are shown in Fig. 34. The solid (dashed) curves are the results for the upper (lower) limit for $\xi(m_\chi)$, the neutrino fluxes. Equilibration of capture and annihilation are included, and the upper (lower) pairs of these curves are for models that give $\Gamma_{\rm detect} = 10^{-4}(10^{-2})\,{\rm m}^{-2}\,{\rm yr}^{-1}$. The model dependence is indicated by the range between the highest and lowest curves. The heavy solid curves show the ratios assuming both the solar and terrestrial signals are at full strength using both the upper and lower limits for $\xi(m_\chi)$. Fig. 34 indicates that for rates near the current detector sensitivity ($10^{-2}\,{\rm m}^{-2}\,{\rm yr}^{-1}$), the Earth signal is comparable to (for $m_\chi \gtrsim 80$ GeV) or greater than (for $m_\chi \lesssim 80$ GeV) the signal from the Sun. On the other hand, it is likely that in future detectors with greater sensitivity, the Sun signal will be stronger.

These results are largely independent of model parameters, within the limits of the assumptions made above, but some of the assumptions that go into the Earth/Sun comparison will not be valid for all realistic and acceptable models. For example, an acceptable relic abundance does not, strictly speaking, fix the annihilation cross section $\sigma_A v$ in the limit of zero relative velocity. This is because p-wave annihilation in the early Universe is often important, especially if the neutralino is less massive than the top quark. If anything, this overestimates $\sigma_A v$, so t/τ for the Earth may be overestimated. As a result, suppression of annihilation relative to capture will often be more important in the Earth than assumed here, and in many realistic models, the Sun/Earth ratio may be larger than shown in Fig. 34. This is illustrated further in Section 11. The Sun/Earth ratio is always $\gtrsim 1$, so the results for direct- and indirect-detection rates discussed below are insensitive (to within a factor of two) to these uncertainties.

The analysis of the case where the WIMP has only axial-vector couplings is much less involved. Such WIMPs are captured only in the Sun – not the Earth – and the capture rate, Eq. (9.19), is relatively simple. The rate for upward muons from annihilation of such particles in the Sun is then

$$\Gamma^{\rm ax}_{\rm detect} = (1.65\times 10^{-4}\,{\rm m}^{-2}\,{\rm yr}^{-1})\tanh(t_\odot/\tau_\odot)\,(m_\chi/{\rm GeV})\,\rho^\chi_{0.3}\sigma^{{\rm H}(40)}_{0\,{\rm spin}} S(m_\chi/m_{\rm H})\,\bar v^{-1}_{270}\,. \qquad (9.55)$$

The values of $\xi(m_\chi)$ are those shown for the Sun in Fig. 33. The analysis of the equilibration timescale is similar to that above. The result is that, in almost all cases of interest, $\tanh(t/\tau) \simeq 1$.

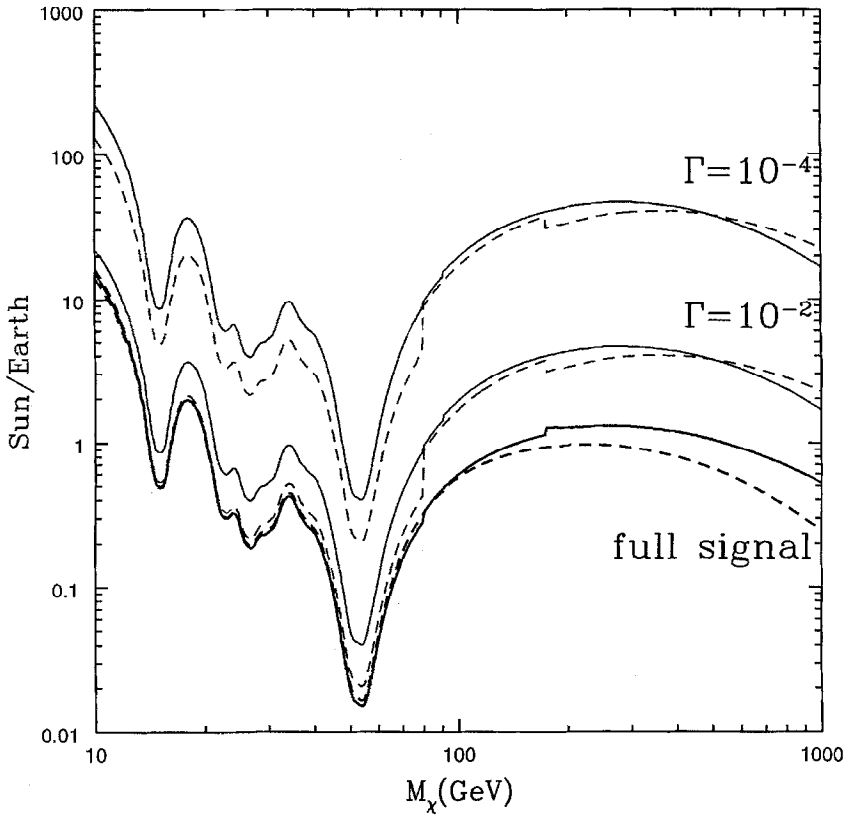

Fig. 34. Ratio of the rate for energetic neutrinos from WIMP annihilation in the Sun versus that from the Earth as a function of WIMP mass for WIMPs with scalar interactions only. The solid (dashed) curves are the results for the upper (lower) limit for $\xi(m_\chi)$, the neutrino fluxes. Equilibration of capture and annihilation are included as described in the text, and the upper (lower) pairs of these curves are for models that give $\Gamma_{\text{detect}} = 10^{-4}(10^{-2})\,\text{m}^{-2}\,\text{yr}^{-1}$. The model dependence is indicated by the range between the highest and lowest curves. The heavy solid curves show the ratios assuming both the solar and Earth signals are at full strength using both the upper and lower limits for $\xi(m_\chi)$.

9.7 Comparison of direct and indirect detection

Both direct-detection and energetic-neutrino experiments seek to detect the same WIMP candidates. Therefore, it is of some interest to compare the relative sensitivities of these experiments to various candidate dark-matter particles for purposes of detector design and search strategies. For each WIMP, there are numerous model parameters that enter the direct-detection rate, and yet other independent parameters that enter the indirect-detection rate, so the ratio of the two rates will generally be different for each model. However, using the discussion of neutrino rates above, it is possible to come up with a somewhat model-independent comparison of direct and indirect rates and to bracket the possible ratios of the two for each WIMP mass [301]. The goal is to come up with a ratio of the rate for elastic scattering in a laboratory detector to the flux of upward muons from neutrinos from WIMP annihilation in the Sun and Earth.

The first thing to note is that both the direct and indirect rates depend primarily on the matrix element for the nucleon–WIMP interaction, f_p. Both indirect and direct event rates depend on whether the interaction is scalar or axial-vector, so we consider the two interactions separately. Consider first, WIMPs with only scalar interactions. Then the event rate for direct detection is given by Eq. (8.21), and the rate for indirect detection is given by Eq. (9.53). The total upward-muon flux will be the sum of the fluxes from annihilation in both the Sun and the Earth. The comparison of direct versus indirect detection depends specifically on the nucleus used in the laboratory detector. For the purpose of illustration, we consider the rate in a germanium detector. The rate in detectors with other compositions can be scaled using Fig. 26. The results for scalar-coupled WIMPs are shown in Fig. 35 as a function of the WIMP mass [301]. The solid (dashed) curves are the ratios (including equilibration properly) for the upper (lower) limit for $\xi(m_\chi)$. The upper (lower) pair of these curves are for WIMPs that give $\Gamma = 10^{-4}(10^{-2})\,\mathrm{m}^{-2}\,\mathrm{yr}^{-1}$. The model-dependent uncertainties are indicated by the range of values between the highest and lowest curves in this plot.

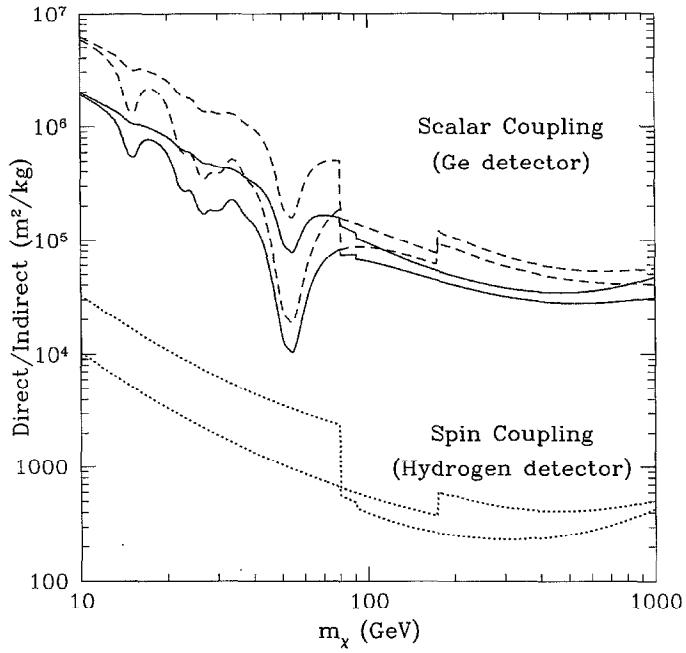

Fig. 35. Direct versus indirect detection of scalar- and spin-coupled WIMPs. For scalar-coupled WIMPs, we plot the ratio of the rate for elastic scattering from Ge in a laboratory detector to the flux of upward muons induced by neutrinos from annihilation in the Sun and Earth as a function of WIMP mass. The solid (dashed) curves are the ratios for the upper (lower) limit for the neutrino fluxes. The upper (lower) pair of these curves are for models that give $\Gamma = 10^{-4}(10^{-2})\mathrm{m}^{-2}\,\mathrm{yr}^{-1}$, and the model dependent uncertainties are indicated by the range of values between the highest and lowest curves. For scalar-coupled WIMPs, the ratios for detectors with different composition can be obtained using the scalings plotted in Fig. 26. For WIMPs with axial-vector (i.e., spin) couplings to nuclei, we plot ratios of the rate for elastic scattering from hydrogen in a laboratory detector to the flux of upward muons induced by neutrinos from annihilation in the Sun. The upper (lower) dotted curve is the ratio for the upper (lower) limit to the neutrino fluxes for spin-coupled WIMPs, and the model-dependent uncertainty is indicated by the range of values between these curves. In both cases, we neglect detector thresholds and backgrounds and assume efficiencies of order unity. From [301].

Now consider WIMPs with axial-vector interactions. Such WIMPs are captured in the Sun by scattering from hydrogen. On the other hand, the spin in the heavier nuclei used in most laboratory detectors is carried at least in part by the neutron. The spin coupling to protons differs from that to neutrons, the relation between the two depending on the details of the model, and there may be significant ambiguities in this relation as well, due to uncertainties in the measured spin content of the nucleon. Therefore, we cannot really obtain a model-independent comparison between indirect rates and scattering rates from detectors with heavier nuclei.

We can, however, make a highly model-independent comparison between indirect rates and rates in a laboratory detector made of hydrogen. Prototypes of such detectors have been tested and larger experiments are currently being considered [325]. The rate for direct detection of axially coupled WIMPs in a hydrogen detector is given by Eq. (8.18) (form-factor suppression can be neglected for scattering from hydrogen), while the upward-muon flux will be given by Eq. (9.55). Both of these detection schemes depend on the same WIMP–hydrogen cross section, so there are no uncertainties from QCD or nuclear physics that enter into the comparison. The results for the ratios of the rate for direct detection versus the upward-muon flux are given, for the allowed range of $\xi(m_\chi)$, in Fig. 35 (the dotted curves). It should be noted that if, in addition, the WIMP has some scalar couplings, there will be additional neutrinos from WIMPs captured in the Sun and Earth through scalar interactions, so the ratio of direct (from scattering off hydrogen) to indirect rates will be even smaller.

So far, we have calculated the ratios of predicted event rates in laboratory detectors to the predicted upward-muon flux in a neutrino detector. To make the comparison between the sensitivities of the two detection techniques more precise, detector thresholds and the backgrounds to be subtracted must be properly considered. For example, consider a direct-detection experiment with 1 kg Ge [305] with background rejection of 99% [306], then the expected background will be roughly 300 per year with a detection efficiency near 100% (for large WIMP masses). And for muon detectors with areas of about 10^4 m^2 [337, 338] with energy thresholds of 3 GeV, the background should coincidentally be about 300 per year (this background can potentially be reduced dramatically with a larger threshold and/or improved muon-energy resolution; for example, although they will not have good energy resolution, AMANDA should be able to distinguish between 10 and 100 GeV muons). However, according to Fig. 35, the rate for detection of scalar-coupled WIMPs is roughly 10–1000 times larger for the Ge experiment than it is for the neutrino experiment, so such a direct-detection experiment would be better suited to detecting scalar-coupled WIMPs [301].

The sensitivity of the above neutrino experiments (with the backgrounds assumed above) would be about 0.005 m^{-2} yr^{-1} after a year. For axially coupled WIMPs, Fig. 35 indicates that with no background and 100% acceptance, a laboratory hydrogen detector would need to be at least 20 g to be comparably sensitive to low-mass WIMPs, and at least 2 kg to be competitive with the neutrino detectors at the high-mass end. Therefore, the neutrino experiments would have the advantage over the 50-g hydrogen experiments currently being discussed [325]. Although these results cannot be generally scaled to direct scattering from other nuclei, we can perform a naive scaling for the purposes of illustration. To do so, we use a naive scaling of the direct-detection rate with nuclear mass and for simplicity assume that axial-vector form factors are the same as the scalar form factors. In addition, assume that the WIMP–neutron coupling is similar to the WIMP–proton coupling. Then the event rate in a 500-g isotopically pure ^{73}Ge detector would be

roughly comparable to the rate in a 10^4-m^2 neutrino detector. However, the relation of the WIMP–neutron coupling to the WIMP–proton coupling differs substantially from one model to the next, it is frequently much smaller than the WIMP–proton coupling, and it may be quite uncertain even for a given model [296]. Therefore, indirect detection would generally seem to have the advantage in probing axially coupled WIMPs.

Before concluding this discussion, it is again worth emphasizing that the relative sensitivities of direct- and indirect-detection schemes depend on a number of experimental factors which we have only touched briefly upon. With that in mind, we summarize the results of the illustrative examples discussed here. Both indirect and direct detection seem to be complementary. Although direct detection seems to be better suited for detection of scalar-coupled WIMPs, the muon detectors will potentially provide a better probe of axially coupled WIMPs.

A numerical survey of several thousand supersymmetric models verified the semi-analytic results plotted in Fig. 35. The result of these numerical calculations seemed to indicate that the majority of the models fall closer to the upper curves (those for purely scalar-coupled WIMPs) than to the lower curves (for purely axially coupled WIMPs). That is, the scalar interactions seem to dominate for most of the neutralinos we have surveyed. This implies, therefore, that direct-detection schemes may have the advantage over indirect-detection techniques for discovery of supersymmetric dark matter. Before jumping to conclusions, however, we should keep in mind that theoretical preferences are fluid. Until recently it was believed that axial-vector couplings were dominant in most supersymmetric models. It is likely that there are yet other WIMP candidates which have not been explored, for which the axial-vector interaction dominates.

Furthermore, in the case of a positive detection of a WIMP, there is much that can be learned about the WIMP from upward-muon rates. For example, the ratio of upward-muon rates from the Sun and Earth could provide information on whether the interactions are scalar or axial-vector, and perhaps even on the cosmological abundance of the WIMP [354]. By measuring the direct- versus indirect-event rates, one could extract information (e.g., from Fig. 35) on the nature of the couplings and perhaps the mass of the WIMP. The observed energy and angular distribution of detected neutrinos could provide information on the WIMP mass [359]. Along similar lines, positive detections by a variety of complementary laboratory detectors could provide information on the nature of the WIMP coupling. Therefore, although some arguments based on current theoretical notions suggest that current laboratory experiments may be more likely to discover neutralinos than the neutrino detectors, the neutrino detectors may be better suited to discovery of other models, and in case of discovery, they will provide valuable information that is complementary to that obtained by the direct experiments.

10. Cosmic rays from WIMP annihilation in the halo

The most promising and reliable methods for the discovery of WIMPs are direct detection in a laboratory experiment and observation of energetic neutrinos from WIMP annihilation in the Sun and/or Earth. Given a particle-physics model and a halo density and velocity dispersion, calculation of these event rates is straightforward and subject to a controlled theoretical uncertainty. Thus, in addition to the potential for discovery, null results from such experiments can be used to rule out dark-matter candidates.

WIMPs may have a number of other potentially observable consequences. The most studied of these is the possibility that annihilation of WIMPs in the Galactic halo can produce anomalous cosmic rays [360]. Although the WIMP is stable, two WIMPs can annihilate into ordinary matter such as quarks, leptons, gauge bosons, etc. in the same way they did in the early Universe. If WIMPs exist in the Galactic halo, then they will occasionally annihilate, and their annihilation products will produce cosmic rays. The difficulty in inferring the existence of particle dark matter from cosmic rays lies in discrimination between WIMP-induced cosmic rays and those from standard "background" sources. As will be argued below, it is quite plausible that WIMPs may produce distinctive cosmic-ray signatures distinguishable from background. It should also be made clear that propagation of cosmic rays in the Galaxy is quite poorly understood. Due to these astrophysical uncertainties, it is difficult to make reliable predictions for a given particle dark-matter candidate, so negative results from cosmic-ray searches cannot generally be used to constrain dark-matter candidates. On the other hand, if observed, these cosmic-ray signatures could provide a smoking-gun signal for the existence of WIMPs in the halo.

The three cosmic-ray annihilation products which could conceivably lead to discovery are antiprotons, positrons, and gamma rays, and each of these will be discussed in a subsection below.

10.1. Cosmic-ray antiprotons

The best place to look for a distinctive cosmic-ray signature is where the background is smallest. The majority of cosmic rays are protons, and most of the rest are heavier nuclei. Only a very small fraction are antiprotons. Cosmic-ray antiprotons are produced in standard propagation models by spallation of primary cosmic rays on hydrogen atoms in the interstellar medium [347]. The exact flux of antiprotons produced by this mechanism actually varies quite a bit in standard propagation models, and the observational situation is equally cloudy. However, there is one feature of the energy spectrum of such secondary antiprotons that is quite generic to standard cosmic-ray models: It is expected that the flux of antiprotons from primary spallation should fall dramatically at low energies, $E_{\rm p} \lesssim 1$ GeV. This is simply because an antiproton at rest must be produced with a large backward momentum in the center-of-momentum frame. This requires a primary cosmic-ray antiproton with a large energy, and the cosmic-ray spectrum falls steeply with energy.

Annihilation of WIMPs, on the other hand, *can* produce low-energy antiprotons [361–366]. WIMPs will annihilate into quarks, leptons, gauge bosons, etc. which will then hadronize and produce, among other end products, antiprotons. There is no reason why the flux of such antiprotons should decrease dramatically at energies less than a GeV. Therefore, observation of low-energy cosmic-ray antiprotons would provide evidence for WIMPs in the halo.

Calculation of the antiproton flux from WIMP annihilation is straightforward. One assumes that the WIMPs have an isothermal distribution in the halo with a density suitable for accounting for the rotation curves. The flux is proportional to the annihilation rate in the halo. The energy spectrum of the antiprotons is determined by the fragmentation functions for producing antiprotons from the various annihilation products, which are obtained from Monte Carlo simulations and from fits to accelerator data. Propagation of the antiprotons through the interstellar medium and solar modulation must also be considered.

In Fig. 36 are shown the cosmic-ray antiproton spectra (from Ref. [361]) expected from models where the dark matter is made up of B-inos of mass 30 GeV (the upper solid curve) or 60 GeV (the

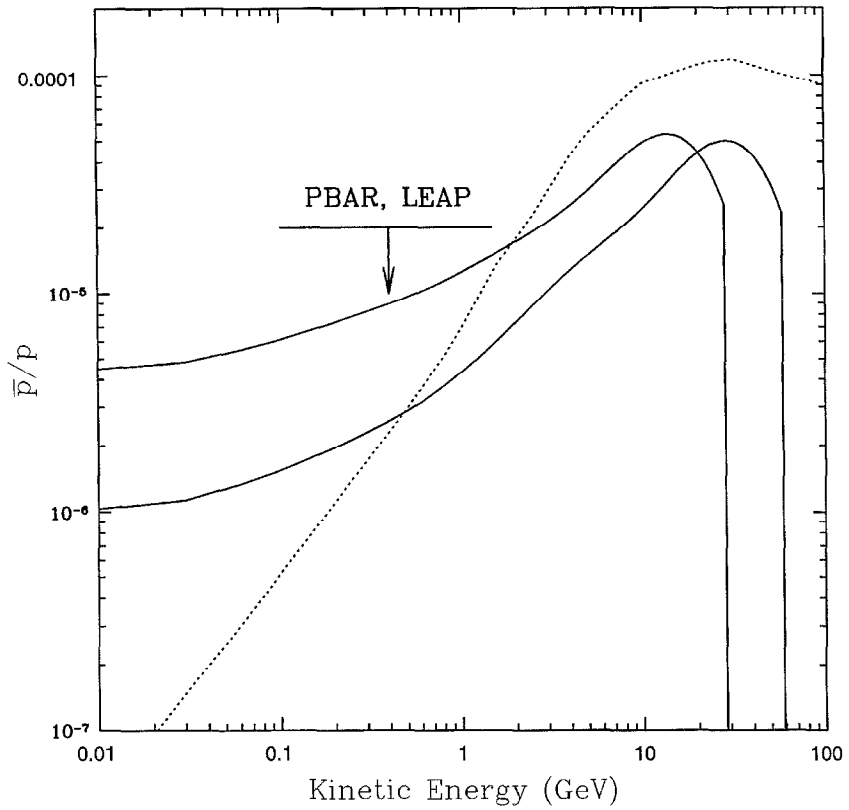

Fig. 36. Observed antiproton/proton ratio as a function of kinetic energy. From Ref. [361].

lower solid curve). For simplicity, the WIMP was chosen to be a B-ino, and it was assumed that the WIMPs contribute closure density, $\Omega_\chi h^2 \simeq 0.25$ with $h = 0.5$ to fix the annihilation cross section. It was also assumed that WIMPs contribute the entire halo density, and standard confinement times and solar-modulation models were used. The dotted curve is the expected background due to spallation in the standard leaky-box model of cosmic-ray propagation. Also shown is the current observational upper limit [367, 368]. As the WIMP mass is increased, the number density in the halo, and therefore the cosmic-ray flux, decrease. As illustrated, observation of low-energy cosmic-ray antiprotons could plausibly provide evidence for the existence of particle dark matter. It should be noted, however, that if the WIMP mass is too large, the antiproton signal would be unobservably small. In addition, even if the WIMP is fairly light, there are considerable astrophysical uncertainties, so it is possible that WIMPs could be the dark matter and still not produce an observable antiproton signal.

The most recent reliable measurements of the cosmic-ray antiproton flux at low energies were by two balloon-borne experiments, the PBAR and ASAP collaborations [367, 368]. They find an upper limit of $\bar{p}/p \lesssim 2 \times 10^{-5}$ roughly in the energy range 100–1000 MeV. The sensitivity to antiprotons in this energy range could be improved by an order of magnitude or more by flying similar experiments at the South Pole, and satellite experiments are also being discussed (see, e.g., Ref. [369]).

10.2. Cosmic-ray positrons

There is also a possibility that annihilation of some WIMP candidates will produce a distinctive cosmic-ray positron signature at high energies [363, 364, 366, 370]. Again, there is a "background" of cosmic-ray positrons from spallation of primary cosmic rays off the interstellar medium. Pions produced when primary cosmic rays interact with protons in the interstellar medium decay to muons which decay to positrons. The flux of positrons, expressed as a fraction of the flux of electrons, decreases slowly with increasing energies.

The showering of WIMP-annihilation products will produce positrons in the same way that antiprotons are produced. The energies of the positrons that come from showering of annihilation products will have a broad energy distribution. The background spectrum of positrons expected from standard production mechanisms is quite uncertain, and precise measurements of the positron energy spectrum are quite difficult, so it is unlikely that positrons from WIMP annihilation with a broad energy spectrum could be distinguished from background.

However, in addition to the positrons that come from decays of hadrons, there is also the possibility that WIMPs may annihilate directly into electron–positron pairs thereby producing a "line" source of positrons [371–373]. Although propagation through the Galaxy would broaden the line somewhat, the observed positron energy spectrum would still have a distinctive peak at an energy equal to the WIMP mass [371]. There are no standard production mechanisms that would produce a positron peak at energies of 10–1000 GeV, so such an observation would be a clear signature of particle dark matter in the halo. It is also interesting to note that some recent measurements of the positron spectrum indicate an increase in the positron fraction at high energies, possibly suggestive of WIMP annihilation, although these results are far from conclusive.

Unfortunately, most of the leading WIMP candidates (e.g., neutralinos) are Majorana particles, and such particles do not annihilate directly into electron–positron pairs due to the helicity suppression. On the other hand, if the WIMP is heavier than the $W^{\pm}$ boson, it can in some cases (for example, if the WIMP is a higgsino) annihilate into monochromatic $W^{+}W^{-}$ pairs, and the W^{+} bosons can then decay directly into positrons with a distinctive energy spectrum peaked at roughly half the WIMP mass [373]. In addition, there will be a continuum of lower energy positrons produced by the other decay channels of the gauge bosons.

Fig. 37 shows the differential positron flux as a fraction of the electron-plus-positron flux, as a function of energy, for a higgsino of mass 120 GeV for two different models of cosmic-ray propagation (the solid and dashed curves) [373]. The dotted curve is the expected background. The peak at higher energies is due to direct decays of gauge bosons produced by WIMP annihilation into positrons, and the broader peak at lower energies comes from the other decay channels of the gauge bosons. The dramatic height of the peak in Fig. 37 is the result of some fairly optimistic, yet reasonable astrophysical assumptions. Again, due to the astrophysical uncertainties, nonobservation of such a signal cannot be used to rule out WIMP candidates.

The most recent measurement of the positron fraction at energies greater than about 10 GeV seems to show an upturn at the highest energies – about 30 GeV – although these results remain controversial [374]. New balloon-borne missions (e.g., the HEAT experiment [375]) should clarify the situation in the near future, and the positron fraction may also be measured more precisely in future space-based experiments.

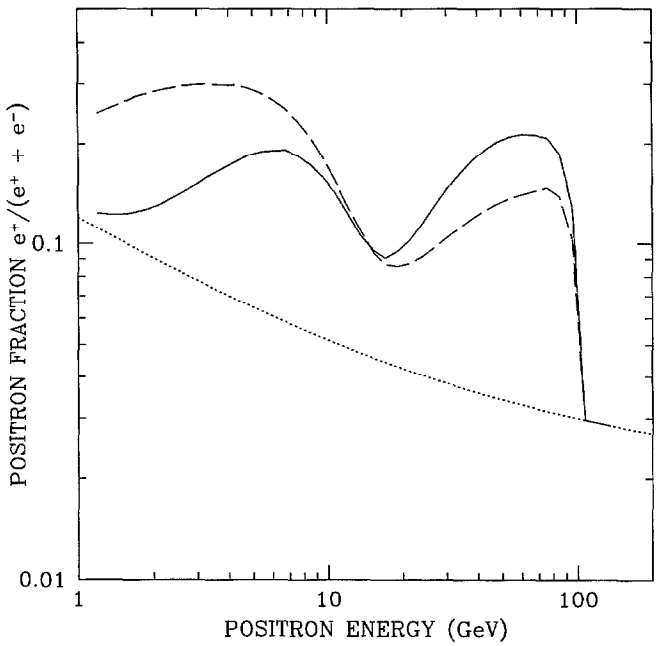

Fig. 37. The differential positron flux divided by the sum of the differential electron and positron fluxes as a function of energy for a neutralino of mass 120 GeV. From Ref. [373].

10.3. Cosmic gamma rays

WIMP annihilation in the halo (and/or Large Magellanic Cloud) may lead to a flux of gamma rays, with both continuum and line contributions. The diffuse background of gamma rays from standard astrophysical sources is poorly understood and precise measurements are difficult; therefore, any inference of the existence of dark matter in the halo from gamma-ray observations must come from fairly distinct gamma-ray signatures. In this section, we will discuss two such signatures: (i) a distinct angular spectrum from WIMP annihilation in the halo [376–378], and (ii) a distinct feature in the gamma-ray energy spectrum [262–265, 379–382]. The first of these signatures is relevant for both continuum and line signals. First we will discuss the qualitative aspects, making order-of-magnitude estimates of the expected gamma-ray fluxes from simple plausible models for the WIMP, and then we will look at results from a recent survey of parameter space for a specific realization of the Galactic halo [266].

When WIMPs annihilate to quarks and leptons (and/or Higgs and gauge bosons if the WIMPs are heavy enough) in the Galactic halo, the subsequent shower from hadronization of the quarks will produce gamma rays with a broad energy distribution centered roughly around one-tenth of the WIMP mass [363, 364, 366, 370, 383–388]. Such a broad continuum signal will in general be difficult to distinguish from background.

WIMPs, essentially by definition, have no direct coupling to photons. However, by virtue of the fact that the WIMP must have some appreciable coupling to ordinary matter (or else annihilation in the early Universe would be too weak to provide $\Omega_\chi h^2 \lesssim 1$), it is almost guaranteed that any

realistic WIMP will couple to photons through loop diagrams, for example, those shown in Fig. 18. Therefore, there will always be some small, but nonzero, cross section for direct annihilation of two WIMPs into gamma rays. Since the typical velocity of WIMPs in the halo ($\sim 300\ \mathrm{km\,s^{-1}}$) is very small compared with the velocity of light, photons produced by annihilation of WIMPs will be monochromatic at an energy equal to the WIMP mass [262–265, 379 382]. No easily imaginable traditional astrophysical source produces monochromatic gamma rays at energies in the range 10–1000 GeV. Therefore, observation of monochromatic gamma rays would provide a "smoking-gun" signal for the existence of WIMPs in the halo.

Consider the characteristic angular dependence of the gamma-ray intensity [376–378] from WIMP annihilation in the Galactic halo. Annihilation of WIMPs in an isothermal halo with core radius a leads to a gamma-ray flux of [376, 389]

$$\frac{\mathrm{d}\mathscr{F}}{d\Omega} = \frac{\sigma_{\chi\chi\to\gamma\gamma} v}{4\pi m_\chi^2} \int_0^\infty \rho^2(r)\, \mathrm{d}r(\psi)$$

$$\simeq (2\times 10^{-12}\ \mathrm{cm^{-2}\,s^{-1}\,sr^{-1}}) \frac{(\sigma_{\gamma\gamma} v/10^{-30}\ \mathrm{cm^3\,s^{-1}})\,(\rho_\chi^{0.4})^2}{(m_\chi/10\ \mathrm{GeV})^2} I(\psi)\,, \tag{10.1}$$

where ψ is the angle between the line of sight and the Galactic center, $r(\psi)$ is the distance along that line of sight, and $\rho_\chi^{0.4}$ is the local WIMP halo density in units of 0.4 GeV cm^{-3}. The quantity $\sigma_{\gamma\gamma} v$ is the cross section times relative velocity v for annihilation of WIMPs into two photons. For monochromatic emission, this is the cross section given in Ref. [266]. For continuum emission this would be the appropriate total cross section for production of gamma rays from all WIMP annihilations; we do not consider this continuum signal further, since for most models it is very difficult to observe.

Fig. 38 shows the result for $I(\psi)$, the angular dependence of the gamma-ray flux, for three values of the ratio R/a, where $R \simeq 8.5$ kpc is the distance of the Sun from the Galactic center. Observation of such a dependence, either in a continuum or a line spectrum, would provide evidence for WIMPs in the halo.

It has been suggested that there may also be an enhancement in the dark-matter density in the Galactic bulge or in the disk, and if this dark matter were made of WIMPs, then annihilation could lead to a strong gamma-ray signal from the Galactic center or the disk [383, 385, 390]. Central halo enhancements could correspond to smooth core distortions with scale of order 100 pc [383, 390], or to more singular power-law distortions extending down to scales of order 1 pc [385]. However, the latter possibility is probably in conflict with observations in several galactic systems [391]. Recently, Gondolo has suggested that the Large Magellanic Cloud (LMC) could be immersed in a halo of dark matter with a central density 10 times that of our own Galaxy, and that annihilation of dark matter therein could lead to a gamma-ray intensity from the LMC roughly ten times stronger than that from our own halo [392], although this estimate comes with significant uncertainties.

We will now make an order-of-magnitude estimate of the expected gamma-ray flux. For example, an order-of-magnitude estimate of the two-photon annihilation cross section that arises from diagrams with slepton loops is

$$\sigma_{\chi\chi\to\gamma\gamma} v \simeq \frac{\alpha^4 m_\chi^2}{m_{\tilde{\mathrm{f}}}^4}\,. \tag{10.2}$$

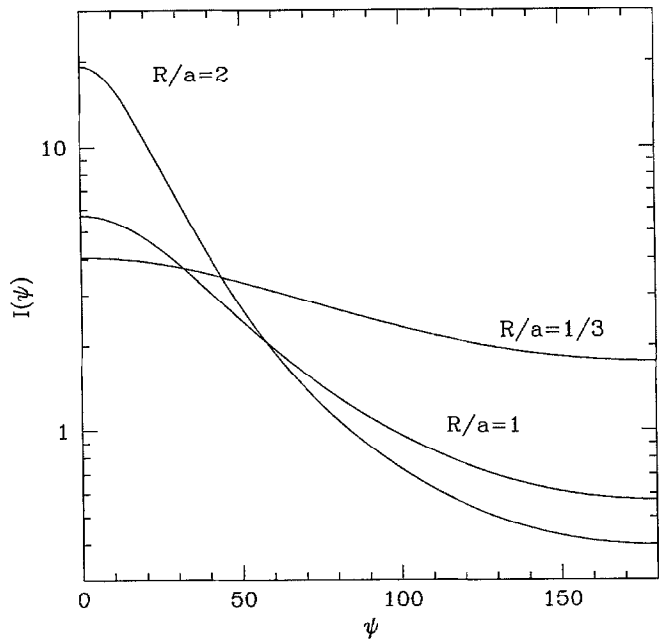

Fig. 38. The intensity of a gamma-ray signal from WIMP annihilation in the halo as a function of the angle ψ between the line of sight and the Galactic center, for several values of R/a. From [376–378].

The slepton is generally the heaviest particle in the loop, so its propagator leads to a suppression $m_{\tilde{l}}^{-4}$ in the cross section. The factor of α^4 in Eq. (10.2) comes from the four couplings in a loop diagram (which are then squared to give a cross section), and the factor of m_χ^2 in the numerator must be included to make the cross section dimensionally correct.

For purposes of illustration, let us focus on the case that the WIMP is a pure B-ino, a linear combination of the supersymmetric partners of the photon and Z boson, which turns out to be the lightest supersymmetric particle in many theories. In this case, the relic abundance turns out to be [361],

$$\Omega_{\tilde{B}} h^2 \simeq 7 \times 10^{-3} \left(\frac{m_{\tilde{q}}}{m_\chi}\right)^2 \left(\frac{m_{\tilde{q}}}{100\ \text{GeV}}\right)^2 . \tag{10.3}$$

Assuming the Universe is flat and that B-inos are the dark matter, then $\Omega_{\tilde{B}} h^2 \simeq 0.25$, and $\sigma_{\chi\chi\to\gamma\gamma} v \simeq 3 \times 10^{-31}\ \text{cm}^3\,\text{s}^{-1}$. If we insert this estimate into Eq. (10.1) we find that the signals in these models, even with optimistic astrophysical assumptions, are at best only marginally observable with current detectors. The standard isothermal halo is broad and flat, and some local density enhancements are required to raise the gamma-ray signal level.

Perhaps the most conservative of the halo enhancement models is that of Ref. [390], along with the closely related calculation of Ref. [383]. Suppose that the center of the Galaxy has a WIMP density enhancement of a factor of ten over that in the standard isothermal halo considered above. Then a detection of a monochromatic gamma-ray emission from the center of the Galaxy becomes possible.

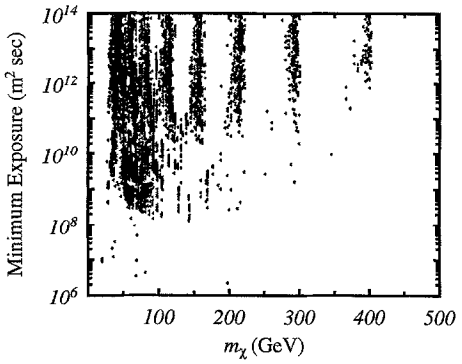

Fig. 39. Minimum exposure required for a 3σ detection of gamma rays from neutralino annihilation in the Galactic center, versus mass of the neutralino, for the survey of supersymmetric parameter space discussed in the text.

To estimate the size of a detector required to see this gamma-ray signature for a generic SUSY dark-matter candidate, we have calculated the flux of gamma rays from annihilation in the Galactic center for a large survey of supersymmetric parameter space [266]. Contributions from all the relevant diagrams, including those with $W^{\pm}$ loops [267] were included. We consider pointed observation of the Galactic center with an atmospheric Cerenkov detector and consider the most important background, which comes from misidentified charged particles [384]. Fig. 39 shows the exposure required for a 3σ detection of gamma rays from neutralino annihilation in the Galactic center for a variety of models [266]. Again, this corresponds to a density enhancement of a factor of ten over that in the standard isothermal halo with $a \simeq 5$ kpc. The SUSY parameter ranges which generated these models were taken to be $50\ \text{GeV} < M_2 < 800\ \text{GeV}$, $50\ \text{GeV} < \mu < 800\ \text{GeV}$, $1 < \tan\beta < 20$, $150\ \text{GeV} < m_A < 600\ \text{GeV}$, and $200\ \text{GeV} < m_{\tilde{q}} < 800\ \text{GeV}$. The grand-unification condition on the gauge couplings was assumed. Models were cut from the plot if they violated known bounds from c^+c^- physics, from the decay $b \to s\gamma$, if they gave Higgs masses in violation of current limits, or if they were inconsistent as models for neutralino dark matter (for example, we obviously require that the LSP is a neutralino). Fig. 39 suggests that a 10^4-m^2 air Cerenkov detector with an exposure of a few years could probe some region of the MSSM parameter space, for this realization of the Galactic halo.

It should always be kept in mind, however, that there are significant uncertainties in astrophysics that could change the rates predicted here for any given particle candidate. Although these uncertainties make it difficult to constrain a given model from null searches for such gamma rays, it is clear that advances in high-energy gamma-ray astronomy could plausibly lead to the discovery of particle dark matter.

11. Sample analysis of the MSSM

11.1. Orientation

In the previous sections, we have reviewed the most important constraints and detection strategies for supersymmetric dark matter, without attempting a global analysis for the MSSM. In

this section, we will indicate the results of such an analysis. Although the following numerical analysis, by its nature, will in time become dated, the physics of the previous sections will be more robust. Therefore we have explicitly separated this model analysis from the discussions of the previous sections.

This section also serves to illustrate the formalism introduced above and summarized in Fig. 62; in particular, we illustrate the use of the numerical code Neutdriver written by the authors and discussed in Appendix B. Interested parties can obtain this code by contacting one of the authors. Finally, we also present some interesting results concerning the detectability of neutralino dark matter.

11.2. SUSY parameter space

The generic supersymmetric (SUSY) model discussed in this review has more than 50 free parameters, and a thorough exploration of this parameter space is not only beyond the scope of this review but would also not be very illuminating. In the examples below, we will specialize to a subset of this space which has only five free parameters. Of course, a more thorough exploration of any region of parameter space can be contemplated with the numerical code. We will use the *practical* SUSY models (see Appendix B) with free parameters m_A, the mass of pseudoscalar Higgs, $\tan\beta$, the ratio of Higgs vacuum expectation values, M_2, a gaugino mass, μ, the Higgsino mass scale, and a common squark and slepton mass scale [i.e., we set all the mass parameters in Eq. (A.73) to be equal]. The A parameter matrices from the soft-breaking Lagrangian have been set to zero. We set all the other parameters using simple relations and approximations. For example, the other gaugino mass, M_1, is set using the usual GUT relation, $M_1 = \frac{5}{3} M_2 \tan^2\theta_W$. All the Higgs masses and couplings are determined from m_A and $\tan\beta$ using the radiative corrections, which depend on the top-quark mass, amongst other parameters. We take $m_t = 170$ GeV throughout. The radiative corrections implemented in the code are those described in Ref. [200]; see Appendix A for more details on the Higgs sector. Note that the sfermion masses are *not* degenerate because mixing still occurs through the D and F terms in the sfermion mass matrices.

As illustrated in Fig. 62, from a particular set of these five parameters in the input-parameter file, the SUSY mass spectrum and couplings can be calculated. From the masses and couplings, all the relevant cross sections can be found (Sections 6 and 7). Also required are additional nuclear and astrophysical data, which are contained in various parameter files. Then, from the cross sections, the relic abundances (Sections 3 and 6), the direct-detection rates (Section 8), the indirect-detection rates (Section 9), as well as various SUSY accelerator detection rates (Section 5), etc. can be calculated. One can then ask and answer many questions. In the following sample analysis, we ask:

1. What regions of SUSY parameter space allow for neutralino dark matter?
2. What event rates are expected in direct-detection experiments? Is it important to build detectors out of materials with nuclear spin, or does the scalar interaction suffice?
3. What event rates are expected in the indirect-detection experiments? How do the rates for neutrinos from the Sun compare with the rates for neutrinos from the Earth?
4. How do the direct and indirect experiments compare with each other – will they compete with or complement one another? Is one method more sensitive than the other?
5. How do various laboratory constraints [such as $\mathrm{Br}(b \to s\gamma)$] affect the above questions?

In attempting to answer these questions, we used our numerical code to calculate all the above quantities for approximately 200 000 sets of SUSY parameters. We considered four values of m_A, (from 170 to 470 GeV), ten values of $\tan\beta$ (2 to 22), two values of sfermion mass scale (200 and 1000 GeV), 35 values of M_2 (10 to 10^4 GeV in logarithmic intervals), and 70 values of $\mu(-10^4$ to 10^4 GeV). We set the A parameters to zero. Thus we are exploring the parameter space shown in Fig. 40. After calculating all the quantities for all these models, we make a series of "cuts", the first of which eliminates models with clearly unacceptable particle physics, such as those with a color-breaking vacuum, or those in which the LSP is not a neutralino. This leaves us with the approximately 51 000 models shown in Fig. 41. We then take into account particle-physics constraints from LEP, CDF, etc. such as the limits on the lightest Higgs mass, the Z^0 width, squark-mass limits and the searches for various SUSY particles discussed in Section 5. In order to make our results conservative, we ignored possible loopholes in many of these accelerator constraints. The cuts made were: lightest squark mass > 150 GeV, $\mathrm{Br}(Z^0 \to \chi_0\chi_0) < 10^{-5}$, $\mathrm{Br}(Z^0 \to \chi_i\chi_j) < 2\times10^{-3}$, $m_{\chi^+} > 45$ GeV, and $m_h > 50$ GeV [1]. This leaves approximately 45 000 models, covering regions of the (M_2, μ) parameter space shown in Fig. 42. Because it is rather new, we study separately the effect of the $\mathrm{Br}(b \to s\gamma)$ limits discussed in Section 5; making the cut $[10^{-4} < \mathrm{Br}(b \to s\gamma) < 4.2\times10^{-4}]$ leaves approximately 14 000 models, which occupy the same regions of parameter space shown in Fig. 42. Thus we have found a large set of SUSY models which satisfy the basic requirement that they are consistent with laboratory experiments.

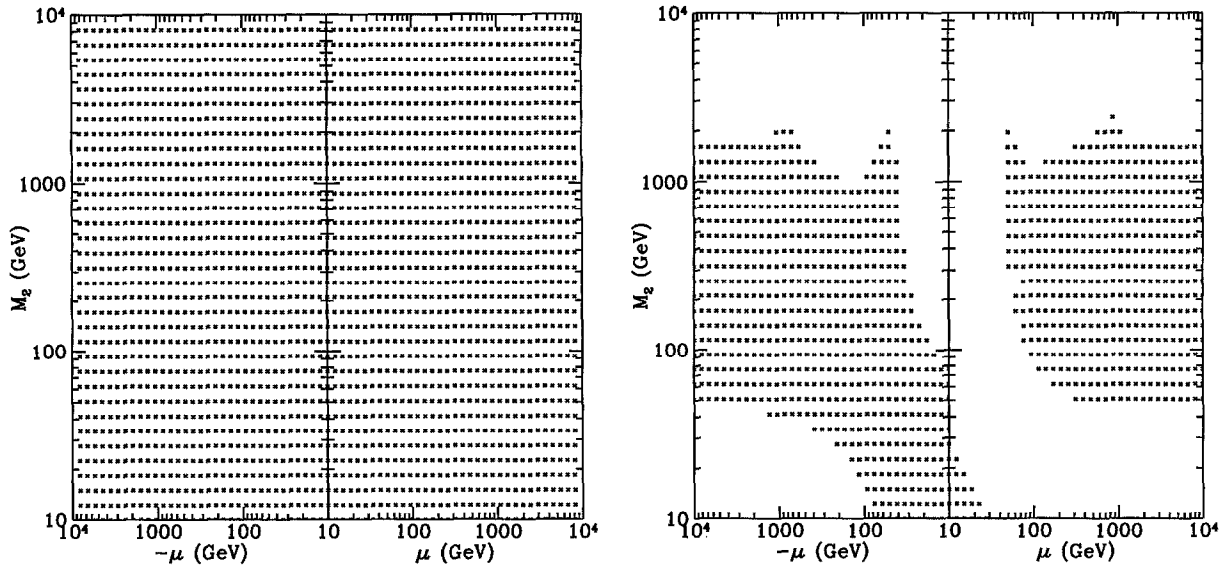

Fig. 40. Parameter space in the MSSM: starting grid of parameter choices. Only two of the five dimensions (μ and M_2) are displayed. The effects of further cuts on the parameter space are shown in Figs. 41–43.

Fig. 41. The models left after eliminating models with vacua which violate colour SU(3) or which do not have the neutralino as the LSP.

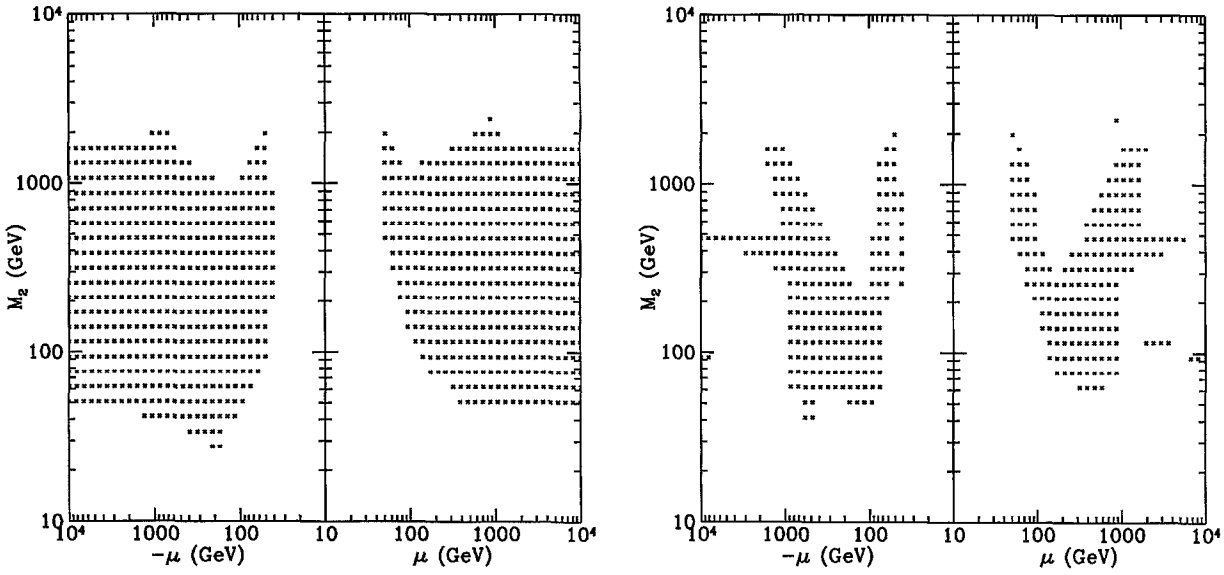

Fig. 42. What is left after implementing several accelerator constraints, including the $Br(b \to s\gamma)$ cut.

Fig. 43. The effect of also requiring that the relic abundance be appropriate for making up the halo dark matter. This figure thus shows the set of acceptable dark-matter models, and it is these models which will be used in all the plots below.

11.3. Relic density

Using this set of models we can see if the neutralino[11] is a suitable dark-matter candidate. In Fig. 44, we plot the neutralino relic abundance $\Omega_\chi h^2$ versus the neutralino mass m_χ for the 14 000 allowed models.[12] Recall from Section 3 that models which predict $\Omega_\chi h^2 > 1$ are ruled out by considerations of the current age of the Universe; those which predict $\Omega_\chi h^2 < 0.025$, while being viable particle-physics models, do not predict enough relic neutralinos to make up the entire dark halo. Thus only those models between the two lines in Fig. 44 are capable of giving the entire dark halo. Our final cut on parameter space is thus to keep only models with $0.025 < \Omega_\chi h^2 < 1$. Approximately 7000 models, covering the regions of parameter space shown in Fig. 43, remain. This is the first interesting result. Even after all the particle-accelerator and relic-abundance constraints are taken into account, there are large numbers of models which can produce neutralino dark matter. The gaugino content of the remaining models can be found by referring to Fig. 6 and Fig. 7 in Section 4. Note that the vertical groupings visible in Fig. 44 at masses near

[11] Recall that we denote the lightest of the four neutralino states as *the* neutralino. Given the cuts above it is also the LSP.

[12] In order to make the plot files less bulky, only a fraction of the allowed points in this and the following figures are actually plotted; but the same range of parameter space is covered.

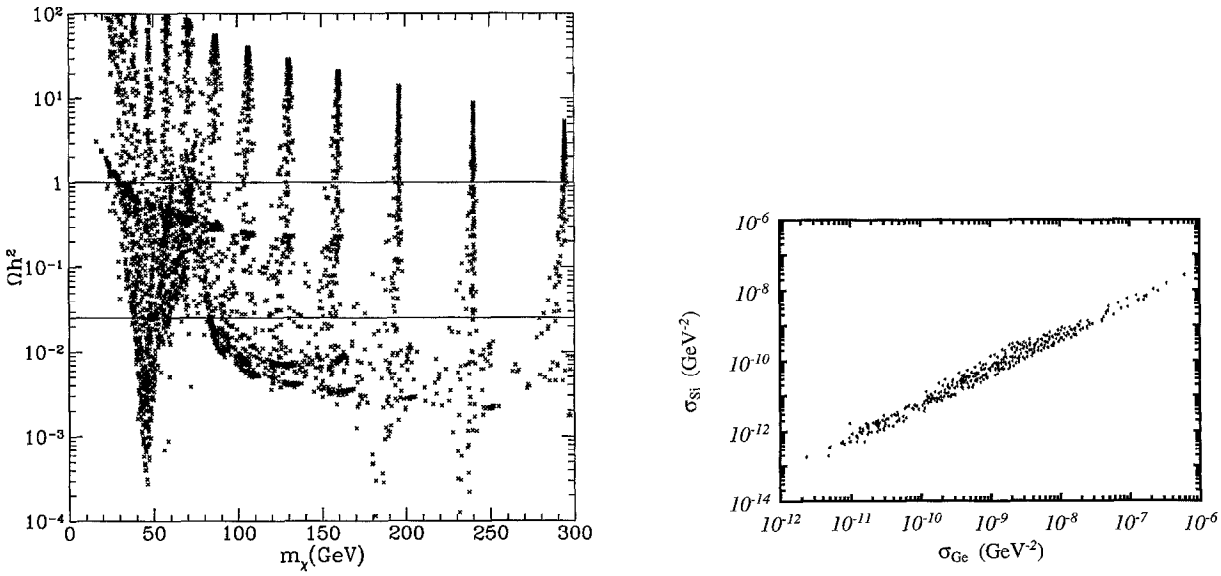

Fig. 44. Scatter plot of relic neutralino density versus neutralino mass for the set of global-SUSY models discussed in the text. Laboratory constraints from LEP measurements and Br(b $\rightarrow$ sγ) are enforced. Models between the lines drawn at $\Omega_\chi h^2 = 0.025$ and $\Omega_\chi h^2 = 1$ are compatible with neutralino dark matter.

Fig. 45. Illustration of the scaling between the ^{29}Si and ^{76}Ge elastic-scattering cross sections. The ratio is very nearly constant and approximately an order of magnitude, indicating the validity of the A^2 scaling of the cross section. The increased spread at lower values is due to the contamination from the spin-dependent cross section, which is noticeable only when the scalar cross section is small. The set of models plotted here is slightly different from those described in the text.

160 GeV, 200 GeV, etc. each correspond to a particular choice of M_2. So one should fill in the gaps due to our finite sampling of parameter space by mentally forming the envelope of the scattered points. However, dips in relic abundance due to the Z^0 pole in the annihilation cross section at 45 GeV, as well as other poles due to Higgs exchange are not due to the finite sampling. We now turn to detection of these "allowed" neutralino dark-matter candidates.

11.4. Elastic-scattering cross sections

As discussed in Section 7, the first step in finding either direct or indirect neutralino detection rates is the calculation of the elastic-scattering cross section of neutralinos off various nuclei. In Fig. 45, we plot the cross section from ^{73}Ge versus the cross section from ^{29}Si. This plot shows several things. First, note the large range in cross sections possible for viable neutralino dark matter. Next note the almost constant ratio, suggesting that a signal in a germanium direct-detection experiment fairly accurately predicts the rate in a silicon detector. Finally, note that the silicon cross section is smaller by a factor of roughly ten, as predicted in Fig. 26.

Next, in Fig. 46, we plot the dependence of the neutralino–germanium cross section on the mass of the lightest Higgs boson. The upper envelope of the scatter plot clearly shows the importance of

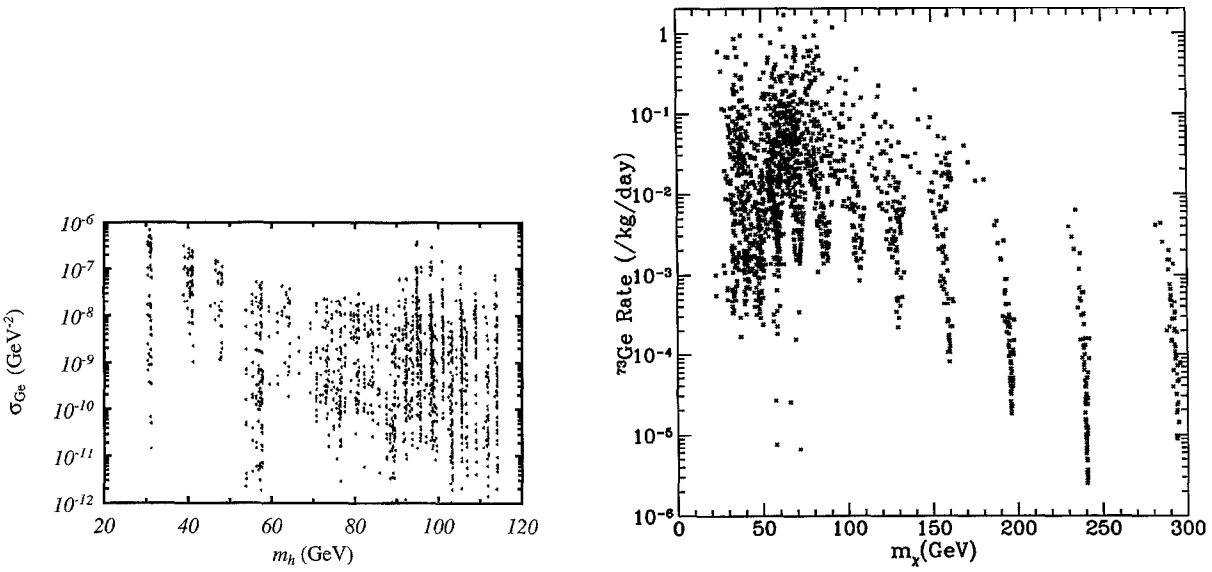

Fig. 46. Dependence of the scalar ^{76}Ge cross section on the lighter Higgs-boson mass. For $m_h \lesssim 70$ GeV, the dependence is clear, indicating that Higgs-boson exchange is playing an important role in the process. The set of models plotted here is slightly different from those described in the text.

Fig. 47. Predicted rate in a ^{73}Ge cryogenic detector versus neutralino mass for the allowed dark-matter models above. All constraints are implemented.

the Higgs exchange in this scattering process. A strong limit on the lightest Higgs mass, from LEP II, would eliminate many models with the largest cross sections and make neutralino detection by either direct or indirect means more difficult.

11.5. Direct-detection rates

To provide examples of expected rates in a direct-detection experiment, we consider the germanium detector discussed in Section 8.2. Using the formulas of Section 8, in Fig. 47 we show a scatter plot of the expected rate versus the neutralino mass. The wide range in expected event rate is due to the wide range in elastic cross sections, which comes from the wide range of Higgs and squark masses considered. Again, many gaps in the scatter plot appear due to finite sampling of the parameter-space grid, but features such as the Z^0 pole at $m_\chi = m_Z/2$ are evident. Note that the envelope of the event rate peaks at about 1 event $\mathrm{kg}^{-1}\,\mathrm{d}^{-1}$ at $m_\chi \approx 80$ GeV, and then falls rapidly for larger masses. As shown in Figs. 46 and 48, lightest Higgs masses as high as 120 GeV are common, due to the radiative corrections and the effect of the heavy top quark. The direct-detection rates are smaller for the models with heavy m_h as shown in Fig. 48. This plot makes it clear that strong limits on the Higgs sector from LEP II would have important effects on the direct-detection experiments.

It has been proposed to use enriched ^{73}Ge in a cryogenic detector to allow the spin-dependent cross section to contribute to the detection rate. In Fig. 49, we plot the spin-only rate and

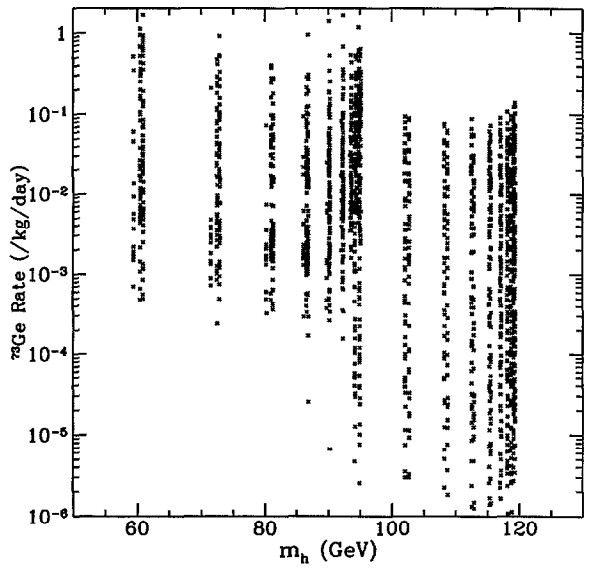

Fig. 48. Predicted rate in a ^{73}Ge cryogenic detector versus lightest scalar Higgs mass for the allowed dark-matter models above. All constraints are implemented. The gaps are due to the incomplete parameter space sampling.

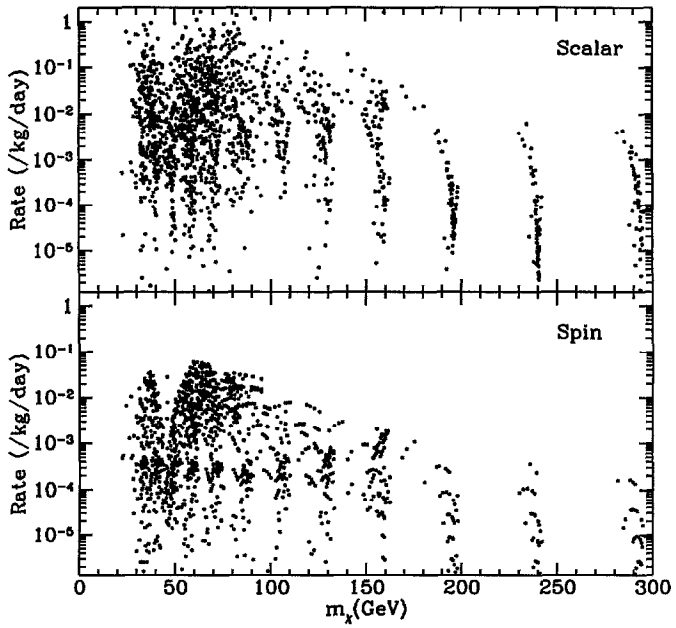

Fig. 49. Predicted rate in a ^{73}Ge cryogenic detector versus neutralino mass for the allowed dark-matter models above. Panel (a) shows only the scalar neutralino–nucleus interaction, while panel (b) shows only the spin interaction. All constraints are implemented.

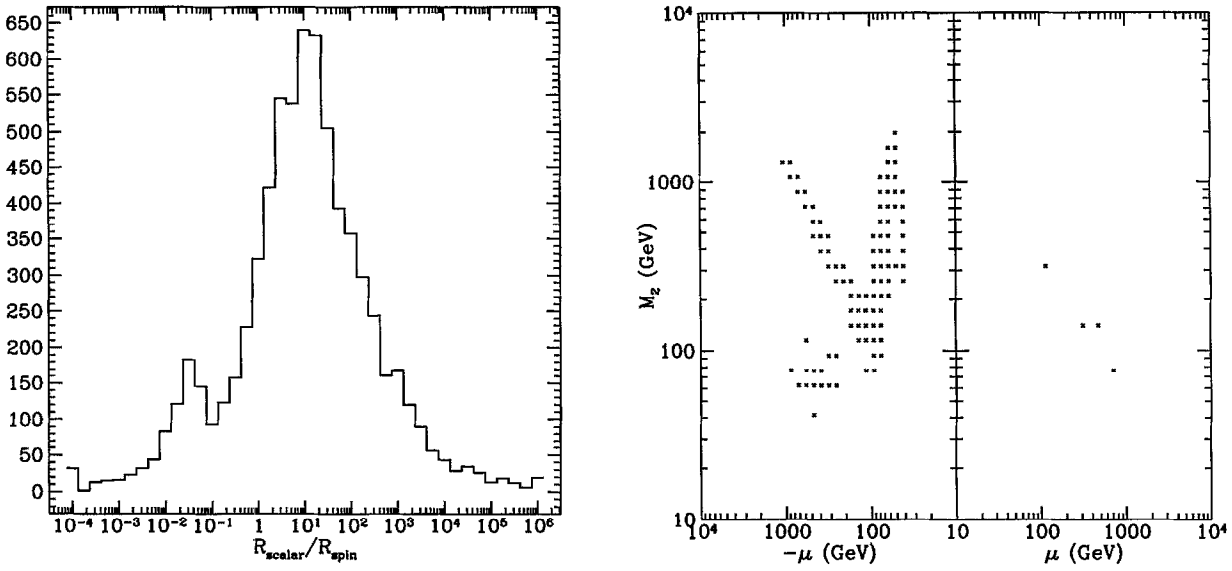

Fig. 50. Histogram of the ratio of scalar rate of spin rate $r = R_{\text{scalar}}/R_{\text{spin}}$ in a ^{73}Ge detector for the allowed dark-matter neutralinos.

Fig. 51. Parameter space for MSSM for specific models: models for which the spin coupled direct-detection rate is ten times larger than the scalar coupled rate. Each point represents an allowed SUSY dark-matter candidate from Fig. 43 which also passes some other criterion.

scalar-only rate for such a detector. We note that the spin-only rate is uniformly smaller than the scalar-only rate. This is shown in another way in Fig. 50 where we histogram the ratio $R_{\text{scalar}}/R_{\text{spin}}$ for all the allowed neutralino models. Typically, the scalar rate dominates the spin rate by a factor > 10, although some models with spin rates larger than scalar rates exist. It therefore seems that, in most cases, a natural germanium detector will do as well as an enriched ^{73}Ge detector.

It is of some interest to see which models have dominant spin interactions and which have dominant scalar interactions, so in Fig. 51, we find the region of (μ, M_2) parameter space for which the spin rate is at least a factor of ten larger than the scalar rate, while in Fig. 52, we show the parameter space where the scalar rate dominates by a factor of ten or more. The large overlap region occurs because these figures are two-dimensional projections of the five-dimensional parameter space. The gaugino/Higgsino content of these areas of parameter space can be found using Fig. 6 from Section 4. We also note that the models with dominant spin rate typically have lower neutralino mass m_χ, higher m_h, and negative μ. It is thus possible to have neutralino dark matter with a dominantly spin interaction, but we note that this typically comes about not due to an enhancement of the spin interaction, but due to a suppression of the scalar interaction. For neutralinos with masses under 100 GeV, there are, however, regions of parameter space with expected rates above 10^{-2} event kg^{-1} d^{-1} and an interaction which is spin dominant.

Next, recalling that the current generation of direct-detection experiments have as a goal a sensitivity of 10^{-2} to 10^{-3} event kg^{-1} d^{-1}, we see from Fig. 47 that a very large area of SUSY parameter space can be probed with current experiments. However, it is also clear that a definitive

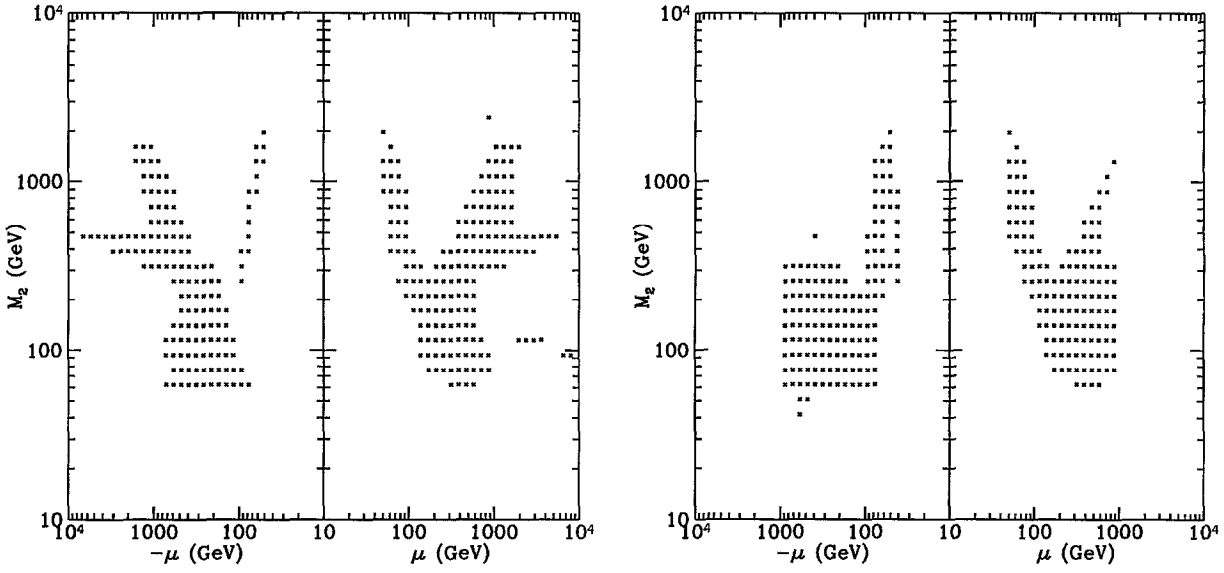

Fig. 52. Models where the scalar rate dominates by a factor of 10.

Fig. 53. Models for which the total direct-detection rate is greater than 10^{-3} event $kg^{-1}\,d^{-1}$, the sensitivity that the next round of experiments hope to reach.

direct search will not be possible with this level of sensitivity since rates below 10^{-3} event $kg^{-1}\,d^{-1}$ are quite possible. The regions of (μ, M_2) parameter space with $R_{\text{direct}} > 10^{-3}$ event $kg^{-1}\,d^{-1}$ are shown in Fig. 53.

We can also discuss the relative merits of detectors made of materials such as fluorine, which has a large spin-interaction cross section. The scatter plots for a ^{19}Fl detector (not shown) are similar to those for a ^{73}Ge detector, with several significant differences. First the scalar rate is ~ 10 times smaller, while the spin rate is a factor of a few larger (compared to Fig. 47). Thus, the fluorine histogram of $R_{\text{scalar}}/R_{\text{spin}}$ differs from Fig. 50; its peak is shifted to about 0.05. The total rate in a fluorine detector is typically smaller than that in a germanium detector by a factor of a few.

Finally, we can explore the impact of the various cuts on the direct-detection search. In Fig. 55, we show the expected rate if the constraint coming from the measurement of $\text{Br}(b \to s\gamma)$ is relaxed. It is interesting that, while many models are eliminated, there is only a moderate effect on the upper envelope of expected event rate for $m_\chi \lesssim 175$ GeV. This can be understood from Fig. 56, where it is seen that the $\text{Br}(b \to s\gamma)$ constraint eliminates parameters which give light *charged* Higgs bosons. Since it is not these, but the lightest neutral Higgs which control the direct rate, the $\text{Br}(b \to s\gamma)$ constraint does not have a major effect in this global search of parameter space. In contrast, however, the current LEP constraints coming from the Higgs and SUSY searches have already had strong effects on direct detection. If it were not for these constraints, much higher event rates would be possible, as would lighter neutralino dark matter [393].

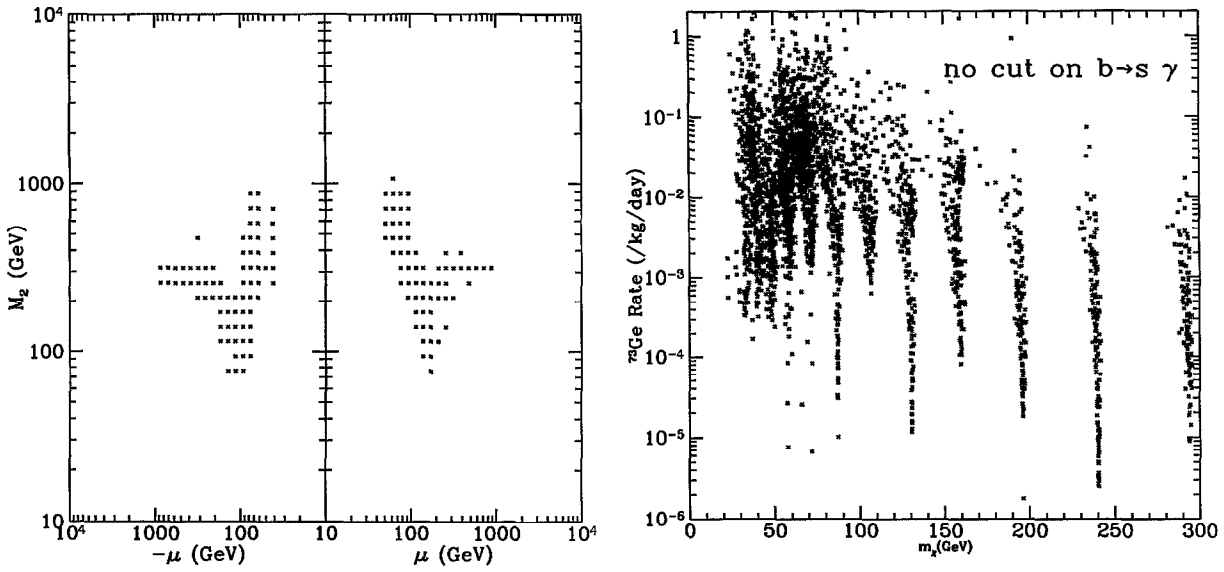

Fig. 54. Models for which the indirect-detection rate Γ is between $10^{-2}\,\mathrm{m}^{-2}\,\mathrm{yr}^{-1}$ and $10^{-4}\,\mathrm{m}^{-2}\,\mathrm{yr}^{-1}$, the sensitivity that the next round of indirect experiments hope to reach.

Fig. 55. Same as Fig. 47 except that the constraint $10^{-4} < \mathrm{Br}(b \to s\gamma) < 4.2 \times 10^{-4}$ has been relaxed.

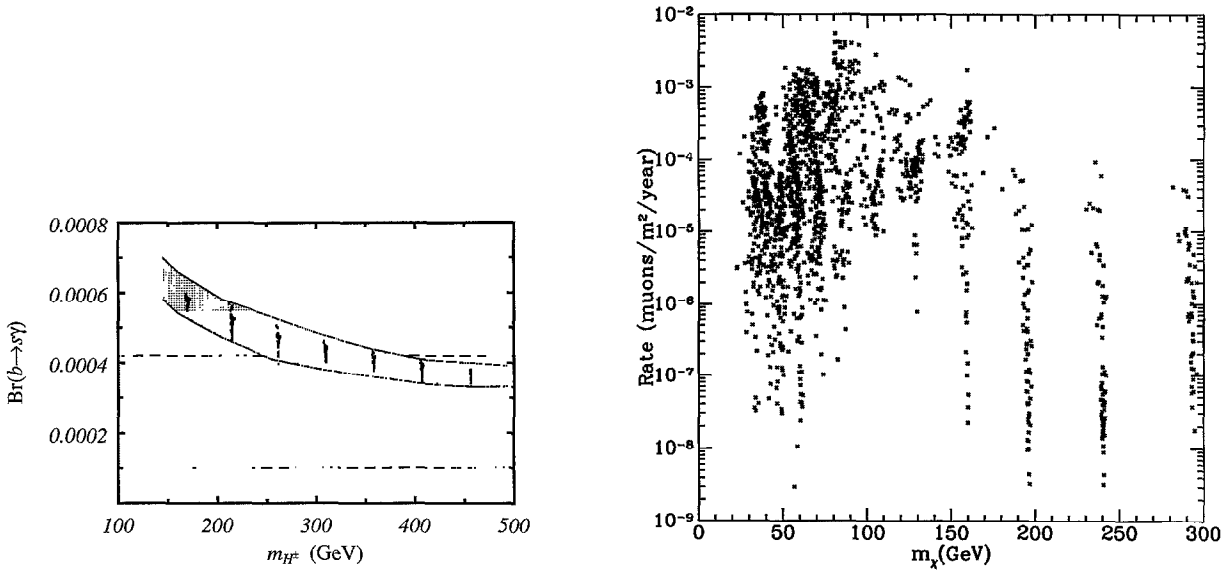

Fig. 56. $\mathrm{Br}(b \to s\gamma)$ for the group of global-SUSY models discussed in the text. Clearly the main contribution to these generic models is from charged-Higgs exchange. The light shaded region indicates the allowed 95% CL limits on the CLEO measurement. Compare to Fig. 8.

Fig. 57. Indirect-detection rate versus neutralino mass. The sum of the rates for upward muons from both the Sun and Earth is shown. Currently planned experiments will be sensitive in the $10^{-2}\,\mathrm{m}^{-2}\,\mathrm{yr}^{-1}$ to $10^{-4}\,\mathrm{m}^{-2}\,\mathrm{yr}^{-1}$ range.

11.6. Indirect-detection rates

Next we turn to the indirect-detection methods described in Section 9. Fig. 57 shows the number of upward muons in astrophysical neutrino detectors such as those described in Section 9.2. These are muons produced by energetic neutrinos from neutralino annihilation in the Sun and Earth. Again, each point in the scatter plot represents an allowed choice of SUSY parameters. Recall that current detectors are sensitive at about the $10^{-2}\,\mathrm{m}^{-2}\,\mathrm{yr}^{-1}$ level and that the next generation of experiments hopes to get to the $10^{-4}\,\mathrm{m}^{-2}\,\mathrm{yr}^{-1}$ level. The parameter space occupied by these models is shown in Fig. 54. The question of the relative signal for neutrinos from the Earth and neutrinos from the Sun is addressed in Fig. 58 and Fig. 59, where the ratio of predicted muons from the Sun and Earth is shown for the allowed models. In Fig. 58 all the allowed models are plotted, while in Fig. 59, only those models which predict rates $10^{-4}\,\mathrm{m}^{-2}\,\mathrm{yr}^{-1} > \Gamma > 10^{-2}\,\mathrm{m}^{-2}\,\mathrm{yr}^{-1}$ are plotted. Models with $\Gamma \gtrsim 10^{-2}\,\mathrm{m}^{-2}\,\mathrm{yr}^{-1}$ have already been excluded and models with $\Gamma < 10^{-4}\,\mathrm{m}^{-2}\,\mathrm{yr}^{-1}$ predict rates too small to be seen in the next round of detectors (see Section 9.6). Note that most neutralinos with masses above 175 GeV have predicted rates below 10^{-4} muons $\mathrm{m}^{-2}\,\mathrm{yr}^{-1}$. We see that for a general neutralino, the Sun is probably a better source of high-energy neutrinos than the Earth.

We could also show the effect of relaxing various cuts such as $\mathrm{Br}(b \to s\gamma)$ on the indirect-detection rate. However, as in the direct case, while many models are added, the envelope of expected rates is not altered appreciably, except at higher neutralino mass.

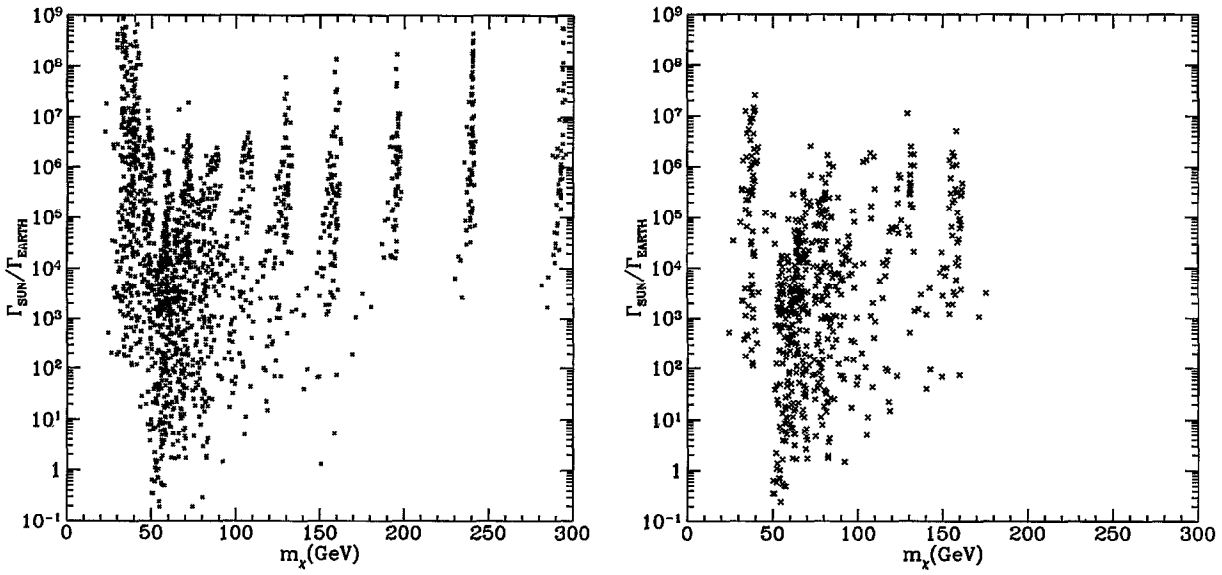

Fig. 58. Ratio of indirect-detection rates for neutrinos from the Sun and Earth versus the neutralino mass. All allowed models are plotted.

Fig. 59. Ratio of indirect-detection rates for neutrinos from the Sun and Earth versus the neutralino mass. Only models which predict rates between $10^{-2}\,\mathrm{m}^{-2}\,\mathrm{yr}^{-1}$ and $10^{-4}\,\mathrm{m}^{-2}\,\mathrm{yr}^{-1}$ are plotted.

11.7. Comparison of direct and indirect rates

In Section 9.7, an attempt at a fairly model-independent comparison of rates for direct and indirect-detection techniques was made following Ref. [301]. In Figs. 60 and 61, we make the same comparison using our set of allowed SUSY models. Here, the ratio of direct to indirect events is plotted versus neutralino mass for a germanium detector; Fig. 60 shows all the allowed models, while Fig. 61 shows only those with $10^{-4}\,\mathrm{m}^{-2}\,\mathrm{yr}^{-1} < \Gamma < 10^{-2}\,\mathrm{m}^{-2}\,\mathrm{yr}^{-1}$. We can conclude that 1-kg-Ge detector has the same sensitivity as a 0.01–1.0 km^2 indirect detector for most dark-matter neutralinos.

11.8. Results from unified models

A complete discussion of the cosmology and phenomenology of the neutralino in SUSY-GUT and SUGRA models is beyond the scope of this work. However, the low-energy limit of such models should be the MSSM explored here, although unification will impose relations between some of the parameters that have been chosen arbitrarily in the illustrative numerical work in this section. As a result, the results for relic abundances and direct- and indirect-detection rates should occupy some subspace of the numerical results shown in the scatter plots here. For some arbitrary set of assumptions about the high-energy theory, it is natural to expect the detection rates to lie below the highest rates we have found, but perhaps also above the lowest rates we plotted. On the other hand, it should be possible (although we have not done so) to find reasonable unified theories

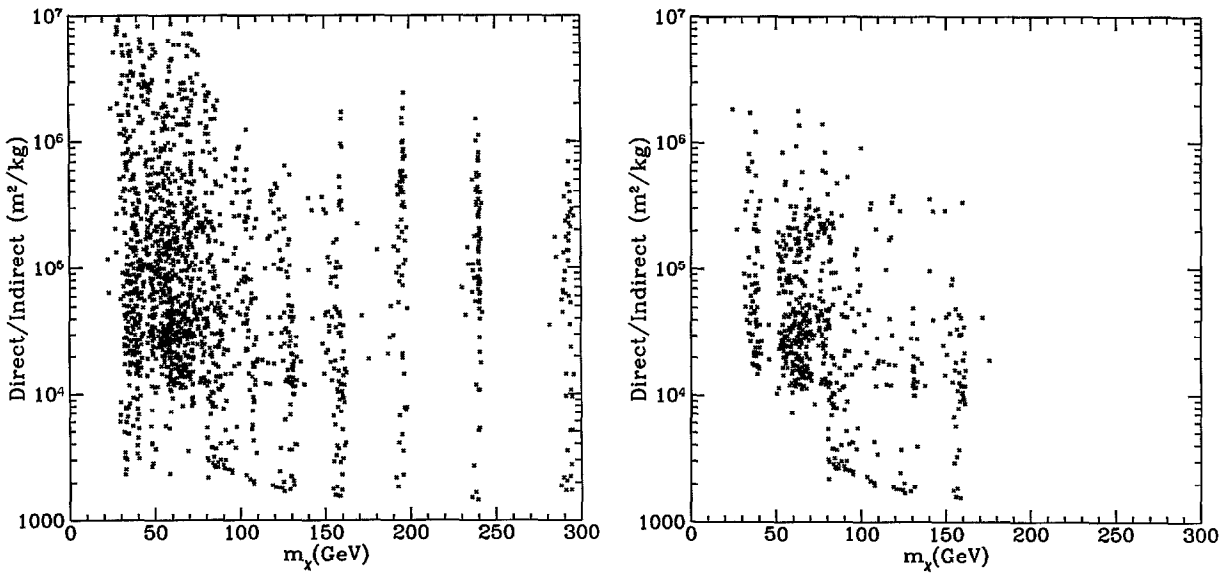

Fig. 60. The ratio of direct to indirect rates is plotted for all allowed models.

Fig. 61. The ratio of direct to indirect rates is plotted for models with indirect rates between $10^{-4}\,\mathrm{m}^{-2}\,\mathrm{yr}^{-1} > \Gamma > 10^{-2}\,\mathrm{m}^{-2}\,\mathrm{yr}^{-1}$.

that give rise to detection rates near the upper envelope of detection rates we plotted for the MSSM.

There have been numerous calculations of neutralino abundances and detection rates in a variety of unified models. For example, Diehl et al. have recently carried out a comprehensive analysis of neutralino relic abundances, direct- and indirect-detection rates, and prospects for accelerator signatures in a class of consistent minimal super-unified models [394]. They impose the constraint that electroweak symmetry be broken and that the phenomenology be consistent with all known laboratory constraints. Their conclusions are in agreement with ours. As expected, their direct- and indirect-detection rates fall within the envelope for the MSSM that we find. Although their rates are generally smaller than ours, it is not clear that this would be true with different assumptions about the form of the unified model. The next generation of direct-detection experiments will provide a better probe of dark matter than the next generation of indirect-detection experiments in the majority of their models. This agrees with our model-independent results for the majority of supersymmetric WIMPs which have primarily scalar couplings. They argue that collider experiments most likely provide the best route to discovery of supersymmetry. Even so, WIMP-detection experiments will be needed to ascertain that the halo is composed of supersymmetric particles.

12. Other particle dark-matter candidates

In this review we have discussed a canonical example of a *thermal* relic particle. A thermal relic is one which, at very early times – when the Universe was at very high temperature – was in thermal equilibrium with the radiation. As discussed in Section 3, when the temperature finally drops below the mass of the would-be relic particle, its number density will "freeze out", and a substantial number of relic particles can be left. The remarkable fact is that a thermal relic with electroweak-scale interactions can give $\Omega \simeq 1$; thus the name weakly interacting massive particle. As we have discussed, such particles may be within reach of current accelerators; thus, many accelerator searches for exotic particles are also searches for the dark matter of the Universe.

Thus far we have focussed primarily on the neutralino, which is perhaps the theoretically best developed and motivated WIMP candidate. However, the first WIMP considered was a heavy fourth-generation neutrino. Also, other particles which arise in supersymmetry may be candidate WIMPs.

12.1. The rise and fall of heavy-neutrino dark matter

The first proposed cold dark-matter candidate in the WIMP class was a stable, heavy ($m_\nu \gtrsim$ GeV), fourth-generation Dirac or Majorana neutrino with standard-model couplings [120–122]. Such a neutrino would couple to the Z^0 boson in the ordinary way and therefore have weak interactions with ordinary matter. Thus, the cosmology of a heavy neutrino is similar to the cosmology of the LSP. The difference, however, is that far fewer parameters are needed to describe the neutrino; its interactions are fixed by gauge symmetry, and the only adjustable scale is its mass.

The relic abundance of a Dirac or Majorana neutrino can be obtained from its annihilation cross section as discussed in Section 3. Neutrino annihilation into light fermions occurs via s-channel exchange of a Z^0 boson. The cross section is proportional to the square of the neutrino mass. For

a Dirac (Majorana) neutrino, the cosmological abundance turns our to be $\Omega_{\bar{\nu}\nu}h^2 \simeq (m_\nu/2\ \mathrm{GeV})^{-2}$ [$\Omega_\nu h^2 \simeq (m_\nu/5\ \mathrm{GeV})^{-2}$] for masses in the range $\mathrm{GeV} \lesssim m_\nu \lesssim m_Z$ [120–122]. Therefore, Dirac (Majorana) neutrino masses less than about 2 (5) GeV are cosmologically inconsistent, and neutrinos with masses slightly larger (say $2\ \mathrm{GeV} \lesssim m_\nu \lesssim 20$ GeV for Dirac neutrinos and $5\ \mathrm{GeV} \lesssim m_\nu \lesssim 50$ GeV for Majorana neutrinos) would be good candidates for the dark matter in our halo. For neutrino masses greater than the electroweak gauge-boson masses, neutrino annihilation into gauge- and Higgs-boson pairs can occur [395]. The cross sections for annihilation into these channels depend somewhat on the associated heavy-lepton and Higgs-boson masses. However, the general result is that the cross section does *not* decrease as the neutrino mass is increased, so the relic abundance of neutrinos with masses $\gtrsim 100$ GeV remains small – perhaps too small to account for the dark matter in the Galactic halo.

This result appears at odds with the unitarity bound discussed in Section 3. There, it was pointed out that the relic abundance should increase at the largest WIMP masses. The solution to this apparent paradox is likely due to the breakdown of the perturbative calculation of the annihilation cross section used in Ref. [395] at neutrino masses $m_\nu \sim$ O(TeV). The neutrino mass is generated via the Higgs mechanism, so the neutrino–Higgs Yukawa couplings are increased as the neutrino mass is raised. Therefore, as the neutrino mass is raised above O(TeV), the theory becomes strongly coupled, perturbation theory breaks down, and it is not even clear whether such a neutrino could exist as a free stable state.

Therefore, the bottom line seems to be that neutrinos in the mass range between roughly 1 GeV and 1 TeV are cosmologically consistent, but that the abundance of those with masses $\gtrsim 10$ GeV would be too small to account for the halo dark matter.

Of course, if there is a cosmic asymmetry between Dirac neutrinos and antineutrinos [128], then the cosmological abundance of neutrinos could be much greater than the canonical value. Similarly, the abundance of either Dirac or Majorana neutrinos could be enhanced by some nonstandard production scenario, as discussed in Section 3.5. With these caveats in mind, it is conceivable that Dirac or Majorana neutrinos could be the halo dark matter.

This simple proposition, however, can be tested by a variety of experiments of the type discussed in this article. In particular, Dirac neutrinos interact with nuclei through a "coherent" vector interaction. Thus, the Dirac-neutrino–nucleus cross section is quite substantial, and this would lead to a significant event rate in a direct-detection experiment. Null results from modified double-beta-decay detectors have ruled out Dirac neutrinos with masses in the range $12\ \mathrm{GeV} \lesssim m_\nu \lesssim 1.4$ TeV as the primary component of the dark matter in the halo [291, 307]. When combined with limits from measurements of the Z^0 width, which rule out a fourth-generation neutrino mass $m_\nu \lesssim m_Z/2$, the direct-detection results rule out Dirac-neutrino dark matter in the mass range $m_\nu \lesssim 1.4$ TeV [396, 397]. Dirac neutrinos with larger masses are in principle consistent, but would be close to the murky regime where the neutrino becomes strongly interacting.

Majorana neutrinos interact only via an axial-vector interaction, and are therefore much more difficult to detect directly. However, such neutrinos would still be captured in the Sun by scattering from hydrogen therein. Annihilation of Majorana neutrinos in the Sun would produce an energetic-neutrino signal from the Sun. Null results from energetic-neutrino searches at Kamiokande rule out Majorana neutrinos with mass less than a few hundred GeV [331].

To sum up, heavy fourth-generation Dirac neutrinos with standard-model couplings cannot be the halo dark matter unless they have masses large enough that they are nearly strongly interacting,

and similarly for Majorana neutrinos, although the accessible mass window is perhaps a bit wider. In either case, the relic-abundance calculation suggests that we should not expect there to be a significant cosmological density of such neutrinos, unless there were exotic production mechanisms in the early Universe, or a cosmological particle–antiparticle asymmetry in the case of Dirac neutrinos. Of course, heavy Dirac or Majorana neutrinos with nonstandard couplings could well be the halo dark matter and still evade detection [398].

Finally, we note that there is not much theoretical motivation for a stable heavy neutrino. Stability of a new particle generally requires a new symmetry. In the case of heavy-neutrino dark matter, the required symmetry does not typically arise from any fundamental principle, and is added in an ad hoc manner.

12.2. Sneutrinos

In some supersymmetric models, the LSP might be a sneutrino, the spin-0 supersymmetric partner of the neutrino. As is the case for the neutralino, the sneutrino relic abundance depends on numerous supersymmetric parameters. For reasonable assumptions, a sneutrino with mass in the range 550 GeV $\lesssim m_{\tilde{\nu}} \lesssim$ 2300 GeV can result in an interesting (i.e., $0.1 \lesssim \Omega_{\tilde{\nu}} h^2 \lesssim 1$) relic density [176]. The sneutrino–nucleus interaction is four times the Dirac-neutrino–nucleus interaction [176], so the direct-detection limits to sneutrino dark matter in our halo are similar to those for heavy neutrinos. The end result is that sneutrino masses above a TeV or so are probably still consistent, although recent results from the Heidelberg–Moscow direct-detection experiment [399] may rule out these masses as well [176].

12.3. Other supersymmetric dark-matter condidates

There are several candidates for supersymmetric-particle dark matter other than the minimal neutralino on which we have focussed and the sneutrino discussed briefly above. These include gravitinos, axinos, and neutralinos in nonminimal models.

Nonminimal neutralinos: Although we have focussed on the minimal supersymmetric extension of the standard model, it is quite plausible that the low-energy manifestation of supersymmetry could be more complicated than the MSSM. The neutralino in these models may also be a suitable dark-matter candidate, and generically, we would expect its interactions to fall within the rather broad range allowed for the general MSSM neutralino. However, the detailed form of the interactions could be different than those presented here [400].

Gravitinos: In supergravity theories, the graviton possesses a supersymmetric partner, called the gravitino, with extremely weak couplings to other matter. Cosmology of the gravitino [401, 402] is significantly more speculative than for the models we have so far discussed, because the physics of the gravitino must be considered at energies and temperatures right up to the Planck scale. Gravitinos will decouple at temperatures of order the Planck scale. If they behave as standard stable thermal relics, with an abundance determined by consideration of this decoupling, then they must have a mass less than a few keV [401]. However, it is generally believed that such a primordial gravitino abundance will be washed out by a later inflationary epoch. Note that this requires an upper bound for the reheating temperature at the end of the inflationary period so that the gravitinos are not regenerated [402, 403]. Another constraint arises from the fact that the

next-lightest supersymmetric particle must decay to a gravitino plus ordinary particles. Since the coupling to gravitinos is so weak, this next-lightest particle will be very long-lived. There is a danger then, that the products of this decay will contain high-energy gamma rays which can photodisintegrate the products of big-bang nucleosynthesis [403]. Generally, the cosmological consequences of gravitinos are dependent on the properties of an associated superparticle produced in gravitino decay. As another example, a scenario involving gravitinos and sneutrinos was considered in Ref. [404].

Axinos: Another possibility for supersymmetric dark matter can be found in models which combine axions and supersymmetry. The axion will have a supersymmetric partner, the axino, with possibly interesting cosmology [148, 405]. The axino may be the lightest supersymmetric particle, or it may decay to the lightest supersymmetric particle. Since the couplings of the axino are weak, it is generally long-lived even when quite heavy. When the axino is the lightest supersymmetric particle, a mass of a few keV implies that it can be warm dark matter. A combined axino–gravitino scenario has been considered in Ref. [406].

13. Conclusions

The evidence that dark matter outweighs luminous matter in the Universe by at least a factor of ten is overwhelming. There are numerous additional arguments that this dark matter must be composed of some new exotic substance. Theories of new physics beyond the standard model provide numerous candidates for the nonluminous component. In particular, theories which involve supersymmetry may be the best candidates for new physics, and a by-product of supersymmetry is a stable new particle – usually the lightest neutralino – which has a cosmological abundance similar to the abundance of dark matter.

Thus, if supersymmetry exists, it is reasonable to expect that the dark matter in the Universe and in the Galactic halo could be neutralinos. There are several avenues toward discovery of such particles in our halo. These include direct detection in a terrestrial laboratory, observation of high-energy neutrinos from neutralino annihilation in the Sun and Earth, or possibly measurement of anomalous cosmic rays produced by annihilation in the halo.

In this review, we have discussed the dark-matter problem, the WIMP solution, and prospects for WIMP detection in some generality. We then specialized to low-energy supersymmetry which embodies a broad class of particle theories in which the WIMP paradigm is realized concretely. The minimal supersymmetric extension of the standard model was described with an emphasis on those elements needed for dark matter. Superparticle masses and couplings and laboratory constraints on them were described, and calculations of cosmological abundances and detection rates were presented in some detail.

13.1. Summary of calculations

Fig. 62 shows a diagrammatic summary of our discussion of supersymmetric dark matter showing the connections between the various calculations and experimental and astrophysical constraints. Below, we summarize the review with a discussion of the various components shown in Fig. 62.

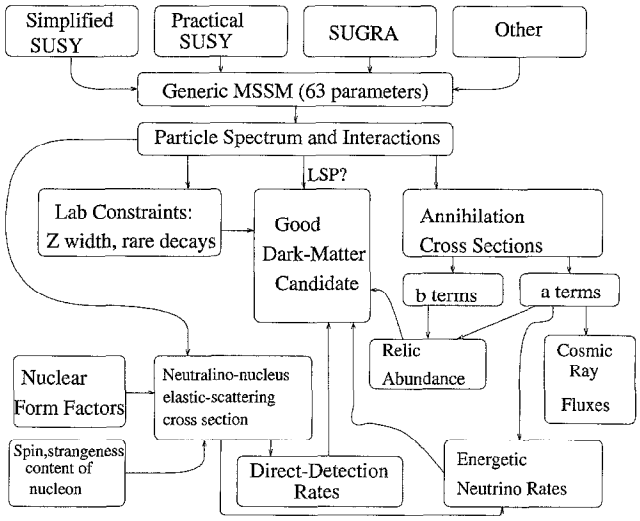

Fig. 62. Diagrammatic summary of calculations needed in the study of supersymmetric dark matter.

A generic minimal supersymmetric extension of the standard model is specified by 63 parameters (masses, mixings, and couplings). A 63-dimensional parameter space is difficult to study, so relations between the various parameters are often assumed. The phenomenology of the full range of the 63-dimensional parameter space can be investigated by restricting ourselves to only a handful of parameters, if these imposed relations are chosen reasonably and properly. Three such sets of relations were described. These model parameterizations are discussed in Section 4 and Appendix A.

First are the *simplified* supersymmetric models, which are specified by six parameters. In these models, all squark and slepton masses are assumed to be degenerate with no sfermion mixing. These *simplified* models are easier to manipulate analytically than the generic MSSM. Furthermore, they have been studied extensively in the literature since they represent a relatively simple class of "toy" models for supersymmetric dark matter. However, the *simplified* models are unrealistic. The *practical* model involves a more correct selection of the low-energy supersymmetric parameters.

Instead of specifying sfermion masses by hand, one should take as input the parameters in the soft supersymmetry-breaking terms in the Lagrangian that give rise to the superparticle masses. The *practical* model parameterization involves specific (although still somewhat arbitrary) relations between these couplings. The final model specification described here is the supergravity (SUGRA) model specification. The MSSM is almost certainly the low-energy limit of some high-energy theory – for example, a grand-unified, supergravity, or string theory – and the 63 MSSM parameters would then be related to a handful of parameters in this more fundamental theory. We have given a brief discussion of supergravity theories, in which the fundamental Lagrangian is specified by nine parameters. There have been numerous other supergravity, SUSY-GUT, and string theories presented in the literature which have some realization of the generic MSSM as their low-energy limit. Therefore, the general discussion in this Report can be applied to these models as well.

Once the Lagrangian of the generic MSSM is specified, the superparticle masses and couplings can be obtained by diagonalization of the mass matrices. First of all, one must check that the vacuum of the theory is neutral (i.e., that there is no charge- or color-breaking vacuum expectation value). Then, if the lightest supersymmetric particle is not a neutralino (nor a sneutrino; see Section 12.2), then there will not be a supersymmetric dark-matter candidate (although the model may still be phenomenologically viable). The model must then satisfy all known accelerator constraints to be acceptable. The most robust and model-independent of these constraints, those which come from Z^0 decays to charginos, neutralinos, and Higgs bosons, and those which come from $b \to s\gamma$ decays, were reviewed in Section 5. The same calculations can be used to forecast sensitivities of next-generation experiments to various models. There may be additional accelerator constraints on the MSSM, but a discussion of how these are obtained from the data for a generic model is quite involved and beyond the scope of this article. For a more complete discussion, see, e.g., Refs. [19, 20].

The next result of interest is the cosmological-abundance calculation described in Section 3. The abundance of a neutralino is determined by its annihilation cross section, the subject of Section 6, and this can be written in terms of the s-wave ("*a* terms") and p-wave ("*b* terms") contributions. If a model is to be cosmologically viable (barring some exotic early-Universe phenomena; Section 3.5), the neutralino should have a relic abundance $\Omega_\chi \lesssim 1$. To be a candidate for the halo dark matter, it should have a relic density in the range $0.01 \lesssim \Omega_\chi h^2 \lesssim 1$. Smaller neutralino relic densities are astrophysically acceptable, although it is unlikely that such models could constitute the primary component of the halo dark matter.

One can then search for experimentally and cosmologically viable WIMPs. The local halo density and velocity distribution are the primary sources of astrophysical uncertainty in the predicted detection rates (Section 2.4). Both direct and energetic-neutrino searches depend primarily on the WIMP–nucleus interaction (Section 7). In addition to the supersymmetric model parameters, these cross sections depend on experimental and theoretical input from QCD and nuclear physics, and these input are currently the source of some uncertainty. The predicted energetic-neutrino rates further depend on the WIMP-annihilation cross sections (but only the *a* terms), the neutrino spectra from WIMP-annihilation products, and the interactions of neutrinos with the solar medium (Section 9.5). The neutrino spectra are another source of uncertainty. In Section 11, we give sample results of all the above calculations and demonstrate the feedback process described in Fig. 62.

In order to be an acceptable dark-matter candidate, a neutralino must be consistent with the constraints already set by the first generation of direct-detection and energetic-neutrino searches, as well as consistent with known accelerator bounds. If a given model violates current limits from direct and indirect searches for particle dark matter, it is still conceivable that the supersymmetric model is viable. This would be the case, for example, if the canonical calculations resulted in a cosmological abundance too small to account for halo dark matter, or if some loophole in the relic-abundance calculation were in operation. The good dark-matter candidates will be the target of forthcoming direct, indirect, and accelerator searches.

The *a* terms of the annihilation cross section are also needed for the flux of anomalous cosmic rays produced by WIMP annihilation in the halo. The sensitivity of current cosmic-ray measurements are sufficient to probe only a very small family of WIMP candidates. Moreover, predicted cosmic-ray fluxes are subject to numerous astrophysical uncertainties, so comparison of a given model with observations is much more imprecise than it is in the case of direct or

energetic-neutrino searches. Still, a cosmic-ray signal is sometimes predicted for models which have very small direct-detection and energetic-neutrino rates, so cosmic-ray searches may provide a complementary avenue towards the discovery of particle dark matter.

13.2. Central results

We now summarize the central results needed for supersymmetric-dark-matter calculations. First we begin with the determination of the superparticle masses. The chargino masses are obtained by diagonalization of the chargino mass matrix, Eq. (A.17), and diagonalization of the neutralino mass matrix, Eq. (A.20), gives the neutralino masses. The Higgs masses are given in Eqs. (A.23) and (A.24). The squark, slepton, and sneutrino masses are obtained by diagonalizing the appropriate mass matrices in Eqs. (A.25)–(A.28). Couplings needed for cross sections throughout the paper are given in Appendix A.

The laboratory constraints to supersymmetric models reviewed here are those from limits to Z^0-boson decay to neutralinos, charginos, and Higgs bosons. The rate for Z decay to charginos and neutralinos is given in Eq. (5.2), and that for decay to h^0A^0 pairs is given in Eq. (5.1). Additional constraints to the Higgs sector come primarily from $b \to s\gamma$ limits. The calculation of the rates for these decays in the MSSM is outlined in Section 5.6.

The cosmological abundance of a WIMP, Ω_χ, is given in terms of the coefficients a and b in the nonrelativistic expansion of the total annihilation cross section, Eq. (6.1), by Eqs. (3.6)–(3.8). The a and b contributions to the total annihilation cross section are listed in Section 6. The results for a and b for all annihilation channels are summarized in Table 2.

The cross section for neutralino–nucleus elastic scattering is crucial for the prediction of direct-detection and energetic-neutrino rates. The cross section can be split up into two parts: that due to the spin interaction and that due to the scalar interaction. The "standard" total cross sections at zero momentum transfer for the spin and scalar interaction, that are used subsequently for direct- and indirect-detection rates, are given in Eqs. (7.16) and (7.36). The differential direct-detection rate is given in terms of an arbitrary form factor $F(Q)$ and WIMP velocity distribution $T(Q)$ in Eq. (8.6). The differential event rate for a WIMP velocity distribution appropriate to an isothermal halo corrected for the solar-system velocity through the halo, but for an arbitrary form factor is given in Eq. (8.17), the central result of Section 8. The total event rates assuming no form-factor suppression and assuming an exponential form factor are given in Eqs. (8.18) and (8.21), respectively.

The rate for observation of upward muons induced by energetic neutrinos from WIMP annihilation in the Sun and Earth is provided in Eq. (9.2). The annihilation rate Γ_A that appears in Eq. (9.2) is written in terms of the capture rate C in Eq. (9.7). The rate for capture in the Sun via the axial-vector interaction is listed in (9.19), and the rates for capture in the Sun and Earth via the scalar interaction for all but a few pathological cases are provided in Eqs. (9.26) and (9.27). The neutrino spectra that appear in the expression, Eq. (9.2), for the upward-muon flux are listed in Section 9.5.

13.3. Concluding remarks

Although our discussion focussed on the neutralino, we might expect similar astrophysical phenomenology for any stable particle with weak couplings to matter (Section 12). The most

commonly discussed WIMPs – apart from MSSM neutralinos – are heavy fourth-generation Dirac or Majorana neutrinos, sneutrinos, or neutralinos in non-minimal supersymmetric models. The study of Dirac and Majorana neutrinos is especially instructive, since most of the available parameter space for these models has been ruled out by a variety of considerations described here.

In this review, we have described calculations for the most general MSSM. Numerically, surveys of the entire parameter space lead to a broad range of relic abundances and detection rates for the entire parameter space, which provides little guidance for experimental searches. Therefore, where possible, we provided general model-independent comparisons of various event rates for models which in some sense are more "likely."

Another avenue which should be (and is currently being) pursued is the study of the low-energy supersymmetric theories which arise from GUT, supergravity, or string theories. By doing so, one can focus on the regions of parameter space that are more "likely" from a fundamental perspective rather than surveying the vast parameter space as we do here. We still do not have an understanding of the 18 parameters of the standard model, so any given theoretical prediction of all 63 SUSY parameters should be taken with a grain of salt. Still, many such theories *can* account for the standard-model particle spectrum to some extent, and these models will similarly suggest relations between superparticle masses. The literature on phenomenology and cosmology of supergravity- or SUSY-GUT-derived low-energy models is quite large. As an example, several authors have argued that a pure B-ino is favored as the LSP in SUSY-GUT and supergravity models, but there is some disagreement about the preferred mass range [407]. Furthermore, some authors claim that naturalness leads to an upper bound to the B-ino mass of order a few hundred GeV [257, 408] (roughly coincident with the cosmological upper bound [132, 134]). More discussions of which models are favored from the viewpoint of unified theories are needed.

Also on the particle-physics front, the spin and strangeness content of the nucleon need to be determined more precisely, and an improved understanding of the relevant nuclear physics would be useful.

In astrophysics, the most important issue for dark-matter detection is the determination of the local halo density. As discussed in Section 2.4, there is potentially a large uncertainty in the local halo density due to imprecise knowledge of the amount and distribution of luminous and nonluminous (MACHOs?) matter in the bulge and disk. Improved dynamical constraints and Galactic models are needed, and the microlensing events toward the bulge must be understood. The halo fraction of MACHOs has been estimated but still needs to be determined to greater precision [64].

Progress in the search for dark matter will most likely come with new experimental developments. The strongest accelerator test of supersymmetry will come with the advent of LEP-II. A large fraction of the Higgs parameter space will be probed by searches for direct production of neutral Higgs bosons. Unfortunately, LEP-II will still be insensitive to some fraction of the models, so it is possible that supersymmetry exists even if it does not make itself manifest at LEP-II.

Predicted rates for detection of dark-matter neutralinos vary over several orders of magnitude. The first generation of direct and indirect searches probed only the most optimistic of these models. The second generation of direct-detection technologies and astrophysical neutrino detectors are currently being assembled. The sensitivity of these experiments to particle dark matter will be increased by an order of magnitude or more, and a significant fraction of the theoretically favored models will be accessible. However, realistically, development of even larger detectors will be needed to test the majority of WIMP candidates currently discussed by theorists.

Acknowledgements

We are indebted to M. Drees, J. Engel, F. Halzen, P. Nath, B. Sadoulet, D. Seckel, M. Srednicki, and T. Ressell for helpful discussions. We thank D. Akerib, S. Barwick, M. Drees, K. Freese, G. Raffelt, P. Smith, D. Spergel, and X. Tata for detailed comments on a preliminary draft. We thank J. Engel also for providing us with nuclear form factors, A. Da Silva and D. Akerib for providing unpublished data, and M. Runyan for checking our numerical code. This work was supported in part (K.G.) by the Center for Particle Astrophysics, an NSF Science and Technology Center operated by the University of California under Cooperative Agreement No. ADT-8809616. M. K. was supported by the W. M. Keck Foundation at the I. A. S. and by the D. O. E. at Columbia under contract DEFG02-92-ER 40699. G. J. was supported by the D.O.E under contract DEFG02-85-ER 40231. K.G. was supported in part by a D.O.E. OJI award and the Alfred P. Sloan Foundation. M.K. acknowledges the hospitality of the CERN Theory Group and the NASA/Fermilab Astrophysics Center where part of this work was completed.

Appendix A. Construction of the MSSM

A.1. Introduction

In this Appendix, we provide the details of the construction of the MSSM which are necessary in order to perform explicit calculations. This means that we write down all of the required interaction terms in complete generality and in a uniform convention. This Appendix can be read as a self-contained introduction to the technical details of supersymmetric-model construction.

A.2. Superfield formalism

The most compact form for the Lagrangian of a supersymmetric field theory is obtained with the superfield formalism [409, 410]. When written in terms of superfields, the theory possesses manifest supersymmetry. It would be well beyond us to give a detailed review of this formalism, and we refer the interested reader to some of the many expositions which are available [16, 152, 153].

Put simply, a superfield is a collection of "component" fields, describing excitations such as fermions, scalar fields, or gauge particles, organized in such a way as to make the action of supersymmetry transformations on these component fields simple when written in terms of the superfield. The various component fields of a given superfield are the members of a supersymmetric multiplet. A superfield is written as a formal polynomial in abstract spinor symbols, which we denote θ_α, $\bar{\theta}_{\dot{\alpha}}$, and which are required to satisfy anticommutation relations, $\{\theta_\alpha, \theta_\beta\} = \{\theta_\alpha, \bar{\theta}_\beta\} = \{\bar{\theta}_\alpha, \bar{\theta}_\beta\} = 0$. These symbols are called the superspace coordinates, and they transform as spinors with respect to Poincare transformations. A generic superfield will look like

$$\Phi(x, \theta_\alpha, \bar{\theta}_{\dot{\alpha}}) = f(x) + \theta_\alpha \psi^\alpha(x) + \bar{\theta}_{\dot{\alpha}} \chi^{\dot{\alpha}}(x) + \theta_\alpha \theta^\alpha m(x) + \bar{\theta}_{\dot{\alpha}} \bar{\theta}^{\dot{\alpha}} n(x) + \theta_\alpha (\sigma^\mu)^{\alpha\dot{\alpha}} \bar{\theta}_{\dot{\alpha}} v_\mu(x)$$

$$+ \theta_\alpha \theta^\alpha \bar{\theta}_{\dot{\alpha}} \bar{\lambda}^{\dot{\alpha}}(x) + \bar{\theta}_{\dot{\alpha}} \theta^{\dot{\alpha}} \theta_\alpha \phi^\alpha(x) + \theta_\alpha \theta^\alpha \bar{\theta}_{\dot{\alpha}} \bar{\theta}^{\dot{\alpha}} d(x) , \tag{A.1}$$

which contains scalar, spinor, and vector component fields. As a necessary feature of the formalism, some of the component fields turn out to be nondynamical; these auxiliary fields can be eliminated using their equations of motion, at the expense of destroying the manifest supersymmetry. As representations for the supersymmetry transformations, superfields are generally reducible. The unique irreducible superfield representations are of two types. The first type of irreducible representation is provided by chiral superfields, which are superfields that satisfy the constraint

$$(\partial/\partial\bar{\theta}^{\dot{\alpha}} + \mathrm{i}\theta^{\alpha}(\sigma^{\mu})_{\alpha\dot{\alpha}}\partial_{\mu})\,\Phi_{\mathrm{chiral}} = 0\ . \tag{A.2}$$

The second type of irreducible representation is provided by vector superfields, which satisfy the constraint

$$\Phi_{\mathrm{vector}} = \Phi^{\dagger}_{\mathrm{vector}}\ , \tag{A.3}$$

These constraints eliminate certain combinations of component fields, but do not destroy manifest supersymmetry. As their names suggest, these fields give supersymmetric versions of two standard types of nonsupersymmetric fields. A chiral superfield turns out to be the appropriate supersymmetric analogue of a chiral fermion field, and a vector superfield turns out to be the appropriate analogue of a gauge field.

In order to construct an action functional, we must remove the scaffolding of superspace coordinates without destroying manifest supersymmetry. A method is provided by the well-known Berezin rules for integration of Grassman-valued variables, $\int \mathrm{d}\theta = 0$; $\int \mathrm{d}\theta\ \theta = 1$. Using this definition, the most general perturbatively renormalizable polynomial action for a theory of a chiral superfield can be written as

$$S = \int \mathrm{d}^4x \left[\int \mathrm{d}^2\theta\, \mathrm{d}^2\theta\ \Phi^{\dagger}\Phi + \int \mathrm{d}^2\theta \{\lambda\Phi + m\Phi\Phi + \kappa\Phi\Phi\Phi\} \right]. \tag{A.4}$$

The second term, involving powers of Φ, is called the superpotential. The first term is correctly identified as a kinetic-energy term, and the minimal coupling prescription for interaction with a vector superfield can be shown to be

$$\int \mathrm{d}^2\theta\, \mathrm{d}^2\bar{\theta}\ \Phi^{\dagger}\Phi \rightarrow \int \mathrm{d}^2\theta\, \mathrm{d}^2\bar{\theta}\ \Phi^{\dagger}\mathrm{e}^{2gV}\,\Phi\ , \tag{A.5}$$

where V is the vector superfield.

The remaining required term is a kinetic term for the vector superfields. The appropriate definition of the kinetic term for a non-Abelian gauge superfield is somewhat involved, and we will not require its explicit form, so we leave that undiscussed. Interested readers can consult Ref. [16].

A.3. Minimal supersymmetric standard model: general discussion

The construction of the minimal supersymmetric standard model proceeds as follows. Consider a supersymmetric field theory, the superfield content of which is sufficient to incorporate the fields of the standard model as components. Allow all those interactions which are gauge-invariant and renormalizable, and allow no more superfields than the minimum required to encompass the fields of the standard model. This defines the minimal supersymmetric standard model (MSSM). The

chiral superfields of the MSSM are the quark and lepton superfields

$$\hat{L}_{\mathrm{L}i},\ \hat{c}_{\mathrm{R}i},\ \hat{Q}_{\mathrm{L}i},\ \hat{d}_{\mathrm{R}i},\ \hat{u}_{\mathrm{R}i}\ , \tag{A.6}$$

together with the Higgs superfields

$$\hat{H}_1,\ \hat{H}_2\ . \tag{A.7}$$

The superfields $\hat{Q}$, $\hat{L}$, $\hat{H}_1$, and $\hat{H}_2$ carry $\mathrm{SU}(2)_{\mathrm{W}}$ indices in the usual way; they are weak doublets. The index i on the quark and lepton superfields is a generation index, and we will consistently use Latin indices i, j, k as generation indices. The vector superfields are those appropriate to the $\mathrm{U}(1)_{\mathrm{Y}} \times \mathrm{SU}(2)_{\mathrm{W}} \times \mathrm{SU}(3)_{\mathrm{c}}$ gauge symmetry,

$$\hat{B},\ \hat{W}^a,\ \hat{G}^a\ . \tag{A.8}$$

We have introduced the hat notation for superfields in order to distinguish them from their ordinary counterparts. The superfields of the MSSM are listed in Table 11.

The existence of two Higgs superfields at first seems nonminimal. However, it is not possible to introduce Yukawa couplings of both up- and down-type quarks to the same Higgs field in the MSSM. One may recall that in the ordinary standard model with one Higgs doublet, down- and up-type quarks couple respectively to H and $H^{\mathrm{c}} = \mathrm{i}\tau_2 H^*$. But in a superpotential for chiral superfields, a superfield cannot appear together with its adjoint; no such supersymmetric term exists. Thus an extra Higgs field is required. Furthermore, it can be shown that the existence of the second Higgs superfield is required to avoid a gauge anomaly which would otherwise result from the unpaired chiral fermion which exists in the Higgs supermultiplet [166].

With the above field content, we write the supersymmetric Lagrangian of the MSSM,

$$\mathscr{L}_{\mathrm{S}} = \mathscr{L}_{\text{vector kinetic}} + \mathscr{L}_{\text{minimal coupling}} + \int \mathrm{d}^2\theta\, \mathscr{W}\ , \tag{A.9}$$

where $\mathscr{W}$ is the superpotential for the chiral superfields,

$$\mathscr{W} = -\mu \hat{H}_1 \hat{H}_2 + \hat{H}_1 h_{\mathrm{e}}^{ij} \hat{L}_{\mathrm{L}i} \hat{e}_{\mathrm{R}j} + \hat{H}_1 h_{\mathrm{d}}^{ij} \hat{Q}_{\mathrm{L}i} \hat{d}_{\mathrm{R}j} - \hat{H}_2 h_{\mathrm{u}}^{ij} \hat{Q}_{\mathrm{L}i} \hat{u}_{\mathrm{R}j}\ . \tag{A.10}$$

Here, μ is the so-called higgsino mass parameter that appears in the neutralino and chargino mass matrices. Weak doublet fields are implicitly contracted using the SU(2) tensor ε_{ab}. The matrices h_n are the Yukawa coupling matrices, related to the fermion mass matrices, M_{e}, M_{u}, and M_{d}, in the usual way,

$$h_{\mathrm{e}} = \frac{g}{\sqrt{2} m_{\mathrm{W}} \cos\beta} M_{\mathrm{e}}; \qquad h_{\mathrm{d}} = \frac{g}{\sqrt{2} m_{\mathrm{W}} \cos\beta} M_{\mathrm{d}}; \qquad h_{\mathrm{u}} = \frac{g}{\sqrt{2} m_{\mathrm{W}} \sin\beta} M_{\mathrm{u}}\ , \tag{A.11}$$

where $\tan\beta$ is the ratio of vacuum expectation values for the Higgs fields.

In actual fact, we have already broken our specified rules for the construction of the Lagrangian. The superpotential written here does not constitute the most general superpotential possible. There exists another class of interactions, the so-called R-parity violating interactions, which we have not included. These interactions produce unsuppressed tree-level baryon- and lepton-number violation. The existence of such interactions would make the MSSM a phenomenological disaster. It is exceptionally convenient that these terms can be eliminated by the imposition of a discrete symmetry, R parity, which is a remnant of a continuous $\mathrm{U}(1)_R$ rephasing symmetry involving the

Table 11
Field content of the MSSM as in Ref. [18]

Superfield	Component Fields	Quantum Numbers (SU(3), SU(2), U(1))	Name
	Matter fields		
Q_L	$\begin{pmatrix} u_L \\ d_L \end{pmatrix} \equiv Q_L$	$(3, 2, \frac{1}{3})$	left-handed quark doublet
	$\begin{pmatrix} \bar{u}_L \\ \bar{d}_L \end{pmatrix} \equiv \bar{Q}_L$		
$\hat{u}_R$	u_L^c	$(3^*, 1, -\frac{4}{3})$	right-handed up-quark singlet
	$\tilde{u}_l^c$		
$\hat{d}_R$	d_L^c	$(3^*, 1, +\frac{2}{3})$	right-handed down-quark singlet
	$\tilde{d}_l^c$		
$\hat{L}_L$	$\begin{pmatrix} v_L \\ e_L \end{pmatrix}$	$(1, 2, -1)$	left-handed lepton doublet
	$\begin{pmatrix} \tilde{v}_L \\ \tilde{e}_L \end{pmatrix}$		
$\hat{e}_R$	e_L^c	$(1, 1, +2)$	right-handed lepton singlet
	$\tilde{e}_L^c$		
	Gauge fields		
$\hat{W}$	$\begin{pmatrix} W^{\pm} \\ W^3 \end{pmatrix}$	$(1, 0, 3)$	$SU(2)_L$ gauge fields
	$\begin{pmatrix} \tilde{W}^{\pm} \\ \tilde{W}^3 \end{pmatrix}$		
$\hat{B}$	B	$(1, 1, +2)$	U(1) gauge field
	$\tilde{B}$		
	Higgs fields		
$\hat{H}_2$	$\begin{pmatrix} \phi_u^+ \\ \phi_u^0 \end{pmatrix}$	$(1, 2, +1)$	up-type higgs doublet
	$\begin{pmatrix} \tilde{\phi}_u^+ \\ \tilde{\phi}_u^0 \end{pmatrix}$		
$\hat{H}_1$	$\begin{pmatrix} \phi_d^+ \\ \phi_d^0 \end{pmatrix}$	$(1, 2, -1)$	down-type higgs doublet
	$\begin{pmatrix} \tilde{\phi}_d^+ \\ \tilde{\phi}_d^0 \end{pmatrix}$		

superspace coordinates. In terms of its action on component fields, $R = (-1)^{3(B-L)+2S}$, where B and L are the baryon and lepton numbers, and S is the spin. The necessity of this restriction is an annoyance, compared to the case of the nonsupersymmetric standard model where baryon and lepton number arise as accidental symmetries of the most general gauge-invariant and renormalizable Lagrangian. Deviations from exact R invariance have been studied to some degree, however

one must then provide a mechanism to explain the required smallness of the deviations. Thus our definition of the MSSM is such that R parity is an exact symmetry. This has the important consequence that there exists a lighest particle with $R = -1$, and this particle must be absolutely stable. It is often called the lighest supersymmetric particle (LSP).

The theory specified by Eqs. (A.9) and (A.10) is a manifestly supersymmetric theory of fields interacting with themselves and with their supermultiplet partners. These partners must, of course, have the same masses as the usual standard-model particles to which they are related, and this is in direct contradiction to experimental facts.[13] So another layer of complexity must be contemplated; somehow supersymmetry must be broken so that the undesirable partners are given masses high enough that they could not have been already discovered in high-energy collisions. On the other hand, this breaking mechanism should not destroy that feature of a supersymmetric theory which is arguably most desirable, the softened ultraviolet behavior of radiative corrections. Such well-behaved breaking is called soft breaking. Following Girardello and Grisaru [167], one can write down the most general gauge-invariant soft supersymmetry-breaking terms involving the fields of the MSSM,

$$\begin{aligned}\mathscr{L}_{\text{soft}} = & -m_1^2|H_1|^2 - m_2^2|H_2|^2 - m_{12}^2(H_1H_2 + H_1^*H_2^*) - \tilde{Q}_{\text{L}i}^\dagger M_{\tilde{\text{Q}}ij}^2 \tilde{Q}_{\text{L}j} - \tilde{u}_{\text{R}i}^\dagger M_{\tilde{\text{u}}ij}^2 \tilde{u}_{\text{R}j} \\ & - \tilde{d}_{\text{R}i}^\dagger M_{\tilde{\text{d}}ij}^2 \tilde{d}_{\text{R}j} - \tilde{L}_{\text{L}i}^\dagger M_{\tilde{\text{L}}ij}^2 \tilde{L}_{\text{L}j} - \tilde{e}_{\text{R}i}^* M_{\tilde{\text{e}}ij}^2 \tilde{e}_{\text{R}j} + H_2 \tilde{Q}_{\text{L}i}(h_{\text{u}}A_{\text{u}})_{ij}\tilde{u}_{\text{R}j} - H_1 \tilde{Q}_{\text{L}i}(h_{\text{d}}A_{\text{d}})_{ij}\tilde{d}_{\text{R}j} \\ & - H_1 \tilde{L}_{\text{L}i}(h_{\text{e}}A_{\text{e}})_{ij}\tilde{e}_{\text{R}j} - \tfrac{1}{2}[M_1 \bar{\tilde{B}}\tilde{B} + M_2 \bar{\tilde{W}}^a \tilde{W}^a + M_3 \bar{\tilde{G}}^a \tilde{G}^a] \,. \end{aligned} \tag{A.12}$$

The fields here are not superfields, but component fields; $\tilde{\psi}$ indicates the scalar partner of a fermion ψ, and $\tilde{V}$ indicates the fermionic partner of a vector boson V. The parameters A_u are materices in flavor space with the dimensions of mass, and the $M_{\tilde{x}}^2$ (for $x = \text{Q, u, d, L, e}$) are each 3×3 symmetric matrices with dimension of mass squared.

These soft-breaking terms are to be understood as terms of an effective Lagrangian at energy scales less than the scale at which the supersymmetry-breaking mechanism is defined, E_{SB}. Being an effective Lagrangian, $\mathscr{L}_{\text{soft}}$ provides a complete description of the symmetry-breaking physics at or below the scale at which that physics is specified, and there is no need to consider the origin of the symmetry breaking when studying the phenomenology of the theory at low energies, $E < E_{\text{SB}}$. However, $\mathscr{L}_{\text{soft}}$ cannot be expected to describe faithfully processes at scales greater than E_{SB}, where it presumably has an origin in some specific dynamical mechanism. It is in this sense that the MSSM is an incomplete theory, and it is in this sense that our earlier comment about the apparent necessity for some new physics in which to embed the softly broken MSSM is meant. Nevertheless, the theory given by $\mathscr{L}_{\text{S}}$ together with $\mathscr{L}_{\text{soft}}$ is a complete description of the possible physics below the scale E_{SB}, as it must be, and no generality is lost by considering it for phenomenological study. The only restrictions we have so far invoked are the restriction on the field content and the restriction on the existence of R-violating interactions.

We have chosen to write the fermionic fields of the resulting theory as four-component spinor fields. Since gauginos and higgsinos are Majorana fermions (two-state particles), this leads to

[13] In fact they must have vanishing mass, since electroweak-symmetry breaking cannot occur if supersymmetry is unbroken.

certain oddities in the interactions (see, e.g., Ref. [20] for further details). However, on the whole it is a more approachable form, due to the familiarity of the associated algebraic manipulations and conventions.

At this point, to make the final step toward the phenomenology of the MSSM, we will eliminate the auxiliary fields, destroying the manifest supersymmetry. In the absence of the soft-supersymmetry-breaking terms, this would be a foolish thing to do. However, because of soft breaking, the vacuum is not supersymmetric, and nothing can be gained by calculating in a manifestly supersymmetric manner. It is after this point that the MSSM can be regarded simply as a normal field theory, with some extra fields and some unusual relations among various coupling constants. The elimination of the auxiliary fields creates various contributions to the Lagrangian in terms of component fields. We now enumerate the types of terms which arise.

For the scalar potential, the elimination of the auxiliary fields gives

$$V_{\text{scalar}} = \tfrac{1}{2} D^a D^a + F_n^* F_n \,, \tag{A.13}$$

where, letting $\{A_n\}$ denote the scalar fields of the theory which are components of the superfields $\{\hat{A}_n\}$,

$$F_n = \frac{\partial \mathscr{W}}{\partial A_n}; \qquad D^a = g A_n^* T^a A_n \,, \tag{A.14}$$

Derivatives of the superpotential with respect to a scalar field are understood according to this rule: in the function $\mathscr{W}$, replace each superfield with its scalar component and then compute the indicated derivative. The T^a are gauge generators. The sum over adjoint group indices, a in Eq. (A.13), is understood to be over all the group generators of $\mathrm{U}(1) \times \mathrm{SU}(2) \times \mathrm{SU}(3)$. We have set the so-called Fayet–Iliopoulos term to zero, as it must generically be very small for phenomenological reasons [166].

For the Yukawa interactions, the elimination of the auxiliary fields gives

$$\mathscr{L}_{\text{Yukawa}} = -\frac{1}{2}\left[\left(\frac{\partial^2 \mathscr{W}}{\partial A_n \partial A_m}\right) \bar{\psi}_n^c P_L \psi_m + \left(\frac{\partial^2 \mathscr{W}}{\partial A_n \partial A_m}\right)^* \bar{\psi}_n P_R \psi_m^c\right], \tag{A.15}$$

which gives the previously mentioned identification of the superpotential couplings with the Yukawa couplings of the fermion fields.

For the gauge interactions, the Lagrangian in terms of component fields is, letting ψ be a fermion field with superpartner $\tilde{\psi}$, and letting V_μ be the gauge boson with superpartner $\tilde{V}$,

$$\begin{aligned}\mathscr{L}_{\text{gauge}} = & -\tfrac{1}{4} F^a_{\mu\nu} F^{\mu\nu a} + \tfrac{1}{2} \mathrm{i} g f_{abc} \bar{\tilde{V}}^a \gamma^\mu \tilde{V}^b V^c_\mu - g V^a_\mu \bar{\psi} \gamma^\mu T^a \psi - \mathrm{i} g V^a_\mu \bar{\tilde{\psi}}^\dagger T^a \overleftrightarrow{\partial}_\mu \tilde{\psi} \\ & - \sqrt{2} g (\bar{\tilde{V}}^a \psi T^a \tilde{\psi} + \bar{\tilde{\psi}} \tilde{V}^a T^a \psi) + g^2 V^a_\mu V^{\mu b} \bar{\tilde{\psi}} T^a T^b \tilde{\psi} \,.\end{aligned} \tag{A.16}$$

A.4. Minimal supersymmetric standard model: spectrum and interactions

Using the above prescriptions for calculating the component field interactions from the superpotential, we will now construct the Lagrangian in terms of component fields. The first step is to diagonalize the various mass matrices to obtain the mass eigenstates.

First, we diagonalize the mass matrices for the charginos and neutralinos, which are the fermionic superpartners of the gauge bosons and Higgs particles. Then we discuss the Higgs sector. Then we diagonalize the sfermion mass matrices. We assume that the familiar fermion mass matrices are already diagonalized. The effect of this diagonalization procedure is to introduce a flavor mixing matrix in the charged-current interactions of the quarks, the Cabibbo–Kobayashi–Maskawa matrix, $V_{\rm CKM}$. In the usual way, there is no observable effect of the diagonalization of the lepton mass matrix, due to the freedom to absorb any rotation by a counter rotation of the neutrino fields. The effect of this rotation on the sfermions will be considered when we discuss their mass matrices. Henceforth, when we write a quark or lepton field, it will be understood to be a mass eigenstate.

Charginos: In the basis $\tilde{W}^{\pm}$–$\tilde{H}^{\pm}$, the chargino mass matrix is

$$M_{\rm ch} = \begin{pmatrix} M_2 & \sqrt{2} m_{\rm W} \sin\beta \\ \sqrt{2} m_{\rm W} \cos\beta & \mu \end{pmatrix}. \tag{A.17}$$

This nonsymmetric matrix is diagonalized by separate rotations of the negatively and positively charged states, $M_{\rm ch}^{\rm diag} = U^{\dagger} M_{\rm ch} V$. The matrices U and V will appear in the interactions of the mass-eigenstate charginos, which will be designated $\chi_n^{\pm} = 1, 2$. Note that our definition is such that the eigenvectors of the mass matrices lie in the columns of the corresponding diagonalization matrices. This differs from the convention of Ref. [20], where the eigenvectors lie in the rows of the diagonalization matrix. The explicit forms for the chargino mixing matrices are

$$U = \begin{pmatrix} \cos\phi_- & -\sin\phi_- \\ \sin\phi_- & \cos\phi_+ \end{pmatrix}$$
$$V = \begin{pmatrix} \cos\phi_+ & -\sin\phi_+ \\ \sin\phi_+ & \cos\phi_- \end{pmatrix}, \tag{A.18}$$

where

$$\tan 2\phi_- = 2\sqrt{2} m_{\rm W} \frac{(\mu \sin\beta + M_2 \cos\beta)}{(M_2^2 - \mu^2 + 2m_{\rm W}^2 \cos 2\beta)}$$
$$\tan 2\phi_+ = 2\sqrt{2} m_{\rm W} \frac{(\mu \cos\beta + M_2 \sin\beta)}{(M_2^2 - \mu^2 + 2m_{\rm W}^2 \cos 2\beta)}. \tag{A.19}$$

We do *not* choose the convention that the masses are positive; instead, the sign of the mass term is allowed to be positive or negative, which corresponds to the CP eigenvalue of the particle. Had we fixed the masses to be positive, this quantum-number information would otherwise appear in the mixing matrix. Of course, the convention cannot change any physical results. The merit of our choice is more clear in the case of the neutralino mass matrix. By allowing the masses to have either sign, it is possible to work with purely real-valued mixing matrices; the subsequent simplification for manipulations of the couplings is worthwhile, especially in numerical calculations.[14]

[14] In this article, we assume that the interactions of the charginos are CP conserving. Then M_1, M_2, and μ are real and U and V are real matrices. Even so, our formalism throughout allows the diagonalization and mass matrices to be complex, so our equations will accommodate CP-violating models as well.

Neutralinos: The neutralino mass matrix, in the $\tilde{B}$–$\tilde{W}^3$–$\tilde{H}_1^0$ – $\tilde{H}_2^0$ basis, is

$$M_{\rm neut} = \begin{pmatrix} M_1 & 0 & -m_Z c_\beta s_W & m_Z s_\beta s_W \\ 0 & M_2 & m_Z c_\beta c_W & -m_Z s_\beta c_W \\ -m_Z c_\beta s_W & m_Z c_\beta c_W & 0 & -\mu \\ m_Z s_\beta s_W & -m_Z s_\beta c_W & -\mu & 0 \end{pmatrix}, \tag{A.20}$$

where $c_\beta = \cos\beta$, $s_\beta = \sin\beta$, $c_W = \cos\theta_W$, and $s_W = \sin\theta_W$. This Hermitian matrix is diagonalized by a unitary transformation of the neutralino fields, $M_{\rm neut}^{\rm diag} = N^\dagger M_{\rm neut} N$. The matrix N will appear in the interactions of mass-eigenstate neutralinos, which will be designated χ_n^0, $n = 1, 4$. In what follows we will consistently use the indices m, n as chargino or neutralino indices. Again, we have defined the diagonalization procedure such that the eigenvectors lie in the columns of the diagonalization matrix. As mentioned above for the chargino states, we allow the masses to have either sign, and this means that the mixing matrices can be chosen to have purely real-valued entries.[15]

Higgs sector: Next we consider the Higgs sector. There are five physical Higgs states, which we denote by $h^0, H^0, H^\pm, A^0$. The neutral CP-even states h^0 and H^0 are mixtures of the neutral components of the interaction-state Higgs fields [19, 411]. The mixing angle is called α, and satisfies

$$\sin 2\alpha = -\sin 2\beta \left(\frac{m_H^2 + m_h^2}{m_H^2 - m_h^2}\right), \qquad \cos 2\alpha = -\cos 2\beta \left(\frac{m_A^2 - m_z^2}{m_H^2 - m_h^2}\right). \tag{A.21}$$

At tree level, the masses of the neutral Higgs bosons are related by

$$m_{H,h}^2 = \tfrac{1}{2}(m_A^2 + m_Z^2 \pm \sqrt{(m_A^2 + m_Z^2)^2 - 4 m_Z^2 m_A^2 \cos^2 2\beta}). \tag{A.22}$$

The ratio of the two vacuum expectation values is $\tan\beta = v_2/v_1$. Any two parameters amongst the masses and angles determine the others. Furthermore, the charged-Higgs-boson mass is related to the pseudoscalar mass by

$$m_{H^\pm}^2 = m_A^2 + m_W^2. \tag{A.23}$$

Beyond tree level there are also corrections which depend on fermion masses, other combinations of standard-model couplings, and sfermion masses. If these quantities are taken as known, it remains true that two of the Higgs parameters suffice to fix the rest.

The radiative corrections to the Higgs sector are somewhat involved in full generality. We refer to the literature for a complete discussion [201–211]. To indicate the nature of the results, we can quote a simplified form for the correction which is often useful,

$$\begin{aligned} m_{h,H}^2 &= \tfrac{1}{2}(m_A^2 + m_Z^2 + \varepsilon \pm \Delta), \\ \Delta &= [(m_A^2 + m_Z^2 + \varepsilon)^2 - 4 m_A^2 m_Z^2 \cos^2 2\beta - 4\varepsilon m_A^2 \sin^2\beta - 4\varepsilon m_Z^2 \cos^2\beta]^{1/2}, \\ \varepsilon &= \frac{3g^2}{8\pi^2} \frac{m_t^4}{m_W^2 \sin^2\beta} \ln(1 + m_t^2/m_t^2). \end{aligned} \tag{A.24}$$

[15] Again, in this article we restrict ourselves to CP-conserving neutralino interactions, so $M_{\rm neut}$ and N will be real matrices, although the formalism presented here allows for CP-violating interactions.

The $H^{\pm}$–A^0 relation, Eq. (A.23), is to a good approximation unchanged by the radiative corrections.

Note that the numerical code described in Appendix B uses a somewhat more general result for the radiative corrections. The appropriate results are given in Eq. (3.77) of Ref. [199]. Numerical results presented at various points in this review were computed using this code.

Squarks, sleptons, and sneutrinos: Finally we must diagonalize the sfermion mass matrices. Note that generally these mass matrices give rise to a mixing between all six sfermions of a given charge. For example, the up-type squark states $\tilde{u}_{Li}$, $\tilde{u}_{Ri}$ will mix amongst themselves, and similarly for the down-type squarks and the charged sleptons. The sneutrinos are slightly different in that there are only three states, $\tilde{\nu}_{iL}$. These 6×6 mass-squared matrices, written in terms of 3×3 blocks, are

$$\tilde{M}_{\mathrm{u}}^2 = \begin{pmatrix} M_{\tilde{\mathrm{Q}}}^2 + M_{\mathrm{u}}^{\dagger}M_{\mathrm{u}} + m_Z^2(\tfrac{1}{2} - e_{\mathrm{u}}s_{\mathrm{W}}^2)\cos 2\beta & M_{\mathrm{u}}(A_{\mathrm{u}} - \mu\cot\beta) \\ (A_{\mathrm{u}}^{\dagger} - \mu^*\cot\beta)M_{\mathrm{u}}^{\dagger} & M_{\tilde{\mathrm{u}}}^2 + M_{\mathrm{u}}^{\dagger}M_{\mathrm{u}} + m_Z^2 e_{\mathrm{u}}s_{\mathrm{W}}^2\cos 2\beta \end{pmatrix}, \tag{A.25}$$

$$\tilde{M}_{\mathrm{d}}^2 = \begin{pmatrix} M_{\tilde{\mathrm{Q}}}^2 + M_{\mathrm{d}}^{\dagger}M_{\mathrm{d}} - m_Z^2(\tfrac{1}{2} - e_{\mathrm{d}}s_{\mathrm{W}}^2)\cos 2\beta & M_{\mathrm{d}}(A_{\mathrm{d}} - \mu\tan\beta) \\ (A_{\mathrm{d}}^{\dagger} - \mu^*\tan\beta)M_{\mathrm{d}}^{\dagger} & M_{\tilde{\mathrm{d}}}^2 + M_{\mathrm{d}}^{\dagger}M_{\mathrm{d}} + m_Z^2 e_{\mathrm{d}}s_{\mathrm{W}}^2\cos 2\beta \end{pmatrix}, \tag{A.26}$$

$$\tilde{M}_{\mathrm{e}}^2 = \begin{pmatrix} M_{\tilde{\mathrm{L}}}^2 + M_{\mathrm{e}}^{\dagger}M_{\mathrm{e}} - m_Z^2(\tfrac{1}{2} - e_{\mathrm{e}}s_{\mathrm{W}}^2)\cos 2\beta & M_{\mathrm{e}}(A_{\mathrm{e}} - \mu\tan\beta) \\ (A_{\mathrm{e}}^{\dagger} - \mu^*\tan\beta)M_{\mathrm{e}}^{\dagger} & M_{\tilde{\mathrm{e}}}^2 + M_{\mathrm{e}}^{\dagger}M_{\mathrm{e}} + e_{\mathrm{e}}m_Z^2 s_{\mathrm{W}}^2\cos 2\beta \end{pmatrix}, \tag{A.27}$$

and the 3×3 sneutrino matrix is

$$\tilde{M}_{\nu}^2 = M_{\tilde{\mathrm{L}}}^2 + \tfrac{1}{2}m_Z^2\cos 2\beta\,, \tag{A.28}$$

where the $M_{\tilde{x}}^2$ and A_x are the matrices of soft-supersymmetry-breaking parameters that appear in Eq. (A.12). The e_i are the electric charges, $e_{\mathrm{u}} = 2/3$, $e_{\mathrm{d}} = -1/3$, and $e_{\mathrm{e}} = -1$. The terms proportional to fermion mass matrices arise from F terms and the terms proportional to a gauge-boson mass arise from D terms, when the Higgs field acquire vacuum expectation values; see Eq. (A.13). These Hermitian matrices are diagonalized by unitary matrices, $\tilde{M}_x^{2\,\mathrm{diag}} = \Theta_x^{\dagger}\tilde{M}_x^2\Theta_x$.[16] We denote the mass-eigenstate charged sfermions by $\tilde{f}_j$ with $j = 1, \ldots, 6$, where f is any one of u, d, e, indicating the family of up-type, down-type, or lepton-type fermions. The sneutrino family is similar except that there are only three states, ν_j with $j = 1,2,3$. It is important to note that we can perform a preliminary rotation of the sfermion fields in generation space, such that the fermion mass matrices, M_{u}, M_{d}, and M_{e}, which appear in the 3×3 blocks are diagonal. We do this by rotating the left and right sfermion fields by the same unitary transformations which were used to rotate the left and right fermions in the process of diagonalizing the fermion mass matrices. This involves a change in the definitions of the matrix soft-breaking parameters A_x and $M_{\tilde{x}}^2$. Since there is no preferred basis in which to specify these matrices, there is no loss of generality implied by this redefinition. This redefinition is most convenient because it then becomes manifest that off-diagonal squark-flavor mixing will not occur in the case of flavor-blind soft supersymmetry

[16] Once again, in our numerical work, we restrict ourselves to CP-conserving squark interactions, so the matrices A_x, $M_{\tilde{x}}^2$, and therefore $\tilde{M}_x^2$ and Θ_x can be chosen to be real. If one allows for CP-violating squark interactions [412], then these matrices will in general be complex. Our formalism is sufficiently general to take into account such CP-violating interactions.

breaking, i.e., in the case that the soft-breaking terms are flavor symmetric; this defines what we mean by flavor-blind soft supersymmetry breaking. In general, radiative corrections involving the fermion Yukawa couplings will induce deviations from flavor-blind soft supersymmetry breaking. This occurs, for example, in supergravity models where the soft-breaking terms are postulated to be flavor blind at a high-energy scale; in this case, the leading logarithmic radiative corrections are summed using the renormalization group, and they lead to flavor mixing in the squark sector. Such corrections must be applied in the basis in which they are calculated. Ideally one would calculate only basis-independent quantities, since only such quantities are truly physical; however, it generally proves convenient to express results in terms of a chosen basis.

From the form of Eqs. (A.25)–(A.27), it is clear that squark and slepton mixing is quite generic. For example, even if all the matrices $M_{\tilde{x}}^2$ are diagonal and the A_x are all zero, there are still off-diagonal terms in the matrices $\tilde{M}_x^2$ proportional to the fermion mass matrices. Thus in this case, there can still be significant mixing between right and left top squarks.

Vacuum alignment: In the context of this model, the vacuum-alignment problem simply means that no scalar field carrying electromagnetic or color charge should acquire a vacuum expectation value. Therefore, the above sfermion mass-squared matrices are required to have strictly positive eigenvalues. This is a minimum requirement which is imposed along with other constraints on the models which are generated automatically by our numerical code. In principle, there are other aspects of the vacuum alignment problem in general models, which lead to (usually mild) constraints on the Higgs sector. A standard example of this is the calculation of Coleman and Weinberg [413].

MSSM interactions: At this point we can list the interactions in terms of the physical mass eigenstates. Many of these interaction terms appear in various forms in the literature [19, 20, 411, 414–416]. We will pay particular attention to the flavor structure and flavor mixing which occurs, as these ingredients very often do not appear in the literature. We choose not to reproduce ghost interactions, so it must be emphasized that these interactions are complete only for diagrams which do not involve gauge-boson or Higgs-boson loops.

First we list all the interactions involving sfermions. These interactions are mainly complicated by sfermion mixing. It is important to handle the general case properly since the general case includes the possibility of FCNCs, which are of great phenomenological interest. In order to state the interactions in the most transparent way, it is best to introduce two projection operators which have the effect of projecting mass-eigenstate sfermion fields onto subspaces corresponding to a particular handedness. Call these projection operators Π_{L} and Π_{R}. They are defined such that

$$\tilde{u}_{\mathrm{L}i} = (\Pi_{\mathrm{L}})_{ik}\Theta^{\mathrm{u}}_{kj}\tilde{u}_j, \qquad \tilde{u}_{\mathrm{R}i} = (\Pi_{\mathrm{R}})_{ik}\Theta^{\mathrm{u}}_{kj}\tilde{u}_j, \tag{A.29}$$

and similarly for the down-type squarks and the charged sleptons. The Θ^{f} are the sfermion mixing matrices defined by the diagonalization procedure given above. The case of sneutrinos is different, since the right-handed family is absent; in this case we have simply $\Pi_{\mathrm{L}} = 1$, $\Pi_{\mathrm{R}} = 0$. An explicit realization of these projection operators as matrices is easily given. Consider, for example, the

up-type squarks with the basis $(\tilde{u}_L, \tilde{c}_L, \tilde{t}_L, \tilde{u}_R, \tilde{c}_R, \tilde{t}_R)$; in this basis the projection matrices are

$$\Pi_L = \begin{pmatrix} 1 & 0 & 0 & 0 & 0 & 0 \\ 0 & 1 & 0 & 0 & 0 & 0 \\ 0 & 0 & 1 & 0 & 0 & 0 \end{pmatrix},$$

$$\Pi_R = \begin{pmatrix} 0 & 0 & 0 & 1 & 0 & 0 \\ 0 & 0 & 0 & 0 & 1 & 0 \\ 0 & 0 & 0 & 0 & 0 & 1 \end{pmatrix}. \tag{A.30}$$

It is also convenient to define 6×6 projection matrices by $\Pi_{LL} = \Pi_L^\dagger \Pi_L$, $\Pi_{RR} = \Pi_R^\dagger \Pi_R$. These products of projection matrices appear in some expressions which are quadratic in sfermion fields. As well, we define the projected CKM matrix $V_{LL} = \Pi_L^\dagger V_{CKM} \Pi_L$, which is a 6×6 matrix. Finally, we have the usual chiral projection operators for Dirac spinors, $P_L = \frac{1}{2}(1-\gamma_5)$, $P_R = \frac{1}{2}(1+\gamma_5)$. The interactions of sfermions with fermions and neutralinos are given by

$$\mathscr{L}_{f\tilde{f}\chi^0} = \sum_{f=u,d,e} \bar{f}_i (P_R X'_{fijn} + P_L W'_{fijn}) \chi^0_n \tilde{f}_j + \bar{\nu}_i P_R X'_{\nu ijn} \chi^0_n \tilde{\nu}_j + \text{h.c.} \tag{A.31}$$

The couplings appearing here are

$$X'_{fijn} = X_{fn} (\Pi_L \Theta_f)_{ij} + Z_{fikn} (\Pi_R \Theta_f)_{kj},$$

$$W'_{fijn} = Y_{fn} (\Pi_R \Theta_f)_{ij} + Z_{fikn} (\Pi_L \Theta_f)_{kj}, \tag{A.32}$$

where

$$X_{fn} = -g\sqrt{2}[T_{3f} N^*_{\tilde{W}n} - \tan\theta_W (T_{3f} - e_f) N^*_{\tilde{B}n}], \quad Y_{fn} = g\sqrt{2} \tan\theta_W e_f N^*_{\tilde{B}n},$$

$$Z_{uijn} = -\frac{g}{\sqrt{2} m_W \sin\beta} (M_u)_{ij} N^*_{\tilde{H}_2 n}, \quad Z_{dijn} = -\frac{g}{\sqrt{2} m_W \cos\beta} (M_d)_{ij} N^*_{\tilde{H}_1 n},$$

$$Z_{eijn} = -\frac{g}{\sqrt{2} m_W \cos\beta} (M_e)_{ij} N^*_{\tilde{H}_1 n}. \tag{A.33}$$

Repeated indices are always summed in the expressions we will write. We have indicated elements of the N matrix using the symbols $\tilde{H}_2$ and $\tilde{H}_1$ to denote components in the defining basis of Eq. (A.20). Recall that we have already diagonalized the quark and lepton mass matrices, so that the mass matrices in the definitions of the Z couplings are diagonal; we have chosen to write them as full matrices in order to use the summation convention without confusion.

The interactions of sfermion currents with vector bosons are given by

$$\begin{aligned}
\mathscr{L}_{\tilde{f}\tilde{f}V} = & -\frac{ig}{\cos\theta_W} Z^\mu \sum_{f=u,d,e,\nu} (T_{3f} - e_f \sin^2\theta_W) \tilde{f}_j^* \overleftrightarrow{\partial}_\mu (\Theta_f^\dagger \Pi_{LL} \Theta_f)_{jk} \tilde{f}_k \\
& + \frac{ig}{\cos\theta_W} Z^\mu \sum_{f=u,d,e,\nu} e_f \sin^2\theta_W \tilde{f}_j^* \overleftrightarrow{\partial}_\mu (\Theta_f^\dagger \Pi_{RR} \Theta_f)_{jk} \tilde{f}_k \\
& - ieA^\mu \sum_{f=u,d,e,\nu} e_f \tilde{f}_j^* \overleftrightarrow{\partial}_\mu \tilde{f}_j - ig_s G^{\mu a} \sum_{q=u,d} \tilde{q}_j^* \overleftrightarrow{\partial}_\mu \tilde{q}_j \\
& - \frac{ig}{\sqrt{2}} [W^{\mu+} \tilde{u}_j^* (\Theta_u^\dagger V_{LL}^\dagger \Theta_d)_{jk} \overleftrightarrow{\partial}_\mu \tilde{d}_k + W^{\mu-} \tilde{d}_j^* (\Theta_d^\dagger V_{LL} \Theta_u)_{jk} \overleftrightarrow{\partial}_\mu \tilde{u}_k] \\
& - \frac{ig}{\sqrt{2}} [W^{\mu+} \tilde{\nu}_j^* (\Theta_\nu^\dagger \Pi_L \Theta_e)_{jk} \overleftrightarrow{\partial}_\mu \tilde{e}_k + W^{\mu-} \tilde{e}_j^* (\Theta_e^\dagger \Pi_L^\dagger \Theta_\nu)_{jk} \overleftrightarrow{\partial}_\mu \tilde{\nu}_k] \,. \qquad \text{(A.34)}
\end{aligned}$$

Here G^μ is the gluon vector potential; A^μ, Z^μ, and W^μ are the usual electroweak vector potentials. Note that Θ_ν is a 3×3 matrix since the sneutrino mass matrix is a 3×3 matrix; see Eq. (A.28).

Seagull terms also arise, coupling the sfermion currents to pairs of vector bosons. These interactions are given by

$$\begin{aligned}
\mathscr{L}_{\tilde{f}\tilde{f}VV} = & e^2 A_\mu A^\mu \sum_{f=u,d,e} e_f^2 \tilde{f}_j^* \tilde{f}_j + g_s^2 G_{\mu a} G_b^\mu \sum_{q=u,d} \tilde{q}_j^* T^a T^b \tilde{q}_j \\
& + \frac{g^2}{\cos^2\theta_W} Z_\mu Z^\mu \sum_{f=u,d,e,\nu} (T_{3f} - e_f \sin^2\theta_W)^2 \tilde{f}_j^* (\Theta_f^\dagger \Pi_{LL} \Theta_f)_{jk} \tilde{f}_k \\
& + \frac{2ge}{\cos\theta_W} A_\mu Z^\mu \sum_{f=u,d,e,\nu} e_f (T_{3f} - e_f \sin^2\theta_W) \tilde{f}_j^* (\Theta_f^\dagger \Pi_{LL} \Theta_f)_{jk} \tilde{f}_k \\
& - \frac{2ge}{\cos^2\theta_W} A_\mu Z^\mu \sum_{f=u,d,e} e_f^2 \sin^2\theta_W \tilde{f}_j^* (\Theta_f^\dagger \Pi_{RR} \Theta_f) \tilde{f}_k \\
& + \frac{1}{2} g^2 W_\mu^+ W^{\mu-} [\tilde{u}_j^* (\Theta_u^\dagger \Pi_{LL} \Theta_u)_{jk} \tilde{u}_k + \tilde{d}_j^* (\Theta_d^\dagger \Pi_{LL} \Theta_d)_{jk} \tilde{d}_k] \\
& + \frac{1}{2} g^2 W_\mu^+ W^{\mu-} [\tilde{\nu}_j^* \tilde{\nu}_j + \tilde{e}_j^* (\Theta_e^\dagger \Pi_{LL} \Theta_{\tilde{e}})_{jk} \tilde{e}_k] \\
& + \frac{g}{\sqrt{2}} \frac{1}{3} \left[eA^\mu - \frac{g s_W^2}{\cos\theta_W} Z^\mu \right] [\tilde{u}_j^* (\Theta_u^\dagger V_{LL} \Theta_d)_{jk} \tilde{d}_k W_\mu^+ + \tilde{d}_j^* (\Theta_d^\dagger V_{LL} \Theta_u)_{jk} \tilde{u}_k W_\mu^-] \\
& - \frac{g}{\sqrt{2}} \left[eA^\mu - \frac{g s_W^2}{\cos\theta_W} Z^\mu \right] [\tilde{\nu}_j^* (\Theta_\nu^\dagger \Pi_L \Theta_e)_{jk} \tilde{e}_k W_\mu^+ + \tilde{e}_j^* (\Theta_e^\dagger \Pi_L^\dagger \Theta_\nu)_{jk} \tilde{\nu}_k W_\mu^-] \\
& + g_s^2 G_\mu^a G^{\mu b} \sum_{q,j} \frac{1}{6} G_\mu^a G^{\mu a} \delta^{ab} \tilde{q}_j^* \tilde{q}_j + \frac{1}{2} d^{abc} \tilde{q}_j^* T^c \tilde{q}_j
\end{aligned}$$

$$+\sqrt{2}gg_{\mathrm{s}}G^{\mu a}[W_{\mu}^{+}\tilde{u}_{j}^{*}T^{a}(\Theta_{\mathrm{u}}^{\dagger}V_{\mathrm{LL}}^{\dagger}\Theta_{\mathrm{d}})_{jk}\tilde{d}_{k}W_{\mu}^{+}\tilde{d}_{j}^{*}T^{a}(\Theta_{\tilde{\mathrm{d}}}^{\dagger}V_{\mathrm{LL}}\Theta_{\mathrm{u}})_{jk}\tilde{u}_{k}]$$

$$+2g_{\mathrm{s}}eA_{\mu}G^{\mu a}\sum_{\mathrm{q}=\mathrm{u,d}}e_{\mathrm{q}}\tilde{q}_{j}^{*}T^{a}\tilde{q}_{j}$$

$$+2g_{\mathrm{s}}\frac{g}{\cos\theta_{\mathrm{W}}}Z_{\mu}G^{\mu a}\sum_{\mathrm{q}=\mathrm{u,d}}(T_{3\mathrm{q}}-e_{\mathrm{q}}\sin^{2}\theta_{\mathrm{W}})\,\tilde{q}_{j}^{*}T^{a}(\Theta_{\tilde{\mathrm{q}}}^{\dagger}\Pi_{\mathrm{LL}}\Theta_{\mathrm{q}})_{jk}\,\tilde{q}_{k}\,. \tag{A.35}$$

The above interactions of sfermion currents with gauge bosons illustrate the nature of the FCNCs in the model. FCNCs arise in this case because $\Pi_{\mathrm{LL}}\neq 1$, and the unitary of the matrices Θ_{f} is not enough to insure a cancellation of flavor-off-diagonal parts of the currents, i.e., $\Theta_{\mathrm{f}}^{\dagger}\Pi_{\mathrm{LL}}\Theta_{\mathrm{f}}\neq 1$. Such projections with Π_{LL} arise necessarily because the weak gauge bosons couple only to left-handed fermions, and supersymmetry dictates they must then couple only to the left sfermions.[17]

The interactions $\mathscr{L}_{\mathrm{f}\tilde{\mathrm{f}}\chi^{0}}$ also generically include FCNCs. For example, consider the part of the vertex $\tilde{d}_{i}^{*}$–d_{j}–χ^{0} proportional to the coefficient $X_{\mathrm{d}n}$. This interaction is the superpartner of the neutral current interaction d_i–d_j–Z^{0}. In the latter case there are no flavor-off-diagonal terms because of the GIM cancellation. But the GIM mechanism cannot operate for the mixed quark–squark vertex since the rotations of the squark fields are independent of the rotations of the quark fields. Note that the leptonic supercurrents are not immune from this phenomena; leptonic flavor-changing neutral currents will also arise generically, with manifestations such as $\Gamma(\mu\rightarrow \mathrm{e}\gamma)\neq 0$.

The supersymmetric charged current interactions are given by

$$\mathscr{L}_{\mathrm{f}\tilde{\mathrm{f}}\chi^{\pm}}=-g[\bar{u}_{i}P_{\mathrm{R}}K_{ijn}^{\mathrm{Ld}}\chi_{n}^{+}\tilde{d}_{j}+\bar{d}_{i}P_{\mathrm{R}}K_{ijn}^{\mathrm{Lu}}(\chi_{n}^{+})^{\mathrm{c}}\tilde{u}_{j}]+\frac{g}{\sqrt{2}\cos\beta}[\bar{u}_{i}P_{\mathrm{R}}J_{ijn}^{\mathrm{Rd}}\chi_{n}^{+}\tilde{d}_{j}+\bar{d}_{i}P_{\mathrm{L}}J_{ijn}^{\mathrm{Lu}}(\chi_{n}^{+})^{\mathrm{c}}\tilde{u}_{j}]$$

$$+\frac{g}{\sqrt{2}\sin\beta}[\bar{u}_{i}P_{\mathrm{L}}J_{ijn}^{\mathrm{Ld}}\chi_{n}^{+}\tilde{d}_{j}+\bar{d}_{i}P_{\mathrm{R}}J_{ijn}^{\mathrm{Ru}}(\chi_{n}^{+})^{\mathrm{c}}\tilde{u}_{j}]$$

$$+\frac{g}{\sqrt{2}\cos\beta}[\nu_{i}P_{\mathrm{R}}J_{ijn}^{\mathrm{Re}}\chi_{n}^{+}\tilde{e}_{j}+\tilde{e}_{i}P_{\mathrm{L}}J_{ijn}^{\mathrm{L}\nu}(\chi_{n}^{+})^{\mathrm{c}}\tilde{\nu}_{j}] \tag{A.36}$$

$$+\mathrm{h.c.},$$

where

$$K_{ijn}^{\mathrm{Ld}}=(V_{\mathrm{CKM}}^{\dagger}\Pi_{\mathrm{L}}\Theta_{\mathrm{d}})_{ij}U_{1n},\qquad K_{ijn}^{\mathrm{Lu}}=(V_{\mathrm{CKM}}\Pi_{\mathrm{L}}\Theta_{\mathrm{u}})_{ij}V_{1n}\,, \tag{A.37}$$

$$J_{ijn}^{\mathrm{Rd}}=\frac{1}{m_{\mathrm{W}}}(V_{\mathrm{CKM}}^{\dagger}M_{\mathrm{d}}\Pi_{\mathrm{R}}\Theta_{\mathrm{d}})_{ij}U_{2n},\qquad J_{ijn}^{\mathrm{Lu}}=\frac{1}{m_{\mathrm{W}}}(V_{\mathrm{CKM}}M_{\mathrm{d}}\Pi_{\mathrm{L}}\Theta_{\mathrm{u}})_{ij}U_{2n}\,,$$

$$J_{ijn}^{\mathrm{Ld}}=\frac{1}{m_{\mathrm{W}}}(V_{\mathrm{CKM}}^{\dagger}M_{\mathrm{u}}\Pi_{\mathrm{L}}\Theta_{\mathrm{d}})_{ij}V_{2n},\qquad J_{ijn}^{\mathrm{Ru}}=\frac{1}{m_{\mathrm{W}}}(V_{\mathrm{CKM}}M_{\mathrm{u}}\Pi_{\mathrm{R}}\Theta_{\mathrm{u}})_{ij}V_{2n}\,, \tag{A.38}$$

[17] This incomplete GIM cancelation involving 6×6 matrices will be recognized by those readers familiar with extensions of the standard model involving right-handed neutrinos.

$$J^{\mathrm{Re}}_{ijn} = \frac{1}{m_{\mathrm{W}}}(M_{\mathrm{e}}\Pi_{\mathrm{R}}\Theta_{\mathrm{e}})_{ij}U_{2n}\,,$$

$$J^{\mathrm{Lv}}_{ijn} = \frac{1}{m_{\mathrm{W}}}(M_{\mathrm{e}}\Theta_{\mathrm{v}})_{ij}U_{2n}\,, \tag{A.39}$$

Again, note that the mass matrices in the above are diagonal by our previous rotations of the fields. No projector appears in the equation for J^{Lv} since the sneutrino mixing matrix is only 3×3. Also note the appearance of the charge-conjugation operation,

$$\psi^{\mathrm{c}} = C\bar{\psi}^{\mathrm{T}}\,. \tag{A.40}$$

The interaction of squarks with quarks and gluinos is given by

$$\begin{aligned}\mathscr{L}_{\mathrm{q\tilde{q}\tilde{G}}} = & -\sqrt{2}g_{\mathrm{s}}\sum_{\mathrm{q=u,d}}\bar{\tilde{G}}^{a}[P_{\mathrm{L}}q_i(\Pi_{\mathrm{L}}\Theta^{*})_{ij} - P_{\mathrm{R}}q_i(\Pi_{\mathrm{R}}\Theta^{*})_{ij}](T_a)^{\mathrm{T}}\tilde{q}^{*}_{j}\\ & + [\bar{q}_iP_{\mathrm{R}}(\Pi_{\mathrm{L}}\Theta)_{ij} - \bar{q}_iP_{\mathrm{L}}(\Pi_{\mathrm{R}}\Theta)_{ij}]T^{a}\tilde{G}^{a}\tilde{q}_j\,.\end{aligned} \tag{A.41}$$

In the following expressions involving the Higgs fields, we have written the interactions only for the squarks. In order to obtain the interactions for the sleptons, make the replacements $\mathrm{u}\to\mathrm{v}$, $\mathrm{d}\to\mathrm{e}$. The interactions with the neutral scalars are

$$\begin{aligned}\mathscr{L}_{\tilde{\mathrm{q}}\tilde{\mathrm{q}}\mathrm{H}^{0}} &= g_{\tilde{\mathrm{u}}_i\tilde{\mathrm{u}}_j\mathrm{H}^{0}}H^{0}\tilde{u}^{*}_{i}\tilde{u}_j + g_{\tilde{\mathrm{d}}_i\tilde{\mathrm{d}}_j\mathrm{H}^{0}}H^{0}\tilde{d}^{*}_{i}\tilde{d}_j\,.\\ \mathscr{L}_{\tilde{\mathrm{q}}\tilde{\mathrm{q}}\mathrm{h}^{0}} &= g_{\tilde{\mathrm{u}}_i\tilde{\mathrm{u}}_j\mathrm{h}^{0}}h^{0}\tilde{u}^{*}_{i}\tilde{u}_j + g_{\tilde{\mathrm{d}}_i\tilde{\mathrm{d}}_j\mathrm{h}^{0}}h^{0}\tilde{d}^{*}_{i}d_j\,,\end{aligned} \tag{A.42}$$

where the couplings are

$$\begin{aligned}g_{\tilde{\mathrm{u}}_i\tilde{\mathrm{u}}_jH^{0}} = & -\frac{gm_{\mathrm{Z}}}{\cos\theta_{\mathrm{W}}}\cos(\alpha+\beta)\{(T_{3\mathrm{u}} - e_{\mathrm{u}}\sin^{2}\theta_{\mathrm{W}})(\Theta^{\dagger}_{\mathrm{u}}\Pi_{\mathrm{LL}}\Theta_{\mathrm{u}})_{jk} + e_{\mathrm{u}}\sin^{2}\theta_{\mathrm{W}}(\Theta^{\dagger}_{\mathrm{u}}\Pi_{\mathrm{RR}}\Theta_{\mathrm{u}})_{jk}\}\\ & -\frac{g}{m_{\mathrm{W}}\sin\beta}\sin\alpha(\Theta^{\dagger}_{\mathrm{u}}[\Pi^{\dagger}_{\mathrm{R}}M^{2}_{\mathrm{u}}\Pi_{\mathrm{R}} + \Pi^{\dagger}_{L}M^{2}_{\mathrm{u}}\Pi_{\mathrm{L}}]\Theta_{\mathrm{u}})_{jk}\\ & -\frac{g\cos\alpha}{2m_{\mathrm{W}}\sin\beta}\{(\Theta^{\dagger}_{\mathrm{u}}\Pi^{\dagger}_{\mathrm{R}}M_{\mathrm{u}}[\mu - A_{\mathrm{u}}\tan\alpha]\Pi_{\mathrm{L}}\Theta_{\mathrm{u}})_{jk} + \mathrm{h.c.}\}\,,\end{aligned} \tag{A.43}$$

$$\begin{aligned}g_{\tilde{\mathrm{d}}_i\tilde{\mathrm{d}}_jH^{0}} = & -\frac{gm_{\mathrm{Z}}}{\cos\theta_{\mathrm{W}}}\cos(\alpha+\beta)\{(T_{3\mathrm{d}} - e_{\mathrm{d}}\sin^{2}\theta_{\mathrm{W}})(\Theta^{\dagger}_{\mathrm{d}}\Pi_{\mathrm{LL}}\Theta_{\mathrm{d}})_{jk} + e_{\mathrm{d}}\sin^{2}\theta_{\mathrm{W}}(\Theta^{\dagger}_{\mathrm{d}}\Pi_{\mathrm{RR}}\Theta_{\mathrm{d}})_{jk}\}\\ & -\frac{g}{m_{\mathrm{W}}\cos\beta}\cos\alpha(\Theta^{\dagger}_{\mathrm{d}}[\Pi^{\dagger}_{\mathrm{R}}M^{2}_{\mathrm{d}}\Pi_{\mathrm{R}} + \Pi^{\dagger}_{L}M^{2}_{\mathrm{d}}\Pi_{\mathrm{L}}]\Theta_{\mathrm{d}})_{jk}\\ & -\frac{g\sin\alpha}{2m_{\mathrm{W}}\cos\beta}\{(\Theta^{\dagger}_{\mathrm{d}}\Pi^{\dagger}_{\mathrm{R}}M_{\mathrm{d}}[\mu - A_{\mathrm{d}}\cot\alpha]\Pi_{\mathrm{L}}\Theta_{\mathrm{d}})_{jk} + \mathrm{h.c.}\}\,,\end{aligned} \tag{A.44}$$

$$g_{\tilde{u},\tilde{u},h^0} = \frac{gm_Z}{\cos\theta_W}\sin(\alpha+\beta)\{(T_{3u} - e_u\sin^2\theta_W)(\Theta_u^\dagger \Pi_{LL}\Theta_u)_{jk} + e_u\sin^2\theta_W(\Theta_u^\dagger \Pi_{RR}\Theta_u)_{jk}\}$$

$$- \frac{g}{m_W\sin\beta}\cos\alpha(\Theta_u^\dagger[\Pi_R^\dagger M_u^2 \Pi_R + \Pi_L^\dagger M_u^2 \Pi_L]\Theta_u)_{jk}$$

$$+ \frac{g\sin\alpha}{2m_W\sin\beta}\{(\Theta_u^\dagger \Pi_R^\dagger M_u[\mu + A_u\cot\alpha]\Pi_L\Theta_u)_{jk} + \text{h.c.}\}\,, \tag{A.45}$$

$$g_{\tilde{d},\tilde{d},h^0} = \frac{gm_Z}{\cos\theta_W}\sin(\alpha+\beta)\{(T_{3d} - e_d\sin^2\theta_W)(\Theta_d^\dagger \Pi_{LL}\Theta_d)_{jk} + e_d\sin^2\theta_W(\Theta_d^\dagger \Pi_{RR}\Theta_d)_{jk}\}$$

$$+ \frac{g}{m_W\cos\beta}\sin\alpha(\Theta_d^\dagger[\Pi_R^\dagger M_d^2 \Pi_R + \Pi_L^\dagger M_d^2 \Pi_L]\Theta_d)_{jk}$$

$$- \frac{g\cos\alpha}{2m_W\cos\beta}\{(\Theta_d^\dagger \Pi_R^\dagger M_d[\mu + A_d\tan\alpha]\Pi_L\Theta_d)_{jk} + \text{h.c.}\}\,. \tag{A.46}$$

The interactions with the pseudoscalar are

$$\mathscr{L}_{\tilde{q}\tilde{q}A^0} = \frac{ig}{2m_W}A^0\{\tilde{d}_j^*(\Theta_d^\dagger \Pi_R^\dagger[\mu M_d + M_d A_d\tan\beta]\Pi_L\Theta_d)_{jk}\tilde{d}_k - \text{h.c.}\}$$

$$+ \frac{ig}{2m_W}A^0\{\tilde{u}_j^*(\Theta_u^\dagger \Pi_R^\dagger[\mu M_u + M_u A_u\cot\beta]\Pi_L\Theta_u)_{jk}\tilde{u}_k - \text{h.c.}\}. \tag{A.47}$$

The interactions with the charged scalar are

$$\mathscr{L}_{\tilde{q}\tilde{q}H^\pm} = -\frac{gm_W\sin 2\beta}{\sqrt{2}}H^+\tilde{u}_j^*(\Theta_u^\dagger \Pi_{LL}\Theta_d)_{jk}\tilde{d}_k + \text{h.c.}$$

$$+ \frac{g}{\sqrt{2}m_W}H^+\tilde{u}_j^*(\Theta_u^\dagger \Pi_L^\dagger[M_d^\dagger M_d\tan\beta + M_u^\dagger M_u\cot\beta]\Pi_L\Theta_d)_{jk}\tilde{d}_k + \text{h.c.}$$

$$+ \frac{g}{\sqrt{2}m_W}H^+\tilde{u}_j^*(\Theta_u^\dagger \Pi_R^\dagger[M_d^\dagger M_u\tan\beta + M_u^\dagger M_d\cot\beta]\Pi_R\Theta_d)_{jk}\tilde{d}_k + \text{h.c.}$$

$$+ \frac{g}{\sqrt{2}m_W}H^+\tilde{u}_j^*(\Theta_u^\dagger \Pi_L^\dagger M_d^\dagger[-\mu + A_d\tan\beta]\Pi_R\Theta_d)_{jk}\tilde{d}_k + \text{h.c.}$$

$$+ \frac{g}{\sqrt{2}m_W}H^+\tilde{u}_j^*(\Theta_u^\dagger \Pi_R^\dagger M_u[-\mu + A_u\cot\beta]\Pi_L\Theta_d)_{jk}\tilde{d}_k + \text{h.c.}\,. \tag{A.48}$$

The following quartic sfermion interactions are relatively uninteresting for phenomenological purposes, but we list them as a further illustration of the appearance of squark flavor mixing.

$$\begin{aligned}
\mathscr{L}_{\tilde{f}\tilde{f}\tilde{f}\tilde{f}} = & -\tfrac{1}{6} g_s^2 [(\tilde{u}_j^* \tilde{u}_j)^2 + (\tilde{d}_j^* \tilde{d}_j)^2 + 3(\tilde{d}_j^* \tilde{u}_k)(\tilde{u}_k^* \tilde{d}_j) - (\tilde{u}_j^* \tilde{u}_j)(\tilde{d}_k^* \tilde{d}_k)]^2 \\
& - \tfrac{1}{8} g^2 [\tilde{u}_j^* (\Theta_u^\dagger \Pi_{LL} \Theta_u)_{jk} \tilde{u}_k \to \tilde{d}_j^* (\Theta_d^\dagger \Pi_{LL} \Theta_d)_{jk} \tilde{d}_k - \tilde{\nu}_j^* \tilde{\nu}_j - \tilde{e}_j^* (\Theta_e^\dagger \Pi_{LL} \Theta_e)_{jk} \tilde{e}_k]^2 \\
& - \tfrac{1}{8} g^2 \tan^2 \theta_W [\tfrac{1}{3} \tilde{u}_j^* (\Theta_u^\dagger \Pi_{LL} \Theta_u)_{jk} \tilde{u}_k + \tfrac{1}{3} \tilde{d}_j^* (\Theta_d^\dagger \Pi_{LL} \Theta_d)_{jk} \tilde{d}_k \\
& - \tfrac{4}{3} \tilde{u}_j^* (\Theta_u^\dagger \Pi_{RR} \Theta_u)_{jk} \tilde{u}_k + \tfrac{2}{3} \tilde{d}_j^* (\Theta_d^\dagger \Pi_{RR} \Theta_d)_{jk} \tilde{d}_k \\
& - \tilde{e}_j^* (\Theta_e^\dagger \Pi_{LL} \Theta_e)_{jk} \tilde{e}_k - \tilde{\nu}_j^* \tilde{\nu}_j + 2\tilde{e}_j^* (\Theta_e^\dagger \Pi_{RR} \Theta_e)_{jk} \tilde{e}_k]^2 \\
& - \frac{g^2}{2m_W^2 \sin^2 \beta} \{ |\tilde{u}_j (\Theta_u^T \Pi_L^\dagger M_u \Pi_R \Theta_u)_{jk} \tilde{u}_k|^2 + |\tilde{d}_j (\Theta_d^T \Pi_L^\dagger M_u \Pi_R \Theta_n)_{jk} \tilde{u}_k|^2 \} \\
& - \frac{g^2}{2m_W^2 \cos^2 \beta} \{ |\tilde{u}_j (\Theta_u^T \Pi_L^\dagger M_d \Pi_R \Theta_u)_{jk} \tilde{d}_k|^2 + |\tilde{d}_j (\Theta_d^T \Pi_L^\dagger M_d \Pi_R \Theta_d)_{jk} \tilde{d}_k|^2 \} \\
& - \frac{g^2}{2m_W^2 \cos^2 \beta} \{ |\tilde{\nu}_j (\Theta_\nu^T M_e \Pi_R \Theta_e)_{jk} \tilde{e}_k|^2 + |\tilde{e}_j (\Theta_e^T \Pi_L^\dagger M_e \Pi_R \Theta_e)_{jk} \tilde{e}_k|^2 \} \, . \qquad \text{(A.49)}
\end{aligned}$$

We will not list the quartic squark–squark–Higgs–Higgs vertices, which can be found in Refs. [411, 415]. The introduction of general squark-flavor mixing follows the above form.

Now we list those interactions involving neutralinos, charginos, and gluinos, without sfermions [20, 411, 415].

$$\mathscr{L}_{W \pm \chi \pm \chi^0} = g W_\mu^- \bar{\chi}_n^0 \gamma^\mu [O_{nm}^L P_L + O_{nm}^R P_R] \chi_m^+ + \text{h.c.} \, , \qquad \text{(A.50)}$$

$$\mathscr{L}_{Z\chi\chi} = \frac{g}{\cos \theta_W} Z_\mu [\bar{\chi}_n^+ \gamma^\mu (O_{nm}'^L P_L + O_{nm}'^R P_R) \chi_m^-] + \frac{1}{2} \frac{g}{\cos \theta_W} Z_\mu [\bar{\chi}_n^0 \gamma^\mu (O_{nm}''^L P_L + O_{nm}''^R P_R) \chi_m^0], \qquad \text{(A.51)}$$

$$\mathscr{L}_{\gamma\chi\chi} = -eA_\mu \bar{\chi}_n^+ \gamma^\mu \chi_i^- \qquad \mathscr{L}_{G\tilde{G}\tilde{G}} = \tfrac{1}{2} i g_s f^{abc} \bar{\tilde{G}}^a \gamma_\mu \tilde{G}^b G^{\mu c} \, . \qquad \text{(A.52)}$$

The couplings appearing in the above are given by

$$\begin{aligned}
O_{nm}''^L &= -O_{nm}''^{R*} = \tfrac{1}{2}(-N_{3n} N_{3m}^* + N_{4n} N_{4m}^*) \, , \\
O_{nm}'^L &= -V_{1n} V_{1m}^* - \tfrac{1}{2} V_{2n} V_{2m}^* + \delta_{nm} \sin^2 \theta_W \, , \\
O_{nm}'^R &= -U_{1n}^* U_{1m} - \tfrac{1}{2} U_{2n}^* U_{2m} + \delta_{nm} \sin^2 \theta_W \, , \\
O_{nm}^L &= -(1/\sqrt{2}) N_{4n} V_{2m}^* + N_{2n} V_{1m}^* \, , \qquad O_{nm}^R = (1/\sqrt{2}) N_{3n}^* U_{2m} + N_{2n}^* U_{1m} \, . \qquad \text{(A.53)}
\end{aligned}$$

Again we note that our convention for the diagonalization matrices differs by transposition from the convention of [20]. The indices of N, U, V refer to the defining basis of Eqs. (A.17) and (A.20).

The following Higgs-boson interactions with neutralinos and charginos are fixed by supersymmetry and gauge symmetry, and thus do not display the model dependence typical of Higgs interactions [20, 411, 415].

$$\mathscr{L}_{H^0 \chi^+ \chi^-} = -g \cos \alpha H^0 \bar{\chi}_n^+ [Q_{nm}^* P_L + Q_{mn} P_R] \chi_m^- - g \sin \alpha H^0 \bar{\chi}_n^+ [S_{nm}^* P_L + S_{mn} P_R] \chi_m^- \, , \qquad \text{(A.54)}$$

$$\mathscr{L}_{h^0\chi^+\chi^-} = g\sin\alpha\, h^0\bar{\chi}_n^+[Q_{nm}^* P_L + Q_{mn}P_R]\chi_m^- - g\cos\alpha\, h^0\bar{\chi}_n^+[S_{nm}^* P_L + S_{mn}P_R]\chi_m^- , \tag{A.55}$$

$$\mathscr{L}_{A^0\chi^+\chi^-} = ig\sin\beta\, A^0\bar{\chi}_n^+[Q_{nm}^* P_L - Q_{mn}P_R]\chi_m^- + ig\cos\beta\, A^0\bar{\chi}_n^+[S_{nm}^* P_L - S_{mn}P_R]\chi_m^- , \tag{A.56}$$

$$\mathscr{L}_{H^0\chi^0\chi^0} = \tfrac{1}{2} gH^0\bar{\chi}_n^0[T_{Hnm}^* P_L + T_{Hnm}P_R]\chi_m^0 , \tag{A.57}$$

$$\mathscr{L}_{h^0\chi^0\chi^0} = \tfrac{1}{2} gh^0\bar{\chi}_n^0[T_{hnm}^* P_L + T_{hmn}P_R]\chi_m^0 , \tag{A.58}$$

$$\mathscr{L}_{A^0\chi^0\chi^0} = \tfrac{1}{2} igA^0\bar{\chi}_n^0[- T_{Anm}P_L + T_{Anm}P_R]\chi_m^0 , \tag{A.59}$$

$$\mathscr{L}_{H^\pm\chi^\pm\chi^0} = - gH^-\bar{\chi}_n^0[Q_{nm}'^L P_L + Q_{nm}'^R P_R]\chi_m^+ + \text{h.c.} \tag{A.60}$$

The couplings appearing here are

$$Q_{nm} = \sqrt{\tfrac{1}{2}}\, U_{2n}V_{1m}, \qquad S_{nm} = \sqrt{\tfrac{1}{2}}\, U_{1n}V_{2m} ,$$

$$Q_{nm}'^L = \cos\beta[N_{4n}^* V_{1m}^* + \sqrt{\tfrac{1}{2}}(N_{2n}^* + \tan\theta_W N_{1n}^*)V_{2m}^*] ,$$

$$Q_{nm}'^R = \sin\beta[N_{3n}U_{1m} - \sqrt{\tfrac{1}{2}}(N_{2n} + \tan\theta_W N_{1n})U_{2m}] ,$$

$$T_{Hnm} = - \cos\alpha\, Q_{nm}'' + \sin\alpha\, S_{nm}'' , \quad T_{hnm} = \sin\alpha\, Q_{nm}'' + \cos\alpha\, S_{nm}'' ,$$

$$T_{Anm} = - \sin\beta\, Q_{nm}''^* + \cos\beta\, S_{nm}''^* ,$$

$$Q_{nm}'' = \tfrac{1}{2}N_{3n}(N_{2m} - \tan\theta_W N_{1m}) + (n \leftrightarrow m) ,$$

$$S_{nm}'' = \tfrac{1}{2}N_{4n}(N_{2m} - \tan\theta_W N_{1m}) + (n \leftrightarrow m) . \tag{A.61}$$

The above interaction terms exhaust those involving the superpartner particles. To finish, we give the interactions involving Higgs bosons with gauge bosons [411, 415], which are fixed by gauge symmetry. We also give the familiar Yukawa interactions and gauge interactions of quarks and leptons.

$$\begin{aligned}\mathscr{L}_{HiHjV} = & - \tfrac{1}{2} igW_\mu^+ H^- \overleftrightarrow{\partial}_\mu [H^0\sin(\alpha-\beta) + h^0\cos(\alpha-\beta) + iA^0] + \text{h.c.} \\ & - \frac{ig}{2\cos\theta_W} Z_\mu [iA^0 \overleftrightarrow{\partial}_\mu (H^0\sin(\alpha-\beta) + h^0\cos(\alpha-\beta))] \\ & + \frac{ig}{2\cos\theta_W}(2\sin^2\theta_W - 1)Z_\mu H^- \overleftrightarrow{\partial}_\mu H^+ - ieA_\mu H^- \overleftrightarrow{\partial}_\mu H^+ ,\end{aligned} \tag{A.62}$$

$$\begin{aligned}\mathscr{L}_{HiVV} = & gm_W W_\mu^+ W^{\mu -}[H^0\cos(\alpha-\beta)h^0\sin(\alpha-\beta)] \\ & + \frac{gm_Z}{2\cos\theta_W} Z_\mu Z^\mu [H^0\cos(\beta-\alpha) + h^0\sin(\beta-\alpha)] ,\end{aligned} \tag{A.63}$$

$$\mathscr{L}_{\mathrm{HiHjVV}} = \tfrac{1}{4} g^2 W_\mu^+ W^\mu \; [(H^0)^2 + (h^0)^2 + (A^0)^2 + 2H^+H^-]$$
$$+ \frac{g^2}{8\cos^2\theta_\mathrm{W}} Z_\mu Z^\mu [(H^0)^2 + (h^0)^2 + (A^0)^2 + 2\cos^2 2\theta_\mathrm{W} H^+H^-]$$
$$+ e^2 A_\mu A^\mu H^+H^- + \frac{eg\cos 2\theta_\mathrm{W}}{\cos\theta_\mathrm{W}} A_\mu Z^\mu H^+H^-$$
$$- \frac{1}{2} g \left[eA_\mu - \frac{g\sin^2\theta_\mathrm{W}}{\cos\theta_\mathrm{W}} Z_\mu \right] [W^{\mu+} H^- (H^0 \sin(\beta-\alpha) - h^0\cos(\beta-\alpha) - \mathrm{i}A^0) + \mathrm{h.c.}] \,. \tag{A.64}$$

The familiar Yukawa interactions are given by

$$\mathscr{L}_{\mathrm{Hff}} = -\frac{g}{2m_\mathrm{W}\sin\beta} \bar{u}_i M_{\mathrm{u}ij} [H^0 \sin\alpha + h^0\cos\alpha - \mathrm{i}\gamma_5 A^0 \cos\beta] u_j$$
$$- \frac{g}{2m_\mathrm{W}\cos\beta} \bar{d}_i M_{\mathrm{d}ij} [H^0\cos\alpha - h^0\sin\alpha - \mathrm{i}\gamma_5 A^0\sin\beta] d_j$$
$$+ \frac{g}{\sqrt{2}m_\mathrm{W}} \{H^+ \bar{u}_i (M_\mathrm{d}\tan\beta P_\mathrm{R} + M_\mathrm{u}\cot\beta P_\mathrm{L})_{ij} d_j + \mathrm{h.c.}\} \,. \tag{A.65}$$

Recall that the fermion mass matrices in the above equation are diagonal by our previous rotations of the quark fields. In order to obtain the Yukawa couplings of charged leptons, simply make the replacements d → e and u → ν in the above expression, noting that the neutrino mass matrix vanishes indentically. Therefore, these terms lead to the following Higgs–fermion–fermion Yukawa couplings. For up-type fermions, the couplings are,

$$h_\mathrm{Auu} = -\frac{gm_\mathrm{u}\cot\beta}{2m_\mathrm{W}}, \quad h_\mathrm{Huu} = -\frac{gm_\mathrm{u}\sin\alpha}{2m_\mathrm{W}\sin\beta}, \quad h_\mathrm{huu} = -\frac{gm_\mathrm{u}\cos\alpha}{2m_\mathrm{W}\sin\beta}, \tag{A.66}$$

where m_u is the fermion mass, and for down-type fermions, the couplings are

$$h_\mathrm{Add} = -\frac{gm_\mathrm{d}\tan\beta}{2m_\mathrm{W}}, \quad h_\mathrm{Hdd} = -\frac{gm_\mathrm{d}\cos\alpha}{2m_\mathrm{W}\cos\beta}, \quad h_\mathrm{hdd} = +\frac{gm_\mathrm{d}\sin\alpha}{2m_\mathrm{W}\cos\beta}, \tag{A.67}$$

where m_d is the fermion mass.

The familiar gauge interactions are given by

$$\mathscr{L}_{\mathrm{Vff}} = -\frac{g}{\sqrt{2}} [W_\mu^+ \bar{u}_i (V_\mathrm{CKM}^\dagger)_{ij} \gamma^\mu P_\mathrm{L} d_j + W_\mu^- d_i (V_\mathrm{CKM})_{ij} \gamma^\mu P_\mathrm{L} u_j]$$
$$- \frac{g}{\sqrt{2}} [W_\mu^+ \bar{\nu}_i \gamma^\mu P_\mathrm{L} e_j + W_\mu^- \bar{e}_i \gamma^\mu P_\mathrm{L} \nu_j] - \frac{g}{\cos\theta_\mathrm{W}} Z_\mu \sum_{\mathrm{f=u,d,e}} \bar{f}_i \gamma^\mu$$
$$\times [(\tfrac{1}{2} - e_\mathrm{f}\sin^2\theta_\mathrm{W}) P_\mathrm{L} - e_\mathrm{f}\sin^2\theta_\mathrm{W} P_\mathrm{R}] f_i - eA_\mu \sum_{\mathrm{f=u,d,e}} e_\mathrm{f} \bar{f}_i \gamma^\mu f_i \tag{A.68}$$

The only remaining interactions are the cubic and quartic interactions within the Higgs sector. The cubic terms are [411, 415],

$$\begin{aligned}\mathscr{L}_{H_iH_jH_k} = & -gm_W H^+H^-[H^0\cos(\beta-\alpha)+h^0\sin(\beta-\alpha)] \\ & -\frac{gm_Z}{4\cos\theta_W}[H^0\cos(\beta+\alpha)-h^0\sin(\beta+\alpha)]\times\{\cos 2\alpha[(H^0)^2-(h^0)^2] \\ & -2H^0h^0\sin 2\alpha-[(A^0)^2+2H^+H^-]\cos 2\beta\} \end{aligned} \tag{A.69}$$

The quartic Higgs self-couplings are given in Ref. [19], see also Ref. [416]. We refrain from listing them here because they are rarely needed in tree-level diagrams, and the appropriate rules for diagrams involving loops of physical Higgs bosons must be supplemented by rules for ghost interactions, which we have already decided not to reproduce here.

A.5. SUSY-GUT and supergravity models

Realistic models of spontaneously broken *global* supersymmetry are particularly difficult to construct due to a combination of problems, the most important of these being a general constraint on the mass spectrum of the theory. Such models require the addition of new gauge symmetries and new chiral superfields in order to insure that all the superpartner particles are massive enough to have avoided detection. This basic constraint on spontaneously broken global supersymmetry derives from the mass supertrace relation for supermultiplets [417],

$$\sum_J(-1)^{2J}(2J+1)m_J^2 = 2\,\mathrm{Tr}\;Q_a\langle D^a\rangle\,, \tag{A.70}$$

where $\langle D^\alpha\rangle$ is the vacuum expectation value of the scalar component of some vector superfield, with charge matrix Q_α. This relation says that the average mass of any supermultiplet is proportional to a vacuum expectation value which is spontaneously breaking the supersymmetry. Clearly, due to observational constraints, this average mass cannot be zero, and we must have some $\langle D^a\rangle \neq 0$. However, no scalar component of a gauge superfield of the MSSM can acquire such a vacuum expectation value since the vacuum alignment would then be incorrect. This means that the vacuum would break a gauge symmetry which should not be broken, such as color or electromagnetism. For a discussion, see Ref. [152]. It is also worth pointing out that the trace of the $U(1)_Y$ generator in the standard model is zero, and so the problem cannot be alleviated by the so-called Fayet–Iliopoulos mechanism [199]. In fact, in order to cancel all mixed gauge-gravitational anomalies in any model, all the U(1) generators must be traceless [418], and the supertrace problem is unavoidable.

Spontaneous breakdown of *local* supersymmetry is a different matter. In this case, the mass supertrace relation gains a term proportional to the gravitino mass squared [164].

$$\sum_J(-1)^{2J}(2J+1)m_J^2 = am_{3/2}^2+\cdots \tag{A.71}$$

thus eliminating the main difficulty. However, this result does not come for free. The symmetry-breaking sector must still be separate from the superfields associated to observed particles; this symmetry-breaking sector must be hidden, interacting with the observable sector only via

gravitational interactions. Realistic models can be constructed with the addition of only one chiral superfield. See Ref. [166] for a discussion.

As discussed in Section 4, the low-energy limit of the supergravity theory will be of the form presented above, assuming a spectrum like that of the standard model at low energies. The main tool for model building with supergravity is the renormalization-group-evolution of the various parameters, used to obtain predictions for the low-energy theory. A great deal of effort has gone into such methods and the analysis of the results. We will simply refer to a few papers which we found to be useful in understanding the subject. Many of the earlier analyses have been outdated due to their assumptions about the mass of the top quark. Others made restrictive assumptions on the size of the Yukawa couplings other than that of the top quark [198]. The required renormalization-group equations, in sufficient generality, are conveniently listed in Ref. [194]. In that reference, a systematic exploration of parameter space is undertaken, with two main assumptions. First, it is assumed that the Kähler potential is minimal. This assumption is open to some debate, and we refer to Ref. [194] for a discussion and references. Second, it is assumed that the b-quark and τ-lepton Yukawa couplings unify at high energies. This assumption is interesting because of its predictive power, although it also is open to debate. Because of these assumptions, the analysis becomes quite difficult. The unification boundary conditions at the high-energy scale must be reconciled with the measured data at the weak scale in order to fix the parameters of the theory. The approximate treatment of this situation is the subject of Ref. [194]. A consistent treatment of the sparticle spectrum was given in Ref. [196], with interesting results for the spectrum in a certain class of models.

Rather than embark on such a difficult analysis, we felt that for our purposes it was best to have a scheme which was relatively easy to implement, although less predictive. In particular, our numerical effort was not pointed toward detailed supergravity calculations but toward detailed astrophysical and cosmological calculations. Thus we settled on the following useful scheme; see Ref. [194] for notational and conceptual details. Consider the supergravity model to be specified by the parameters (see below and Section 4 for more discussion)

$$A,\ M,\ m,\ h_{\mathrm{b}}(M_{\mathrm{X}}),\ h_{\mathrm{t}}(M_{\mathrm{X}}),\ h_{\tau}(M_{\mathrm{X}})\ . \tag{A.72}$$

These couplings can be evolved down to the wake scale, at which point we can extract $\tan\beta$ from knowledge of m_{τ} and $\mu(M_{\mathrm{Z}})$, $B(M_{\mathrm{Z}})$ from the condition of electroweak-symmetry breaking. Furthermore, all the other weak scale soft-breaking parameters are as well determined. Then μ and B can be evolved back up to the GUT scale, in order to see what values they must take there.

Compared to the standard procedure, this method loses the minimality assumption for the Kähler potential. The physical importance of this is unclear due to the unclear status of this assumption. Furthermore, one should take more care with thresholds and use a consistent sparticle spectrum [196].

A.6. Parameterizations

A.6.1. Bringing everything together

In Section 4, we briefly discussed the parameterization of the MSSM and of a certain class of SUGRA models. In this section we will explicitly give what we found to be the most useful forms in

which to parameterize these models. Three of these forms are variants of the MSSM, each based on certain physical assumptions, and the fourth is the form we prefer for SUGRA parameterization. These forms standardize certain sets of assumptions which appear throughout the literature. Each of these forms is supported explicitly by the code which we have written to perform the various numerical calculations, and this is the main motivation for collecting these parameterizations here. The differences between the three forms given for the MSSM all pertain to the sfermion sector; it is the proliferation of soft-breaking parameters in the sfermion sector which dominates the parameter count in the MSSM.

A.6.2. Generic MSSM parameterization

The most general minimal supersymmetric standard model (MSSM) contains 63 parameters. This is over and above the usual standard-model parameters, such as the fermion masses and gauge couplings, which are treated separately. Support for these *generic* models is required in order to access all of parameter space in the MSSM. These 63 parameters are: 3 neutralino mass parameters M_i, the parameters μ and $\tan\beta$, the pseudoscalar Higgs mass m_A, 18 parameters in the three independent symmetric 3×3 squark mass-squared parameter matrices $M^2_{\tilde{Q}}$, $M^2_{\tilde{u}}$, $M^2_{\tilde{d}}$, 12 parameters in the two independent symmetric 3×3 slepton mass-squared parameter matrices $M^2_{\tilde{L}}$, $M^2_{\tilde{e}}$, and 27 parameters in the three independent 3×3 soft-breaking A-parameter matrices, A_u, A_d, A_e.

A.6.3. Practical MSSM parameterization

The most useful form of the MSSM, for nonspecialized calculational studies, restricts the sfermion parameter space by assuming that the sfermion mass-squared parameter matrices and the soft-breaking A-parameter matrices are flavor diagonal, but no other restrictions are made. As we have emphasized in our discussion of sfermion mixing, this does not mean that sfermion mixing is absent. Sfermion mixing through the D terms and F terms in the action, as well as through the A parameters in the soft-breaking Lagrangian, will still occur as it must; the restriction only implies the absence of flavor mixing from the matrices $M^2_{\tilde{f}}$ of Eqs. (A.25)–(A.27). This form of the model specification will be occasionally inadequate for studies of flavor-related issues, such as FCNC interactions, but will be otherwise complete. We call this form the *practical* model specification.

Explicitly, the restrictions on the *generic* parameterization which produce the *practical* parameterization are that, in Eqs. (A.25)–(A.27), the mass-squared parameter matrices are diagonal,

$$
\begin{aligned}
&M^2_{\tilde{Q}} = \mathrm{diag}(m^2_{Q11}, m^2_{Q22}, m^2_{Q33}), \quad M^2_{\tilde{u}} = \mathrm{diag}(m^2_{u11}, m^2_{u22}, m^2_{u33}) ,\\
&M^2_{\tilde{d}} = \mathrm{diag}(m^2_{d11}, m^2_{d22}, m^2_{d33}) , \quad M^2_{\tilde{L}} = \mathrm{diag}(m^2_{L11}, m^2_{L22}, m^2_{L33}) ,\\
&M^2_{\tilde{e}} = \mathrm{diag}(m^2_{e11}, m^2_{e22}, m^2_{e33}) , \quad A_u = \mathrm{diag}(A_{u11}, A_{u22}, A_{u33}) ,\\
&A_d = \mathrm{diag}(A_{d11}, A_{d22}, A_{d33}) , \quad A_e = \mathrm{diag}(A_{e11}, A_{e22}, A_{e33}) .
\end{aligned}
\tag{A.73}
$$

Furthermore, in the gaugino sector, a GUT relation of the form

$$
M_1 = \tfrac{5}{3} M_2 \tan^2\theta_W , \tag{A.74}
$$

is often assumed. This assumption is independent of, and is not included in, the definition of a *practical* model parameterization.

A.6.4. Simplified MSSM parameterization

A common MSSM model specification for calculations is that which forces all sfermion mixing to vanish, and further assumes the GUT relation, Eq. (A.74), in the neutralino sector. This leaves only six free parameters, which are the single gaugino mass parameter M_2, the higgsino mass parameter μ, $\tan\beta$, a common squark mass, a common slepton mass, and the mass of the pseudoscalar Higgs boson. The assumption of identical physical masses in the sfermion sector and the attendant assumption of vanishing mixing is unrealistic. However, such a parameter selection may be useful as a simplified "toy" model, and it has been used in much of the literature on supersymmetric dark matter.

The explicit restrictions on the soft-breaking matrices, such as given above, cannot be given in any simple form. This is because the cancelations between D-term mixing and explicit mixing, which are necessary to yield matrices proportional to the identity in Eqs. (A.25)–(A.27), cannot be inverted in any useful way. Support for this *simplified* model specification in our numerical code is provided primarily for comparison with past studies.

A.6.5. SUGRA parameterization

As discussed in Section 4, we parameterize SUGRA models by nine parameters, $\mu(M_X)$, $h_b(M_X)$, $h_\tau(M_X)$, $h_t(M_X)$, α_X, M_X, A, M, and m. No demand for Yukawa-coupling unification is made.

The unification scale and the unified gauge coupling are determined in terms of the measured gauge couplings, leaving seven parameters. Of these, one is fixed by use of a measured weak-scale mass, in particular the mass of the Z is useful. See the discussion in the subsection above. This leaves the six free parameters $h_b(M_X)$, $h_\tau(M_X)$, $h_t(M_X)$, A, M, and m. These six parameters are used to specify a supergravity-model input set for our numerical calculations.

Each model gives rise to a unique set of *generic* parameters as a low-energy effective description of the theory. This low-energy description is fixed by the renormalization-group analysis, and all calculations proceed as if for a *generic* model from that point.

Appendix B. User's guide for Neutdriver

Most of the numerical results in this paper were calculated using a specialized code written by the authors for this task. This code is available in the form of a program, written in ANSI C, called `Neutdriver`, which is available for general use. It can be obtained by contacting one of the authors. In this section we describe some of the features of this code, pertaining to the types of supersymmetric model parameterizations which were discussed in Section A.5.

Input of model parameters can be given in one of four forms, each corresponding to one of the cases described above, i.e., *generic* models, *practical* models, *simplified* models, or SUGRA models. The input files provide easy access to these parameters. Furthermore, the parameterizations are automatically consistent, in the sense that it is not possible to assign conflicting values to any input parameters; each represents a truly independent quantity.

The *generic* and *practical* model calculations are relatively straightforward applications of the results presented throughout this review. The *simplified* model calculations are handled in a slightly different manner since that parameterization is essentially unphysical. The SUGRA model

calculations first solve the renormalization group evolution as discussed above in order to obtain a *generic* model representation, for which calculations then proceed as usual. Our treatment of the SUGRA models is somewhat naive, as discussed above, and for those users interested in supergravity studies, it is recommended that they produce appropriate *generic* model parameterizations from their own supergravity code. Such *generic* parameterizations are then easily fed into Neutdriver.

The program Neutdriver is designed to allow access to all physics parameters of the MSSM through easily maintained input files. The code is modular and portable and has been successfully compiled and run on several platforms. Output is file-based, with configurable format, and is easily manipulated by standard tools such as awk in the Unix environment. There is also a set of supermongo macros available for reading, cutting and plotting the program output. For a detailed description of the program Neutdriver, please refer to its documentation.

References

[1] Particle Data Group, Phys. Rev. D 50 (1994) 1173.
[2] G. 't Hooft, in: Recent Developments in Gauge Theories, Proc. NATO Advanced Summer Institute, Cargese, 1979, eds. G. 't Hooft et al. (Plenum, New York, 1980) p. 135.
[3] S. Dimopoulos, S.A. Raby and F. Wilczek, Phys. Today 44 (1991) 25.
[4] U. Amaldi, W. de Boer and H. Fürstenau, Phys. Lett. B 260 (1991) 447.
[5] C.S. Li, R.J. Oakes and T.C. Yuan, Phys. Rev. D 43 (1991) 3759; G.L. Kane, G.A. Ladinsky and T.C. Yuan, Phys. Rev. D 45 (1992) 124.
[6] M. Kamionkowski and D.N. Spergel, Astrophys. J. 432 (1994) 7.
[7] K.A. Olive, G. Steigman, D.N. Schramm, T.P. Walker and H. Kang, Astrophys. J. 376 (1991) 51.
[8] S. Tremaine and J.E. Gunn, Phys. Rev. Lett. 42 (1979) 407.
[9] M.W. Goodman and E. Witten, Phys. Rev. D 31 (1986) 3059.
[10] J. Wasserman, Phys. Rev. D 33 (1986) 2071.
[11] J. Silk, K. Olive and M. Srednicki, Phys. Rev. Lett. 55 (1985) 257.
[12] L.M. Krauss, K. Freese, D.N. Spergel and W.H. Press, Astrophys. J. 299 (1985) 1001.
[13] K. Freese, Phys. Lett. B 167 (1986) 295.
[14] L.M. Krauss, M. Srednicki and F. Wilczek, Phys. Rev. D 33 (1986) 2079.
[15] T. Gaisser, G. Steigman and S. Tilav, Phys. Rev. D 34, (1986) 2206.
[16] J. Wess and J. Bagger, Supersymmetry and Supergravity, 2nd Ed. (Princeton University Press, Princeton, 1992).
[17] P. West, Introduction to Supersymmetry and Supergravity (World Scientific, Singapore, 1986).
[18] R.N. Mohapatra, Unification and Supersymmetry (Springer, New York, 1986).
[19] J.F. Gunion, H.E. Haber, G. Kane and S. Dawson, The Higgs Hunter's Guide (Addison-Wesley, Redwood City, 1990).
[20] H.E. Haber and G.L. Kane, Phys. Rep. 117 (1985) 75.
[21] J.R. Primack, B. Sadoulet and D. Seckel, Annu. Rev. Nucl. Part. Sci. B 38 (1988) 751.
[22] J. Rich, D. Lloyd and M. Spiro, Phys. Rep. 151 (1987) 239.
[23] J. Engel, S. Pittel and P.Vogel, Int. J. Mod. Phys. E 1 (1992) 1.
[24] P.F. Smith and J.D. Lewin, Phys. Rep. 187 (1990) 203.
[25] Proc. of the 5th Int. Workshop on Low Temperature Detectors, Berkeley, California, 29 July–3 August 1993, in J. Low Temp. Phys. 93 (1993) 185.
[26] For reviews of current and future energetic-neutrino detectors, see, e.g., High Energy Neutrino Astrophysics, eds. V.J. Stenger, J.G. Learned, S. Pakvasa and X. Tata (World Scientific, Singapore, 1992); Neutrino 94, Proc. 16th International Conference on Neutrino Physics and Astrophysics, Eilat, Israel, 29 May–3 June 1994, eds. A. Dar, G. Eilam and M. Gronau (North-Holland, Amsterdam, 1995) [Nuclear Physics (Proc. Suppl.) B38]; T.K. Gaisser, F. Halzen and T. Stanev, Phys. Rep. 258 (1995) 174.

[27] K.M. Ashman, Proc. Astron. Soc. Pac. 104 (1992) 1109.
[28] V. Trimble, Annu. Rev. Astron. Astrophys. 25 (1989) 425.
[29] M. Fich and S. Tremaine, Annu. Rev. Astron. Astrophys. 29 (1991) 409.
[30] J. Binney and S. Tremaine, Galactic Dynamics (Princeton University Press, Princeton, 1987).
[31] E.W. Kolb and M.S. Turner, The Early Universe (Addison-Wesley, Redwood City, 1989).
[32] P.J.E. Peebles, Principles of Physical Cosmology (Princeton University Press, Princeton, 1993).
[33] F. Zwicky, Helv. Phys. Acta 6 (1933) 110.
[34] M. Davis and J. Huchra, Astrophys. J. 254, (1982) 437.
[35] R.D. Kirshner et al., Astron. J. 88 (1983) 1285.
[36] K.G. Begeman, A.H. Broeils and R.H. Sanders, Mon. Not. R. Astron. Soc. 249 (1991) 523.
[37] D. Zaritsky, Publ. Astron. Soc. Pac. 394 (1992) 1.
[38] J.A. Tyson and P. Fischer, Astrophys. J. Lett. 446 (1995) L55.
[39] U.G. Briel, J.P. Henry and H. Bohringer, Astron. Astrophys. 259 (1992) L31.
[40] S.D.M. White et al., Nature 366, (1993) 429.
[41] M.S. Smith, L.H. Kawano and R.A. Malaney, Astrophys. J. Suppl. Ser. 85 (1993) 219.
[42] T.P. Walker et al., Astrophys. J 376 (1991) 51.
[43] J.R. Primack, SCIPP-95-10, astro-ph/9503020, to appear in: Proc. 1994 Summer Study on High Energy Physics: Particle and Nuclear Astrophysics and Cosmology in the Next Millenium, Snowmass, CO, 29 June–14 July 1994.
[44] G. Steigman and J.E. Felten, OSU-TA-24/94, to appear in: Proc. St. Petersburg Gamow Seminar, St. Petersburg, Russia, 12–14 September 1994, eds. A.M. Bykov and A. Chevalier, Sp. Sci. Rev., in press (Kluwer, Dordrecht).
[45] A. Dekel, Annu. Rev. Astron. Astrophys. 32 (1994) 371.
[46] M.A. Strauss and J.A. Willick, Phys. Rep. 261 (1995) 271.
[47] A. Yahil, T. Walker and M. Rowan-Robinson, Astrophys. J. Lett. 301 (1986) L1.
[48] E. Bertschinger and A. Dekel, Astrophys. J. Lett. 336, (1989) L5.
[49] M.J. Hudson et al., Mon. Not. R. Astron. Soc. 274 (1995) 305.
[50] M. Davis and A. Nusser, in: Dark Matter, Proc. 5th Annual October Astrophysics Conference in Maryland: International Conference on Dark Matter, College Park, MD, 10–12 Oct 1994, eds. S.S. Holt and C.L. Bennett (American Institute of Physics, New York, 1995).
[51] M. Kamionkowski, B. Ratra, D.N. Spergel and N. Sugiyama, Astrophys. J. Lett. 434 (1994) L1).
[52] W. Hu, E.F. Bunn and N. Sugiyama, Astrophys. J. Lett. 446 (1995) L59.
[53] M. Kamionkowski, D.N. Spergel and N. Sugiyama, Astrophys. J. Lett. 426 (1994) L57; G. Jungman, M. Kamionkowski, A. Kosowsky and D.N. Spergel, CU-TP-703, astroph/9507080, submitted to Phys. Rev. Lett.
[54] A. Renzini, Ann. N.Y. Acad Sci. 688 (1994) 124.
[55] Jacoby et al., Publ. Astron. Soc. Pac. 104 (1992) 599.
[56] A.G. Riess, W.H. Press and R.P. Kirshner, Astrophys. J. Lett. 438 (1995) L17; B.P. Schmidt et al., Astrophys. J. 432 (1994) 42.
[57] W. Freedman et al., Nature 371 (1994) 757.
[58] J.H. Applegate, C.J. Hogan and R.J. Scherrer, Phys. Rev. D 35 (1987) 1151.
[59] F. Wilezek, Int. J. Mod. Phys. A 7 (1992) 3911; M. Fukugita and C.J. Hogan, Nature 354 (1992) 17.
[60] K. Jedamzik, G.M. Fuller and G.J. Mathews, Astrophys. J. 423 (1994) 50; R.A. Malaney and G.J. Mathews, Phys. Rep. 229 (1993) 145.
[61] A. Songalia et al., Nature 368 (1994) 599.
[62] D. Tytler and X. Fan, Bull, Am. Astron. Soc. 26 (1994) 1424.
[63] C. Alcock et al. (MACHO Collaboration), Nature 365 (1993) 621.
[64] C. Alcock et al. (MACHO Collaboration), Phys. Rev. Lett. 74 (1995) 2867.
[65] E. Aubourg et al. (MACHO Collaboration), Nature 365 (1993) 623.
[66] A. Udalski et al. (OGLE Collaboration), Acta Astron. 44 (1994) 165.
[67] C. Kochanek, astro-ph/9505068.
[68] D. Lynden-Bell, Mon. Not. R. Astron. Soc. 136 (1967) 101.
[69] D. Zaritsky et al., Astrophys. J. 345 (1989) 759.

[70] L. Blitz, in: Dark Matter, Proc. 5th Annual October Astrophysics Conference in Maryland: International Conference on Dark Matter, College Park, MD, 10–12 Oct 1994, eds. S.S. Holt and C.L. Bennett (American Institute of Physics, New York, 1995).
[71] S.R. Kulkarni, L. Blitz and C. Heiles, Astrophys. J. Lett. 259 (1982) L63.
[72] F.J. Kerr and D. Lynden-Bell, Mon. Not. R. Astron. Soc. 221 (1986) 1023.
[73] M.R. Merrifield, Astron. J. 103 (1992) 1552.
[74] M. Fich, L. Blitz and A.A. Stark, Astrophys. J. 342 (1989) 272.
[75] N.W. Evans and J. Jijina, Mon. Not. R. Astron. Soc. 267 (1994) L21; N.W. Evans, Mon. Not. R. Astron. Soc. 267 (1994) 333; ibid. 260 (1993) 191.
[76] C. Alcock et al. (MACHO Collaboration), Astrophys. J. 449 (1995) 28.
[77] E. Gates and M.S. Turner, Phys. Rev. Lett. 72 (1994) 2520.
[78] E.I. Gates, G. Gyuk and M.S. Turner, Phys. Rev. Lett. 74 (1995) 3724.
[79] EROS Collaboration: M. Moniez and C. Magneville, talks given at the Microlensing Workshop, Livermore, CA, 13–15 January 1995.
[80] MACHO Collaboration; M. Lehner, W. Sutherland, D. Bennett and K. Griest, talks given at the Microlensing Workshop, Livermore, CA, 13–15 January 1995.
[81] E.I. Gates, G. Gyuk and M.S. Turner, Astrophys. J. Lett. 449 (1995) L123.
[82] J.N. Bahcall, M. Schmidt and R.M. Soneira, Astrophys. J. 265 (1983) 730.
[83] J.A.R. Caldwell and J.P. Ostriker, Astrophys. J. 251 (1981) 61.
[84] M.S. Turner, Phys. Rev. D 33 (1986) 889.
[85] R.A. Flores, Phys. Lett. B 215, (1988) 73.
[86] K. Griest, unpublished; early version: talk at Snowmass 94.
[87] Ref. [30], p. 226.
[88] J.H. Oort, Bull. Astron. Inst. Neth. 6 (1960) 249; J.N. Bahcall, Astrophys. J. 287 (1984) 926; K. Kuijken and G. Gilmore, Astrophys. J. Lett. 367 (1991) L9; J.N. Bahcall, C. Flynn and A. Gould, Astrophys. J. 389 (1992) 234.
[89] H.S. Zhao, D.N. Spergel and R.M. Rich, Astrophys. J. Lett. 108 (1995) 2154.
[90] K. Kuijken and G. Gilmore, Astrophys. J. Lett. 367 (1991) L9.
[91] C. Flynn and B. Fuchs, Mon. Not. R. Astron. Soc. 270 (1995) 471.
[92] J.N. Bahcall, C. Flynn and A. Gould, Astrophys. J. 389 (1992) 234.
[93] D.N. Spergel and D.O. Richstone, in: Dark Matter, Proc. XXII Rencontres de Moriond, Les Arcs, Savoie, France, 8–15 March 1988, eds. J. Audouze and J. Tran Thanh Van (Editions Frontiers, Gif-sur-Yvette, 1988).
[94] H. Rix, astro-ph/9501068, talk given at IAU Symposium 169: Unsolved Problems of the Milky Way, The Hague, August, 1994.
[95] G. Blumenthal, R. Flores, J. Primack and M.J. Rees, Astrophys. J. 301 (1986) 27; B. Ryden and J.E. Gunn, in: Dark Matter in the Universe, eds. G.R. Knapp and J. Kormendy (Reidel, Dordrecht, 1987).
[96] J.D. Anderson, E.L. Lau, A.H. Taylor, D.A. Dicus, D.C. Teplitz and V.L. Teplitz, DOE-ER40200-143 (1988).
[97] B. Paczyński, Astrophys. J. 304 (1986) 1.
[98] B.J. Carr, Comm. Astrophys. 14 (1990) 257.
[99] B.J. Carr, Annu. Rev. Astron. Astrophys. 32 (1994) 531.
[100] J. Shaham and A. Dekel, Astron. Astrophys. 74 (1979) 186.
[101] K. Griest Astrophys. J. 366 (1991) 412.
[102] R.J. Nemiroff, Astron. Astrophys. 247 (1991) 73; A. De Rujula, P. Jetzer and E. Masso, Astron. Astrophys. 254 (1992) 99.
[103] D.J. Hegyi and K.A. Olive, Phys. Lett. B 126 (1983) 28.
[104] O.E. Gerhard and J. Silk, Nature, submitted; F. De Paolis, P. Jetzer and M. Roncadelli, Phys. Rev. Lett. 74 (1995) 14.
[105] D. Pfenniger, F. Combes and L. Martinet, Astron. Astrophys. 285 (1994) 79.
[106] R.N. Henriksen and L.M. Widrow, astro-ph/9402002.
[107] S.D.M. White, C.S. Frenk and M. Davis, Astrophys. J. 274 (1983) L1-5.
[108] O.E. Gerhard and D.N. Spergel, Astrophys. J. Lett. 389 (1992) L9.
[109] J.A. Holtzman, Astrophys. J. Suppl. 71 (1989) 1; M. Davis, F.J. Summers and D. Schlegel, Nature 359 (1992) 393; J.R. Primack and J.A. Holtzman, Astrophys. J. 405 (1993) 428; A. Klypin et al., Astrophys. J. 416 (1993) 1.

[110] M.S. Turner, Phys. Rep. 197 (1990) 67.
[111] G. Raffelt, Phys. Rep. 198 (1990) 1.
[112] C. Hagmann et al., astro-ph/9508013, to appear in: Perspectives in Particle Physics, Atomic Physics and Gravitation, Proc. 30th Rencontres de Moriond, Villars-sur-Ollon, Switzerland, 21–28 January 1995; S. Matsuki, ibid; K. van Bibber et al., UCRL-JC-118357 (1988).
[113] J.E. Kim, Phys. Rep. 150 (1987) 1.
[114] A. Jaffe and J.A. Frieman, Phys. Rev. D 45 (1992) 2674.
[115] K.G. Begeman, A.H. Broeils and R.H. Sanders, Mon. Not. R. Astron. Soc. 249 (1991) 532.
[116] P. Mannheim, Astrophys. J. 419 (1993) 150.
[117] Ya.B. Zel'dovich, Zh. Eksp. Teor. Fiz. 48, (1965) 986.
[118] Ya.B. Zel'dovich, L.B. Okun and S.B. Pikelner, Usp. Fiz. Nauk. 84 (1965) 113.
[119] H.-Y. Chiu, Phys. Rev. Lett. 17 (1966) 712.
[120] B.W. Lee and S. Weinberg, Phys. Rev. Lett. 39 (1977) 165.
[121] P. Hut, Phys. Lett. B 69 (1977) 85.
[122] M.I. Vysotskii A.D. Dolgov and Ya. B. Zel'dovich, JETP Lett. 26 (1970) 188.
[123] J.E. Gunn et al., Astrophys. J. 223 (1978) 1015.
[124] G. Steigman et al., Astron. J. 83 (1978) 1050.
[125] J. Ellis, J.S. Hagelin, D.V. Nanopoulos, K.A. Olive and M. Srednicki, Nucl. Phys. B 238 (1984) 453.
[126] J. Bernstein, L. Brown and G. Feinberg, Phys. Rev. D 32 (1985) 3261.
[127] R. Scherrer and M.S. Turner, Phys. Rev. D 33 (1986) 1585; ibid. D 34 (1986) 3263(E).
[128] K. Griest and D. Seckel, Nucl. Phys. B 283 (1987) 681.
[129] M. Srednicki, R. Watkins and K.A. Olive, Nucl. Phys. B 310 (1988) 693.
[130] K. Griest, Phys. Rev. Lett. 61 (1988) 666.
[131] K. Griest, Phys. Rev. D 38 (1988) 2357; FERMILAB-Pub-89/139-A (E).
[132] K.A. Olive and M. Srednicki, Phys. Lett. B 230 (1989) 78.
[133] K.A. Olive and M. Srednicki, Nucl. Phys. B 355, (1991) 208.
[134] K. Griest, M. Kamionkowski and M.S. Turner, Phys. Rev. D 41 (1990) 3565.
[135] A. Bottino et al., Astropart. Phys. 2 (1994) 67.
[136] H. Goldberg, Phys. Rev. Lett. 50 (1983) 1419.
[137] K. Griest and D. Seckel, Phys. Rev. D 43 (1991) 3191.
[138] P. Gondolo and G. Gelmini, Nucl. Phys. B 360 (1991) 145.
[139] P. Nath and R. Arnowitt, Phys. Rev. Lett. 70 (1993) 3696; P. Nath and R. Arnowitt, Phys. Lett. B 299, (1993) 58.
[140] S. Mizuta and M. Yamaguchi, Phys. Lett. B 298, (1993) 120.
[141] J. March-Russell, Phys. Lett. B 296 (1992) 364; M. Dine, R.G. Leigh, P. Huet, A. Linde and D. Linde, Phys. Rev. D 46 (1992) 550; M.E. Carrington, Phys. Rev. D 45 (1992) 2933.
[142] G.F. Giudice, Phys. Rev. D 45 (1992) 3177.
[143] J.R. Espinosa, M. Quirós and F. Zwirner, Phys. Lett. B 307 (1993) 106.
[144] L. Knox and M.S. Turner, Phys. Rev. Lett. 70 (1993) 371.
[145] J.D. Barrow, Nucl. Phys. B 208 (1982) 501.
[146] M. Kamionkowski and M.S. Turner, Phys. Rev. D 42 (1990) 3310.
[147] K.A. Olive and J. Silk, Phys. Rev. Lett. 55 (1985) 2362; J. Ellis, D.V. Nanopoulos and S. Sarkar, Nucl. Phys. B 259 (1985) 175; J. Ellis, J.E. Kim and D.V. Nanopoulos, Phys. Lett. B 145 (1984) 181.
[148] K. Rajagopal, M.S. Turner and F. Wilczek, Nucl. Phys. B 358 (1991) 447.
[149] D.E. Winget et al., Astrophys. J. 315 (1987) L77.
[150] J.G. Bartlett, A. Blanchard, J. Silk and M.S. Turner, Science 267 (1995) 980.
[151] K. Griest and M. Kamionkowski, Phys. Rev. Lett. 64 (1990) 615.
[152] H.P. Nilles, Phys. Rep. 110 (1984) 1.
[153] M. Sohnius, Phys. Rep. 128 (1985) 39.
[154] E. Farhi and L. Susskind, Phys. Rep. 74 (1981) 277.
[155] S. Coleman and J. Mandula, Phys. Rev. 159 (1967) 1251.
[156] R. Haag, J. Lopuszanski and M. Sohnius, Nucl. Phys. B 88 (1975) 257.

[157] P.G.O. Freund, Supersymmetry (Cambridge University Press, Cambridge, 1986).
[158] P. van Nieuwenhuizen, Phys. Rep. 68 (1981) 189.
[159] P. van Nieuwenhuizen and J. Vermaseren, Phys. Lett. B 65 (1976) 263.
[160] N. Marcus and A. Sagnotti, Nucl. Phys. B 256 (1985) 77; M. Goroff and A. Sagnotti, Phys. Lett. B 160 (1985) 81.
[161] S. Deser and B. Zumino, Phys. Rev. Lett. 38 (1977) 1433.
[162] E. Cremmer, B. Julia, J. Scherk, P. van Nieuwenhuizen, S. Ferrara and L. Girardello, Phys. Lett. B 79 (1978) 231.
[163] E. Cremmer, B. Julia, J. Scherk, S. Ferrara, L. Girardello and P. van Nieuwenhuizen, Nucl. Phys. B 147 (1979) 105.
[164] E. Cremmer, S. Ferrara, L. Girardello and A. van Proeyen, Nucl. Phys. B 212 (1983) 413.
[165] A.H. Chamseddine, R. Arnowitt and P. Nath, Phys. Rev. Lett. 49 (1982) 970.
[166] H.P. Nilles, Phys. Lett. B 115, (1982) 193.
[167] L. Girardello and M.T. Grisaru, Nucl. Phys. B 194 (1982) 65.
[168] F. Zwirner, Phys. Lett. B 132 (1983) 103; R. Barbieri and A. Masiero, Nucl. Phys. B 267 (1986) 679; G.G. Ross and J.W.F. Valle, Phys. Lett. B 151 (1985) 375; J. Ellis et al., Phys. Lett. B 150 (1985) 142; S. Dawson, Nucl. Phys. B 261 (1985) 297; V. Barger, G.F. Giudice and T. Han, Phys. Rev. D 40 (1989) 2987; D. Comelli, A. Masiero, M. Pietroni and A. Riotto, Phys. Lett. B 324 (1994) 397.
[169] R. Kuchimanchi and R.N. Mohapatra, Phys. Rev. D 48 (1993) 4352; J.C. Romao, C.A. Santos and J.W.F. Valle, Phys. Lett. B 288 (1992) 311; S. Martin, Phys. Rev. D 46 (1992) 2769.
[170] B. de Wit and P.Z. Freedman, Phys. Rev. D 12 (1975) 2286.
[171] M. Kobayashi and M. Maskawa, Prog. Theor. Phys. 49 (1973) 652; N. Cabibbo, Phys. Rev. Lett. 10 (1963) 531.
[172] S. Weinberg, Phys. Rev. Lett. 19 (1967) 1264; A. Salam and J.C. Ward, Phys. Lett. 13 (1964) 168; S. Glashow, Nucl. Phys. 22 (1961) 579.
[173] H. Georgi, Weak Interactions and Modern Particle Theory (Benjamin Cummings, Menlo Park, 1984).
[174] S. Wolfram, Phys. Lett. B 82 (1979) 65.
[175] P.F. Smith and J.R.J. Bennett, Nucl. Phys. B 149 (1979) 525.
[176] T. Falk, K.A. Olive and M. Srednicki, Phys. Lett. B 339 (1994) 248.
[177] P. Langacker and M. Luo, Phys. Rev. D 44 (1991) 817.
[178] J. Ellis, S. Kelley and D.V. Nanopoulos, Phys. Lett. B 260 (1991) 131.
[179] S. Dimopoulos and H. Georgi, Nucl. Phys. B 193 (1981) 150.
[180] M.B. Einhorn and D.R.T. Jones, Nucl. Phys. B 196 (1982) 475.
[181] J. Ellis, D.V. Nanopoulos and S. Rudaz, Nucl. Phys. B 202 (1982) 43; P. Nath, R. Arnowitt and A.H. Chamseddine, Phys. Rev D 32 (1985) 2348; J. Hisano, H. Murayama and T. Yanagida, Nucl. Phys B 402 (1993) 46.
[182] J.M. Frere, D.R.T. Jones and S. Raby, Nucl. Phys. B 222 (1983) 11.
[183] J. Polchinski and L. Susskind, Phys. Rev. D 26 (1982) 3661.
[184] H.P. Nilles, M. Srednicki and D. Wyler, Phys. Lett. B 120 (1983) 346.
[185] A.B. Lahanas, Phys. Lett. B 124 (1983) 341.
[186] L. Alvarez-Gaume, J. Polchinski and M.B. Wise, Nucl. Phys. B 221 (1983) 495.
[187] J. Bagger and E. Poppitz, Phys. Rev. Lett. 71 (1993) 2380.
[188] L.E. Ibanez, Phys. Lett. B 118 (1982) 73.
[189] L.E. Ibanez, Nucl. Phys. B 218 (1983) 514.
[190] J. Ellis, D.V. Nanopoulos and K. Tamvakis, Phys. Lett. B 121 (1983).
[191] H.P. Nilles, Nucl. Phys. B 217 (1983) 366.
[192] H. Georgi and S. Glashow, Phys. Rev. Lett. 3 (1974) 438.
[193] L. Hall, J. Lykken and S. Weinberg, Phys. Rev. D 27 (1983) 2359.
[194] M. Drees and M. Nojiri, Nucl. Phys. B 369 (1992) 54.
[195] P. Langacker and N. Polonsky, Phys. Rev. D 49 (1994) 1454; V. Barger, M. Berger and P. Ohmann, Phys. Rev. D 47 (1993) 1093; M. Carena, S. Pokorski and C. Wagner, Nucl. Phys. B 406 (1993) 59; B. Ananthanarayan, G. Lazarides and Q. Shafi, Phys. Rev. D 44 (1991) 1613; A. Buras, J. Ellis, M. Gaillard and D. Nanopoulos, Nucl. Phys. B 135 (1978) 66; M. Chanowitz, J. Ellis and M. Gaillard, Nucl. Phys. B 128 (1977) 506.
[196] G.G. Ross and R. Roberts, Nucl. Phys. B 377 (1992) 571.
[197] K. Babu and R. Mohapatra, Phys. Rev. Lett. 70 (1993) 2845.
[198] L.E. Ibanez and C. Lopez, Nucl. Phys. B 233 (1984) 511.

[199] H. Haber, in: Recent Directions in Particle Theory, Lectures at TASI-92, eds. J. Harvey and J. Polchinski (World Scientific, Singapore, 1993).
[200] H. Haber, in: Testing the Standard Model, Lectures at TASI-90, eds. M. Cvetic and P. Langacker (World Scientific, Singapore, 1991).
[201] M. Berger, Phys. Rev. D 41 (1990) 225.
[202] H.E. Haber and R. Hempfling, Phys. Rev. Lett. 66 (1991) 1815.
[203] P.H. Chankowski, S. Pokorski and J. Rosiek, Phys. Lett. B 274 (1992) 191.
[204] P.H. Chankowski, S. Pokorski and J. Rosiek, Phys. Lett. B 281 (1992) 100.
[205] A. Brignole, Phys. Lett. B 277 (1992) 313.
[206] J. Ellis, G. Ridolfi and F. Zwirner, Phys. Lett. B 257 (1991) 83.
[207] Y. Okada, M. Yamaguchi and T. Yanagida, Prog. Theor. Phys. 85 (1991) 1.
[208] Y. Okada, M. Yamaguchi and T. Yanagida, Phys. Lett. B 262 (1991) 54.
[209] R. Barbieri, M. Frigeni and F. Caravaglios, Phys. Lett. B 258 (1991) 167.
[210] R. Barbieri and M. Frigeni, Phys. Lett. B 258 (1991) 395.
[211] J.R. Espinosa and M. Quiros, Phys. Lett. B 267 (1991) 27.
[212] D. Buskulic et al. (ALEPH Collaboration), Phys. Lett. B 313 (1993) 312.
[213] D. DeCamp et al. (ALEPH Collaboration), Phys. Lett. B 265 (1991) 475.
[214] M. Akrawy et al. (OPAL Collaboration), Z. Phys. C 49 (1991) 1.
[215] B. Adeva et al. (L3 Collaboration), Phys. Lett. B 251 (1990) 311.
[216] P. Abreu et al. (DELPHI Collaboration), Nucl. Phys. B 367 (1991) 511.
[217] C. Dionisi et al., Proc. ECFA Workshop: LEP 200, eds. A. Bohm and W. Hoogland (CERN, Geneva, 1987).
[218] M. Chen et al., Phys. Rep. 159 (1988) 201.
[219] A. Bartl, W. Majerotto and N. Oshimo, Phys. Lett. B 216 (1989) 233.
[220] D. DeCamp et al. (ALEPH Collaboration), Phys. Rep. 216 (1992) 253.
[221] J.L. Feng and M.J. Strassler, Phys. Rev. D 51 (1995) 4661.
[222] L. Roszkowski, Phys. Lett. B 278 (1992) 147.
[223] K. Hidaka, Phys. Rev. D44 (1991) 927.
[224] F. Abe et al. (CDF Collaboration), Phys. Rev. Lett. 69 (1992) 3439.
[225] H. Baer, C. Kao and X. Tata, Phys. Rev. D 48 (1993) 5175.
[226] H. Baer, C. Kao and X. Tata, Phys. Rev. D 48 (1993) R2978.
[227] L. Clavelli et al., Phys. Rev. D 47 (1993) 1973; L. Clavelli, Phys. Rev. D 46 (1992) 2112.
[228] J. Lopez et al., Phys. Lett. B 313 (1993) 241.
[229] M. Gaillard and B. Lee, Phys. Rev. D 10 (1974) 897.
[230] S. Glashow, J. Iliopoulos and L. Maiani, Phys. Rev. D 2 (1970) 1285.
[231] R. Barbieri and R. Gatto, Phys. Lett. B 110 (1982) 211.
[232] J.F. Donoghue, H.P. Nilles and D. Wyler, Phys. Lett. B 128 (1983) 55.
[233] J. Ellis and D.V. Nanopoulos, Phys. Lett. B 110 (1982) 44.
[234] A.V. Lahanas and D.V. Nanopoulos, Phys. Lett. B 129 (1983) 461.
[235] J. Hagelin, S. Kelley and T. Tanaka, Nucl. Phys. B 415 (1994) 293; J. Hagelin, S. Kelley and T. Tanaka, Mod. Phys. Lett. A 8 (1993) 2737.
[236] M. Dugan, B. Grinstein and L. Hall, Nucl. Phys. B 255 (1985) 413.
[237] M.S. Alam et al. (CLEO Collaboration), Phys. Rev. Lett. 74 (1995) 2885.
[238] R. Ammar et al. (CLEO Collaboration), Phys. Rev. Lett. 71 (1993) 674.
[239] B. Grinstein and M. Wise, Phys. Lett. B 201 274 (1988): W. Hou and R. Willey, Phys. Lett. B 202 (1988) 591.
[240] S. Bertolini, F. Borzumati and A. Masiero Nucl. Phys. B 294 321 (1987); S. Bertolini, F. Borzumati, A. Masiero and G. Ridolfi, Nucl. Phys. B 353 (1991) 591.
[241] R. Barbieri and G. Giudice, Phys. Lett. B 309 (1993) 86.
[242] V. Barger, M. Berger and R. Phillips, Phys. Rev. Lett. 70 (1993) 1368.
[243] J.L. Hewett, Phys. Rev. Lett. 70 (1993) 1045.
[244] Y. Okada, Phys. Lett. B 315 (1993) 119.
[245] R. Garisto and J.N. Ng, Phys. Lett. B 315 (1993) 372.

[246] J. Wu, R. Arnowitt and P. Nath, Phys. Rev. D 51 (1995) 1371.
[247] N. Cabibbo and L. Maiani, Phys. Lett. B 79 (1978) 109.
[248] F. Borzumati, M. Drees and M. Nojiri, Phys. Rev. D 51 (1995) 341; P. Nath and R. Arnowitt, Phys. Lett. B 336 (1994) 395.
[249] R. Arnowitt and P. Nath, Phys. Rev. Lett. 74 (1995) 4592.
[250] I. Bigi and F. Gabbiani, Nucl. Phys. B 352 (1991) 309.
[251] F. Gabbiani and A. Masiero, Nucl. Phys. B 322 (1989) 235.
[252] M. Drees, G. Jungman, M. Kamionkowski and M.M. Nojiri, Phys. Rev. D 49 (1994) 636.
[253] M. Drees and M.M. Nojiri, Phys., Rev. D 47 (1993) 376.
[254] L. Roszkowski, Phys. Rev. D 50 (1994) 4842.
[255] J. Wells, UM-TH-94-10 (1994).
[256] M. Kamionkowski, Phys. Rev. D 44 (1991) 3021.
[257] L. Roszkowski, Phys. Lett. B 262 (1991) 59.
[258] J. McDonald, K. A. Olive and M. Srednicki, Phys. Lett. B 283 (1992) 80.
[259] F. Bloch and A. Nordsieck, Phys. Rev. 52 (1937) 54; D. Yennie, S. Frautschi and H. Suura, Ann. Phys. 13 (1961) 379.
[260] T. Kinoshita, J. Math. Phys. 3 (1962) 650; T.D. Lee and M. Nauenberg, Phys. Rev. 133 (1964) 1549.
[261] R. Flores, K. Olive and S. Rudaz, Phys. Lett. B 232 (1989) 377.
[262] L. Bergstrom, Nucl. Phys. B 325 (1989) 647.
[263] S. Rudaz, Phys. Rev. D 39 (1989) 3549.
[264] L. Bergstrom Phys. Lett. B 225 (1989) 372.
[265] G.F. Giudice and K. Griest, Phys. Rev. D 40 (1989) 2549.
[266] G. Jungman and M. Kamionkowski, Phys. Rev. D 51 (1995) 3121.
[267] L. Bergstrom and J. Kaplan, Astropart. Phys. 2 (1994) 261.
[268] J. Ellis and R.A. Flores, Phys. Lett. B 263 (1991) 259.
[269] T. Ressell et al., Phys. Rev. D 48 (1993) 5519.
[270] R.L. Jaffe and A. Manohar, Nucl. Phys. B 337 (1990) 509.
[271] L.M. Krauss and P. Romanelli, Phys. Rev. D 39 (1989) 1225.
[272] R. Flores, K.A. Olive and M. Srednicki, Phys. Lett. B 237 (1990) 72.
[273] A. Ashman et al., Phys. Lett. B 206 (1988) 364.
[274] D. Adams et al. (The Spin Muon Collaboration), CERN-PPE/94-57 (1994).
[275] J. Engel, S. Pittel, E. Ormand and P. Vogel, Phys. Lett. B 275 (1992) 119.
[276] By V. Dimitrov, J. Engel and S. Pittel, Phys. Rev. D 51 (1995) 291.
[277] S. Raby and G.B. West, Phys. Lett. B 202 (1988) 47.
[278] R. Barbieri, M. Frigeni and G.F. Giudice, Nucl. Phys. B 313 (1989) 725.
[279] G. Gelmini, P. Gondolo and E. Roulet, Nucl. Phys. B 351 (1991) 623.
[280] M. Srednicki and R. Watkins, Phys. Lett. B 225 (1989) 140.
[281] M. Drees and M.M. Nojiri, Phys. Rev. D 47 (1993) 4226.
[282] M. Drees and M. Nojiri, Phys. Rev. D 48 (1993) 3483.
[283] T.P. Cheng, Phys. Rev. D 38 (1988) 2869.
[284] H.-Y. Cheng, Phys. Lett. B 219 (1989) 347.
[285] J. Gasser, H. Leutwyler and M.E. Sainio, Phys. Lett. B 253 (1991) 252.
[286] A. Bottino et al., Mod. Phys. Lett. 7 (1992) 733.
[287] N. Christ, private communication.
[288] T. Hatsuda and T. Kunihiro, Nucl. Phys. B 387, (1992) 705.
[289] M.A. Shifman, A.I. Vainshtein and V.I. Zakharov, Phys. Lett. B 78 (1978) 443.
[290] A.I. Vainshtein, V.I. Zakharov and M.A. Shifman, Usp. Fiz. Nauk. 130 (1980) 537 [Sov. Phys. Usp. 23 (1980) 429].
[291] S.P. Ahlen et al., Phys. Lett. B 195 (1987) 603.
[292] K. Freese, J. Frieman and A. Gould, Phys. Rev. D 37 (1988) 3388.
[293] J. Engel, Phys. Lett. B 264 (1991) 114.
[294] H.V. Klapdor-Kleingrothaus, in: Proc. Neutrinos in Cosmology, Astro, Particle, and Nuclear Physics, Erice, Italy, 1993, eds. A. Faessler, Prog. Part. Nucl. Phys. 32 (1994) 261.

[295] V.A. Bednyakov, H.V. Klapdor-Kleingrothaus and S.G. Kovalenko, Phys. Rev. D 50 (1994) 7128.
[296] M. Kamionkowski, L.M. Krauss and M.T. Ressell, IASSNS-HEP-94/14.
[297] A. Drukier and L. Stodolsky, Phys. Rev. D 30 (1984) 2295.
[298] K. Griest, Phys. Rev. D 37 (1988) 2703.
[299] A. Drukier, K. Freese and D. Spergel, Phys. Rev. D 33 (1986) 3495.
[300] B. Sadoulet, private communication.
[301] M. Kamionkowski, K. Griest, G. Jungman and B. Sadoulet, Phys. Rev. Lett. 74 (1995) 5174.
[302] D.N. Spergel, Phys. Rev. D 37 (1988) 1353.
[303] J.I. Collar and F.T. Avignone, Phys. Rev. D 47 (1993) 5238.
[304] J.I. Collar and F.T. Avignone, Astropart. Phys. 3 (1995) 37.
[305] P.D. Barnes et al., J. Low Temp. Phys. 93 (1993) 79.
[306] T. Shutt et al., Phys. Rev. Lett. 69 (1992) 3425; ibid. (1992) 3531.
[307] D.O. Caldwell et al., Phys. Rev. Lett. 61 (1988) 510.
[308] D. Reusser et al., Phys. Lett. B 235 (1991) 143.
[309] D.O. Caldwell et al., Phys. Rev. Lett. 65 (1990) 1305.
[310] W. Seidel et al., J. Low Temp. Phys. 93 (1993) 797; P. Colling et al., Nucl. Instrum. Meth. A 354 (1995) 408.
[311] M. Minowa et al., J. Low Temp. Phys. 93 (1993) 803.
[312] A.T. Lee et al., Phys. Rev. Lett. 71 (1993) 1395.
[313] K. Pretzl, J. Low Temp. Phys. 93 (1993) 439.
[314] N. Spooner and P.F. Smith, Phys. Lett. B 314 (1993) 430.
[315] A. Bottino et al., Phys. Lett. B 293 (1992) 460; C. Bacci et al., Phys. Lett. B 295 (1992) 330.
[316] K. Fushimi et al., Phys. Rev. C 47 (1993) 425.
[317] P.F. Smith, in: Sources of Dark Matter in the Universe, Proc. 1st Int. Symp., ed. D.B. Cline (World Scientific, Singapore, 1994) p. 227.
[318] S.R. Bandler et al., J. Low Temp. Phys. 93 (1993) 715; ibid (1993) 785.
[319] J. Seguinot et al., CERN preprint CERN-LAA 92-004 (1992); G.J. Davies et al., Phys. Lett. B 320 (1994) 395; J Park et al., in: Sources of Dark Matter in the Universe, Proc. 1st Int. Symp. ed. D.B. Cline (World Scientific, Singapore, 1994), p. 288.
[320] D. Snowden-Ifft et al., Phys. Rev. Lett. 70 (1993) 2348; ibid, 74 (1995) 4133.
[321] J. Engel, M.T. Ressell, I.S. Towner and W.E. Ormand, hep-ph/9504322.
[322] F.T. Avignone and J.I. Collar, Nucl. Instrum. Meth. B 95 (1995) 349.
[323] T. More et al., J. Low Temp. Phys. 93 (1993) 387.
[324] H.J. Maris and S. Tamura, Phys. Rev. B 47 (1991) 143.
[325] K.N. Buckland, M.J. Lehner, G.E. Masek and M. Mojaver, Phys. Rev. Lett. 73 (1994) 1067.
[326] J.D. Lewin and P.F. Smith, Rutherford Appleton Laboratory Report RAL-TR/95/024.
[327] J. Ellis and R.A. Flores, Phys. Lett. B 212 (1988) 375.
[328] H. Ejiri, K. Fushimi and H. Ohsumi, Phys. Lett. B 317 (1993) 14.
[329] G.D. Starkman and D.N. Spergel, Phys. Rev. Lett. 74 (1995) 2623.
[330] M. Mori et al. (Kamiokande Collaboration), Phys. Lett. B 278 (1991) 217.
[331] M. Mori et al. (Kamiokande Collaboration), Phys. Lett. B 289 (1992) 463.
[332] M. Mori et al. (Kamiokande Collaboration), Phys. Rev. D 48 (1993) 5505.
[333] J.M. LoSecco et al. (IMB Collaboration), Phys. Lett. B 188 (1987) 388.
[334] R. Svoboda et al., Astrophys. J. 315 (1987) 420.
[335] Frejus Collaboration, presented by H.J. Daum, Topical Seminar on Astrophysics and Particle Physics, San Miniato, Italy, 1989.
[336] E. Diehl, Ph.D. Thesis, University of Michigan, 1994.
[337] R.J. Wilkes, in: Proc. 22nd Annual SLAC Summer Institute on Particle Physics: Particle Physics, Astrophysics and Cosmology (School: 8–16 August 1994 followed by Topical Conference: 17–19 August 1994), Stanford, CA, 8–19 August 1994.
[338] D.M. Lowder et al., Nature 353 (1991) 331.

[339] L. Resvanis, Europhys. News 23 (1992) 172.
[340] F. Halzen, T. Stelzer and M. Kamionkowski, Phys. Rev. D 45 (1992) 4439.
[341] A. Bottino et al., Astropart. Phys. 3 (1995) 65.
[342] D. Seckel, T. Stanev and T.K. Gaisser, Astrophys. J. 382 (1991) 652.
[343] S. Ritz and D. Seckel, Nucl. Phys. B 304 (1988) 877.
[344] J. Edsjo, Nucl. Phys. B 43 (1995) 265; Ph.D. Thesis, Uppsala University (1993).
[345] G. Jungman and M. Kamionkowski, Phys. Rev. D 51 (1995) 328.
[346] L.V. Volkova, Yad. Fiz. 31 (1980) 784 [Sov. J. Nucl. Phys. 31 (1980) 1510].
[347] T.K. Gaisser, Cosmic Rays and Particle Physics (Cambridge University Press, Cambridge, 1990).
[348] M. Mori et al. (Kamiokande Collaboration), Phys. Lett. B 270 (1991) 89.
[349] M.M.Boliev et al., Bull. Acad. Sci. USSR, Phys. Ser. 55 (1991) 126 [Izv. Akad. Nauk. SSSR, Fiz. 55 (1991) 748.
[350] A. Gould, Astrophys. J. 321 (1987) 571.
[351] W.H. Press and D.N. Spergel, Astrophys. J. 296 (1985) 679.
[352] A. Gould, Astrophys. J. 321 (1987) 560.
[353] M. Nauenberg, Phys. Rev. D 36 (1987) 1080.
[354] A. Gould, Astrophys. J. 388 (1991) 338.
[355] J. Rich and C. Tao, DAPNIA-SPP-95-01, to appear in: Proc. 1994 Summer Study on High Energy Physics: Particle and Nuclear Astrophysics and Cosmology in the Next Millenium, Snowmass, CO, 29 June–14 July 1994.
[356] C. Peterson, D. Schlatter, I. Schmitt and P.M. Zerwas, Phys. Rev. D 27 (1983) 105.
[357] M. Abramowitz and I.A. Stegun, eds., Handbook of Mathematical Functions (Dover, New York, 1970) p. 228.
[358] F. Abe et al. (CDF Collaboration), Phys. Rev. Lett. 73 (1994) 225.
[359] J. Edsjo and P. Gondolo, hep-ph/9504283; F. Halzen, private communication, 1994.
[360] M. Kamionkowski, in: Particle Astrophysics, Atomic Physics, and Gravitation, Proc. XIV Moriond Workshop, Villars sur Ollon, Switzerland, 22–29 January 1994, eds. J. Tran Thanh Van, G. Fontaine and E. Hinds (Editions Frontieres, Gif-sur-Yvette, 1994).
[361] G. Jungman and M. Kamionkowski, Phys. Rev. D 49 (1994) 2316.
[362] A. Bottino, C. Favero, N. Fornengo and G. Mignola, Astropart. Phys. 3 (1995) 77.
[363] J. Silk and M. Srednicki, Phys. Rev. Lett. 53 (1984) 624.
[364] J. Ellis et al., Phys. Lett. B 214 (1989) 403.
[365] F. Stecker, S. Rudaz and T. Walsh, Phys. Rev. Lett. 55 (1985) 2622.
[366] F. Stecker and A. Tylka, Astrophys. J. 336 (1989) L51.
[367] M. Salamon et al., Astrophys. J. 349 (1990) 78.
[368] R.E. Streitmatter et al. Proc. 21st ICRC, OG 7.3-2, Adelaide, Vol. 3 (1990) p. 277.
[369] R.L. Golden et al., Nuovo Cimento B 105 (1990) 191.
[370] S. Rudaz and F. Stecker, Astrophys. J 325 (1988) 16.
[371] M.S. Turner and F. Wilczek, Phys. Rev. D 42 (1990) 1001.
[372] A.J. Tylka, Phys. Rev. Lett. 63 (1989) 840.
[373] M. Kamionkowski and M.S. Turner, Phys. Rev. D 43 (1991) 1774.
[374] D. Muller and K.K. Tang, Astrophys. J. 312 (1987) 183.
[375] D. Muller, private communication.
[376] M.S. Turner, Phys. Rev. D 34 (1986) 1921.
[377] J. Gunn et al., Astrophys. J. 233 (1978) 1015.
[378] F. Stecker, Astrophys. J. 223 (1978) 1022.
[379] M. Srednicki, S. Theissen and J. Silk, Phys. Rev. Lett. 56 (1986) 263.
[380] S. Rudaz, Phys. Rev. Lett. 56 (1986) 2128.
[381] L. Bergstrom and H. Snellman, Phys. Rev. D 37 (1988) 3737.
[382] A. Bouquet, P. Salati and J. Silk, Phys. Rev. D 40 (1989) 3168.
[383] H. Bloemen and J. Silk, Astrophys. J. Lett. 313 (1987) 47.
[384] M. Urban et al., Phys. Lett. B 293 (1992) 149.
[385] V. Berezinsky, A. Bottino and G. Mignola, Phys. Lett. B 325 (1994) 136.
[386] F. Stecker, Phys. Lett. B 201 (1988) 529.

[387] H.U. Bengtsson, P. Salati and J. Silk, Nucl. Phys. B 346 (1990) 129.
[388] V. Berezinsky, A. Bottino and V. de Alfaro, Phys. Lett. B 274 (1992) 122.
[389] M. Kamionkowski, in: The Gamma Ray Sky with Compton GRO and SIGMA, Proc. School, Les Houches, France, 25 January–4 February 1994, eds. M. Signore, P. Salati and G. Vedrenne (Kluwer Academic, Dordrecht, 1995).
[390] J.R. Ipser and P. Sikivie, Phys. Rev. D 35 (1987) 3695.
[391] J. Flores and J. Primack, Astrophys. J. 427 (1994) L1.
[392] P. Gondolo, Nucl. Phys. (Proc. Suppl.) B 35 (1994) 148.
[393] L. Roszkowski, Phys. Lett. B 252 (1990) 471; K. Griest and L. Roszkowski, Phys. Rev. D 46 (1992) 3309.
[394] E. Diehl et al., hep-ph/9502399.
[395] K. Enqvist, K. Kainulainen and J. Maallampi, Nucl. Phys. B317 (1989) 647.
[396] K. Griest and J. Silk, Nature 343 (1990) 26.
[397] L.M. Krauss, Phys. Rev. Lett. 64 (1990) 999.
[398] P. Chardonnet, P. Salati and P. Fayet, Nucl. Phys. B 394 (1993) 35.
[399] M. Beck, Nucl. Phys. (Proc. Suppl.) B 35 (1994) 150; M. Beck et al., Phys. Lett. B 336 (1994) 141.
[400] R.A. Flores, K.A. Olive and D. Thomas, Phys. Lett. B 263 (1991) 425; J. Ellis, J.F. Gunion, H.E. Haber, L. Roszkowski and F. Zwirner, Phys. Rev. D 39 (1989) 844; B.R. Greene and P.J. Miron, Phys. Lett. B 168 (1986) 226; S.A. Abel, S. Sarkar, and I.B. Whittingham, Nucl. Phys. B 392 (1993) 83.
[401] H. Pagels and J.R. Primack, Phys. Rev. Lett. 48 (1982) 223; S. Weinberg, Phys. Rev. Lett. 48 (1982) 1303.
[402] D.V. Nanopoulos, K.A. Olive and M. Srednicki, Phys. Lett. B 127 (1983) 30; M.Yu. Khlopov and A.D. Linde, Phys. Let. B 138 (1985) 265; J. Ellis, E. Kim, and D.V. Nanopoulos, Phys. Lett. B 145 (1984) 181; R. Juskiewicz, J. Silk and A. Stebbins, Phys. Lett. B 158 (1983) 463.
[403] T. Moroi, H. Muruyama and M. Yamaguchi, Phys. Lett. B 303 (1993) 289.
[404] V.S. Berezinsky, Phys. Lett. B 261 (1991) 71.
[405] E.J. Chun, J.E. Kim and H.P. Nilles, Phys. Lett. B 287 (1992) 123.
[406] E.J. Chun, H.B. Kim and J.E. Kim, Phys. Rev. Lett. 72 (1994) 1956.
[407] B. Ananthanarayan and Q. Shafi, Phys. Rev. D 50 (1994) 5986; J.L. Lopez, D.V. Nanopoulos and K.Yuan, Nucl. Phys. B 370 (1992) 445; C. Kolda, L. Roszkowski, J.D. Wells and G.L. Kane, Phys. Rev. D 50 (1994) 3498.
[408] G.W. Anderson and D.J. Castaño, Phys. Lett. B 347 (1995) 300; Phys. Rev. D 52 (1995) 1693.
[409] A. Salam and J. Strathdee, Nucl. Phys. Lett. B 76 (1974) 477.
[410] S. Ferrara, J. Wess and B. Zumino, Phys. Lett. B 51 (1974) 239.
[411] J.F. Gunion and H.E. Haber, Nucl. Phys. B 272 (1986) 1.
[412] T. Falk, K.A. Olive and M. Srednicki, Phys. Lett. B 354 (1995) 99.
[413] S. Coleman and E. Weinberg, Phys. Rev. D 7 (1973) 1888.
[414] J.F. Gunion and H.E. Haber, Nucl. Phys. B 278 (1986) 449.
[415] J. Gunion and H. Haber, UCD-92-31 (1992).
[416] J. Gunion and H. Haber, G. Kane and S. Dawson, SCIPP-92/58 (1992).
[417] S. Ferrara, L. Girardello and F. Palumbo, Phys. Rev. D 20 (1979) 403.
[418] L. Alvarez-Gaume and E. Witten, Nucl. Phys. B 234 (1984) 269.
[419] F. Iachello, L.M. Krauss and G. Maino, Phys. Lett. B 254 (1991) 220.
[420] Data acquired by the UCB/UCSB/LBL experiment at Oroville using a high-purity germanium ionization detector kindly provided by A. Da Silva, unpublished.